

Nonequilibrium phase transitions in chiral fluid  
dynamics including dissipation and fluctuation

Dissertation

zur Erlangung des Doktorgrades  
der Naturwissenschaften

vorgelegt beim Fachbereich Physik  
der Johann Wolfgang Goethe - Universität  
in Frankfurt am Main

von

Marlene Nahrgang  
aus Stadtallendorf

Frankfurt 2011

D 30



Nonequilibrium phase transitions in chiral fluid dynamics including dissipation  
and fluctuation

Vom Fachbereich Physik der  
Johann Wolfgang Goethe - Universität  
als Dissertation angenommen.

Dekan: Prof. Dr. Michael Huth

Erstgutachter: Prof. Dr. Marcus Bleicher  
Zweitgutachter: Prof. Dr. Horst Stöcker  
Datum der Disputation: 13. Juli 2011



Diese Arbeit beruht auf folgenden Publikationen:

- [Sch09] T. Schuster, M. Nahrgang, M. Mitrovski, R. Stock, M. Bleicher,  
“Analysis of the baryon-, proton-, and charged particle kurtosis in heavy ion collisions within a relativistic transport approach”, [arXiv:0903.2911 [hep-ph]].  
submitted to Phys. Lett. B
- [Nah09] M. Nahrgang, M. Bleicher,  
“The phase transition in chiral fluid dynamics”, Acta Phys. Polon. B Proc. Suppl. **2**  
(2009) 405.
- [Nah10a] M. Nahrgang,  
“Fluid dynamics with a critical point”, Russ. Phys. J. **53** (2010) 103.
- [Nah10b] M. Nahrgang, M. Bleicher,  
“Non-equilibrium fluctuations at the QCD phase transition”, J. Phys. Conf. Ser. **270**  
(2010) 012059.
- [Nah11a] M. Nahrgang, C. Herold, S. Schramm, M. Bleicher,  
“Hybrid approaches to heavy ion collisions and future perspectives”, [arXiv:1103.0753  
[hep-ph]].
- [Nah11b] M. Nahrgang, S. Leupold, C. Herold, M. Bleicher,  
“Nonequilibrium chiral fluid dynamics including dissipation and noise”, [arXiv:1105.0622  
[nucl-th]].  
accepted by Phys. Rev. C
- [Nah11c] M. Nahrgang, S. Leupold, M. Bleicher,  
“Equilibration and relaxation times at the chiral phase transition including reheating”, [arXiv:1105.1396 [nucl-th]].  
submitted to Phys. Lett. B
- [Nah11d] M. Nahrgang, M. Bleicher, S. Leupold, I. Mishustin,  
“The impact of dissipation and noise on fluctuations in chiral fluid dynamics”, [arXiv:1105.1962  
[nucl-th]].



# Contents

<b>1. Introduction</b>	<b>1</b>
<b>2. The phase diagram of quantum chromodynamics</b>	<b>7</b>
2.1. Quantum chromodynamics . . . . .	7
2.1.1. The classical Lagrangian . . . . .	7
2.1.2. The running coupling constant . . . . .	8
2.1.3. Chiral symmetry . . . . .	9
2.2. Thermodynamics of phase transitions . . . . .	10
2.2.1. Second order phase transition . . . . .	11
2.2.2. First order phase transition . . . . .	13
2.3. Lattice QCD . . . . .	15
2.4. Heavy-ion collisions . . . . .	16
2.4.1. Simulations of heavy-ion collisions . . . . .	17
2.4.2. Critical fluctuations . . . . .	21
2.4.3. Formation of disoriented chiral condensates . . . . .	24
2.4.4. Experimental status . . . . .	25
2.5. Model studies . . . . .	27
<b>3. Nonequilibrium methods in finite temperature quantum field theory</b>	<b>31</b>
3.1. Imaginary-time formalism . . . . .	32
3.2. Real-time formalism . . . . .	34
3.2.1. Generating functional on the real-time contour . . . . .	35
3.2.2. Real-time propagators . . . . .	38
3.3. Dissipation and fluctuation . . . . .	42
3.3.1. Boltzmann kinetic theory . . . . .	43
3.3.2. Langevin theory . . . . .	43
3.3.3. Dissipation-fluctuation theorem . . . . .	44
3.4. The influence functional method . . . . .	46
3.4.1. Path integral formulation of the density matrix . . . . .	46
3.4.2. The influence functional . . . . .	47
3.5. The closed time path effective action . . . . .	49
3.6. The two-particle irreducible effective action . . . . .	52
<b>4. Chiral fluid dynamics I</b>	<b>57</b>
4.1. The linear sigma model with constituent quarks . . . . .	57
4.1.1. Mean-field thermodynamics . . . . .	58
4.1.2. Phase diagram of the linear sigma model with constituent quarks . . . . .	60
4.1.3. Thermal equilibrium . . . . .	64

4.2.	Dynamics of the chiral fields and the quarks . . . . .	64
4.3.	Numerical implementation . . . . .	66
4.3.1.	Staggered leap-frog algorithm . . . . .	66
4.3.2.	SHASTA fluid dynamic code . . . . .	67
4.3.3.	Initial conditions . . . . .	68
4.3.4.	Equation of state . . . . .	68
4.3.5.	The inclusion of the source term . . . . .	70
4.4.	Results . . . . .	70
4.4.1.	Equilibrium expansion . . . . .	71
4.4.2.	Off-equilibrium expansion . . . . .	75
<b>5.</b>	<b>Selfconsistent system-heat bath coupling</b>	<b>81</b>
5.1.	The influence functional for the linear sigma model with constituent quarks	81
5.1.1.	Explicit calculation of the influence functional . . . . .	82
5.1.2.	The noise kernel and fluctuations . . . . .	85
5.1.3.	The semiclassical equations of motion . . . . .	85
5.2.	The 2PI effective action for the linear sigma model with constituent quarks .	86
5.2.1.	The explicit form of $\Gamma_2[\sigma, S]$ and the self energy . . . . .	87
5.2.2.	The coupled equations of motion . . . . .	88
5.2.3.	The thermodynamic quantities of the quark fluid . . . . .	90
5.3.	The equation of motion for the sigma field . . . . .	90
5.3.1.	Lowest order . . . . .	90
5.3.2.	The damping kernel . . . . .	91
5.3.3.	Correlation of the noise fields . . . . .	96
5.4.	Discussion of the hard-mesonic heat bath . . . . .	97
5.5.	Energy-momentum conservation . . . . .	98
<b>6.</b>	<b>Equilibration and relaxation times</b>	<b>101</b>
6.1.	Numerical implementation of the Langevin equation . . . . .	101
6.2.	Equilibration for a global, isothermal heat bath . . . . .	102
6.2.1.	First order phase transition . . . . .	103
6.2.2.	Critical point . . . . .	106
6.3.	The energy dissipation . . . . .	108
6.4.	Equilibration for a heat bath with reheating . . . . .	111
6.4.1.	First order phase transition . . . . .	111
6.4.2.	Critical point . . . . .	111
<b>7.</b>	<b>Chiral fluid dynamics II</b>	<b>115</b>
7.1.	Energy-momentum conservation . . . . .	116
7.2.	Supercooling and reheating . . . . .	117
7.2.1.	Constant damping coefficient $\eta = 2.2/\text{fm}$ . . . . .	117
7.2.2.	Constant damping coefficient $\eta = 10/\text{fm}$ . . . . .	118
7.2.3.	Temperature dependent damping coefficient $\eta = \eta(T)$ . . . . .	120
7.3.	The intensity of sigma fluctuations . . . . .	122
7.4.	Correlation length at the critical point . . . . .	128



7.5. Momentum anisotropy . . . . .	129
<b>8. Summary and outlook</b>	<b>133</b>
<b>Appendix</b>	<b>139</b>
<b>A. SU(2) and SU(3)</b>	<b>139</b>
<b>B. The Grassmann algebra</b>	<b>141</b>
B.1. The basic formulation . . . . .	141
B.2. Differentiation . . . . .	141
B.3. Integration . . . . .	142
<b>C. The one-loop partition function in imaginary time formalism</b>	<b>143</b>
C.1. The free propagators in imaginary time . . . . .	143
C.2. Partition function for free bosons . . . . .	143
C.3. Partition function for free fermions . . . . .	145
<b>D. Parametrization of the equation of state</b>	<b>147</b>
<b>E. Feynman rules on the closed time path</b>	<b>149</b>
<b>F. Energy conservation in nonequilibrium chiral fluid dynamics</b>	<b>151</b>
F.1. Constant damping coefficient $\eta = 2.2/\text{fm}$ . . . . .	151
F.2. Constant damping coefficient $\eta = 10/\text{fm}$ . . . . .	151
F.3. Temperature dependent damping coefficient $\eta = \eta(T)$ . . . . .	152
<b>G. Energy density in nonequilibrium chiral fluid dynamics</b>	<b>153</b>
G.1. Constant damping coefficient $\eta = 2.2/\text{fm}$ . . . . .	153
G.2. Constant damping coefficient $\eta = 10/\text{fm}$ . . . . .	153
G.3. Temperature dependent damping coefficient $\eta = \eta(T)$ . . . . .	154
<b>H. Sigma field in nonequilibrium chiral fluid dynamics</b>	<b>155</b>
H.1. Constant damping coefficient $\eta = 2.2/\text{fm}$ . . . . .	155
H.2. Constant damping coefficient $\eta = 10/\text{fm}$ . . . . .	155
H.3. Temperature dependent damping coefficient $\eta = \eta(T)$ . . . . .	156
<b>Bibliography</b>	<b>157</b>
<b>Deutsche Kurzfassung</b>	<b>173</b>
<b>Danke!</b>	<b>181</b>
<b>Akademischer Lebenslauf</b>	<b>183</b>
<b>Meine akademischen Lehrer</b>	<b>185</b>



# List of Figures

1.1.	Phase diagram from lattice QCD and heavy-ion collisions. . . . .	2
1.2.	A pictorial view of the phase diagram of QCD inspired by model calculations	3
2.1.	Thermodynamic potential, critical point. . . . .	13
2.2.	Thermodynamic potential, first order phase transition. . . . .	14
2.3.	Trace anomaly, energy density and pressure from lattice QCD. . . . .	20
2.4.	Effective kurtosis in UrQMD. . . . .	24
2.5.	Fluctuations from NA49 . . . . .	26
2.6.	Effective net-proton kurtosis from STAR. . . . .	27
2.7.	The chiral and confinement crossover transition at $\mu_B = 0$ in the PNJL model	28
2.8.	The chiral and confinement crossover transition at $\mu_B = 0$ for the PQM model.	29
2.9.	The phase diagram in the PQM model. . . . .	30
3.1.	Loop diagrams in $\phi^4$ theory. . . . .	35
3.2.	The time path contour. . . . .	37
4.1.	The effective potential at $g = 3.3$ . . . . .	62
4.2.	The effective potential at $g = 5.5$ . . . . .	62
4.3.	The effective potential at $g = 3.63$ . . . . .	63
4.4.	The equilibrium value of the sigma field $\sigma_{\text{eq}}$ . . . . .	63
4.5.	The equilibrium value of the sigma mass $m_\sigma$ . . . . .	64
4.6.	The variance of the sigma fluctuations in equilibrium. . . . .	65
4.7.	Equation of state in equilibrium. . . . .	69
4.8.	Time evolution of the energy density, critical point. . . . .	71
4.9.	Time evolution of the energy density, first order phase transition. . . . .	72
4.10.	Time evolution of the sigma field, critical point. . . . .	72
4.11.	Time evolution of the sigma field, first order phase transition. . . . .	73
4.12.	Average and variance of the sigma field. . . . .	73
4.13.	Average and variance of the temperature. . . . .	74
4.14.	Total energy, critical point. . . . .	76
4.15.	Total energy, first order phase transition. . . . .	76
4.16.	Time evolution of the energy density in a critical point scenario and an off-equilibrium expansion. . . . .	77
4.17.	Time evolution of the energy density in a scenario with first order phase transition and an off-equilibrium expansion. . . . .	77
4.18.	Time evolution of the sigma field in a critical point scenario and an off-equilibrium expansion. . . . .	78

4.19. Time evolution of the sigma field in a scenario with first order phase transition and an off-equilibrium expansion. . . . .	78
4.20. Average and variance of the sigma field. . . . .	79
4.21. Average and variance of the temperature. . . . .	79
5.1. The only diagram for $\Gamma_2[\sigma, S]$ . . . . .	88
5.2. Temperature dependence of the damping coefficient for all phase transition scenarios. . . . .	95
6.1. The distribution of the sigma field for $T = 160$ MeV. . . . .	103
6.2. Average of the sigma field, first order phase transition, $T > T_{sp}^{(2)}$ . . . . .	104
6.3. Average of the sigma fluctuations, first order phase transition, $T > T_{sp}^{(2)}$ . . . . .	104
6.4. The average of the sigma field for $T = 125$ MeV. . . . .	105
6.5. The distribution of the sigma field at $T_c = 123.27$ MeV. . . . .	106
6.6. Average of the sigma field, first order phase transition, $T < T_c$ . . . . .	107
6.7. Average of the sigma fluctuations, first order phase transition, $T < T_c$ . . . . .	107
6.8. Time evolution of the scaled noise average of the sigma field, critical point. . . . .	108
6.9. Time evolution of the noise averaged variance of the sigma fluctuations, critical point. . . . .	109
6.10. Energy dissipation for a scenario with a first order phase transition and for a critical point scenario . . . . .	110
6.11. Time evolution of the volume averaged sigma field, first order phase transition, with reheating. . . . .	112
6.12. Time evolution of the volume averaged temperature, first order phase transition, with reheating. . . . .	112
6.13. Time evolution of the volume averaged sigma field, critical point, with reheating. . . . .	114
6.14. Time evolution of the volume averaged sigma field, critical point, with reheating. . . . .	114
7.1. Average and variance of the sigma field, $\eta = 2.2/\text{fm}$ . . . . .	117
7.2. Average and variance of the temperature, $\eta = 2.2/\text{fm}$ . . . . .	118
7.3. Average and variance of the sigma field, $\eta = 10/\text{fm}$ . . . . .	119
7.4. Average and variance of the temperature, $\eta = 10/\text{fm}$ . . . . .	119
7.5. Average and variance of the sigma field, $\eta = \eta(T)$ . . . . .	120
7.6. Average and variance of the temperature, $\eta = \eta(T)$ . . . . .	121
7.7. Transverse momentum spectra, critical point, $\eta = \eta(T)$ . . . . .	123
7.8. Transverse momentum spectra, first order, $\eta = \eta(T)$ . . . . .	124
7.9. Intensity of sigma fluctuations, $\eta = 2.2/\text{fm}$ , critical point. . . . .	124
7.10. Intensity of sigma fluctuations, $\eta = 10/\text{fm}$ , critical point. . . . .	125
7.11. Intensity of sigma fluctuations, $\eta = \eta(T)$ , critical point. . . . .	125
7.12. Deviation of the sigma field from equilibrium, critical point. . . . .	126
7.13. Intensity of sigma fluctuations, $\eta = 2.2/\text{fm}$ , first order phase transition. . . . .	126
7.14. Intensity of sigma fluctuations, $\eta = 10/\text{fm}$ , first order phase transition. . . . .	127
7.15. Intensity of sigma fluctuations, $\eta = \eta(T)$ , first order phase transition. . . . .	127

7.16. Deviation of the sigma field from equilibrium, first order phase transition. .	128
7.17. Correlation length, constant damping. . . . .	130
7.18. Momentum anisotropy, temperature-dependent damping. . . . .	131
F.1. The total energy of the system for $\eta = 2.2/\text{fm}$ . . . . .	151
F.2. The total energy of the system for $\eta = 10/\text{fm}$ . . . . .	151
F.3. The total energy of the system for $\eta = \eta(T)$ . . . . .	152
G.1. Time evolution of the energy density for $\eta = 2.2/\text{fm}$ . . . . .	153
G.2. Time evolution of the energy density for $\eta = 10/\text{fm}$ . . . . .	153
G.3. Time evolution of the energy density for $\eta = \eta(T)$ . . . . .	154
H.1. Time evolution of the sigma field for $\eta = 2.2/\text{fm}$ . . . . .	155
H.2. Time evolution of the sigma field for $\eta = 10/\text{fm}$ . . . . .	155
H.3. Time evolution of the sigma field for $\eta = \eta(T)$ . . . . .	156



## List of Tables

- 6.1. Relaxation of the averaged sigma field and final temperatures for a scenario with a first order phase transition and reheating of the heat bath. . . . . 113
- 6.2. Relaxation of the averaged sigma field and final temperatures for a critical point scenario and reheating of the heat bath. . . . . 113





# 1. Introduction

More than 99 percent of the mass of the visible matter in our universe emerges at the phase transition from a plasma of quarks and gluons to a world mainly built from hadrons, protons and neutrons. In nature this phase transition potentially appears shortly,  $10^{-5}$  seconds, after the Big Bang at temperatures of around  $10^{12}$  Kelvin. Besides the early universe the core of superdense stars could be a place for this phase transition. It has two interesting aspects: the spontaneous breaking of chiral symmetry and the transition between partonic and hadronic degrees of freedom. Above the phase transition temperature, up- and down-quarks have very small but finite current masses of 1.5 and 3 MeV. The origin of this current mass is searched for at the Large Hadron Collider (LHC) in form of the Higgs boson. Below the phase transition, protons and neutrons form with a mass of about 940 MeV, which corresponds to a constituent quark mass of about 300 MeV. This mass is generated at the chiral phase transition. The current quark mass breaks chiral symmetry explicitly. Compared to hadronic masses, however, it is small enough to consider chiral symmetry an approximate symmetry of the strong interaction. While the theory itself is approximately chirally symmetric, the ground state of the strong interaction is not. Chiral symmetry is, thus, spontaneously broken. From Goldstone's theorem we know that every spontaneously broken symmetry is accompanied by a massless mode, the so-called Goldstone boson. The lightest meson, the pion, is considered the Goldstone boson of chiral symmetry. Its finite mass is generated by the current quark mass.

The fundamental theory of the strong interaction between quarks and gluons and between nucleons in the atomic nuclei is quantum chromodynamics (QCD). The charge of QCD is called color and has three aspects, red, blue and green. In none of the experiments conducted since the dawn of high-energy particle physics a single, isolated quark has ever been observed. In the final state quarks are always bound in color-neutral hadrons. This peculiar phenomenon is called confinement and has its origin in the non-Abelian structure of QCD. Unlike the photon in quantum electrodynamics, whose success is the triumph of the concept of quantum field theories, the gauge boson mediating the strong force, the gluon, itself carries color charge. Gluons, thus, interact with each other. As a direct consequence of this, the strong interaction becomes stronger at larger distances or lower energies. At smallest distances or highest energies the interaction becomes small and the quarks are asymptotically free. The key aspect here is the running coupling obtained from quantizing the classical QCD. It poses a severe technical problem to working with the theory. The predictive power of quantum field theories lies mainly in the perturbative treatment of its interactions. At energies of the quark-hadron phase transition the coupling constant of QCD is of the order of one and any perturbative analysis must break down.

As it is the case for the phase diagram of water, the transition between the two phases can

## 1. Introduction

---

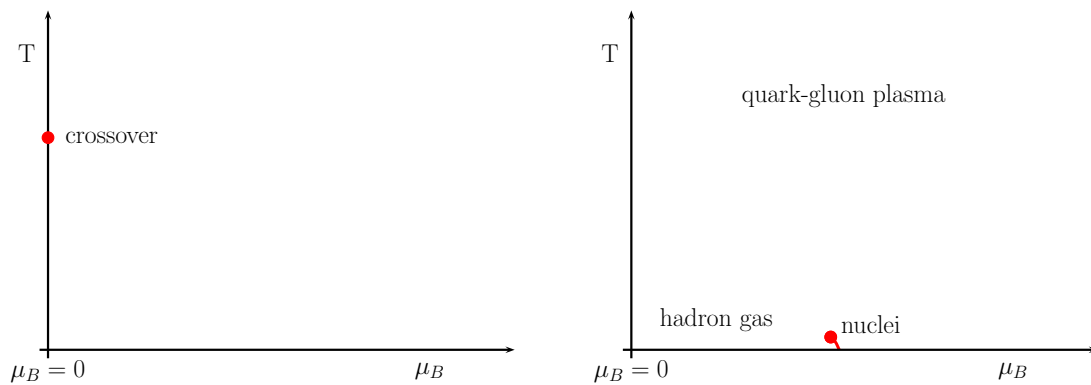


Figure 1.1.: What we know about the phase diagram of QCD from lattice calculations (left) and from heavy-ion collisions (right).

proceed continuously or discontinuously. A discontinuous phase transition, also called a first order phase transition, has a coexistence region, where both phases are stable equilibrium states. At a continuous phase transition, also called a second order phase transition, this coexistence region vanishes. We find that microscopically different systems show the same universal behavior at a second order phase transition. Here, the correlation length and the fluctuations become large and the properties are thus dominated by a couple of macroscopic parameters, like the system's dimension. In the phase diagram of water the first order phase transition line ends at higher temperatures and pressures. Beyond this end point the definition of phases is unclear. We rather see a fast phase change than a real phase transition. This is a so-called crossover transition. More interestingly, the end point of the first order phase transition line is a single point of a second order phase transition. This is called the critical point of water. Here, the growth of the correlations up to the wavelength of light can be observed as opalescence: the originally transparent fluid turns opaque at the critical point.

An analogous investigation of the QCD phase diagram is complicated by two issues: the technically challenging QCD interaction and the fact that we cannot simply put strongly interacting matter in a box and heat or compress it.

For the study of the phase diagram of QCD you have three possible ways to go.

- First, you are brave and solve the partition function of QCD. This necessarily involves nonperturbative methods, the most promising of which is lattice QCD. With large numerical power QCD is solved on a discretized space-time lattice. This method is, however, only feasible at zero or very small baryonic densities, where it shows that the phase transition is a crossover. The left plot of figure 1.1 shows what we know about the phase diagram from lattice QCD.
- Second, you are strong and collide heavy ions at ultrarelativistic energies. Neutron stars are too far in space and astrophysical observations are too indirect to draw definite conclusions. The Big Bang is too long back in time. You, thus, have to create systems close to the phase transition of QCD in your laboratory. The endeavour of

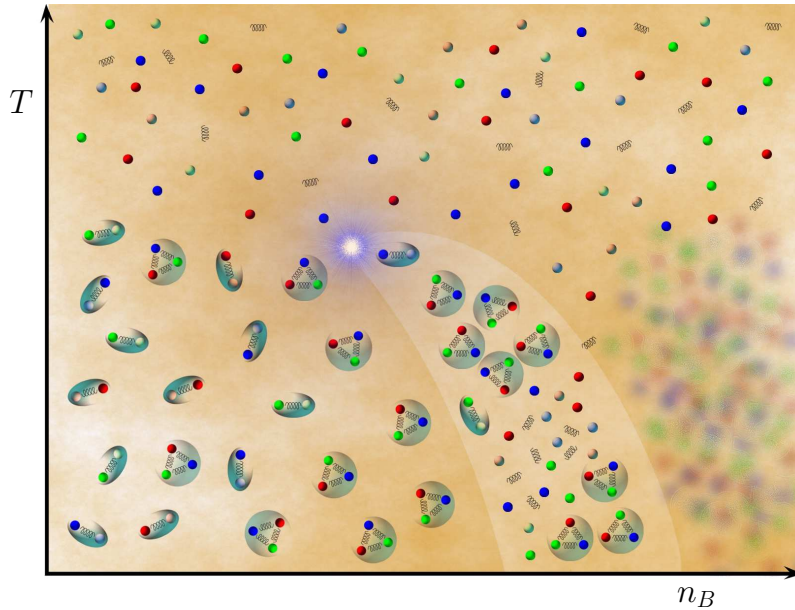


Figure 1.2.: A pictorial view of the phase diagram of QCD inspired by model calculations, which strongly suggest a first order phase transition at higher baryonic densities. In order to see the coexistence region of the first order phase transition the phase diagram is shown in the  $T$ - $n_B$  plane. The first order phase transition line ends in a critical point. At even higher baryonic densities there is space for more exotic phases of QCD, like the quarkyonic matter, the color-superconducting phase and the color-flavor locked phase.

heavy-ion collisions started with relatively low energies to study nuclear structure and the liquid-gas phase transition of nuclear matter. With the possibility of building more powerful accelerators at CERN (Organisation européenne pour la Recherche nucléaire) and BNL (Brookhaven National Laboratory) and faster and more accurate detectors it became possible to collide heavy ions at ultrarelativistic energies. A broad variety of observables has been proposed to study the properties of the quark-gluon plasma and of the QCD phase transition in heavy-ion collisions. Yet, none of them has unambiguously explained the available data. The search for a conjectured critical point and the onset of deconfinement has led to the low energy beam scan at RHIC (Relativistic Heavy Ion Collider), BNL, basically looking for an increase of event-by-event fluctuation measures. The upcoming accelerator project FAIR (Facility for Anti-proton and Ion Research) at GSI Helmholtzzentrum für Schwerionenforschung will provide excellent conditions for the study of the phase transition at higher densities at the CBM (Compressed Baryonic Matter) experiment. The right plot of figure 1.1 shows the phase diagram as seen from heavy-ion collisions.

- Third, you are creative and phenomenologically construct an effective field theoretical model of QCD. Creativity is not unlimited as these models should give a good quantitative description of experimentally measured quantities like cross sections and cover qualitative aspects of the phase diagram, like chiral symmetry and/or

confinement. There are indeed a couple of models that meet these requirements and they can describe certain parameter regions of the phase diagram. These model studies strongly suggest a first order phase transition at high baryonic densities and lower temperatures. This line ends in a critical point. A pictorial view of the phase diagram inspired by model studies is shown in figure 1.2.

This thesis contributes to the ambitious goal of theoretically understanding the phase transition of QCD under realistic conditions of heavy-ion collisions. It is located between the phenomenological approach of effective models and the realistic modeling of heavy-ion experiments. While the prediction of most observables is based on thermodynamics it is unclear if the matter, which is created in heavy-ion collisions, is in thermal equilibrium at the phase transition. Here, relaxation times become large, whereas the dynamics of a heavy-ion collision is very fast.

Even if the system is in equilibrium above the phase transition it is likely to be driven out of equilibrium as it cools through the phase transition. At a second order phase transition this is called critical slowing down and severely limits the growth of the correlation length. As a consequence, one expects any signal of a critical point to be weakened in a dynamic nonequilibrium situation. Signals of a first order phase transition, however, are based on nonequilibrium effects, such as supercooling. Here, parts of the system remain in the high-temperature phase for some time even below the transition temperature. In this work we wish to approach both questions:

- How much of a signal of the critical point survives in the nonequilibrium of a dynamic environment?
- How much of a signal of the first order phase transition is developed in the nonequilibrium situation of a heavy-ion collision?

To answer these questions, we develop a coupled nonequilibrium approach based on finite temperature quantum field theoretical methods. Our starting point is the Lagrangian of the linear sigma model with constituent quarks. It is an effective low energy model of QCD with a pointlike interaction between quarks and mesons focussing on the aspect of chiral symmetry. The dynamics of the quark fields lead to a dynamic symmetry breaking in the mesonic sector of the model. Inspired by the success of fluid dynamic simulations of heavy-ion collisions we treat the quarks in local thermal equilibrium and reduce their dynamics to the evolution of their energy and momentum density. Due to the pressure built up the system expands and cools. This cooling drives the chiral phase transition for the pion and sigma fields. With focus on the order parameter of chiral symmetry, the sigma field, we obtain the nonequilibrium dynamics of the chiral fields within two functional methods, the influence functional and the two-particle irreducible effective action. From the interaction of the chiral fields with the quark fluid we obtain a Langevin equation of motion including damping and noise terms. While the influence functional method relies on an intuitive separation between the quark fluid as a heat bath and the chiral fields as the explicitly propagated variables, the two-particle irreducible effective action is the basis for a selfconsistent scheme. On the one hand, it allows for a nonequilibrium evolution

---

of the chiral fields, equivalent to that derived from the influence functional. On the other hand, we obtain the equilibrium energy density and pressure of the quark fluid depending on the external parameters, the chiral fields, within the same framework. The relation between the energy density and the pressure is called the equation of state and needed for the fluid dynamic expansion. In our coupled approach we also take the back reaction of the damping of the chiral fields into account. The energy that dissipates from the chiral fields to the quark fluid is taken into account as a source term in the fluid dynamic expansion. By this procedure we achieve energy and momentum conservation of the entire system to good precision.

A brief introduction to QCD and a summary of the achievements and challenges of the different approaches to the phase diagram are outlined in chapter 2. Chapter 3 first introduces the quantum field theoretical basics for the study of relativistic many-body systems at finite temperature. After a discussion of the general aspects of nonequilibrium, such as irreversibility and the origin of dissipation and fluctuation, the functional methods applied in this work are introduced. A first naïve propagation of the chiral fields coupled to the fluid dynamic expansion of the quarks in standard mean-field approximation results in a classical equation of motion for the chiral fields. We call this the off-equilibrium expansion. These results are presented in chapter 4. Next, we consistently derive the nonequilibrium propagation of the sigma field including dissipation and noise and the fluid dynamic equations for the propagation of the quarks and antiquarks in chapter 5. The issues of energy-momentum conservation of the entire system are discussed. In the following we present the numerical implementation and results. In chapter 6 we investigate the relaxational dynamics of the sigma field in a static heat bath and the energy dissipation from the field during relaxation. In chapter 7 we finally present the evolution of the fully coupled system of the sigma field and the quark fluid. With our consistent approach of coupling the nonequilibrium dynamics to a realistic expansion of heavy-ion collisions we are able to study thermalization and relaxation times, as well as nonequilibrium effects of the phase transition such as supercooling, reheating, fluctuations and correlations. We summarize the methods, achievements and open challenges of this work in chapter 8.

## *1. Introduction*

---

## 2. The phase diagram of quantum chromodynamics

In this chapter, we present the contemporary understanding of the phase diagram of QCD. Its predominant feature is the transition between partonic degrees of freedom in the deconfined phase at high temperatures and high net-baryon densities and the hadronic degrees of freedom in the confined phase at low temperatures and low net-baryon densities. This phase transition has two aspects: the spontaneous breaking of chiral symmetry and the confinement-deconfinement transition. We introduce the basic properties of QCD in section 2.1 and give a brief reminder of the thermodynamics of phase transitions in section 2.2. Next, we present the three approaches to the QCD phase diagram: first principle QCD calculations on the lattice, section 2.3, the experimental study of the phase diagram by heavy-ion collisions, section 2.4 and effective low energy models of QCD in section 2.5.

### 2.1. Quantum chromodynamics

The quark model [Gel64] was successful in explaining the baryon and meson multiplets known experimentally if one added one additional quantum number, color, to avoid violations of the Pauli principle. All experimentally detected excitations of the strong interaction are color neutral. It was later discovered that non-Abelian gauge theories are asymptotically free and thus are able to have confining properties in the infrared regime [GroWil74, Wil74b]. The quantum theory of the strong interaction can be formulated completely in terms of the underlying degrees of freedom, quarks and gluons.

#### 2.1.1. The classical Lagrangian

QCD is a non-Abelian gauge theory with  $SU_c(3)$  color gauge invariance coupled to fermions. The classical Lagrangian of QCD ignoring the heavier quarks reads

$$\mathcal{L} = \sum_{q=u,d,s} \bar{q}^{\alpha} (i\gamma^{\mu} D_{\mu,\alpha\beta} - m_q \delta_{\alpha\beta}) q^{\beta} + \mathcal{L}_{YM} \quad (2.1)$$

with the Yang-Mills part [YanMil54]

$$\mathcal{L}_{YM} = -\frac{1}{4} F_{\mu\nu}^a F_a^{\mu\nu}. \quad (2.2)$$

The covariant derivative in the fundamental representation of the  $SU_c(3)$  Lie Algebra reads

$$D_{\mu} = \partial_{\mu} + ig t_a A_{\mu}^a \quad (2.3)$$

and the gluon field strength is given by

$$F_{\mu\nu}^a = \partial_\mu A_\nu^a - \partial_\nu A_\mu^a - gf_{bc}^a A_\mu^b A_\nu^c. \quad (2.4)$$

In the above equations, the quark field  $q^\alpha$ ,  $\alpha = \{1, 2, 3\}$  is the  $SU_c(3)$  triplet, the gluon field  $A_\mu^a$ ,  $a = 1, \dots, 8$  the  $SU_c(3)$  octet,  $m_q$  are the quark masses,  $g$  is the dimensionless coupling and  $\gamma^\mu$  the Dirac matrices. The matrices  $t^a$  are the generators of  $SU(3)$  fulfilling the commutation relations of a Lie algebra

$$[t_a, t_b] = if_{abc}t^c. \quad (2.5)$$

See appendix A for the explicit form of  $t^a$  and the structure constants  $f_{abc}$ .

### 2.1.2. The running coupling constant

Because quantum effects in QCD become more important at low energies the classical Lagrangian is of little use for the real dynamics of the theory. We have to quantize QCD in order to learn more. Due to high momenta in intermediate quantum loops quantization introduces ultraviolet divergences. QCD is a renormalizable theory and these divergences can be absorbed in renormalizing the parameters of the Lagrangian. The renormalized coupling constant is of special interest. After renormalization it depends on the renormalization scale  $\Lambda$ . The renormalization group equation reads

$$\Lambda \frac{\partial g}{\partial \Lambda} = \beta. \quad (2.6)$$

We define the strong coupling constant

$$\alpha_s(\Lambda) = \frac{g^2(\Lambda)}{4\pi} \quad (2.7)$$

with the initial condition to equation (2.6)  $\alpha_s(\Lambda_{\text{QCD}}) = g$ .

The  $\beta$ -function on the right hand side of (2.6) is to lowest order

$$\beta(g) = -\frac{1}{4\pi} \left( 11 - \frac{2}{3}N_f \right) g^3, \quad (2.8)$$

with the number of quark flavors  $N_f$ . The explicit solution of equation (2.6) for the strong coupling constant is then

$$\alpha_s(\Lambda) = \frac{2\pi}{\left( 11 - \frac{2}{3}N_f \right) \ln(\Lambda^2/\Lambda_{\text{QCD}}^2)}. \quad (2.9)$$

For large  $\Lambda$  the coupling  $\alpha_s(\Lambda)$  becomes logarithmically small while it diverges at  $\Lambda_{\text{QCD}}$ , which is experimentally found to be  $\Lambda_{\text{QCD}} \approx 200$  MeV. Perturbative calculations in QCD are, therefore, only meaningful for energies large compared to  $\Lambda_{\text{QCD}}$ . This behavior of the strong coupling is reflected in the anti-screening property of the QCD vacuum. It has a non-trivial structure with nonperturbative gluon and quark condensates. The gluon condensate lowers the energy density of the QCD vacuum below that of a perturbative vacuum, playing an essential role for the confinement property.

The quark condensate serves as an order parameter for the dynamic breaking of chiral symmetry.



### 2.1.3. Chiral symmetry

Besides the unbroken  $SU_c(3)$  gauge symmetry the QCD Lagrangian has a number of other symmetries. Here, we concentrate on chiral symmetry. For free massless Dirac particles helicity is a good quantum number. The generalized concept for an interacting theory is chirality. According to the chirality operator the quark fields can be split into left- and right-handed quarks

$$q_L = \frac{1}{2}(1 - \gamma_5)q \quad (2.10)$$

$$q_R = \frac{1}{2}(1 + \gamma_5)q, \quad (2.11)$$

with the  $\gamma_5$  Dirac matrix. The Lagrangian (2.1) becomes

$$\mathcal{L} = \sum_{q=u,d,s} (\bar{q}_R^\alpha i\gamma^\mu D_{\mu,\alpha\beta} q_R^\beta + \bar{q}_L^\alpha i\gamma^\mu D_{\mu,\alpha\beta} q_L^\beta) - m_q \delta_{\alpha\beta} (\bar{q}_R^\alpha q_L^\beta + \bar{q}_L^\alpha q_R^\beta) + \mathcal{L}_{\text{YM}}. \quad (2.12)$$

One sees that the QCD interaction does not mix left- and right-handed states. The term involving the mass of the quarks, however, does. The existence of finite quark masses breaks chiral symmetry explicitly. The masses of the light up- and down-quarks (and to some extent of the strange quark) are very small compared to hadronic masses. Energies at the phase transition of QCD are not high enough for heavier quarks to play an important role. In this sector we can, thus, speak of chiral symmetry as an approximate symmetry of QCD. The chiral group structure is

$$U_L(3) \times U_R(3) = U_V(1) \times SU_V(3) \times SU_A(3) \times U_A(1). \quad (2.13)$$

The transformations under  $U_V(1)$  change the phase of all quarks equally. This symmetry is present in the Lagrangian even for finite quark masses. It reflects that baryon number is an exactly conserved quantum number of the strong interaction. The symmetry  $U_A(1)$  is also exact on the classical level, but broken in the quantized QCD by axial anomaly.

Let us take a closer look at the remaining symmetry groups. For simplicity, here, we consider the  $SU_V(2) \times SU_A(2)$  subgroup with equal masses for the two lightest quarks  $m_u = m_d$ . The Lagrangian (2.1) is invariant under a transformation  $H_V \in SU_V(2)$ , for which

$$q \rightarrow H_V q = \exp(i\vec{\Theta} \frac{\vec{\tau}}{2}) q \quad (2.14)$$

with parameters  $\Theta$ . In the transformation (2.14),  $\vec{\tau}$  are the Pauli isospin matrices. This invariance reflects the well realized isospin symmetry  $m_u \simeq m_d$ . For a pionic state the transformation  $H_V$  is an isospin rotation

$$\vec{\pi} = i\vec{q}\vec{\tau}\gamma_5 q \rightarrow i\vec{q}\vec{\tau}\gamma_5 q + \vec{\Theta} \times (i\vec{q}\vec{\tau}\gamma_5 q) = \vec{\pi} + \vec{\Theta} \times \vec{\pi}. \quad (2.15)$$

According to Noether's theorem there is an associated conserved current with this symmetry. It is the vector current

$$\vec{V}_\mu = \bar{q}\gamma_\mu \frac{\vec{\tau}}{2} q. \quad (2.16)$$

## 2. The phase diagram of quantum chromodynamics

---

Under a transformation  $H_A \in \text{SU}_A(2)$  with

$$q \rightarrow H_A q = \exp(i\gamma_5 \vec{\Theta} \frac{\vec{\tau}}{2}) q \quad (2.17)$$

the mass term of the Lagrangian with two flavors and  $m_u = m_d$  is not invariant. It rotates a pionic state into a sigma-like state

$$\vec{\pi} = i\bar{q}\vec{\tau}\gamma_5 q \rightarrow i\bar{q}\vec{\tau}\gamma_5 q + \vec{\Theta}(i\bar{q}q) = \vec{\pi} + \vec{\Theta}\sigma. \quad (2.18)$$

The current associated with this approximate axial-vector symmetry is the axial-vector current

$$\vec{A}_\mu = \bar{q}\gamma_\mu\gamma_5\frac{\vec{\tau}}{2}q. \quad (2.19)$$

The crucial point is now that an approximate chiral symmetry, more precisely an approximate invariance under  $\text{SU}_A(2)$  transformations, implies the existence of approximately degenerate hadronic states with the same mass. This is, however, not observed in the hadronic spectra. The solution to this is that chiral symmetry is spontaneously broken at low temperatures. A symmetry is called spontaneously broken if it is realized at the level of the Lagrangian but is not present in the true ground state. The most famous example of a spontaneously broken symmetry in physics is that of a ferromagnet. While the spin-spin interaction is rotational invariant the ground state has a finite macroscopic magnetization pointing in some direction. Rotational  $\text{O}(3)$  symmetry is broken to rotational symmetry around this distinguished direction. The excitations in the other two directions have massless modes, spin waves. According to the Goldstone theorem there is one massless Goldstone boson for every remaining unbroken generator of a spontaneously broken continuous symmetry. In the case of QCD the sigma field with the quantum numbers of the vacuum acquires a finite expectation value by the spontaneous breaking of chiral symmetry. In terms of quarks this refers to the finite quark condensate. The massless Goldstone modes are the pions. Their finite, but small, mass comes from explicit symmetry breaking by the finite quark masses.

Before we come to the achievements and challenges of the different approaches to the QCD phase transition, lattice QCD, heavy-ion collisions and effective models, we give a brief overview about the physics of phase transitions.

### 2.2. Thermodynamics of phase transitions

The key quantity of any thermodynamic study is the partition function. In the grand-canonical ensemble it is the Gibbs sum over all states

$$Z(T, \mu_i) = \text{Tr} \exp\left(-\frac{H - \sum_i \mu_i N_i}{T}\right) = \sum_n \left\langle n \left| \exp\left(-\frac{H - \sum_i \mu_i N_i}{T}\right) \right| n \right\rangle, \quad (2.20)$$

with the Hamiltonian  $H$  of the system and the conserved charges  $N_i$  with their chemical potentials  $\mu_i$ . The phases of strongly interacting matter are typically characterized by temperature  $T$  and the baryochemical potential  $\mu_B$ . Then,

$$Z(T, \mu) = \sum_n \exp\left(-\frac{E_n - \mu_B B_n}{T}\right) = \exp\left(-\frac{V\Omega(T, \mu)}{T}\right), \quad (2.21)$$

with the energies  $E_n$  and the baryon number  $B_n$ .  $V$  is the volume of the system. This defines the thermodynamic potential  $\Omega(T, \mu_B)$ , which describes the state of the system. All thermodynamic quantities can be obtained from the thermodynamic relations by partial differentiation. The pressure is given by

$$p(T, \mu) = -\Omega(T, \mu_B). \quad (2.22)$$

There is usually a quantity that changes in a characteristic way at the phase transition and that can be used to distinguish the phases. This is the order parameter of the phase transition. In Ginzburg-Landau theory [GinLan50] it is used to expand the thermodynamic potential in a power series. According to the second law of thermodynamics, the principle of the increase of entropy, the equilibrium states are at the minima of the thermodynamic potential.

Phase boundaries are defined where the thermodynamic potential is non-analytic in any of the parameters, which in addition to  $T$  and  $\mu_B$  can be an external field or the order parameter.

The transition between two phases can either be continuous or discontinuous depending on whether the first derivative of  $\Omega$  with respect to any one of the parameters is continuous or discontinuous. In the old Ehrenfest classification [Ehr33] phase transitions are called  $n$ th order if the first discontinuity appears in the  $n$ th derivative. We also speak of a first order phase transition meaning a discontinuous phase transition and of a second order phase transition meaning a continuous phase transition. A crossover, formally a phase transition of infinite order, does not allow for a clear phase separation and is, therefore, rather a rapid phase change than a real phase transition.

Phase transitions in a phase diagram can either be of one type of this classification, or change the order as one goes along the line of the phase transition. When a first order phase transition line terminates, there is a critical point, which is a second order phase transition. Beyond the critical point the phase transition is a crossover. A typical example for a such a behavior is the phase diagram of water.

We now explain the main features of second and first order phase transitions.

### 2.2.1. Second order phase transition

Let us consider a Ginzburg-Landau functional  $\phi$ , which is an expansion in powers of an appropriate order parameter  $\sigma$  of the phase transition

$$\phi(T, \sigma) = \phi_0(T) + a(T - T_c)\sigma^2 + b\sigma^4, \quad (2.23)$$

with  $a > 0, b > 0$ . From minimizing  $\phi$  with respect to  $\sigma$  one finds the equilibrium values

$$\sigma_{\text{eq}} = \begin{cases} 0 & , \text{ for } T > T_c \\ \sqrt{\frac{a}{2b}(T - T_c)} & , \text{ for } T < T_c \end{cases}. \quad (2.24)$$

In the symmetric phase for  $T > T_c$  the order parameter vanishes. In the unsymmetric phase for  $T < T_c$  it has a finite value.  $\phi(T, \sigma)$  is sketched in figure 2.1. One sees that the high-temperature minimum,  $\sigma_{\text{eq}} = 0$ , changes continuously to the low-temperature

## 2. The phase diagram of quantum chromodynamics

---

minimum at finite  $\sigma$ . At the critical temperature  $T_c$  the potential becomes very flat at the minimum. The Landau-Ginzburg functional (2.23) for  $\sigma = \sigma_{\text{eq}}$  is the thermodynamic potential

$$\phi(T) = \begin{cases} \phi_0(T) & , \text{ for } T > T_c \\ \phi_0(T) + \frac{a^2}{2b}(T_c - T)^2 & , \text{ for } T < T_c \end{cases} . \quad (2.25)$$

The entropy

$$S(T) = -\frac{\partial\phi(T)}{\partial T} = \begin{cases} S_0(T) & , \text{ for } T > T_c \\ S_0(T) + \frac{a^2}{b}(T_c - T) & , \text{ for } T < T_c \end{cases} , \quad (2.26)$$

is continuous over the phase transition. For the heat capacity, which is a second derivative of  $\phi$ , we find a discontinuity at  $T = T_c$

$$C(T) = -T\frac{\partial S(T)}{\partial T} = \begin{cases} C_0(T) & , \text{ for } T > T_c \\ C_0(T) - \frac{a^2}{b}T & , \text{ for } T < T_c \end{cases} . \quad (2.27)$$

The systems behavior under a small perturbation in form of an external field  $h$  in  $\phi$

$$\phi_h(T, \sigma) = \phi_0(T) + a(T - T_c)\sigma^2 + b\sigma^4 - hV\sigma , \quad (2.28)$$

is quantified by the susceptibility

$$\chi = \left( \frac{\partial\sigma}{\partial h} \right) \Big|_{T, h \rightarrow 0} . \quad (2.29)$$

The derivative of the equilibrium condition  $\partial\phi_h(T, \sigma)/\partial\sigma = 0$  with respect to  $h$

$$\left( \frac{\partial}{\partial h} \frac{\partial\phi_h}{\partial\sigma} \right) (T, \sigma) \Big|_{T, h \rightarrow 0} = \left( \frac{\partial\sigma}{\partial h} \right) \Big|_{T, h \rightarrow 0} \frac{\partial^2\phi_h(T, \sigma)}{\partial^2\sigma} = 0 \quad (2.30)$$

reads

$$\chi(2a(T - T_c) + 12b\sigma^2) = V . \quad (2.31)$$

For the susceptibility in the limit  $h \rightarrow 0$  with (2.24) we get

$$\chi(T) = \begin{cases} \frac{V}{2a(T - T_c)} & , \text{ for } T > T_c \\ -\frac{V}{4a(T - T_c)} & , \text{ for } T < T_c \end{cases} . \quad (2.32)$$

The susceptibility diverges for  $T \rightarrow T_c$  because the curvature of  $\phi$  at the minimum is very flat at  $T = T_c$ .

The probability for fluctuations of the order parameter around its equilibrium value  $\delta\sigma = \sigma - \sigma_{\text{eq}}$  is

$$P[\delta\sigma] \propto \exp\left(-\frac{\Delta\phi_h}{T}\right) , \quad (2.33)$$

with  $\Delta\phi = 1/2\delta\sigma^2(\partial^2\phi/\partial^2\sigma)|_T$  in Gaussian approximation. Then, the size of the fluctuations diverges with the susceptibility at  $T \rightarrow T_c$

$$\langle(\Delta\sigma)^2\rangle = \frac{T_c\chi}{V}. \quad (2.34)$$

If one takes spatial fluctuations of  $\sigma(\vec{r})$  into account a term  $1/2(\partial\sigma/\partial\vec{r})^2$  is added to  $\phi$ . In Gaussian approximation one can calculate the correlation function of these spatial fluctuations. It is for  $\vec{r} = \vec{r}_1 - \vec{r}_2$

$$G(\vec{r}) = \langle\sigma(\vec{r}_1)\sigma(\vec{r}_2)\rangle = \sigma_{\text{eq}}^2 + \frac{1}{r} \exp\left(-\frac{r}{\xi}\right). \quad (2.35)$$

The typical length, over which these fluctuations are correlated, is the correlation length  $\xi$ . In Ginzburg-Landau theory

$$\xi = \left(\sqrt{\frac{\partial\phi(T,\sigma)}{\partial\sigma}\bigg|_{\sigma=\sigma_{\text{eq}}}}\right)^{-1} \propto (\sqrt{T-T_c})^{-1}. \quad (2.36)$$

It diverges as  $T$  approaches  $T_c$ .

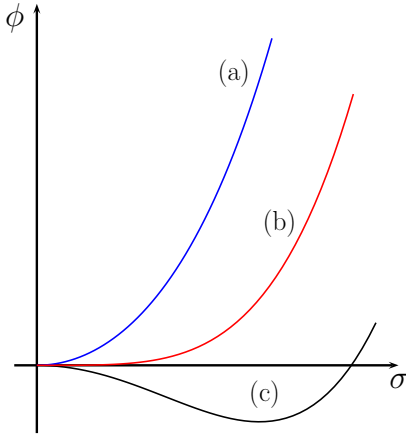


Figure 2.1.: The thermodynamic potential for a cooling scenario with a critical point at different temperatures: in (a) for  $T > T_c$ , in (b) for  $T = T_c$  and in (c) for  $T < T_c$ .

For spatial dimensions  $d < 4$  the large fluctuations at the second order phase transition lead to a breakdown of the Landau-Ginzburg perturbative expansion of  $\phi$ . A more elaborate concept to treat the infrared divergences caused by the soft fluctuations is the renormalization group (RG) [Wil74a].

Since long-range correlations determine the physics at the critical point the microscopic details of the interaction become irrelevant. Starting from a microscopic Hamiltonian the short distance fluctuations are gradually integrated out generating a class of Hamiltonians with scale dependent parameters. The existence of an infrared fixed point in the parameter space of Hamiltonians indicates universality. Critical phenomena depend only on macroscopic properties, such as the dimensionality, of the system and very different physical systems can be described by the same method. The QCD critical point is in the universality class of the  $\mathcal{O}(4)$  Ising-model in three dimensions [Wil92].

These critical phenomena, large fluctuations and correlations, are the basis for locating a conjectured critical point in the QCD phase diagram.

### 2.2.2. First order phase transition

In order to study a first order phase transition in the Ginzburg-Landau theory the coefficient  $b$  in the functional (2.23) must be negative,  $b < 0$ , and a term of sixth order must be

## 2. The phase diagram of quantum chromodynamics

included to stabilize the potential. Let us assume the following Ginzburg-Landau functional

$$\phi(T, \sigma) = \phi_0(T) + a(T - T_{\text{sp}}^{(2)})\sigma^2 + b\sigma^4 + c\sigma^6, \quad (2.37)$$

where  $a$  and  $c$ . In figure 2.2 a sketch of the shape of  $\phi(T, \sigma)$  is shown for several temperatures. At high temperatures there is one minimum at small  $\sigma$ . There is a temperature, the upper spinodal temperature  $T_{\text{sp}}^{(2)} > T_c$ , below which a second local minimum forms at larger  $\sigma$ . At the transition temperature  $T_c$  the two minima are degenerate. For temperatures  $T_c > T > T_{\text{sp}}^{(1)}$  the minimum at large  $\sigma$  is the global minimum, but the minimum at small  $\sigma$  still exists. It vanishes for temperatures below  $T < T_{\text{sp}}^{(1)}$ .

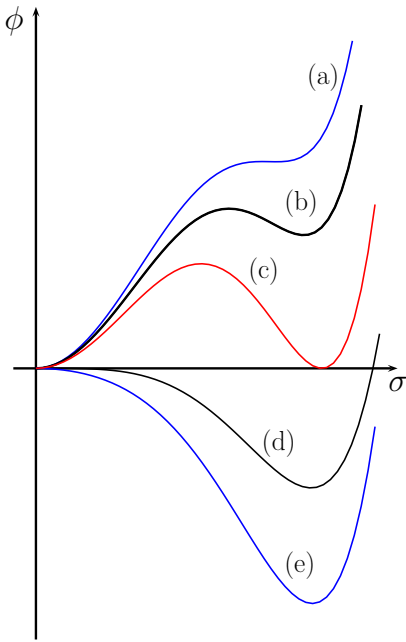


Figure 2.2.: The thermodynamic potential for a cooling scenario with a first order phase transition at different temperatures: in (a) for  $T = T_{\text{sp}}^{(1)}$ , in (b) for  $T_{\text{sp}}^{(1)} > T > T_c$ , in (c) for  $T = T_c$ , in (d) for  $T_c > T > T_{\text{sp}}^{(2)}$  and in (e) for  $T = T_{\text{sp}}^{(2)}$ .

The interesting region of the first order phase transition is between  $T_{\text{sp}}^{(1)}$  and  $T_{\text{sp}}^{(2)}$ , where there are two minima, which are separated by a barrier. At  $T_c$  these two minima are degenerate and the pressure of the two phases is the same. Therefore, the two corresponding phases coexist. Above and below  $T_c$  the respective global minimum is the stable equilibrium state. A real system that is cooled through the phase transition might stay in the high-temperature minimum even below the phase transition. This is a thermodynamically unstable state and the system is supercooled. In this nonequilibrium situation there are two interesting phenomena to be observed, nucleation and spinodal decomposition.

Nucleation is the thermal decay of the system in an unstable phase. In order to relax to the global minimum, i.e. the thermodynamically stable phase, the thermal fluctuations of the system must be of the same order as the latent heat given by height of the barrier [Bin73, Bin87].

Spinodal decomposition is the reaction of the system to a highly nonequilibrium configuration. When the supercooled system does not decay via nucleation, as thermal excitations might be too small, the unstable minimum disappears during further cooling. The curvature of the thermodynamic potential changes from being positive to negative at the lower spinodal temperature  $T = T_{\text{sp}}^{(1)}$ .

Here, like in equilibrium at a second order phase transition the curvature of the potential and the associated mass vanishes. This leads to an instability of the soft field modes. The phenomena of spinodal decomposition has extensively been investigated in condensed matter physics (e.g. [Bro99]) but also gained attention in heavy-ion physics as giving rise to potential signatures for the first order phase transition [Ran96, Ran97, Mis99b, Gav99, Cho04, Ran04, Sas08]. One of them is the

formation of disoriented chiral condensates, which is discussed in section 2.4.3.

## 2.3. Lattice QCD

As we have seen in the previous section it is a theoretically well-defined task to locate the phase boundaries of QCD. We need to evaluate the partition function (2.21) of QCD, which can be written as a path integral in Euclidean space

$$Z(T, \mu) = \int \mathcal{D}(A, q, q^\dagger) \exp(-S_E) = \int \mathcal{D}A \det F[A] \exp(-S_{YM}). \quad (2.38)$$

The singular points mark the phase boundaries. In (2.38) the fermionic determinant of

$$F[A] = i\gamma^\mu D_{\mu,\alpha\beta} - i\mu_B - m_q \delta_{\alpha\beta} \quad (2.39)$$

is taken over Dirac, flavor, isospin and space-time indices.

As well defined as the task is, there is no analytical method yet to evaluate the partition function (2.38) for the region in  $T$  and  $\mu_B$  that is of interest for the phase transition. Straightforward perturbation theory converges poorly for the relevant temperature regimes and advanced resummation techniques, like the Hard Thermal Loop (HTL) [Bra92, Fre92, Bla94] approach, give reliable results only for temperatures clearly above the critical temperature.

Lattice QCD is a powerful method for first principle calculations of the thermodynamic properties of QCD. It can shed light on the intrinsically nonperturbative region of the phase transition. The basis of lattice QCD is to define the gauge fields and the fermionic action on a discretized and finite space-time lattice. There are, however, a lot of technical problems when working with lattices instead of continuous space-time. Thermodynamic quantities are obtained only in the continuum limit and by extrapolating to infinite volumes. Moreover, defining fermions on the lattice leads to the problem of fermion-doubling, which is related to the fact that chiral symmetry is broken on the lattice. All of these difficulties can reliably be overcome at vanishing baryochemical potential  $\mu_B = 0$  by highly sophisticated methods. Here, the special power of lattice QCD lies in the Monte-Carlo evaluation of the path integral in (2.38). Monte-Carlo methods and importance sampling are possible because  $F[A]$  is positive-definite. One does not need to evaluate the integral for all possible configurations because most of them are exponentially suppressed by  $\exp(-S_E)$ . One randomly chooses field configurations corresponding to a probability proportional to  $\exp(-S_E)$ . Different approaches nowadays agree that the phase transition at zero baryochemical potential is a crossover [Aok06] with transition temperatures between  $T_C = [145, 165]$  MeV [WUPBUD10, HotQCD10]. The remaining discrepancies stem from the different fermion actions and from the determination of  $T_C$  from different observables, the chiral susceptibility, the quark number susceptibility and observables related to the confinement-deconfinement phase transition. It is remarkable that at zero baryochemical potential the chiral phase transition and the confinement-deconfinement phase transition occur around the same critical temperature.

For finite  $\mu_B$  things are more difficult. The fermionic determinant in (2.38) is complex and the probability interpretation is not possible anymore. This is the so called sign problem. There are some methods to overcome this problem.

The earliest method that allowed for a prediction of the location of a critical point at  $T_E = 162 \pm 2$  MeV and  $\mu_E = 360 \pm 40$  MeV [Fod02, Fod04] is reweighting. In importance sampling of Monte-Carlo calculations reweighting techniques are used for simulations of phase transitions [Fer88]. In the context of finite density lattice calculations one can extrapolate from zero to finite baryochemical potential by multiplying with a reweighting factor. Several problems of this method have been pointed out since then [Eji06, Spl05]. They basically revealed that the found point lies on the critical line of phase-quenched QCD, which means working with  $|\det F|$  instead of  $\det F$  in (2.38).

A direct way to extend calculations from zero baryochemical potential to small values of  $\mu_B$  is the Taylor expansion of the pressure in  $\mu_B$  [All02]

$$p = \sum_{n=0}^{\infty} \chi_{2n}(T) \mu_B^{2n} \quad (2.40)$$

where the coefficients  $\chi_{2n}$  are calculated at  $\mu_B = 0$

$$\chi_0 = p(T, \mu_B = 0), \quad \chi_{2n}(T) = \frac{1}{2n!} \left. \frac{\partial^{2n} p}{\partial \mu_B^{2n}} \right|_{\mu_B=0}. \quad (2.41)$$

The breakdown of the series expansion indicates a singular behavior in the thermodynamic potential. The position of the critical point is given by the radius of convergence of the Taylor expansion and the corresponding temperature. In two-flavor QCD the critical point found with this method is located at  $T^c = 0.95 T_{\mu_B=0}^c$  and  $\mu_B^c / T^c = 1.1 \pm 0.2$  where  $T_{\mu_B=0}^c$  is the crossover temperature at vanishing baryochemical potential [Gav05].

The sign problem is circumvented easily when exploring the phase diagram at imaginary  $\mu_B$  [deF02]. However, one also has to rely on a truncated Taylor expansion of the observables to perform an analytic continuation to real baryochemical potentials. Within this method the surface of the first order chiral phase transition for small quark masses and the first order deconfinement phase transition for heavy quarks extending to finite  $\mu_B$  has been established [deF03, deF06]. For the current order of truncation of the Taylor expansion the regions of first order phase transition seems to shrink in the plane of the quark masses. To this order no critical point is found for physical quark masses. For a review of lattice QCD at finite temperature and density see [Phi10].

Since calculations at finite  $\mu_B$  do not agree, neither on the location nor on the existence of a critical point, first principle calculations on the lattice give definite results only for zero baryochemical potential. Next, we explain how heavy-ion collisions can elucidate the phase diagram of QCD.

### 2.4. Heavy-ion collisions

The QCD phase diagram can partly be scanned in heavy-ion collisions. By colliding heavy nuclei at ultrarelativistic energies one creates strongly interacting matter at high temperatures or high baryonic densities. There are good indications that at the highest energies available, first for gold (Au) nuclei at RHIC with  $\sqrt{s_{NN}} = 200$  GeV [STAR05, PHENIX05,



PHOBOS05, BRAHMS05], and now for lead (Pb) nuclei at the LHC with runs performed at  $\sqrt{s_{NN}} = 2.76$  TeV [ALICE08] and design energies up to  $\sqrt{s_{NN}} = 5.5$  TeV the quark-gluon plasma can be created in the laboratory. By changing the collision energy one probes different regions of the QCD phase diagram. At high energies one reaches high temperatures and high energy densities but low baryochemical potentials, because the colliding nuclei essentially punch through each other. While the incident baryons of the two accelerated nuclei follow their original trajectories at beam rapidities they deposit energy into the overlap region of the collision and thereby highly excite the QCD vacuum. The system at midrapidity is dominated by quark-antiquark pairs to be measured as mesons in the detectors. With decreasing collision energies the nucleons of the incident nuclei are stopped and the rapidity distribution of net baryons is shifted to midrapidity. The systems created have a lower energy density and a lower temperature, but higher baryonic densities. Mid-energy regions of the QCD phase diagram have been investigated in an energy scan at the CERN Super Proton Synchrotron SPS with  $E_{\text{lab}} = 20 - 158A$  GeV. From the statistical model fit to particle multiplicity ratios the chemical freeze-out points  $T_{\text{fr}}$  and  $\mu_{B,\text{fr}}$  of the systems are obtained [BrM95, BrM96, Cle99, Bec02]. They indicate that indeed the system created reaches temperatures and baryochemical potentials that come close to the theoretically predicted region of the phase transition. One should, however, be careful with assigning thermodynamic parameters such as temperatures and baryochemical potentials to the entire system. During the whole course of a heavy-ion collision the system is highly dynamic, the relevant degrees of freedom might change from hadronic to partonic and back and different parts of the collision region can behave differently. We must expect that the system equilibrates at least locally to speak meaningfully of temperatures and baryochemical potentials. Systems at low collision energies,  $E_{\text{lab}} = 2 - 11A$  GeV, were investigated at the Alternating Gradient Synchrotron (AGS), which nowadays serves as a pre-accelerator for RHIC.

This already shows that the full description of heavy-ion collisions poses a huge challenge to theory. We will briefly explain approaches to simulate the dynamics of heavy-ion collisions, followed by the description of critical fluctuations and disoriented chiral condensates. Finally the experimental status is reviewed.

### 2.4.1. Simulations of heavy-ion collisions

We briefly introduce the Boltzmann transport and the fluid dynamic approach to describe the dynamics of a heavy-ion collision.

#### Transport approach to heavy-ion collisions

The Boltzmann transport approach solves the Boltzmann equation of relativistic kinetic theory for the one-particle distribution function  $f_i(x, p)$  for each particle species  $i$

$$p^\mu \partial_\mu f_i(x, p) = C_i, \quad (2.42)$$

where  $C_i$  is the collision term describing the possible scattering processes in the underlying theory. Here, all cross sections have to be known, either from calculations within a particular model or from experimental data. In hadronic transport models the dynamics

is predominated by the excitation of hadron strings and resonances [Bas98, Ble99, Cas99]. Some models treat the hadronic and a partonic stage separately [Cas08] based on a quasi-particle approach. While most models violate detailed balance by including  $2 \rightarrow n$  processes only and thus cannot describe equilibration of a system in a certain volume, the partonic BAMPS model [Xu05] successfully included  $3 \rightarrow 2$  processes to study the equilibration of partonic systems. Transport approaches have been very successful in reproducing multiplicity spectra at various collision energies [Bas99, Ble00, Bra04]. In these microscopic approaches neither hadronization nor the actual phase transition are explained. Transport simulations thus cannot make any predictions on how the phase transition is dynamically realized in heavy-ion collisions.

For the validity of kinetic transport approaches the mean free path of the system must be large so that subsequent collisions can be treated incoherently and quantum interference effects can be neglected. It is doubtful that the hot and dense phase of a heavy-ion collision meets this requirement. We now present a complementary approach.

### Fluid dynamic simulations

Systems with a small mean free path can reach local thermal equilibrium on a much shorter time scale than the global dynamics. These systems can be described fluid dynamically by energy-momentum and charge conservation. Nonrelativistic fluid dynamics are well studied even in the nonideal case by solving the Navier-Stokes equations. They include effects of viscosities up to first order and are parabolic differential equations. It was soon realized that the relativistic analog to the Navier-Stokes equations is not causal. To derive hyperbolic and thus causal dissipative fluid dynamic equations for relativistic matter one must include terms up to at least second order in the dissipative quantities. The solution of these equations are nontrivial and require large computational and conceptual effort. Surprisingly enough the high values of elliptic flow measured in a heavy ion collision at RHIC are compatible with relativistic ideal fluid dynamics [Kol01b, Kol01a] or imply very small viscosities [Hei06, Rom07, Luz08] near the conjectured lower bound of AdS/CFT calculations  $\eta/s = 1/4\pi$  [Bai08, Son07]. In ideal fluid dynamics local equilibration is taken to be instantaneous because the mean free path of the particles is infinitely small. It is a longstanding issue to explain this early equilibration on a microscopic basis [Xu05, Xu07] and determine the initial time  $\tau_0$  after which the fluid dynamic treatment can be applied. Viscous fluid dynamic calculations in  $2 + 1$  dimensions take a finite relaxation time into account [Son09a, Son09b]. These values, however, are estimates from different theories (see references in [Son09b]). No full (3+1)d viscous fluid dynamic code has been developed and tested reliably yet, although there is ongoing work [Mol10].

The conservation of energy and momentum leads to the following hyperbolic differential equation

$$\partial_\mu T^{\mu\nu} = 0, \quad (2.43)$$

with the energy-momentum tensor of an ideal fluid

$$T^{\mu\nu} = (e + p)u^\mu u^\nu - pg^{\mu\nu}, \quad (2.44)$$

where  $e$  is the energy density,  $p$  is the pressure,  $u^\mu = \gamma(1, \vec{v})$  is the local four-velocity of the fluid,  $\gamma = (1 - \vec{v}^2)^{-1/2}$  the relativistic gamma factor and  $g^{\mu\nu} = \text{diag}(1, -1, -1, -1)$

the metric tensor. For any conserved charge, such as net-baryon number or strangeness, there is an additional equation for the respective charge current

$$\partial_\mu N^\mu = 0, \quad (2.45)$$

where  $N^\mu = nu^\mu$  and  $n$  the charge density. Note, that the energy density, the pressure and the charge density are quantities in the local rest frame of the fluid.

**Equation of state** The most important input to the fluid dynamic expansion of the system is the equation of state, which connects the local rest frame quantities  $p = p(e, n)$  and closes the fluid dynamic equations. It strongly influences the dynamics of the system and can naturally describe the phase transition in local equilibrium. It is at this point where the basic interactions between the particles of the fluid play a role. Model equations of state are the hadron resonance gas [Zsc02], the bag model [Cho74a, Cho74b] and the chiral equation of state [Pap99, Zsc07]. The hadron resonance gas does not describe a phase transition and can be used for comparing fluid dynamic calculations with hadronic transport models. The equation of state of the bag model has a strong first order phase transition for all baryochemical potentials with a large latent heat. The chiral equation of state is obtained from a chiral hadronic Lagrangian that includes all baryons from the lowest flavor-SU(3) octet and the multiplets of scalar, pseudo-scalar, vector and axial-vector mesons. Recently a deconfinement equation of state has been derived by including partonic degrees of freedom in the chiral Lagrangian [Dex10], very much in the same manner as the Polyakov-loop extension of quark meson models. It has been successfully implemented to include investigations on the confinement-deconfinement transition to the framework of a hybrid model [Ste10], which combines hadronic transport and fluid dynamics [Tea01, And06, Hir07, Pet08].

For a QCD equation of state from first principles we have to rely on lattice QCD calculations. The quantity accessible in lattice calculations is the finite temperature contribution to the trace of the energy-momentum tensor, the so-called trace anomaly

$$\frac{e - 3p}{T^4} = T \frac{\partial}{\partial T} \left( \frac{p}{T^4} \right). \quad (2.46)$$

The pressure is then obtained from integration by choosing an appropriate integration constant  $p_0$ , which can be adjusted for zero temperature or to the pressure of a hadron gas at  $T_0 = 100$  MeV. The trace anomaly, pressure and the energy density are shown in figure 2.3. Due to the liberation of color degrees of freedom one sees an increase of the energy density and the pressure around the transition temperature. As mentioned before these calculations are performed only at  $\mu_B = 0$ .

**Initial conditions** Unlike hadronic transport models one-fluid fluid dynamics cannot describe a heavy-ion collision for all times, but only after an initial time  $\tau_0$  when local thermal equilibrium is established. Besides the equation of state the fluid dynamic evolution depends crucially on the initial conditions. These are an external input to the fluid dynamic evolution and can be obtained from models. There are essentially three approaches

## 2. The phase diagram of quantum chromodynamics

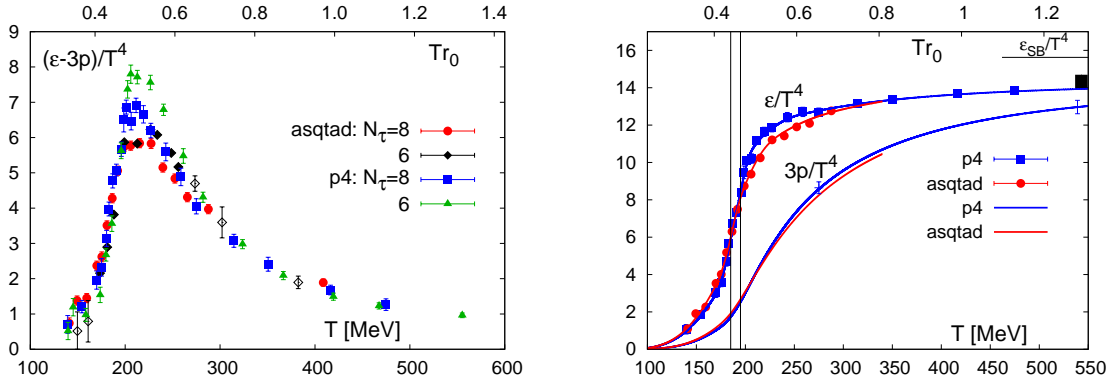


Figure 2.3.: The left figure shows the trace anomaly calculated on the lattice for two different actions and temporal extents. The right figure shows the energy density and the pressure obtained from the trace anomaly. The black band in the upper right corner indicates the systematic error from the integration for the pressure with  $T_0 = 100$  MeV. Both figures are taken from [Baz09].

to the initial conditions. The Glauber model [Gla70] gives initial energy and baryon densities from binary collisions in the geometric overlap region of the collision. It considers the mean free path of baryons passing through each other and takes the elementary baryon-baryon cross sections for the computation of the multiple collision process. The color glass condensate (CGC) [Gel10] is an effective theory of slow dynamic color fields that couple to fast color sources, which are frozen on the timescale of the field dynamics. With random initial distributions of color sources the CGC can be applied to heavy-ion collisions describing the gluon saturation of the wave function of the colliding nuclei [McL94a, McL94b, McL94c]. The energy-momentum tensor after the collision is then given from the solution of the classical Yang-Mills equations. The resulting state is called the Glasma [Lap06] and consists of chromo-electromagnetic fields extended longitudinally and screened transversally, the color flux tubes. Initial conditions for fluid dynamics can be obtained from the KNL parametrization of the gluon saturation [Hir04, Kuh06]. In hybrid models [Tea01, And06, Hir07, Pet08] the initial state can be calculated in hadronic transport models, from which the thermodynamic quantities are obtained by assuming sudden thermalization.

**Freeze-out** The fluid dynamic prescription propagates only densities. At later stages of the heavy-ion collision the system has expanded and diluted to a degree where the further applicability of fluid dynamics is questionable. Fluid dynamic densities are transferred to particles by the Cooper-Frye freeze-out equation [CooFry74]

$$E \frac{dN}{d^3p} = \int_{\sigma} d\sigma_{\mu} p^{\mu} f(p^{\mu} u_{\mu}, T, x). \quad (2.47)$$

It connects the boosted phase-space distribution  $f(x, p)$  and the momentum-space distribution  $dN/d^3p$  along the hypersurface  $\sigma$ . In hybrid models the obtained particles are put

back into hadronic transport models to include the final hadronic interactions after the freeze-out.

**Fluid dynamics with a critical point** In [Non04] an equation of state was constructed from the assumption that the QCD critical point is in the same universality class as the three-dimensional Ising model. A mapping from the Ising model variables to the QCD relevant parameters  $\mu_B$  and  $T$  gives a singular part of the equation of state near the critical point. It is matched smoothly to a nonsingular equation of state known from the hadron gas. The major finding is that isentropic trajectories are attracted by a critical point, which raised hopes that an existing critical point in heavy-ion collisions also attracts the system and that critical phenomena are seen over a wider range of beam energies. It is, however, possible that this behavior is an artificial effect of the matching between the two equations of state [Nak09].

Since fluid dynamics only propagates thermal averages one cannot study the propagation of critical fluctuations at the phase transition. In the remainder of this section we present the suggested observables for a critical point and give an overview of the experimental results.

## 2.4.2. Critical fluctuations

Having in mind the striking thermodynamic features of diverging correlations and fluctuations in a system at the critical point the main observables suggested are event-by-event fluctuations. In this section we describe the main ideas of how critical fluctuations of the order parameter can presumably be seen in data from heavy-ion collisions.

### Event-by-event fluctuations

At a critical point the correlation length  $\xi$  diverges. Susceptibilities and fluctuations of the order parameter are proportional to positive powers of the correlation length  $\xi$  and thus diverge with it. In [Ste99] it was proposed to use the induced critical phenomena to discover the critical point of QCD in heavy-ion experiments. Let us assume that the system created in a heavy-ion collision is in thermal equilibrium. Then the order parameter of chiral symmetry, the sigma field, shows critical behavior. The effect of these critical fluctuations on the pions can be obtained from a coupling  $G\sigma\pi\pi$  with an unknown coupling constant  $G$ . The microscopic correlator of the event-by-event fluctuations of pion multiplicities

$$\langle \Delta n_p \Delta n_k \rangle = \langle n_p n_k \rangle - \langle n_p \rangle \langle n_k \rangle \quad (2.48)$$

is calculated for an effective potential

$$\Omega(\sigma) = \frac{1}{2} m_\sigma^2 \sigma^2 + G\sigma\pi\pi. \quad (2.49)$$

It can be evaluated diagrammatically from the forward scattering of two pions with momenta  $p$  and  $k$  by the exchange of a sigma. The most divergent contribution comes from

## 2. The phase diagram of quantum chromodynamics

---

the sigma in the zero mode. Ignoring less divergent terms (2.48) is

$$\langle \Delta n_p \Delta n_k \rangle = v_p^2 \delta_{pk} + \frac{1}{m_\sigma^2} \frac{G^2}{T} \frac{v_p^2 v_k^2}{\omega_p \omega_k}, \quad (2.50)$$

where  $v_p^2 = \langle (\Delta n_p)^2 \rangle = \langle n_p \rangle (1 + \langle n_p \rangle)$  is the mean square average for the thermodynamic fluctuations of the occupation number in an ideal Bose gas, with the Bose-Einstein distribution  $n_p = (\exp(\epsilon_p/T) - 1)^{-1}$ . As the sigma mass  $m_\sigma$  vanishes at the critical point the second term in equation (2.50) gives a diverging contribution.

With (2.50) also the variance of the distribution of mean transverse momentum  $p_T$

$$\sigma_{p_T}^2 = \frac{1}{\langle N \rangle^2} \sum_{pk} \Delta p_T \Delta k_T \langle \Delta n_p \Delta n_k \rangle, \quad (2.51)$$

where  $\langle N \rangle$  is the average particle multiplicity in the acceptance, diverges at the critical point. As seen in (2.50) and (2.51),  $\sigma^2 \propto \zeta^2$  for the variance of the fluctuations, as it should be in the  $\mathcal{O}(4)$  universality class. In order to give a realistic prediction for the size of these fluctuation measures one has to estimate the coupling  $G$ , correct for the detector acceptance, use the statistical model fit for the freeze-out temperature and chemical potential and take finite size effects into account. For a finite system the correlation length cannot exceed the size of the system. In the study of [Ste99] it does, therefore, not diverge but grow to the size of the system itself. Their estimates are made for correlation lengths  $\zeta \lesssim 6$  fm.

It is also known that the baryon number susceptibility  $\chi_B$  and the charge number susceptibility  $\chi_C$  diverge at the critical point as seen in model studies. In [Hat03] it was argued that the net-baryon density can mix with the chiral condensate  $\langle \bar{\psi} \psi \rangle$ , because it has the same quantum numbers. A mixing of the isospin density with the chiral condensate, however, is strictly forbidden by exact  $SU_V(2)$  symmetry. A small explicit breaking of the isospin symmetry by a finite mass difference of up- and down quarks  $m_u - m_d > 0$  only gives a negligible mixing. Therefore, the diverging fluctuations in net-baryon number can completely be seen in fluctuations of the net-proton number, an experimentally accessible quantity. In [Hat03] the size of the fluctuations in the net-proton number were estimated along the same lines as for pions assuming another coupling  $g\sigma\bar{p}p$  of the protons  $p$  to the sigma field.

### Critical slowing down

Finite time effects due to the phenomena of critical slowing down turn out to be more limiting on the growth of  $\zeta$  than finite size effects. The relaxation times at a critical point become infinitely long. Even if the system is in thermal equilibrium above  $T_c$  it is necessarily driven out of equilibrium when crossing the critical point. Investigating a phenomenological equation for the time development of the sigma mass  $m_\sigma$

$$\frac{d}{dt} m_\sigma(t) = -\Gamma[m_\sigma(t)] \left( m_\sigma(t) - \frac{1}{\zeta_{\text{eq}}(t)} \right), \quad (2.52)$$

with parameters in  $\Gamma[m_\sigma(t)]$  from the dynamic universality class [HohHal77] of QCD and the temperature mapping of the  $\mathcal{O}(3)$  Ising model to determine  $\zeta_{\text{eq}}(t)$  it is found that the correlation length grows only to about 1.5 – 2.5 fm [Ber00, Son04, Asa06]. This will severely diminish the potential signal of the critical point obtained from (2.51).

### Higher moments and the kurtosis

A solution might be to look for fluctuation observables that grow with larger powers of the correlation length  $\zeta$ . It was found in [Ste09] that these include higher order susceptibilities. The suggested observables are the quadratic and quartic susceptibilities of baryons ( $B$ ), protons ( $P$ ) and charged particles ( $Q$ ):

$$\chi_2 = \frac{1}{VT^3} \langle \delta N^2 \rangle \quad (2.53)$$

$$\chi_3 = \frac{1}{VT^3} \langle \delta N^3 \rangle \quad (2.54)$$

$$\chi_4 = \frac{1}{VT^3} (\langle \delta N^4 \rangle - 3\langle \delta N^2 \rangle^2) \quad (2.55)$$

where  $\langle \delta N^n \rangle = \langle (N - \bar{N})^n \rangle$  are the  $n$ th central moments of the respective distribution for  $N = B, P, Q$ . The ratio of the quartic to the quadratic susceptibilities represents the kurtosis  $K(\delta N)$  times the variance of the distribution, a well known statistical quantity:

$$\frac{\chi_4}{\chi_2} = \frac{\langle \delta N^4 \rangle}{\langle \delta N^2 \rangle} - 3\langle \delta N^2 \rangle = K(\delta N) \langle \delta N^2 \rangle \equiv K^{\text{eff}}. \quad (2.56)$$

Analyzing the effective kurtosis instead of the kurtosis itself has the advantage that it eliminates the  $1/N$  behavior as expected from the central limit theorem and removes the explicit dependence on system size. The kurtosis of a Gauss distribution is zero,  $K_{\text{Gauss}} = 0$ , and the effective kurtosis of a Poisson distribution is one,  $K_{\text{Poisson}}^{\text{eff}} = 0$ . The skewness, which describes the asymmetry of the distribution, is defined as

$$\kappa_3^{\text{eff}} = \frac{\chi_3}{\chi_2^{3/2}}, \quad (2.57)$$

and is obviously zero for a Gaussian distribution. The net-proton skewness diverges as  $\kappa_3^{\text{eff}} \propto \zeta^{9/2}$  and the effective kurtosis diverges as  $K^{\text{eff}} \propto \zeta^7$  [Ste09]. Even for a relatively small increase of the correlation length at the critical point the kurtosis is expected to grow significantly. The experimental measurements of the higher moments of distributions are, however, not a trivial task and high statistics are needed. Fluctuations in susceptibilities have been studied in a variety of models [Roe07, Sto09, Sas08, Asa09] and on the lattice for  $\mu_B = 0$  [Che09]. The energy dependence of the effective kurtosis of net-baryon, net-proton and net-charge number within the UrQMD transport model of heavy-ion collisions, which conserves charge and baryon number explicitly in each event, is given in figure 2.4. The net-baryon number effective kurtosis is especially affected by the conservation constraints [Sch09]. The experimentally accessible net-proton number effective kurtosis is affected only for very low energies.

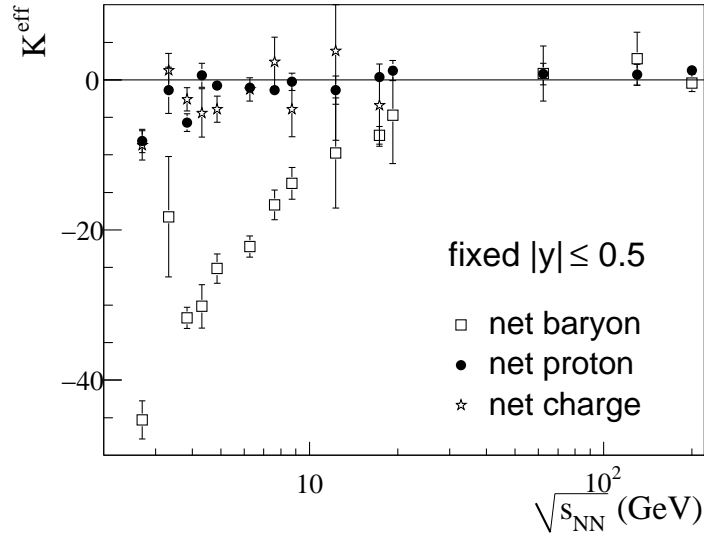


Figure 2.4.: Effective kurtosis for the net-charge, net-proton and net-baryon number distributions at midrapidity ( $|y| < 0.5$ ) as calculated from UrQMD at various beam energies for central Pb+Pb/Au+Au reactions. The figure is taken from [Sch09].

### 2.4.3. Formation of disoriented chiral condensates

The formation of disoriented chiral condensates (DCC) was proposed as one of the predominant signatures of chiral restoration in heavy-ion collisions [Bjo92, Raj93, Ran96, Mis99b, Cho04]. The pseudoscalar condensate  $\langle \bar{q}\vec{\tau}\gamma_5 q \rangle$  might acquire finite values as a result of spinodal decomposition of the system. These states are misaligned to the true vacuum expectation value. It is a strong nonequilibrium effect. The domains of these disoriented condensates subsequently decay and, thus, lead to an excess of low-momentum pions. This is expected to be seen as large collective fluctuations of different isospin directions of the pions, i.e. in the number of produced neutral pions in comparison to produced charged pions in heavy-ion experiments. As it is difficult to measure extreme low momentum pions in heavy-ion collisions none of these signatures have been observed yet. The best candidate for DCC formation is a class of unexplained cosmic ray events, the CENTAUROS [Lat80]. The forming of DCCs was studied in effective chiral models for a quench scenario assuming that the effective potential of the long wavelength modes suddenly changes from its shape in the chirally restored phase for  $T > T_c$  to the classical potential at  $T = 0$  [Bjo92, Raj93]. This certainly is a strong assumption in comparison to the real evolution of a heavy-ion collision. It can, however, naturally occur at the upper spinodal temperature of a first order phase transition [Sca99]. Nonequilibrium quantum field theoretical methods applied to  $\phi^4$  theory allow for a systematic study of the formation of DCCs. In the  $1/N$  expansion of the closed time path effective action [Coo95] and for two-loop calculations within the influence functional method [Gle93, Gre97] equations of motion were derived. In the latter the soft modes are assumed to be in contact with the



thermal bath of hard modes. The interaction between these two sectors leads to damping and noise terms in the propagation of the soft modes. In [Ris98] similar calculations were performed for the chirally broken phase in the  $\mathcal{O}(N)$  chiral model.

In [Bir97] the probability of an instability that could lead to a DCC event is investigated by describing the evolution of the chiral fields that are in contact with a thermal heat bath. The chiral fields are propagated according to effective Langevin equations and the expansion and cooling of the system is modeled by scaling. The strength of instabilities is measured as the time integral over tachyonic masses [Ran96, Ran97] and turns out to be comparably large for the most extreme events. In [Xu00] a detailed study of DCC formation in Markovian and non-Markovian Langevin scenarios showed that the resulting distributions of the total pion number are non-Poissonian. The rare DCC events are expected to be seen in higher order cumulants.

#### 2.4.4. Experimental status

This section will briefly summarize the available experimental data on event-by-event fluctuations that are relevant for the phase transition, from the CERN SPS data, to the present RHIC low beam energy scan and concluding with a outlook to the CBM experiment at FAIR.

##### NA49 at the Super Proton Synchrotron (SPS), CERN

At the CERN SPS the NA49 detector collected Pb+Pb data in an energy scan program over an energy range  $E_{\text{lab}} = 20 - 158A$  GeV and the event-by-event fluctuations were analyzed. At low energies the  $K/\pi$  fluctuations [NA49-02] show an increase, which was attributed to the onset of deconfinement [Gor04]. Figure 2.5 shows the energy dependence of fluctuations in the multiplicity of negatively charged hadrons quantified by the scaled variance  $\omega$ , which is the variance divided by the mean of the multiplicity distribution, in the left plot and in transverse momentum of negatively charged hadrons given by  $\phi_{p_T}$ , where mixed-event fluctuations are subtracted [NA49-08a]. The data is compared to the predictions from [Ste99] for a location of the critical point taken from lattice calculations [Fod04]. One sees no evidence for a critical point in the data, which rather agree with UrQMD [Ble99] calculations without a phase transition.

##### Beam energy scan at the Relativistic Heavy Ion Collider (RHIC), BNL

Recently, the beam energy scan program [Cai09] was run at RHIC pursuing the major goal of the discovery and location of the critical point, the onset of signals of the quark-gluon plasma and new physics like the chiral magnetic effect [Kha08]. In 2010 Au+Au data was taken at energies  $\sqrt{s_{NN}} = 7.7, 11.5$  and 39 GeV. For 2011 it is planned to additionally run the collider at  $\sqrt{s_{NN}} = 27$  and 18 GeV, which would then cover the phase diagram up to a baryochemical potential of  $\mu_B \simeq 420$  MeV. Due to the collider type experiments at RHIC the detector acceptance is independent of the beam energy. This is one advantage of the RHIC experiments compared to NA49. It has also been possible to collect more statistics than was available at the SPS. Existing measurements at higher en-

## 2. The phase diagram of quantum chromodynamics

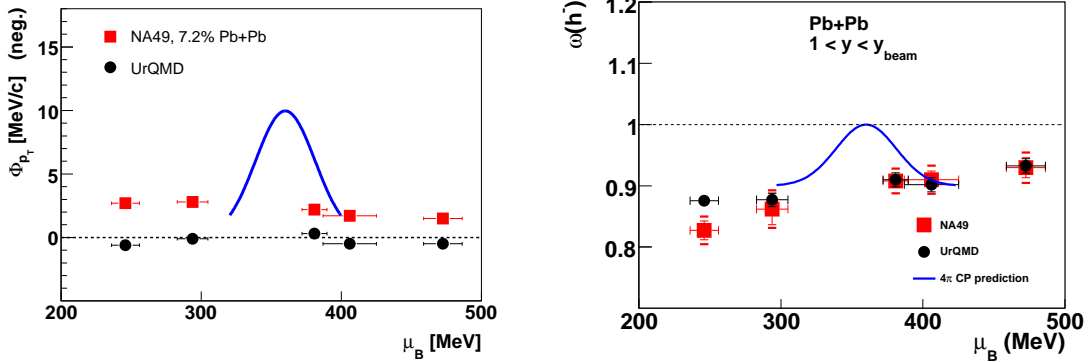


Figure 2.5.: The energy dependence of the scaled variance  $\omega$  of negatively charged hadrons (left plot) and the  $\phi_{p_T}$  measure of transverse-momentum fluctuations of negatively charged hadrons (right plot) as measured with NA49 (red dots). The data is compared to a prediction of enhanced fluctuations at a critical point [Ste99, Fod04] (blue line) and calculations from UrQMD [Ble99] (black dots). The data shows no evidence for a critical point behavior. Both figures are taken from [NA49-08a].

energies  $\sqrt{s_{NN}} = 200$  and  $62.4$  GeV and with less statistics from a previous test run at the injection energy from AGS  $\sqrt{s_{NN}} = 19.6$  GeV show that the STAR collaboration is able to measure higher moments of charged particle distributions and the net-proton kurtosis [STAR10]. In figure 2.6, they are plotted as the effective kurtosis,  $\kappa\sigma^2$ , and compared to model calculations. On the upper axis the corresponding values of  $\mu_B$  are shown. As expected, these measurements do not show a nonmonotonic behavior of the effective kurtosis up to  $\mu_B \simeq 200$  MeV. For the beam energy scan a nonmonotonic behavior of the kurtosis is the key observable.

### The Compressed Baryonic Matter (CBM) experiment at FAIR

The region of highest baryon densities is especially interesting to study in the QCD phase diagram. First, the discovery of a first order phase transition between confined and deconfined and chirally broken and restored symmetry would prove the existence of a critical point, which could then be located by looking at the weakening of the signal of the first order phase transition. Second, the mechanisms of chiral symmetry restoration are assumed to work differently at high densities and low temperatures than at high temperatures but low densities. Different exotic phases of QCD come into play, such as quarkyonic matter [McL07] and color-superconducting phases [Alf07]. Third, the high-density region of the QCD phase diagram could exist in dense neutron and quark stars. Its equation of state is a key ingredient to the understanding of supernova explosions [Gen93].

According to the freeze-out parameter obtained by statistical model fits highest baryonic densities will not be reached with the lowest energies in the RHIC beam energy scan, but at energies between  $E_{lab} = 15 - 40$  GeV [Ran06], which lie in the energy range of the future FAIR accelerator. Here, the CBM detector is designed to analyze heavy-ion colli-

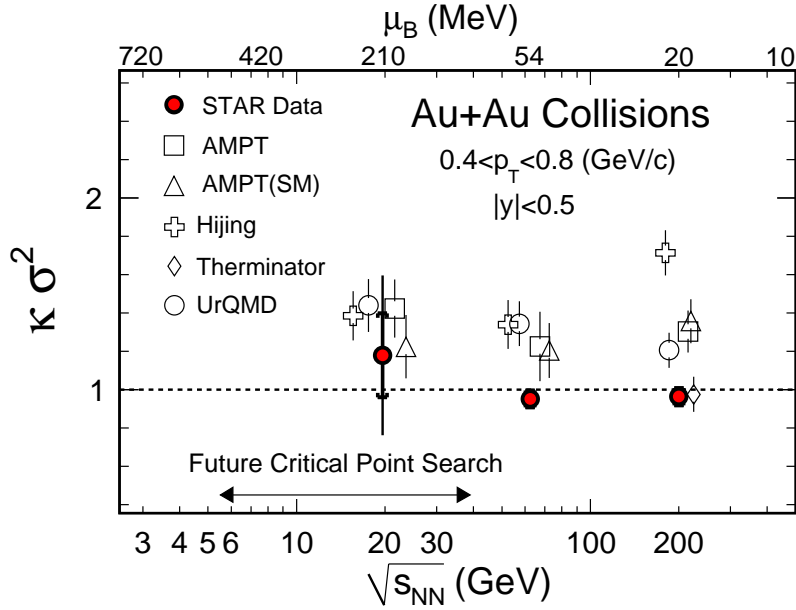


Figure 2.6.: Energy dependence of the effective net-proton kurtosis. STAR measurements are compared to model calculations. The energy range of the energy scan is indicated by the lower arrow. Figure taken from [STAR10].

sions at large baryochemical potentials and densities. The FAIR accelerator will provide high-luminosity beams of excellent quality, which guarantees high statistics for reliable analysis. The physics goals of CBM as well as the detector design are explained in detail in [CBM].

None of the conducted experiments so far have given any decisive answers about the nature of the QCD phase transition. Experimentally, even at  $\mu_B = 0$  a phase transition is not ruled out. In order to improve theoretically one turns to the study of effective models of QCD that capture essential aspects of the phase transition.

## 2.5. Model studies

The investigation of effective low energy models of QCD is a theoretical approach, which is complementary to the first principle lattice calculations. These models capture essential symmetries and therefore give insight into mechanisms of low energy processes. The two most prominent models describing spontaneous chiral symmetry breaking are the linear sigma model [Gel60, Gel64] with constituent quarks [Jun96, Ber03, Tet03, Sch08] and the Nambu-Jona-Lasinio (NJL) model [NaJoLa61a, NaJoLa61b]. In these models the gluonic degrees of freedom act only as a pointlike coupling  $G$  between the quarks. For  $N_f = 2$  the

## 2. The phase diagram of quantum chromodynamics

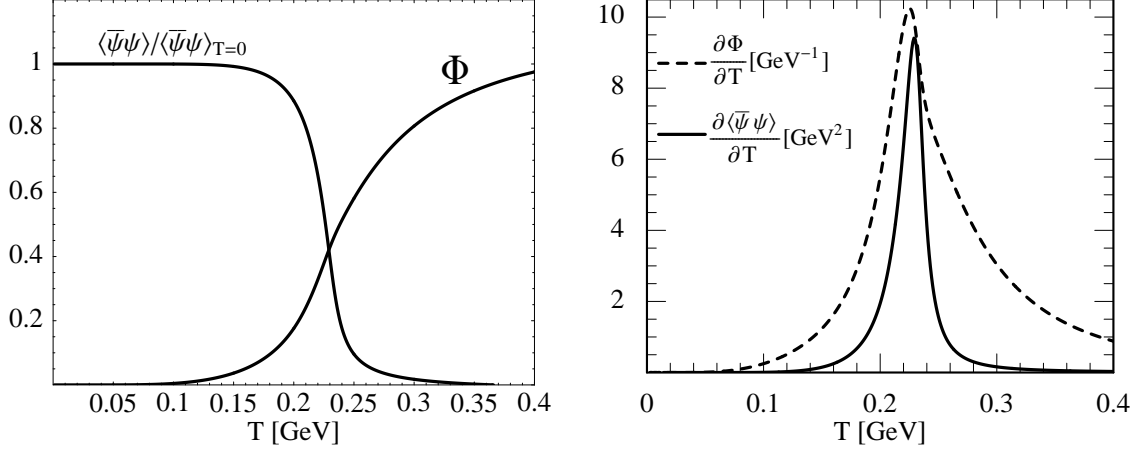


Figure 2.7.: The chiral and confinement crossover transition at  $\mu_B = 0$  in the PNJL model. The left plot shows the temperature dependence of the scaled chiral condensate and the traced Polyakov loop. From the inflection point one sees in the right plot that the transition temperatures for both cases coincide perfectly. Both figures are taken from [Rat06].

interaction is given in the scalar and the pseudoscalar channel by

$$\mathcal{L}_{\text{int}} = \frac{G}{2} ((\bar{q}q)^2 + (\bar{q}i\gamma_5\vec{\tau}q)^2), \quad (2.58)$$

where  $\vec{\tau}$  are the SU(2) Pauli matrices in isospin space. The linear sigma model with constituent quarks treats the meson fields, sigma and pions, as dynamic degrees of freedom. It can be thought of as a partly bosonized version of the NJL model. In the present work we use the linear sigma model with constituent quarks to describe the chiral phase transition. It is explained in more detail in section 4.1.

Both models have been applied extensively to study the chiral aspect of the QCD phase diagram in mean-field approximation and beyond [Sca01a, Bub03, Bar05]. However, they have the shortcoming that quark confinement at low temperatures cannot be described, since the color SU(3) symmetry in these models is global, instead of local as in QCD.

In the limit of infinitely heavy quarks the Z(3) center symmetry of QCD becomes exact with the traced Polyakov loop as the corresponding order parameter. For dynamic quarks it is broken due to string breaking and the formation of quark-antiquark pairs. The Polyakov loop is a thermal Wilson line in imaginary time with periodic boundary conditions

$$L = \mathcal{P} \exp \left[ i \int_0^\beta d\tau A_4 \right] \quad (2.59)$$

where  $\beta = 1/T$  and the temporal component of the gauge field  $A_4 = iA_0$ . Taking the trace of the Polyakov loop (2.59) gives

$$\phi = \frac{1}{N_c} \text{Tr} L, \quad (2.60)$$

with the number of colors  $N_c$ . Polyakov-loop extended NJL (PNJL) models [Rat06, Roe06] and Polyakov-loop extended linear sigma (PQM) models include the traced Polyakov

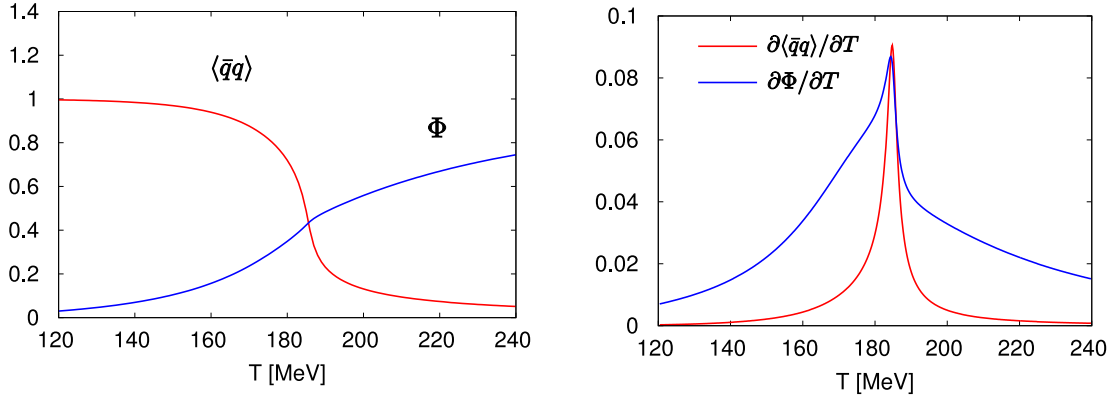


Figure 2.8.: The chiral and confinement crossover transition at  $\mu_B = 0$  for the PQM model. Both figures are taken from [Sch07].

loop  $\phi$  as a classical field coupled to the quarks in addition to the order parameter of chiral symmetry. The Lagrangian of the PNJL model reads

$$\mathcal{L} = \bar{q}[i\gamma^\mu \partial_\mu - m]q + \frac{G}{2} ((\bar{q}q)^2 + (\bar{q}i\gamma_5 \vec{\tau}q)^2) + U(\phi, \phi^*; T) \quad (2.61)$$

with the covariant derivative  $D^\mu = \partial^\mu - iA^\mu$  and  $A^\mu = \delta_0^\mu A^0$ . Here, the coupling  $g$  is absorbed in the definition  $A^\mu = gt^a A_a^\mu$  with the SU(3) gauge field  $A_a^\mu$ .

The effective potential  $U(\phi, \phi^*; T)$  must be Z(3) symmetric. There are different parametrizations with a simple  $\phi^3$  term [Rat06] or a logarithmic term motivated by the SU(3) Haar measure [Rat07, Roe07]. The parameters of the effective potential are fitted to pure-gauge lattice data. Thus, the effective potential itself describes a first order phase transition. In combination with dynamic quarks it correctly turns into a crossover transition at zero baryochemical potential as shown in figure 2.7. As in lattice QCD calculations the chiral and the deconfinement phase transition coincide.

In order to investigate the phase diagram of the PNJL model one needs to include the baryochemical potential  $\mu_B = 3\mu_q$  in the Lagrangian (2.61). It adds a term  $\mathcal{L}^\mu = \gamma_0 \mu_q \bar{q}q$ . The traced Polyakov loop  $\phi$  and its conjugate  $\phi^*$  are identical for  $\mu_B = 0$ , while they differ in the presence of quarks [Dum05]. A detailed study of the phase diagram of the PNJL model including diquark degrees of freedom  $\Delta$  and corrections beyond mean-field is given in [Roe07].

The aspects of confinement are incorporated into the linear sigma model with constituent quarks in very much the same way as for the NJL model. The phase transition for  $\mu_B = 0$  in the PQM model [Sch07, Sto09] is shown in figure 2.8. and the phase diagram in figure 2.9.

In the Polyakov-loop extended models confinement is implemented on a statistical level. The weight of free quarks and antiquarks in the thermodynamic potential is exponentially suppressed as the critical temperature is approached from above. Below  $T_c$  only three-quark states contribute.

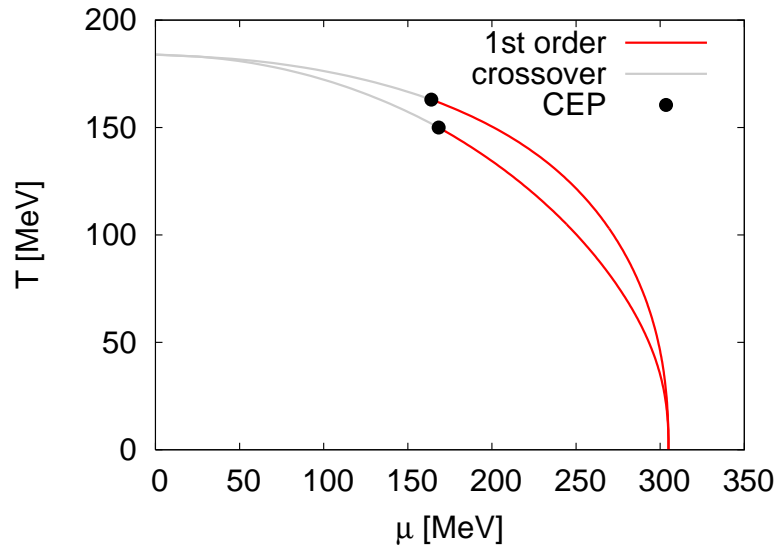


Figure 2.9.: The phase diagram in the PQM model. The figure is taken from [Sch07].

In summary, we have made a lot of progress in the understanding of the QCD phase diagram since the development of efficient numeric lattice QCD calculations, the running of powerful heavy-ion experiments and the detailed study of improved effective models. However, none of these approaches alone has decisively presented the phase diagram of QCD. Most promising will be a combined approach. In this thesis we will embed an effective model with a chiral phase transition in a realistic simulation of a heavy-ion collision. The fast dynamics of a heavy-ion collision necessarily lead to nonequilibrium effects. These play an important role at the phase transition, either due to critical slowing down at a critical point or nucleation and spinodal decomposition at a first order phase transition. In the next chapter we introduce the quantum field theoretical basis for a derivation of a consistent nonequilibrium setup at finite temperature.

### 3. Nonequilibrium methods in finite temperature quantum field theory

Due to the fast dynamics in a heavy-ion collision and long relaxation times at a critical point and the coexistence region at a first order phase transition, nonequilibrium effects are important at the phase transition, which occurs at finite temperature. In this chapter we first introduce the methods of finite temperature quantum field theory and then discuss its application to nonequilibrium concepts.

The development of quantum field theory at finite temperature was motivated by the intensified studies of matter under extreme temperature conditions. Especially the possibility of spontaneous symmetry breaking and restoration has led to the necessity of methods to describe relativistic many-body systems at finite temperatures [DolJac73]. There are two different formalisms. For equilibrium properties the broadly applied imaginary- or Euclidean-time formalism [Mat55] is most suitable. We introduce the basic concepts of the imaginary-time formalism in section 3.1. A real-time approach is needed to study dynamic properties. This so-called closed time path formalism [Sch61, Kel64] is introduced in section 3.2. A detailed description and comparison of both formalisms can be found in [Lan86, Kap94, Das97].

Nonequilibrium statistical mechanics deals with a couple of interesting issues and concepts. Probably the most important point concerns the origin of the obvious time irreversibility of the macroscopic evolution of a system. Irreversibility is one essential ingredient that leads to the nonequilibrium effect of dissipation. The other one is some kind of coarse graining of parts of the system. Starting from off-equilibrium initial conditions dissipation will cause the relaxation of the system to its equilibrium state. In section 3.3 we introduce the basic ideas on dissipation and fluctuations in the Boltzmann kinetic theory and the Langevin theory. The relation of nonequilibrium statistical mechanics and quantum fields is intricate. On one hand, one can ask for quantum field theoretical explanations for the thermalization of relativistic many-body systems. On the other hand, some quantum field processes can be linked to nonequilibrium thermodynamics induced by quantum fluctuations. We introduce two different approaches to derive dissipation and fluctuation within quantum field theoretical methods. The first one, the influence functional method, relies on a clear separation of sectors in the physical system that allows a splitting into relevant and irrelevant variables. This is explained in section 3.4. The second method is based on truncating the Schwinger-Dyson hierarchy. The closed time path effective action, which is one-particle irreducible (1PI), outlined in section 3.5, gives the evolution of the mean field, while the two-particle irreducible (2PI) effective action, explained in section 3.6, selfconsistently gives both the evolution of the mean field and the fluctuations on the level of the two-point function. These methods will be applied in the next chapter to formulate the coupled evolution of the chiral fields and the quark fluid.

A detailed and self-contained description of the interplay of nonequilibrium statistical mechanics and quantum field theory can be found in [Cal08].

### 3.1. Imaginary-time formalism

Imaginary-time formalism is based on the formal analogy between inverse temperature  $\beta = 1/T$  and imaginary time  $\tau = it$ . This analogy is seen best by comparing the path integral representation of the transition amplitude for a field theory with the Hamiltonian  $H$  to the definition of the partition function for a statistical quantum system with temperature  $T$ . The transition amplitude between two states is

$$\begin{aligned} \langle \phi(x_1) | \phi(x_2) \rangle &= \langle \phi_1 | \exp(-iH(t_1 - t_2)) | \phi_2 \rangle \\ &= \mathcal{N} \int \mathcal{D}\phi \exp(iS), \end{aligned} \quad (3.1)$$

with an irrelevant normalization constant  $\mathcal{N}$ , and the action

$$S[\phi] = \int_{t_2}^{t_1} dt \int d^3x \mathcal{L}. \quad (3.2)$$

The path integral in (3.1) is taken over paths  $\phi$  respecting the boundary conditions

$$\phi(x_1) = \phi_1 \quad (3.3a)$$

$$\phi(x_2) = \phi_2. \quad (3.3b)$$

We compare (3.1) to the definition of the partition function (2.20) with particle number  $N$

$$\begin{aligned} Z(\beta) &= \int d\phi_1 \left\langle \phi_1 \left| \exp\left(-\frac{H - \mu N}{T}\right) \right| \phi_1 \right\rangle \\ &= \mathcal{N} \int \mathcal{D}\phi \exp(-S_E). \end{aligned} \quad (3.4)$$

Here, the Euclidean action reads

$$S_E = \int_0^\beta d\tau \int d^3x (\mathcal{L}_E + \beta\mu N). \quad (3.5)$$

We see that one can transform the path integral representation of the transition amplitude (3.1) into that of the partition function (3.4) by substituting  $\tau = it$  in (3.1) and formally identifying  $\tau$  with  $\beta = 1/T$ .

As it is a crucial issue in finite temperature quantum field theory let us take a closer look at the boundary conditions in (3.4). With (3.3) and the definition of the trace operation we see that the path integral is taken over all paths in the complex time plane with periodic boundaries of the field variables

$$\phi(\vec{x}, \beta) = \phi(\vec{x}, 0). \quad (3.6)$$



Before we show the consequences of these boundary conditions we go one step back and look at the operator formalism. The thermal average of any hermitian operator  $A$  is

$$\langle A \rangle_\beta = \frac{1}{Z(\beta)} \text{Tr} \rho(\beta) A. \quad (3.7)$$

The thermal average of the correlation function of any two hermitian operators  $A$  and  $B$  is

$$\langle AB \rangle_\beta = \frac{1}{Z(\beta)} \text{Tr} \rho(\beta) AB. \quad (3.8)$$

In the Heisenberg picture the time evolution of the operator  $A$  is given by

$$A(t) = \exp(iHt) A \exp(-iHt) \quad (3.9)$$

and the thermal correlation function reads

$$\begin{aligned} \langle A(t)B(t') \rangle_\beta &= \frac{1}{Z(\beta)} \text{Tr} \rho(\beta) A(t)B(t') \\ &= \frac{1}{Z(\beta)} \text{Tr} \exp(-\beta H) A(t) \exp(\beta H) \exp(-\beta H) B(t') \\ &= \frac{1}{Z(\beta)} \text{Tr} A(t+i\beta) \exp(-\beta H) B(t') \\ &= \frac{1}{Z(\beta)} \text{Tr} \exp(-\beta H) B(t') A(t+i\beta) \\ &= \langle B(t')A(t+i\beta) \rangle_\beta, \end{aligned} \quad (3.10)$$

where the explicit form of the density matrix  $\rho(\beta)$  at  $\mu = 0$  and the cyclic property of the trace have been used. Especially for  $B = A$  it is

$$\langle A(t)A(t') \rangle_\beta = \langle A(t')A(t+i\beta) \rangle_\beta. \quad (3.11)$$

Note that this holds independently of the statistics of the operators  $A$  and  $B$ , for both bosons and fermions. The consequences, however, are different for bosonic and fermionic Green's functions, where  $A = B^\dagger = \phi$ . From (3.11) with the appropriate rotation to Euclidean space

$$\begin{aligned} G(\vec{x}, \tau; \vec{y}, 0) &= \frac{1}{Z(\beta)} \text{Tr} \left( \rho(\beta) \mathcal{T}_\tau [\phi(\vec{x}, \tau) \phi^\dagger(\vec{y}, 0)] \right) \\ &= \pm G(\vec{x}, \tau; \vec{y}, \beta), \end{aligned} \quad (3.12)$$

where the upper sign refers to bosonic fields and the lower sign to fermionic fields and  $\mathcal{T}_\tau$  is the imaginary-time ordering operator and  $0 \leq \tau \leq \beta$ . These are the so called KMS-boundary conditions [Kub57, MarSch59]. Imaginary-time ordering gives, analogously to the zero temperature Green's functions,

$$\begin{aligned} G(\vec{x}, \tau; \vec{x}', \tau') &= \langle \mathcal{T}_\tau \phi(\vec{x}, \tau) \phi^\dagger(\vec{x}', \tau') \rangle \\ &= \Theta(\tau - \tau') \phi(\vec{x}, \tau) \phi^\dagger(\vec{x}', \tau') \pm \Theta(\tau' - \tau) \phi^\dagger(\vec{x}', \tau') \phi(\vec{x}, \tau). \end{aligned} \quad (3.13)$$

Due to its role in finding solutions to the dynamic equations of the field variables, the periodic and antiperiodic boundary conditions should be inherited by the field variables. However, from the path integral formulation in (3.4) we find the periodic boundary conditions (3.6) only. Within the coherent state formalism the correct antiperiodic boundary conditions for fermions

$$\phi(\vec{x}, \beta) = -\phi(\vec{x}, 0) \quad (3.14)$$

arise from the trace definition in the path integral formalism [Bro92].

Since the Green's functions are defined on a finite time interval with periodic (bosons) and antiperiodic (fermions), boundary conditions, their Fourier transforms are only defined on discrete frequencies

$$G(\tau) = \frac{1}{\sqrt{2\beta}} \sum_n \exp(-i\omega_n \tau) G(\omega_n) \quad (3.15a)$$

$$G(\omega_n) = \frac{1}{\sqrt{2\beta}} \int_{-\beta}^{\beta} d\tau \exp(i\omega_n \tau) G(\tau). \quad (3.15b)$$

Then, we find

$$G(\tau + \beta) = \frac{1}{\sqrt{2\beta}} \sum_n \exp(-i\omega_n(\tau + \beta)) G(\omega_n) = \pm G(\tau), \quad (3.16)$$

which leads to the Matsubara frequencies for bosons

$$\exp(-i\omega_n \beta) = 1 \quad \Leftrightarrow \quad \omega_n = \frac{2n\pi}{\beta} \quad (3.17a)$$

and for fermions

$$\exp(-i\omega_n \beta) = -1 \quad \Leftrightarrow \quad \omega_n = \frac{(2n+1)\pi}{\beta}. \quad (3.17b)$$

The imaginary-time formalism is best suited to calculate equilibrium quantities. As an example the explicit one-loop calculation of the bosonic and fermionic partition function is given in appendix C. But since time is traded in for temperature the imaginary-time formalism cannot be used in a straightforward manner to calculate dynamic and nonequilibrium processes. For this purpose we introduce the real-time formalism in the next section.

## 3.2. Real-time formalism

The imaginary-time formalism presented in the previous section is very successful in calculating thermodynamic properties of quantum field theories. It allows for a consistent diagrammatic perturbation expansion very much like at zero temperature [Kap94]. The discrete Matsubara frequencies appear in internal and external lines of the Feynman diagrams. While in the internal lines they are integrated over by a couple of well-established Matsubara sums, the external lines define Green's functions on discrete points in the complex time plane. At the basis of imaginary-time formalism we completely gave up the



Figure 3.1.: Examples of a loop diagram for the self energy in  $\phi^4$  theory (left) and in  $\phi^4$  theory with finite vacuum expectation value (right).

time variable in favor of the inverse temperature. As a consequence, we obtained Green's functions with an unphysical representation of time and energy. Interesting finite temperature phenomena like dynamic symmetry breaking and nonequilibrium phenomena necessarily require a real-time description. In order to treat these dynamic problems the finite temperature Green's functions need to be continued analytically to the real axis. One direct approach is motivated by the calculation of loop diagrams as the self energy in the left plot of figure 3.1 in  $\phi^4$  theory, where sums over Matsubara frequencies are evaluated by expressing them as a sum of two contour integrals, one at  $T = 0$  and one at  $T > 0$ . This suggests a continuation of the propagators like

$$\frac{1}{\omega_n^2 + \vec{k}^2 + m^2} \rightarrow \frac{i}{k^2 - m^2 + i\epsilon} + \frac{2\pi}{\exp(\beta|k_0|) - 1} \delta(k^2 - m^2). \quad (3.18)$$

There are, however, examples where this continuation leads to mathematical singularities [DolJac73]. Finite expectation values in the  $\phi^4$  theory, which are typical for spontaneously broken symmetries, lead to cubic interactions and therefore to diagrams like in the right plot of figure 3.1. In its evaluation one encounters squares of the delta function in (3.18) which are mathematically not defined.

There is a way out: the closed time path or real-time formalism, which was explicitly motivated by studies on nonequilibrium systems [Sch61, Kel64]. It involves a contour running parallel to the real-time axis from some initial time  $t_i$  to some fixed time  $t$  and back to  $t_i$ . It evokes an effective doubling of the degrees of freedom, one on the upper, one on the lower branch, and, thus, a  $2 \times 2$  matrix structure of the Green's functions. This more involved setup is the price to pay for a consistent real-time formalism of finite temperature quantum field theory.

In this section we establish the real-time formalism by following the time evolution of the density matrix and give the real-time propagators for noninteracting bosons and fermions.

### 3.2.1. Generating functional on the real-time contour

Consider a quantum system that is either in or out of equilibrium and described by the density matrix

$$\rho(t) = \frac{\exp(-\beta H(t))}{\text{Tr} \exp(-\beta H(t))} \quad (3.19)$$

with a Hamilton operator  $H(t)$  that is allowed to explicitly depend on time to reflect the possibility of nonequilibrium. For notational simplicity we work with  $\mu = 0$ . The time

evolution of the density matrix is then

$$\rho(t) = U(t, t')\rho(t')U(t', t) \quad (3.20)$$

with the time evolution operator

$$U(t, t') = \mathcal{T} \exp(-i \int_{t'}^t dt'' H(t'')), \quad (3.21)$$

which satisfies

$$i \frac{\partial U(t, t')}{\partial t} = H(t)U(t, t'). \quad (3.22)$$

Let us initially neglect all correlations leading to the explicit time dependence of the Hamilton operator. In many systems the details of the initial conditions have little influence on the long-time behavior of the system. We can think of the interaction being turned on adiabatically. This is the Bogoliubov initial condition [Bog62]. Then  $H(t \leq t_i) = H_0$ . The initial density matrix is

$$\rho(t_i) = \frac{\exp(-\beta H_0)}{\text{Tr} \exp(-\beta H_0)} = \frac{U(t_{-\infty} - i\beta, t_{-\infty})}{\text{Tr} U(t_{-\infty} - i\beta, t_{-\infty})} \quad (3.23)$$

for a large negative time  $t_{-\infty} < t_i$ . Then, for times  $t > t_i$

$$\rho(t) = U(t, t_i)\rho(t_i)U(t_i, t) = \frac{U(t, t_i)U(t_{-\infty} - i\beta, t_{-\infty})U(t_i, t)}{\text{Tr} U(t_{-\infty} - i\beta, t_{-\infty})}. \quad (3.24)$$

The time evolution of the thermal average of any operator  $A$  is

$$\begin{aligned} \langle A(t) \rangle &= \text{Tr} \rho(t) A(t) \\ &= \text{Tr} \frac{U(t, t_i)U(t_{-\infty} - i\beta, t_{-\infty})U(t_i, t)A(t)}{\text{Tr} U(t_{-\infty} - i\beta, t_{-\infty})} \\ &= \text{Tr} \frac{U(t_{-\infty} - i\beta, t_{-\infty})U(t_i, t)A(t)U(t, t_i)U(t_i, t_{-\infty})U(t_{-\infty}, t_i)}{\text{Tr} U(t_{-\infty} - i\beta, t_{-\infty})} \\ &= \text{Tr} \frac{U(t_{-\infty} - i\beta, t_{-\infty})U(t_{-\infty}, t_i)U(t_i, t)A(t)U(t, t_i)U(t_i, t_{-\infty})}{\text{Tr} U(t_{-\infty} - i\beta, t_{-\infty})} \\ &= \text{Tr} \frac{U(t_{-\infty} - i\beta, t_{-\infty})U(t_{-\infty}, t)A(t)U(t, t_{-\infty})}{\text{Tr} U(t_{-\infty} - i\beta, t_{-\infty})} \\ &= \text{Tr} \frac{U(t_{-\infty} - i\beta, t_{-\infty})U(t_{-\infty}, t_{+\infty})U(t_{+\infty}, t)A(t)U(t, t_{-\infty})}{\text{Tr} U(t_{-\infty} - i\beta, t_{-\infty})U(t_{-\infty}, t_{+\infty})U(t_{+\infty}, t_{-\infty})}, \end{aligned} \quad (3.25)$$

where the cyclic property of the trace,  $U(t_1, t_2)U(t_2, t_3) = U(t_1, t_3)$  for  $t_1 < t_2 < t_3$  and that  $U(t_{-\infty} - i\beta, t_{-\infty})$  and the fact that  $U(t_{-\infty}, t_i)$  commute were used.

The time evolution of the system in the complex time plane is clear. It runs from a large negative time  $t_{-\infty}$  to the time  $t$  where the operator  $A$  is introduced and further to a large positive time  $t_{+\infty}$ . From there it runs back to  $t_{-\infty}$  and then down to  $t_{-\infty} - i\beta$ . This contour

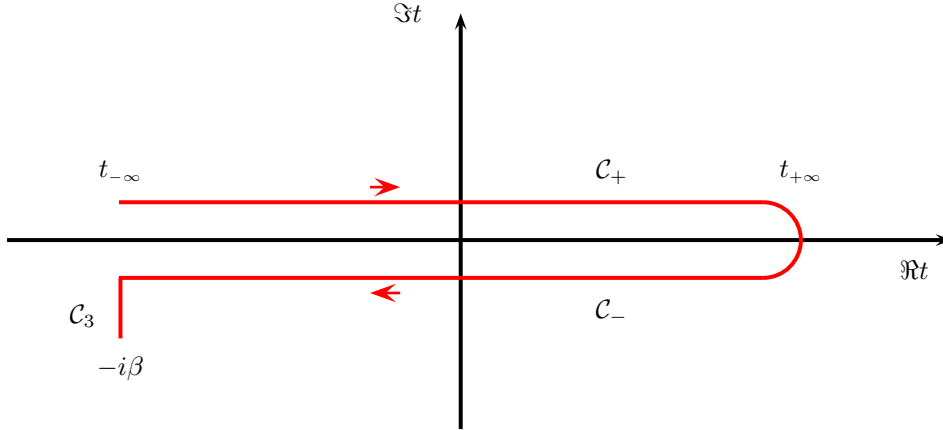


Figure 3.2.: The complete time path contour with the real-time paths  $\mathcal{C}_+$  and  $\mathcal{C}_-$  and the imaginary-time path  $\mathcal{C}_3$

is shown in figure 3.2. From the denominator in (3.25) we see that the partition function of the system along the contour  $\mathcal{C}$  is given by

$$Z(\beta) = \text{Tr}U(t_{-\infty} - i\beta, t_{-\infty})U(t_{-\infty}, t_{+\infty})U(t_{+\infty}, t_{-\infty}). \quad (3.26)$$

This leads to the definition of a generating functional with a source  $J_{\mathcal{C}}$  defined along the contour  $\mathcal{C}$

$$Z[J_{\mathcal{C}}] = \text{Tr}U_{J_{\mathcal{C}}}(t_{-\infty} - i\beta, t_{-\infty})U_{J_{\mathcal{C}}}(t_{-\infty}, t_{+\infty})U_{J_{\mathcal{C}}}(t_{+\infty}, t_{-\infty}). \quad (3.27)$$

For a time-independent Hamilton operator and a constant source along the contour  $J_{\mathcal{C}} = J$  we have  $U_{J_{\mathcal{C}}}(t_{-\infty}, t_{+\infty})U_{J_{\mathcal{C}}}(t_{+\infty}, t_{-\infty}) = 1$  and obtain again the generating functional in imaginary time.

It can be shown that for the assumption made above about the uncorrelated initial state, with  $t_i \rightarrow \infty$ , the generating functional factorizes into the real part of the contour  $\mathcal{C}$ ,  $\mathcal{C}_+$  and  $\mathcal{C}_-$  and in the imaginary part,  $\mathcal{C}_3$  in figure 3.2, [Lan86]

$$Z[J_{\mathcal{C}}] = Z_{\mathcal{C}}[J_{\mathcal{C}_{+,-}}]Z_3[J_3]. \quad (3.28)$$

The propagator cannot connect a point that is on  $\mathcal{C}_3$  with another that is on either  $\mathcal{C}_+$  or  $\mathcal{C}_-$ . In the calculation of Green's functions, and therefore for the dynamics of the system, the imaginary part  $Z_3$  can be ignored, and we will use the index  $\mathcal{C}$  for the real branches of the contour only.

The path integral formulation of the generating functional on the contour is

$$Z[J_{\mathcal{C}}] = \int \mathcal{D}\phi \exp \left[ i \int_{\mathcal{C}} dt \int d^3x (\mathcal{L} + \{J_{\mathcal{C}}\phi\}) \right]. \quad (3.29)$$

As we will see in later chapters  $Z_3$ , cannot be ignored for the calculation of thermodynamic quantities like the energy or the pressure.

### Notations and conventions along the closed contour

Here, we first introduce the notations for performing calculations along the contour. The contour integration consists of the integration along the upper branch  $\mathcal{C}_+$  and the lower branch  $\mathcal{C}_-$

$$\int_{\mathcal{C}} dt = \int_{-\infty}^{\infty} dt_+ - \int_{-\infty}^{\infty} dt_- . \quad (3.30)$$

The step function on the contour is defined as

$$\Theta_{\mathcal{C}}(t - t') = \begin{cases} \Theta(t - t'), & \text{for } t, t' \text{ on } \mathcal{C}_+ \\ \Theta(t' - t), & \text{for } t, t' \text{ on } \mathcal{C}_- \\ 0, & \text{for } t \text{ on } \mathcal{C}_+, t' \text{ on } \mathcal{C}_- \\ 1, & \text{for } t' \text{ on } \mathcal{C}_+, t \text{ on } \mathcal{C}_- . \end{cases} \quad (3.31)$$

The delta function

$$\delta_{\mathcal{C}}(t - t') = \begin{cases} \delta(t - t'), & \text{for } t, t' \text{ on } \mathcal{C}_+ \\ -\delta(t' - t), & \text{for } t, t' \text{ on } \mathcal{C}_- \\ 0, & \text{otherwise} \end{cases} \quad (3.32)$$

satisfies

$$\int_{\mathcal{C}} dt' \delta_{\mathcal{C}}(t - t') f(t') = f(t) , \quad (3.33)$$

for any function  $f$  defined on the contour. The doubling of the contour suggests to write the field variables and the sources as doublets

$$\phi = \begin{pmatrix} \phi_+ \\ \phi_- \end{pmatrix} , \quad (3.34a)$$

$$J = \begin{pmatrix} J_+ \\ J_- \end{pmatrix} . \quad (3.34b)$$

Before we will be concerned with the matrix structure of Green's functions on the real-time contour, let us first summarize a couple of general properties of finite-temperature Green's functions.

#### 3.2.2. Real-time propagators

We define the time-ordered Green's function as the average of a time-ordered product of annihilation and creation operators  $\phi$  and  $\phi^\dagger$

$$iG(x, x') = \langle \mathcal{T} \phi(x) \phi^\dagger(x') \rangle , \quad (3.35)$$

with the time-ordering operator  $\mathcal{T}$  that arranges a product of operators according to their time arguments. It puts the operator with the earliest time to the right and the one with the latest time to the left. For fermions, this operation includes a minus sign when the

reordering consists of an odd number of permutations. We can separately define the following correlation functions

$$iG^>(x, x') = \langle \phi(x) \phi^\dagger(x') \rangle, \quad (3.36a)$$

$$iG^<(x, x') = \pm \langle \phi^\dagger(x') \phi(x) \rangle, \quad (3.36b)$$

where the upper sign belongs to bosonic and the lower sign to fermionic operators. With the density matrix for finite  $\mu$  we write explicitly

$$\begin{aligned} iG^<(x, x')|_{t=0} &= \pm \text{Tr} \rho \phi^\dagger(x') \phi(\vec{x}, 0) \\ &= \pm \text{Tr} \exp[-\beta(H - \mu N)] \exp[\beta(H - \mu N)] \phi(\vec{x}, 0) \rho \phi^\dagger(x') \\ &= \pm \text{Tr} \rho \exp[\beta(H - \mu N)] \phi(\vec{x}, 0) \exp[-\beta(H - \mu N)] \phi^\dagger(x'). \end{aligned} \quad (3.37)$$

Due to the commutation relation for both fermions and bosons

$$[\phi, N]_- = \phi \quad (3.38)$$

the effect of  $\phi$  on any function of  $N$  can be determined to be

$$\begin{aligned} \exp[\beta(H - \mu N)] \phi(\vec{x}, 0) \exp[-\beta(H - \mu N)] &= \exp(\beta H) \phi(\vec{x}, 0) \exp(-\beta H) \exp(\beta \mu) \\ &= \phi(\vec{x}, -i\beta) \exp(\beta \mu). \end{aligned} \quad (3.39)$$

We find a reformulation of the KMS boundary conditions (3.12)

$$iG^<(x, x')|_{t=0} = \pm \exp(\beta \mu) iG^>(x, x')|_{t=-i\beta}, \quad (3.40)$$

which is an important relation between  $G^<$  and  $G^>$ .

In a general situation the Green's functions can have an additional dependence on the center variable. Then, the Fourier transform becomes the Wigner function. Here, we wish to restrict the discussion to translationally invariant systems in equilibrium. We can introduce the Fourier transform of  $G^<$  and  $G^>$  with respect to the relative coordinate. The KMS condition in momentum space becomes

$$G^<(\vec{p}, \omega) = \pm \exp(-\beta(\omega - \mu)) G^>(\vec{p}, \omega). \quad (3.41)$$

By defining the spectral function

$$A(\vec{p}, \omega) = iG^>(\vec{p}, \omega) - iG^<(\vec{p}, \omega), \quad (3.42)$$

(3.41) can be reexpressed as

$$iG^>(\vec{p}, \omega) = (1 \pm n_{B/F}(\omega)) A(\vec{p}, \omega) \quad (3.43a)$$

$$iG^<(\vec{p}, \omega) = \pm n_{B/F}(\omega) A(\vec{p}, \omega) \quad (3.43b)$$

with the Fermi-Dirac  $n_F(\omega)$  and the Bose-Einstein  $n_B(\omega)$  distribution functions.

Diagrammatic schemes for perturbation theory are based on this set of Green's functions (3.35) and (3.36) [FetWal71]. There is another set of physical Green's functions, which facilitates the expressions of statistical and dynamical information of the system. These are the retarded, advanced and correlated Green's functions

$$G_{\text{ret}}(x, x') = \Theta(x_0 - x'_0)[G^>(x, x') - G^<(x, x')] \quad (3.44a)$$

$$G_{\text{adv}}(x, x') = \Theta(x'_0 - x_0)[G^<(x, x') - G^>(x, x')] \quad (3.44b)$$

$$G_{\text{cor}}(x, x') = G^>(x, x') \pm G^<(x, x'). \quad (3.44c)$$

In momentum space there is an especially useful and simple relation between the spectral function and the retarded Green's function

$$G_{\text{ret}}(\vec{p}, \omega) = \int \frac{dp'_0}{2\pi} \frac{A(\vec{p}, p'_0)}{\omega - p'_0 + i\epsilon}. \quad (3.45)$$

The spectral function is given by the imaginary part of the retarded Green's function

$$A(\vec{p}, p'_0) = -2\Im G_{\text{ret}}(\vec{p}, \omega). \quad (3.46)$$

From (3.43) and (3.46) we see that it is enough to evaluate the retarded Green's function in order to determine the full dynamical and statistical information about the system.

Green's functions on the contour are time ordered along the contour. This is the contour ordering. It consists of an ordinary time ordering on the upper branch and a reverse time ordering on the lower branch. The anti-time ordering operator is denoted by  $\mathcal{T}_a$ . Together they form

$$iG_{\mathcal{C}}(t - t') = \langle \mathcal{T}_{\mathcal{C}}(\phi(t)\phi^\dagger(t')) \rangle, \quad (3.47)$$

with the contour-ordering operator  $\mathcal{T}_{\mathcal{C}}$ . The Green's functions adopt a  $2 \times 2$  matrix structure depending on the branches where the time arguments lie

$$G_{\mathcal{C}} = \begin{pmatrix} G_{++} & G_{+-} \\ G_{-+} & G_{--} \end{pmatrix}. \quad (3.48)$$

The individual components are, according to (3.47),

$$iG_{++}(x, x') = \langle \mathcal{T}\phi(x)\phi^\dagger(x') \rangle \quad \text{for } t, t' \text{ on } \mathcal{C}_+, \quad (3.49a)$$

$$iG_{+-}(x, x') = \pm \langle \phi^\dagger(x')\phi(x) \rangle \quad \text{for } t \text{ on } \mathcal{C}_+, t' \text{ on } \mathcal{C}_-, \quad (3.49b)$$

$$iG_{-+}(x, x') = \langle \phi(x)\phi^\dagger(x') \rangle \quad \text{for } t' \text{ on } \mathcal{C}_+, t \text{ on } \mathcal{C}_-, \quad (3.49c)$$

$$iG_{--}(x, x') = \langle \mathcal{T}_a\phi(x)\phi^\dagger(x') \rangle \quad \text{for } t, t' \text{ on } \mathcal{C}_-. \quad (3.49d)$$

Only three out of these four Green's functions are independent. We find the following relations between the four matrix components

$$\begin{aligned} iG_{++}(x, x') &= \Theta(x_0 - x'_0)\langle \phi(x)\phi(x')^\dagger \rangle \pm \Theta(x'_0 - x_0)\langle \phi(x')^\dagger\phi(x) \rangle \\ &= \Theta(x_0 - x'_0)iG_{-+}(x, x') + \Theta(x'_0 - x_0)iG_{+-}(x, x') \end{aligned} \quad (3.50a)$$



and

$$\begin{aligned} iG_{--}(x, x') &= \Theta(x'_0 - x_0) \langle \phi(x) \phi(x')^\dagger \rangle \pm \Theta(x_0 - x'_0) \langle \phi(x')^\dagger \phi(x) \rangle \\ &= \Theta(x'_0 - x_0) iG_{-+}(x, x') + \Theta(x_0 - x'_0) iG_{+-}(x, x'). \end{aligned} \quad (3.50b)$$

Alternatively, we can choose the physical Green's functions to describe the system. Their relations to the contour Green's functions are easily found

$$G_{\text{ret}}(x, x') = G_{++}(x, x') - G_{+-}(x, x') = G_{-+}(x, x') - G_{--}(x, x') \quad (3.51a)$$

$$G_{\text{adv}}(x, x') = G_{++}(x, x') - G_{-+}(x, x') = G_{+-}(x, x') - G_{--}(x, x') \quad (3.51b)$$

$$G_{\text{cor}}(x, x') = G_{++}(x, x') + G_{--}(x, x') = G_{+-}(x, x') + G_{-+}(x, x'). \quad (3.51c)$$

### Bosonic real-time propagators for a free theory

For a noninteracting Klein-Gordon field we obtain the retarded Green's function as the only solution of

$$(-\square - m^2)D_{\text{ret}}(x, x') = -\delta(x - x') \quad (3.52)$$

with causal boundary conditions. It is

$$D_{\text{ret}}(p) = \frac{1}{p^2 - m^2 + i\epsilon \text{sign}(p_0)}. \quad (3.53)$$

The spectral function becomes

$$A(p) = 2\pi \text{sign}(p_0) \delta(p^2 - m^2). \quad (3.54)$$

From the general relations (3.36), (3.44) and (3.51) we then find the contour Green's functions

$$iD_{++}(p) = \frac{1}{p^2 - m^2 + i\epsilon} - 2i\pi n_B(|p^0|) \delta(p^2 - m^2) \quad (3.55a)$$

$$iD_{+-}(p) = -2i\pi (n_B(|p^0|) + \theta(-p^0)) \delta(p^2 - m^2) \quad (3.55b)$$

$$iD_{-+}(p) = -2i\pi (n_B(|p^0|) + \theta(p^0)) \delta(p^2 - m^2) \quad (3.55c)$$

$$iD_{--}(p) = -\frac{1}{p^2 - m^2 - i\epsilon} - 2i\pi n_B(|p^0|) \delta(p^2 - m^2). \quad (3.55d)$$

Correlation functions can be calculated by functional derivatives of the generating functional. For the two-point function

$$\langle \mathcal{T}_C(\phi(t)\phi(t')) \rangle = (-i)^2 \frac{1}{Z[J_C]} \frac{\delta^2 Z[J_C]}{\delta J_C(x) \delta J_C(x')} \Big|_{J_C=0}. \quad (3.56)$$

The generating functional can be evaluated by completing the square

$$Z[J_C] = \left[ \int \mathcal{D}\phi \exp(i \int d^4x \mathcal{L}_0) \right] \exp \left( -\frac{1}{2} \int_C d^4x \int_C d^4x' J_C(x) D_C(x - x') J_C(x') \right) \quad (3.57)$$

with the free Klein-Gordon Lagrange density  $\mathcal{L}_0$ .

### Fermionic real-time propagators for a free theory

In exactly the same manner one derives the contour Green's functions for noninteracting fermions starting from the retarded Green's function, which solves

$$(i\cancel{\partial} - m)S_{\text{ret}}(x, x') = \delta(x - x'). \quad (3.58)$$

It is

$$S_{\text{ret}}(p) = \frac{1}{\cancel{p} - m + i\epsilon \text{sign}(p_0)}, \quad (3.59)$$

and the spectral function

$$A(p) = 2\pi(\cancel{p} + m)\text{sign}(p_0)\delta(p^2 - m^2). \quad (3.60)$$

Again by applying the general relations (3.36), (3.44) and (3.51) we find

$$iS_{++}(p) = (\cancel{p} + m) \left( \frac{1}{p^2 - m^2 + i\epsilon} + 2i\pi n_F(|p^0|) \delta(p^2 - m^2) \right) \quad (3.61a)$$

$$iS_{+-}(p) = 2i\pi(\cancel{p} + m)(n_F(|p^0|) - \Theta(-p^0))\delta(p^2 - m^2) \quad (3.61b)$$

$$iS_{-+}(p) = 2i\pi(\cancel{p} + m)(n_F(|p^0|) - \Theta(p^0))\delta(p^2 - m^2) \quad (3.61c)$$

$$iS_{--}(p) = (\cancel{p} + m) \left( -\frac{1}{p^2 - m^2 - i\epsilon} + 2i\pi n_F(|p^0|) \delta(p^2 - m^2) \right). \quad (3.61d)$$

The propagators can be obtained from the generating functional

$$Z[\bar{\eta}, \eta] = Z_0 \exp \left[ - \int_C d^4x d^4y \bar{\eta}_C(x) S_C(x, y) \eta_C(y) \right] \quad (3.62)$$

by differentiating with respect to the external sources  $\bar{\eta}_C$  and  $\eta_C$ . Here, we have to take care about the Grassmann nature of the fermionic fields, see appendix B. Any two-point function is given by

$$\langle T\psi(x_1)\bar{\psi}(x_2) \rangle = \frac{1}{Z_0} \left( -i \frac{\delta}{\delta \bar{\eta}(x_1)} \right) \left( i \frac{\delta}{\delta \eta(x_2)} \right) Z[\bar{\eta}, \eta] \Big|_{\bar{\eta}=\eta=0}. \quad (3.63)$$

### 3.3. Dissipation and fluctuation

The real-time formalism is the theoretical background to address dynamic problems in nonequilibrium systems including dissipation and fluctuations. There are two basic concepts of dissipation: the Boltzmann kinetic theory of dilute gases and the Langevin theory of Brownian motion. The latter naturally leads to the important relation between dissipation and fluctuation formulated in the dissipation-fluctuation theorem.

### 3.3.1. Boltzmann kinetic theory

In kinetic theory it was Boltzmann's achievement to explain the origin of macroscopic irreversibility by the molecular chaos assumption, which was later reformulated in terms of the truncation of the Bogoliubov-Born-Green-Kirkwood-Yvon (BBGKY) hierarchy. The BBGKY hierarchy is the coupled set of equations of motion of the  $n$ -particle distribution function  $f_n(x_1, p_1; \dots; x_n, p_n)$ . To lowest order the evolution of the one-particle distribution function  $f_1(x_1, p_1)$  is governed by a collisional integral over a two-particle distribution function  $f_2(x_1, p_1; x_2, p_2)$ . It is assumed that the initial state of any two particles is uncorrelated. This is called molecular chaos. Then, the two-particle distribution function can be written as a product of the one-particle distribution functions  $f_2(x_1, p_1; x_2, p_2) = f_1(x_1, p_1)f_1(x_2, p_2)$ . The result is the famous Boltzmann equation (2.42), mentioned in the discussion on microscopic transport theories. After the collision the two particles are correlated. It is this point, at which the irreversibility enters.

### 3.3.2. Langevin theory

In the Langevin description dissipation is introduced by a separation of the entire system into relevant degrees of freedom, called the system, which is propagated explicitly, and irrelevant degrees of freedom, called the environment, which by a subsequent coarse graining acts as a heat bath. This separation is obvious for systems that show a clear separation in scales, e.g. time scales. While the hard modes have short relaxation times, they equilibrate fast. The soft modes have longer time scales and consequently equilibrate more slowly. If there is no clear separation the splitting of the entire system into relevant and irrelevant variables is guided by what is accessible in measurements or what is of special interest for the investigation. One separation procedure is the splitting into a mean field and fluctuations, which connects the Langevin theory with the truncation idea of Boltzmann's kinetic theory. Giving a physical interpretation to the mean field and the fluctuations one obtains a system-environment splitting without an ad hoc separation of scales. We will see the advantages of this method in a later chapter. Dissipation enters the dynamics of the system variables by ignoring details of the environment and only considering its average effect on the system. This loss of information about the environment is called coarse graining. It can be obtained by tracing of a density matrix, integrating out fast modes or truncating the hierarchy of correlations.

In classical Brownian motion the system is a heavy particle of mass  $M$  that interacts with particles of mass  $m$  with  $m \ll M$ . The lighter particles move faster and are assumed to be in thermal equilibrium at a temperature  $T$ . The heavy particle undergoes collisions with the lighter particles. The average effect of these collisions is a frictional force, which is phenomenologically characterized by a damping coefficient  $\eta$ , and a stochastic force  $\zeta(t)$ . The equation of motion is then given by a Langevin equation

$$M\ddot{x} + M\eta\dot{x} = \zeta(t). \quad (3.64)$$

Due to the assumed clear separation between the relaxation times of the heavy particle and the lighter particles the correlation time of  $\zeta(t)$  is assumed to be infinitely short so that these fluctuations are Markovian. Then,  $\zeta(t)$  is fully determined by its mean and

variance

$$\langle \xi(t) \rangle = 0, \quad (3.65a)$$

$$\langle \xi(t)\xi(t') \rangle = \lambda\delta(t-t'). \quad (3.65b)$$

The coefficient  $\lambda$  is a measure of the strength of the fluctuations. Because of the stochastic force on the right hand side of equation (3.64) the trajectories  $x(t)$  are also a stochastic quantity. The physical description of the system is given by an ensemble of trajectories rather than one deterministic trajectory.

The solution for the velocity  $v(t) = \dot{x}(t)$  of equation (3.64) is readily obtained by the retarded Green's function and reads

$$v(t) = v_0 \exp(-\eta t) + \int_0^t dt' \exp(-\eta(t-t'))\xi(t'). \quad (3.66)$$

For long times  $t \gg \eta^{-1}$  we require that the heavy particle reaches thermal equilibrium with the heat bath. Then, by virtue of the energy equipartition theorem the average kinetic energy of the heavy particle becomes

$$\frac{1}{2}M\langle v(t)^2 \rangle = \frac{1}{2}k_B T. \quad (3.67)$$

With (3.65a) and (3.65b)

$$\langle v(t)^2 \rangle = v_0^2 \exp(-2\eta t) + \frac{\lambda}{2\eta M^2}(1 - \exp(-2\eta t)) \rightarrow \frac{\lambda}{2\eta M^2} \quad \text{for } t \gg \eta^{-1}. \quad (3.68)$$

From this we find the Einstein relation [Ein05]

$$\lambda = 2\eta M k_B T. \quad (3.69)$$

By (3.69) we see that the dissipation, given by the damping  $\eta$ , and the fluctuations, characterized by the strength of the stochastic force  $\lambda$ , are related. They have indeed the same microscopic origin, which manifests in the dissipation-fluctuation theorem. We now elucidate this relation on more general grounds.

### 3.3.3. Dissipation-fluctuation theorem

The discussion in this section closely follows the presentation in [LaLiPi80]. Let us consider a homogeneous system described by the variable  $x$ . The equilibrium value for  $x$  is at the maximum of the entropy

$$S = -\frac{\Omega}{k_B T} \quad (3.70)$$

where  $\Omega$  is the free energy of the system. We may choose the coordinates such that in equilibrium  $x = 0$ . Then the probability of fluctuations around the equilibrium value is given by

$$P(x) = \text{const.} \exp(S(x)) = \text{const.} \exp\left(-\frac{\Omega(x)}{k_B T}\right). \quad (3.71)$$

For a small fluctuation  $x$  the entropy can be expanded around  $x = 0$  to second order

$$S(x) = S(0) - \frac{1}{2}\kappa x^2. \quad (3.72)$$

Thus, the probability distribution for thermal fluctuations around equilibrium are Gaussian

$$P(x) = \sqrt{\frac{\kappa}{2\pi}} \exp\left(-\frac{\kappa}{2}x^2\right), \quad (3.73)$$

with the proper normalization and the variance

$$\langle x^2 \rangle = \frac{1}{\kappa}. \quad (3.74)$$

We now wish to introduce dynamics for the variable  $x$  with the requirement that for any deviation significantly larger than  $\sqrt{\langle x^2 \rangle}$ ,  $x$  relaxes to its equilibrium value. For the thermodynamic force

$$F = -\frac{\partial S}{\partial x} = \kappa x \quad (3.75)$$

we find a linearized equation of motion

$$\dot{x} = -\zeta F = -\zeta \kappa x = -\eta x \quad (3.76)$$

with a proportionality factor  $\zeta$  for the dynamics and the damping coefficient  $\eta$ . This dynamical law relaxes  $x$  to its equilibrium value  $x = 0$ . We know, however, that in the real equilibrium situation  $x$  fluctuates around its mean. We, therefore, add a stochastic force  $\zeta$ , the noise, to equation (3.76):

$$\dot{x} = -\eta x + \zeta(t). \quad (3.77)$$

The solution to equation (3.77) is

$$x(t) = x_h(t) + \int^t dt' \zeta(t') \exp(-\eta(t-t')). \quad (3.78)$$

To establish the correct equilibrium state with fluctuations of the variable  $x$  given by (3.74) the variance of the noise  $\zeta$  must be

$$\langle \zeta(t) \zeta(t') \rangle = \langle 2\eta x^2 \rangle \delta(t-t') = \frac{2\eta}{\kappa} \delta(t-t'). \quad (3.79)$$

We see again that based on general arguments the damping coefficient, the variance of the Langevin fluctuations and the equilibrium fluctuations are related. In the next sections we will obtain more insight about the microscopic origin of dissipation and fluctuation when we derive the Langevin equations from quantum field theoretical methods.

### 3.4. The influence functional method

The influence functional method [Fey63, Gre98] gives a reduced description of the entire system with focus on the evolution of the relevant variables. The details of the environment are eliminated by integrating out the environmental fields in a path integral over the closed time path contour of the real time description of finite temperature quantum field theory, see section 3.2. The influence of the environment on the dynamics of the system is encoded in the influence functional. In terms of the Langevin theory, the basis of this method is a clear separation of the relevant variables from the irrelevant variables.

#### 3.4.1. Path integral formulation of the density matrix

Let us assume a system that has a clear physical discrepancy between two sectors: the system described by the field  $\phi$  and the environment with the field  $\Phi$ . The environmental field is assumed to be in thermal equilibrium. We will, therefore, refer to the environment as the heat bath. The equilibrium density matrix, for notational simplicity at  $\mu = 0$ , of the entire system described by the Hamiltonian  $H$ ,

$$\rho_\beta = \frac{1}{Z_\beta} \exp(-\beta H), \quad (3.80)$$

can be written as a Euclidean functional integral

$$\rho_\beta(\bar{\phi}, \bar{\Phi}, \bar{\phi}', \bar{\Phi}') = \frac{1}{Z_\beta} \int \mathcal{D}\bar{\phi} \int \mathcal{D}\bar{\Phi} \exp(-S^E[\bar{\phi}, \bar{\Phi}]), \quad (3.81)$$

where the path integrals are taken over all paths  $\bar{\phi}(\tau)$  and  $\bar{\Phi}(\tau)$  for  $0 \leq \tau \leq \beta$  with

$$\bar{\phi}(0) = \bar{\phi}' \quad \bar{\phi}(\beta) = \bar{\phi} \quad (3.82a)$$

$$\bar{\Phi}(0) = \bar{\Phi}' \quad \bar{\Phi}(\beta) = \bar{\Phi}. \quad (3.82b)$$

The initial density matrix describes the state of the entire system at initial time  $t_i$ ,

$$\rho_i(\phi_i, \Phi_i, \phi'_i, \Phi'_i) = \int d\bar{\phi} \int d\bar{\phi}' \lambda(\phi_i, \bar{\phi}, \phi'_i, \bar{\phi}') \rho_\beta(\bar{\phi}, \Phi_i, \bar{\phi}', \Phi'_i) \quad (3.83)$$

The function  $\lambda$  gives the initial deviation of the system variable  $\phi$  from its equilibrium value  $\bar{\phi}$ . Since the heat bath degrees of freedom  $\Phi$  and  $\Phi'$  are equilibrated initially and for all times it is

$$\bar{\Phi}' = \Phi'_i \quad (3.84a)$$

$$\bar{\Phi} = \Phi_i. \quad (3.84b)$$

The time evolution of the density matrix of the entire system is given by

$$\rho(t) = \exp(-iHt) \rho_i \exp(iHt) \quad (3.85)$$

with the time evolution operator  $U(t_f, t_i) = \exp(-iH(t_f - t_i))$ . It can be expressed via a path integral

$$U(\phi_f, \Phi_f, t_f; \phi_i, \Phi_i, t_i) = \int \mathcal{D}\phi \int \mathcal{D}\Phi \exp(iS[\phi, \Phi]). \quad (3.86)$$

The path integral runs over all paths  $\phi(s)$  and  $\Phi(s)$  for  $t_i \leq s \leq t_f$  with

$$\phi(t_i) = \phi_i \quad \phi(t_f) = \phi_f \quad (3.87a)$$

$$\Phi(t_i) = \Phi_i \quad \Phi(t_f) = \Phi_f. \quad (3.87b)$$

With this we can write equation (3.85) in path integral representation

$$\begin{aligned} \rho(\phi_f, \Phi_f, \phi'_f, \Phi'_f; t_f) &= \int d\phi_i \int d\phi'_i \int d\Phi_i \int d\Phi'_i U(\phi_f, \Phi_f, t_f; \phi_i, \Phi_i, t_i) \times \\ &\quad \times \rho_i(\phi_i, \Phi_i, \phi'_i, \Phi'_i) U^*(\phi'_f, \Phi'_f, t_f; \phi'_i, \Phi'_i, t_i) \\ &= \int d\phi_i \int d\phi'_i \int d\Phi_i \int d\Phi'_i \int d\bar{\phi} \int d\bar{\phi}' \frac{1}{Z_\beta} \lambda(\phi_i, \bar{\phi}, \phi'_i, \bar{\phi}') \times \\ &\quad \times \int \mathcal{D}\phi \int \mathcal{D}\Phi \int \mathcal{D}\phi' \int \mathcal{D}\Phi' \int \mathcal{D}\bar{\phi} \int \mathcal{D}\bar{\Phi} \times \\ &\quad \times \exp(iS[\phi, \Phi] - iS[\phi', \Phi] - S^E[\bar{\phi}, \bar{\Phi}]). \end{aligned} \quad (3.88)$$

The path integral is over all  $\phi(s)$ ,  $\phi(s)'$ ,  $\Phi(s)$  and  $\Phi(s)'$  in real time  $t_i \leq s \leq t_f$  with

$$\phi(t_i) = \phi_i \quad \phi(t_f) = \phi_f \quad (3.89a)$$

$$\Phi(t_i) = \Phi_i \quad \Phi(t_f) = \Phi_f \quad (3.89b)$$

$$\phi'(t_i) = \phi'_i \quad \phi'(t_f) = \phi'_f \quad (3.89c)$$

$$\Phi'(t_i) = \Phi'_i \quad \Phi'(t_f) = \Phi'_f. \quad (3.89d)$$

and for the imaginary time part with  $\bar{\phi}(\tau)$  and  $\bar{\Phi}(\tau)$  for  $0 \leq \tau \leq \beta$  with

$$\bar{\phi}(0) = \bar{\phi}' \quad \bar{\phi}(\beta) = \bar{\phi} \quad (3.89e)$$

$$\bar{\Phi}(0) = \bar{\Phi}' \quad \bar{\Phi}(\beta) = \bar{\Phi}_i. \quad (3.89f)$$

The path integral for the environmental variable describes a continuous contour due to the equilibrium condition (3.84) from  $\Phi_f$  to  $\Phi'_f$ .

### 3.4.2. The influence functional

The action  $S[\phi, \Phi] = \int_{t_i}^{t_f} \mathcal{L}(\phi, \Phi)$  can be divided into three parts

$$S[\phi, \Phi] = S_0[\phi] + S_0[\Phi] + S_{\text{int}}[\phi, \Phi] \quad (3.90)$$

Integrating out the environmental degrees of freedom  $\Phi$  gives the state of the system that is described by the reduced density matrix  $\rho_r = \text{Tr}_\Phi \rho$ . When we want to write this in the path integral formalism we have to be careful how the trace is incorporated in the current formalism. Depending on whether we are dealing with bosonic or fermionic degrees of

freedom it gives periodic or antiperiodic boundary conditions, as was discussed in section 3.1.

For bosons the path integral in

$$\begin{aligned}
 \rho_r(\phi_f, \phi'_f; t_f) &= \int d\Phi_f \rho(\phi_f, \Phi_f, \phi'_f, \Phi_f; t_f) \\
 &= \int d\phi_i \int d\phi'_i \int d\bar{\phi} \int d\bar{\phi}' \frac{1}{Z_\beta} \lambda(\phi_i, \bar{\phi}, \phi'_i, \bar{\phi}') \times \\
 &\quad \times \int \mathcal{D}\phi \int \mathcal{D}\phi' \int \mathcal{D}\bar{\phi} \exp(iS_0[\phi] - iS_0[\phi'] - S_0^E[\bar{\phi}]) \times \\
 &\quad \times \int d\Phi_i \int d\Phi'_i \int \mathcal{D}\Phi \int \mathcal{D}\Phi' \int \mathcal{D}\bar{\Phi} \times \\
 &\quad \times \exp(iS_0[\Phi] + iS_{\text{int}}[\phi, \Phi] - iS_0[\Phi'] - iS_{\text{int}}[\phi', \Phi'] - S_0^E[\bar{\Phi}] - S_{\text{int}}^E[\bar{\phi}, \bar{\Phi}]),
 \end{aligned} \tag{3.91}$$

is taken over all paths with the boundary conditions specified in (3.89) and the additional periodic boundary condition  $\Phi'_f = \Phi_f$ , while for fermions the trace operation gives the antiperiodic boundary condition  $\Phi'_f = -\Phi_f$ .

Again we want to apply the Bogoliubov initial conditions [Bog62] and neglect the initial correlations between the system and the environment. The interaction is then adiabatically turned on. As a consequence, the initial density matrix factorizes in system and environment variables

$$\begin{aligned}
 \rho_i(\phi_i, \Phi_i, \phi'_i, \Phi'_i) &= \int d\bar{\phi} \int d\bar{\phi}' \frac{1}{Z_\beta} \lambda(\phi_i, \bar{\phi}, \phi'_i, \bar{\phi}') \int \mathcal{D}\bar{\phi} \exp(-S_0^E[\bar{\phi}]) \int \mathcal{D}\bar{\Phi} \exp(-S_0^E[\bar{\Phi}]) \\
 &= \rho_i^S(\phi_i, \phi'_i) \otimes \rho_i^E(\Phi_i, \Phi'_i).
 \end{aligned} \tag{3.92}$$

In equation (3.91) this means that  $S_{\text{int}}^E[\bar{\phi}, \bar{\Phi}] = 0$ .

Then, the reduced density matrix is

$$\begin{aligned}
 \rho_r(\phi_f, \phi'_f; t_f) &= \int d\phi_i \int d\phi'_i \rho_i^S(\phi_i, \phi'_i) \int \mathcal{D}\phi \int \mathcal{D}\phi' \times \\
 &\quad \times \exp(iS_0[\phi] - iS_0[\phi'] + iS_{\text{IF}}[\phi, \phi'])
 \end{aligned} \tag{3.93}$$

with the influence functional defined as

$$\begin{aligned}
 \exp(iS_{\text{IF}}[\phi, \phi']) &= \int d\Phi_i \int d\Phi'_i \rho_i^E(\Phi_i, \Phi'_i) \int \mathcal{D}\Phi \int \mathcal{D}\Phi' \times \\
 &\quad \times \exp(iS_0[\Phi] + iS_{\text{int}}[\phi, \Phi] - iS_0[\Phi'] - iS_{\text{int}}[\phi', \Phi']).
 \end{aligned} \tag{3.94}$$

Important properties of the influence functional are

$$S_{\text{IF}}[\phi, \phi'] = -S_{\text{IF}}^*[\phi', \phi], \tag{3.95a}$$

$$S_{\text{IF}}[\phi, \phi] = 0. \tag{3.95b}$$

The latter expresses that in the physical equilibrium case the influence functional vanishes.



In order to evaluate the explicit form of the influence functional we are often forced to make a perturbative expansion in the coupling between the two sectors. We expand the exponential function of  $S_{\text{int}}$  in equation (3.94)

$$\begin{aligned} \exp(iS_{\text{IF}}[\phi, \phi']) &= \int d\Phi_i \int d\Phi'_i \rho_i^{\text{E}}(\Phi_i, \Phi'_i) \int \mathcal{D}\Phi \int \mathcal{D}\Phi' \exp(iS_0[\Phi] - iS_0[\Phi']) \times \\ &\quad \times \left( 1 + i(S_{\text{int}}[\phi, \Phi] - S_{\text{int}}[\phi', \Phi']) - \frac{1}{2}(S_{\text{int}}[\phi, \Phi] - S_{\text{int}}[\phi', \Phi'])^2 + \dots \right) \end{aligned} \quad (3.96)$$

For a treatment in ordinary perturbation theory one has to assume that the coupling between the relevant and the irrelevant variables is a small number. In many cases this is not actually the case.

There is a large number of applications of the influence functional method in nonequilibrium field theory, especially for the  $\phi^4$  theory [Gle93, Gre97, Ris98].

### 3.5. The closed time path effective action

The effective action is a useful quantity to study spontaneous symmetry breaking. The expectation value in equilibrium is given by the global minimum of the effective action. In equilibrium the effective action can be calculated in imaginary time formalism from the partition function, see appendix C. In nonequilibrium we have to apply the closed time path formalism presented in section 3.2 in order to obtain real and causal equations of motion for the true expectation value.

In a first step we want to construct the close time path effective action, from which by the variational principle we obtain the equation of motion for the mean field. Simultaneously, we want to ensure that the expectation value of the deviation from the mean field vanishes. This is achieved by a Legendre transformation of the  $W[J]$  functional with a specific value for the source  $J$ . The generating functional is

$$Z[J] = \exp[iW[J]] = \int \mathcal{D}\Phi \exp\left[i\left(S[\Phi] + J^A \Phi^A\right)\right] \quad (3.97)$$

where the following notation is used for the closed time path:  $S[\Phi] = \int_{\mathcal{C}} d^4x \mathcal{L}[\Phi]$  and  $J^A \Phi^A = \int_{\mathcal{C}} d^4x J^a(x) \Phi^a(x)$ , with  $a = \{+, -\}$ . Recall that the imaginary time path of the complete contour does not contribute to dynamical properties and is neglected, as discussed in section 3.2.1. The effective action is the Legendre transformation of  $W[J] = -i \ln Z[J]$

$$\Gamma[\phi] = W[J] - J^A \phi^A \quad (3.98)$$

with the mean field

$$\phi^A = \frac{\delta W[J]}{\delta J^A} = \langle \Phi^A \rangle_J. \quad (3.99)$$

Then, the specific value of the source can be determined to be

$$J^A = -\frac{\delta \Gamma}{\delta \phi^A}. \quad (3.100)$$

For a vanishing external source  $J^A = 0$  equation (3.100) gives the dynamics of the physical mean field. Inserting (3.100) into (3.98) gives an implicit equation for the effective action

$$\Gamma[\phi] = -i \ln \int \mathcal{D}\Phi^A \exp \left[ i \left( S[\Phi^A] - \frac{\delta\Gamma}{\delta\phi^A} (\Phi^A - \phi^A) \right) \right]. \quad (3.101)$$

In (3.101) we make the substitution  $\varphi^A = \Phi^A - \phi^A$  and construct a new action  $\hat{S}$  that contains only quadratic and higher terms in the new fields  $\varphi$

$$\hat{S}[\varphi] = S[\phi + \varphi] - S[\phi] - \frac{\delta S[\phi]}{\delta\phi^A} \varphi^A. \quad (3.102)$$

This method is called the background field method [Jac74, IIIItMa75]. If, for example, the original action is a  $\phi^4$  theory the new action additionally contains cubic interactions in the new fields  $\varphi$ . The couplings now depend on the mean field  $\phi$ . Inserting (3.102) into (3.101) gives

$$\Gamma[\phi] = S[\phi] - i \ln \int \mathcal{D}\varphi^A \exp \left[ i \left( \hat{S}[\varphi] - \left( \frac{\delta\Gamma}{\delta\phi^A} - \frac{\delta S}{\delta\phi^A} \right) \varphi^A \right) \right]. \quad (3.103)$$

The closed time path effective action consists of two parts, the classical action  $S[\phi]$  and a quantum correction

$$\Gamma_1[\phi] = -i \ln \int \mathcal{D}\varphi^A \exp \left[ i \left( \hat{S}[\varphi] - \frac{\delta\Gamma_1[\phi]}{\delta\phi^A} \varphi^A \right) \right]. \quad (3.104)$$

It is of the form of a generating functional for a new theory given by the action  $\hat{S}$ . The generating functional in (3.104), however, is evaluated at a specific value of the source. It is exactly this source (3.100) that gives the required constraint that the fluctuations around the mean field vanish on average. We now prove that indeed

$$\langle \varphi^A \rangle = \int \mathcal{D}\varphi^A \varphi^A \exp \left[ i \left( \hat{S}[\varphi] - \frac{\delta\Gamma_1[\phi]}{\delta\phi^A} \varphi^A \right) \right] = 0. \quad (3.105)$$

Taking the functional derivative with respect to  $\phi$  of (3.104) yields

$$i \frac{\delta\Gamma_1[\phi]}{\delta\phi^A} = \frac{i \int \mathcal{D}\varphi^A \left( \frac{\delta\hat{S}[\varphi]}{\delta\phi^A} - \frac{\delta^2\Gamma_1[\phi]}{\delta\phi^A\delta\phi^B} \varphi^B \right) \exp \left[ i \left( \hat{S}[\varphi] - \frac{\delta\Gamma_1[\phi]}{\delta\phi^A} \varphi^A \right) \right]}{\int \mathcal{D}\varphi^A \exp \left[ i \left( \hat{S}[\varphi] - \frac{\delta\Gamma_1[\phi]}{\delta\phi^A} \varphi^A \right) \right]} \quad (3.106)$$

and thus

$$\int \mathcal{D}\varphi^A \left( \frac{\delta\hat{S}[\varphi]}{\delta\phi^A} - \frac{\delta\Gamma_1[\phi]}{\delta\phi^A} - \frac{\delta^2\Gamma_1[\phi]}{\delta\phi^A\delta\phi^B} \varphi^B \right) \exp \left[ i \left( \hat{S}[\varphi] - \frac{\delta\Gamma_1[\phi]}{\delta\phi^A} \varphi^A \right) \right] = 0. \quad (3.107)$$

Comparing

$$\frac{\delta\hat{S}[\varphi]}{\delta\phi^A} = \frac{\delta S[\phi + \varphi]}{\delta\phi^A} - \frac{\delta S[\phi]}{\delta\phi^A} - \frac{\delta^2 S[\phi]}{\delta\phi^A\delta\phi^B} \varphi^B \quad (3.108)$$

with

$$\frac{\delta \hat{S}[\varphi]}{\delta \varphi^A} = \frac{\delta S[\varphi + \varphi]}{\delta \varphi^A} - \frac{\delta S[\varphi]}{\delta \varphi^A} \quad (3.109)$$

it is

$$\frac{\delta \hat{S}[\varphi]}{\delta \varphi^A} = \frac{\delta \hat{S}[\varphi]}{\delta \varphi^A} - \frac{\delta^2 S[\varphi]}{\delta \varphi^A \delta \varphi^B} \varphi^B. \quad (3.110)$$

For (3.107) we obtain

$$\begin{aligned} & \int \mathcal{D}\varphi^A \left( \frac{\delta \hat{S}[\varphi]}{\delta \varphi^A} - \frac{\delta^2 S[\varphi]}{\delta \varphi^A \delta \varphi^B} \varphi^B - \frac{\delta \Gamma_1[\varphi]}{\delta \varphi^A} - \frac{\delta^2 \Gamma_1[\varphi]}{\delta \varphi^A \delta \varphi^B} \varphi^B \right) \exp \left[ i \left( \hat{S}[\varphi] - \frac{\delta \Gamma_1[\varphi]}{\delta \varphi^A} \varphi^A \right) \right] \\ &= \int \mathcal{D}\varphi^A \left( \frac{\delta \hat{S}[\varphi]}{\delta \varphi^A} - \frac{\delta \Gamma_1[\varphi]}{\delta \varphi^A} \right) \exp \left[ i \left( \hat{S}[\varphi] - \frac{\delta \Gamma_1[\varphi]}{\delta \varphi^A} \varphi^A \right) \right] \\ & \quad + \int \mathcal{D}\varphi^A \frac{\delta^2 \Gamma_1[\varphi]}{\delta \varphi^A \delta \varphi^B} \varphi^B \exp \left[ i \left( \hat{S}[\varphi] - \frac{\delta \Gamma_1[\varphi]}{\delta \varphi^A} \varphi^A \right) \right]. \quad (3.111) \end{aligned}$$

The first term on the right hand side of (3.111) vanishes because it can be written as

$$\int \mathcal{D}\varphi^A \left( -i \frac{\delta}{\delta \varphi^A} \right) \exp \left[ i \left( \hat{S}[\varphi] - \frac{\delta \Gamma_1[\varphi]}{\delta \varphi^A} \varphi^A \right) \right] = 0 \quad (3.112)$$

and the second term gives

$$\frac{\delta^2 \Gamma_1[\varphi]}{\delta \varphi^A \delta \varphi^B} \langle \varphi^B \rangle = 0, \quad (3.113)$$

where the matrix  $(\delta^2 \Gamma_1[\varphi]) / (\delta \varphi^A \delta \varphi^B)$  is nonsingular because of the property of the Legendre transformation, with (3.100)

$$\frac{\delta}{\delta J^A} \frac{\delta \Gamma[\varphi]}{\delta \varphi^B} = -\delta^{AB}. \quad (3.114)$$

From this with the chain rule one finds

$$-\delta^{AB} = \frac{\delta \varphi^C}{\delta J^A} \frac{\delta^2 \Gamma[\varphi]}{\delta \varphi^C \delta \varphi^B} = \frac{\delta^2 W[J]}{\delta J^A \delta J^C} \frac{\delta^2 \Gamma[\varphi]}{\delta \varphi^C \delta \varphi^B}. \quad (3.115)$$

These two matrices are inverses of each other. It then follows from (3.113) that  $\langle \varphi \rangle = 0$ .

In summary, we have shown that the closed time path effective action is a sum of the classical action  $S$  plus a quantum correction  $\Gamma_1$ . With equation (3.100) we have obtained a dynamic law for the mean field under the constraint that the fluctuations around the mean field vanish on average.

We now turn to the evaluation of the effective action. An efficient method is the loop expansion [Jac74] that is equivalent to an expansion in powers of  $\hbar$ . One can obtain a loop expansion for  $W[J]$  from its functional integral definition (3.97). Working with  $\ln Z[J]$  instead of  $Z[J]$  itself has the advantage that disconnected diagrams cancel in the graphical evaluation. Performing the Legendre transformation it can be proven to all orders in the loop expansion that the one-particle reducible diagrams cancel [Jac74]. These classes are

effectively resummed in the mean field. The closed time path effective action for bosons to one-loop order is

$$\Gamma[\phi] = S[\phi^A] + \frac{i}{2} \ln \det(\mathcal{D}_{AB}^{-1}) + \mathcal{O}(\hbar^2) \quad (3.116)$$

with the propagator

$$i\mathcal{D}_{AB}^{-1} = \frac{\delta^2 S}{\delta\phi^A \delta\phi^B}. \quad (3.117)$$

The higher order corrections can be computed from the systematic loop-expansion of the interaction part of the action  $\hat{S}_{\text{int}}$ .

One possible way to address nonperturbative aspects is the large  $N$  expansion, where  $N$  is the number of identical fields. It allows for a systemic investigation by ordering in powers of  $1/N$  [CoJaTo74, Roo74]. It has been applied to obtain the dynamics of spontaneous symmetry breaking by many authors [Coo94, Coo97, Boy98, Boy99].

### 3.6. The two-particle irreducible effective action

Within the functional method approach it became possible to sum large classes of ordinary perturbative diagrams contributing to the effective action  $\Gamma[\phi]$ . In this section we pursue this strategy further and show how the perturbation series can be even more simplified. In ordinary perturbation theory the quantity of interest is expanded into a power series according to orders of a small parameter, mostly a small coupling between the interacting fields. In many theories this assumption is not true and the coupling is actually not a small parameter. The formalism of the  $n$ -particle irreducible effective action is selfconsistent because one does not expand the dynamic degree of freedom itself but derives an equation of motion for each level of approximation separately. Thus, one can derive one closed set of equations of motion for the mean field, the propagators and all correlations up to the  $n$ -point function at the level of the  $n$ -particle irreducible effective action. A full description of the quantum theory requires the knowledge of all  $n$ -point functions. In the previous section we restricted ourselves to the equation of motion for the one-point function, the mean field, with the constraint that all higher correlations vanish. This was a large simplification since the mean field is fully inherent in the formalism. One does not have to calculate an infinite number of Feynman diagrams to obtain the mean field. These classes of diagrams are summed.

We now go one step further and extend the approach of the closed time path effective action to the two-point function. This means we restrict our analysis to diagrams where internal lines are given by the full propagator instead of some perturbative object. The remaining graphs do not contain subgraphs that can be disconnected by cutting two lines, they are two-particle irreducible.

This original functional formalism [LutWar60] was extended to yield transport equations in a quantum theory that preserve the macroscopic conservation laws and are thermodynamically consistent in the equilibrium limit [LeeYan60, BayKad61, Bay62]. These can be found from a certain class of approximations to the Schwinger-Dyson equation for the two-point function  $G$ . Here, the self energy  $\Sigma$  as a functional of  $G$  must be approximated

in a way that there exists a functional  $\Phi$  of  $G$ , for which

$$\frac{\delta\Phi}{\delta G} = \Sigma. \quad (3.118)$$

These approximations are called  $\Phi$ -derivable. In the path integral formulation of this approach [CoJaTo74] it turns out that the  $\Phi$ -functional is identical to the nontrivial part of the two-particle irreducible (2PI) effective action. In [Iva99] this selfconsistent approach is generalized to arbitrary nonequilibrium many-body systems. Renormalization of  $\Phi$ -derivable approximations is studied in [Hee02a, Hee02b, Hee02c].

To formulate the 2PI formalism we relax the constraint on the deviation  $\varphi^A$  from the mean field  $\phi^A$  such that also the fluctuations around it are known. We then have one additional two-point source,  $K^{AB} = K^{ab}(x, x')$  to enforce the second constraint on the two-point function. The procedure is now analogous to the derivation of the 1PI effective action. We have to perform a double Legendre transformation, one associated with each source. From this we obtain the equations of motion for the mean field and the propagator as the stationary conditions.

The 2PI generating functional is then

$$\exp[iW[J, K]] = \int \mathcal{D}\Phi \exp \left[ i \left( S[\Phi] + J^A \Phi^A + \frac{1}{2} \Phi^A K^{AB} \Phi^B \right) \right] \quad (3.119)$$

In order to benefit most from our derivation of the 1PI effective action we can formally consider equation (3.119) as a generating functional with one source  $J^A$  for a theory with the action

$$S^K[\Phi] = S[\Phi] + \frac{1}{2} \Phi^A K^{AB} \Phi^B, \quad (3.120)$$

where the two-point source  $K^{AB}$  contributes as a mass term. Starting from one Legendre transformation with respect to the source  $J^A$

$$\Gamma^K[\phi] = W[J, K] - J^A \phi^A \quad (3.121)$$

with

$$\phi^A = \frac{\delta W[J, K]}{\delta J^A} = \langle \Phi^A \rangle_{J, K}, \quad (3.122a)$$

$$J^A = -\frac{\delta \Gamma^K[\phi]}{\delta \phi^A}, \quad (3.122b)$$

we can perform the same steps as in the previous section to arrive at

$$\Gamma^K[\phi] = S^K[\phi] + \Gamma_1^K[\phi] \quad (3.123)$$

with the quantum correction

$$\Gamma_1^K[\phi] = -i \ln \int \mathcal{D}\varphi^A \exp \left[ i \left( \hat{S}^K[\phi] - \frac{\delta \Gamma_1^K[\phi]}{\delta \phi^A} \varphi^A \right) \right]. \quad (3.124)$$

Here, the new action  $\hat{S}^K$  is obtained by a shift of the field in  $S^K$  in the same way as  $\hat{S}$  was obtained from  $S$  by taking into account the additional shift by the  $K^{AB}$ -induced mass term. To arrive at a loop expansion we can again split  $S^K$  into a free and an interacting part

$$\begin{aligned}\hat{S}^K &= \frac{1}{2}\phi^A \frac{\delta^2 S^K}{\delta\phi^A \delta\phi^B} \phi^B + \hat{S}_{\text{int}} \\ &= \frac{1}{2}\phi^A \frac{\delta^2 S}{\delta\phi^A \delta\phi^B} \phi^B + \frac{1}{2}\phi^A K^{AB} \phi^B + \hat{S}_{\text{int}}.\end{aligned}\quad (3.125)$$

The free inverse propagator  $(G_0^K)^{-1}$  of the theory with action  $S^K$  relates to the inverse free propagator  $G_0^{-1}$  of the theory with action  $S$  by

$$(G_0^K)^{-1} = G_0^{-1} - iK^{AB}.\quad (3.126)$$

We now perform a second Legendre transformation of  $\Gamma_1^K[\phi]$  with respect to the source  $K^{AB}$

$$\Gamma[\phi, G] = \Gamma^K[\phi] - \frac{\delta\Gamma^K[\phi]}{\delta K^{AB}} K^{AB}.\quad (3.127)$$

With

$$\begin{aligned}\frac{\delta\Gamma^K[\phi]}{\delta K^{AB}} &= \frac{\delta W[J, K]}{\delta K^{AB}} + \frac{\delta W[J, K]}{\delta J^C} \frac{\delta J^C}{\delta K^{AB}} - \frac{\delta J^C}{\delta K^{AB}} \Phi^C \\ &= \frac{\delta W[J, K]}{\delta K^{AB}} \\ &= \frac{1}{2}(\phi^A \phi^B + G^{AB}),\end{aligned}\quad (3.128)$$

equation (3.127) becomes

$$\Gamma[\phi, G] = \Gamma^K[\phi] - \frac{1}{2}K^{AB} \phi^A \phi^B - \frac{1}{2}\text{Tr}KG.\quad (3.129)$$

With the first Legendre transformation (3.121) this is equivalent to simultaneously performing a double Legendre transformation of  $W[J, K]$  with respect to both sources

$$\Gamma[\phi, G] = W[J, K] - J^A \phi^A - \frac{1}{2}K^{AB}(\phi^A \phi^B + G^{AB}).\quad (3.130)$$

The stationary conditions can directly be written down

$$\frac{\delta\Gamma[\phi, G]}{\delta\phi^A} = -J^A - \frac{1}{2}K^{AB} \phi^B\quad (3.131)$$

$$\frac{\delta\Gamma[\phi, G]}{\delta G^{AB}} = -\frac{1}{2}K^{AB}.\quad (3.132)$$

In the absence of the sources this gives the equations of motion for the physical mean field  $\phi^A$  and the physical propagator  $G^{AB}$ .

To one-loop level we can use the bosonic one-loop result (3.116) for  $\Gamma^K[\phi]$  to insert into (3.129)

$$\Gamma[\phi, G] = S[\phi] + \frac{i}{2} \ln \det(G_0^{-1} - iK^{AB}) - \frac{1}{2} \text{Tr}KG + \mathcal{O}(\hbar^2). \quad (3.133)$$

To this order the full propagator is  $G^{-1} = G_0^{-1} - iK^{AB}$ . We can eliminate the source and ignore the constant terms. To go beyond one loop we add an additional term

$$\Gamma[\phi, G] = S[\phi] + \frac{i}{2} \ln \det G^{-1} + \frac{i}{2} \text{Tr}G_0^{-1}G + \Gamma_2[\phi, G]. \quad (3.134)$$

For the proper self-energy

$$\Sigma^{AB} = (G_0^{AB})^{-1} - (G^{AB})^{-1} \quad (3.135)$$

the effective potential (3.134) becomes with  $\ln \det A = \text{Tr} \ln A$

$$\Gamma[\phi, G] = S[\phi] + \frac{i}{2} \text{Tr} \ln G^{-1} + \frac{i}{2} \text{Tr} \Sigma G + \Gamma_2[\phi, G]. \quad (3.136)$$

where we ignored a constant term. Then, the equation of motion for the propagator (3.132) with  $K^{AB} = 0$  can be calculated. With  $\delta \Sigma / \delta G = 1/G^2$  it is

$$\frac{\delta \Gamma[\phi, G]}{\delta G^{AB}} = \frac{i}{2} \Sigma + \frac{\delta \Gamma_2[\phi, G]}{\delta G^{AB}} = 0 \quad (3.137)$$

we find for the self energy

$$\Sigma^{AB} = 2i \frac{\delta \Gamma_2[\phi, G]}{\delta G^{AB}}. \quad (3.138)$$

Since the proper self-energy contains only one-particle irreducible diagrams and variation with respect to the propagators corresponds to cutting the respective line in the diagram, the  $\Gamma_2$  functional can only contain two-particle irreducible diagrams.

For fermions the 2PI effective action can be derived in very much the same way taking into account the Grassmann nature of the fermionic fields. The main difference appears already on the one-loop level, where the fermionic functional determinant comes to the power one instead of  $-1/2$  for bosons. We assume a vanishing fermionic expectation value  $\langle q \rangle = \langle \bar{q} \rangle = 0$ . Then, the 2PI effective action for fermions is

$$\Gamma[S] = -i \text{Tr} \ln S^{-1} - i \text{Tr} S_0^{-1} S + \Gamma_2[S], \quad (3.139)$$

where  $S$  is the full and  $S_0$  is the free fermionic propagator.

In this chapter we have discussed the quantum field theoretical basis, which we use in the remaining chapters to gradually develop a consistent nonequilibrium model of chiral fluid dynamics. We start in the next chapter with a one-loop derivation of the coupled dynamics of the quarks and the chiral fields from the linear sigma model with constituent quarks.





## 4. Chiral fluid dynamics I

Chiral fluid dynamics combines the dynamics of heavy-ion collisions with the explicit propagation of the chiral fields at the chiral phase transition. The common idea of chiral fluid dynamics [Mis99a, Sca99, Pae03] is to embed a low energy effective model of QCD into a fluid dynamic simulation of a heavy-ion collision. In [Mis99a] an additional dilaton field was included in the explicit dynamics to model scale invariance breaking in QCD. Strong nonlinear oscillations were found for all the classical fields at the phase transition. From these oscillations the particle production of sigmas, pions and glueballs was calculated. In [Pae03] initial fluctuations were propagated deterministically through the phase transition.

A model that is particularly well suited for this combined approach is the linear sigma model with constituent quarks. The linear sigma model with nucleons [Gel60] has been studied for years as the prototype effective model of dynamic chiral symmetry breaking. The coupling to dynamic quark degrees of freedom instead of nucleons yields the additional feature that the quarks with light current masses obtain a heavy mass at the phase transition and thus turn into constituent quarks [Jun96, Ber03, Tet03, Sch08]. We will present this model, its thermodynamics and phase structure in section 4.1.

To lowest order the time evolution of the chiral fields is given by the classical equations of motion. Thus, the chiral fields are explicitly propagated out of equilibrium with the quarks, the dynamics of which is reduced to a fluid dynamic evolution of densities. This gives rise to the name chiral fluid dynamics. We present these coupled dynamics in section 4.2. We numerically implement the chiral fluid dynamics for the linear sigma model with constituent quarks in section 4.3 and present results on the time evolution of the fields and the fluid in section 4.4. We call this the off-equilibrium expansion to distinguish between the full nonequilibrium approach including dissipation and fluctuations that is developed in the main chapters of this thesis.

Still, many of the ideas, concepts and notations introduced and used in this chapter will be relevant in later chapters.

Some calculations in this chapter have been presented in [Nah09, Nah10a].

### 4.1. The linear sigma model with constituent quarks

In section 2.5 we gave an overview of the studies of effective models of QCD. One of them, which describes the chiral phase transition, is the linear sigma model with constituent quarks. Here, the  $\sigma$  and  $\pi$  mesons couple to quarks. The Lagrangian reads

$$\mathcal{L} = \bar{q}(i\gamma^\mu\partial_\mu - g(\sigma + i\gamma_5\vec{\tau}\vec{\pi}))q + \frac{1}{2}\partial_\mu\sigma\partial^\mu\sigma + \frac{1}{2}\partial_\mu\vec{\pi}\partial^\mu\vec{\pi} - U(\sigma, \vec{\pi}), \quad (4.1)$$

where  $q = (u, d)$  is the constituent quark field,  $\sigma$  the sigma field and  $\vec{\pi}$  the pion fields. Together they form the chiral field  $\phi = (\sigma, \vec{\pi})$ . The strength of the coupling between the quarks and the chiral fields is  $g$ . In the vertex for the pion-quark coupling the  $\gamma_5$  matrix enters to account for the pseudoscalar nature of the  $\pi$  mesons and the isospin Pauli matrices  $\vec{\tau}$  for the isospin degeneracy of the pions. The interaction between the chiral fields is given by the potential

$$U(\sigma, \vec{\pi}) = \frac{\lambda^2}{4} (\sigma^2 + \vec{\pi}^2 - v^2)^2 - h_q \sigma - U_0. \quad (4.2)$$

The Lagrangian (4.1) is invariant under  $SU_L(2) \times SU_R(2)$  symmetry transformations if the explicit symmetry breaking term  $h_q$  vanishes in the potential (4.2). The parameters in (4.2) are chosen such that chiral symmetry is spontaneously broken in the vacuum, where  $\langle \sigma \rangle = f_\pi = 93$  MeV and  $\langle \vec{\pi} \rangle = 0$ . The explicit symmetry breaking term taking into account the finite quark masses is  $h_q = f_\pi m_\pi^2$  with the pion mass  $m_\pi = 138$  MeV. With these requirements,  $v^2 = f_\pi^2 - m_\pi^2 / \lambda^2$ . Choosing  $\lambda^2 = 20$  yields a realistic vacuum sigma mass  $m_\sigma^2 = 2\lambda^2 f_\pi^2 + m_\pi^2 \approx 604$  MeV. In order to have zero potential energy in the ground state the term  $U_0 = m_\pi^4 / (4\lambda^2) - f_\pi^2 m_\pi^2$  is subtracted. At a coupling  $g = 3.3$  the constituent quark mass in vacuum is  $m_q = 306.9$  MeV.

The Lagrangian (4.1) treats the quarks and antiquarks and the mesons on equal footing. In the real world confining forces recombine quarks and antiquarks in mesons and baryons below the confinement critical temperature. The aspect of confinement is not included in the linear sigma model with constituent quarks. We can, thus, investigate the pure effect of the chiral phase transition. In extensions of the model gluons are included on the level of the dilaton field [Mis99a] or the Polyakov loop [Sch07, Sto09], mentioned already in section 2.5.

#### 4.1.1. Mean-field thermodynamics

For a system in the volume  $V$ , which is in thermodynamic equilibrium at a temperature  $T$  and quark chemical potential  $\mu_q = \mu_B/3$  the grand-canonical partition functions reads

$$Z = \int \mathcal{D}\bar{q}\mathcal{D}q\mathcal{D}\sigma\mathcal{D}\vec{\pi} \exp \left[ \int d^4x (\mathcal{L} + \mu_q \bar{q} \gamma^0 q) \right]. \quad (4.3)$$

It can be explicitly calculated in the mean-field approximation for the chiral fields. This means that the chiral fields are replaced by their expectation values and quantum fluctuations around the mean field are neglected. This approach is justified at high  $T$  and  $\mu_B$  where the mesonic resonances are heavy but it is not capable of capturing all phenomena at the phase transition. At this point it is our intention to study the dynamics of the phase transition qualitatively and we do not aim at the extraction of critical exponents for example. We should, however, keep in mind that the mean-field approach is of limited use for the quantitative study of fluctuations [Sto09].

In the mean-field approximation the partition function of the linear sigma model with constituent quarks can be evaluated along the same lines as the partition function for free fermions, see appendix C.3.

The thermodynamic potential in mean-field approximation is

$$\Omega(T, \mu_q) = -\frac{T}{V} \ln Z = U(\sigma, \vec{\pi}) + \Omega_{q\bar{q}}, \quad (4.4)$$

with the chiral potential  $U(\sigma, \vec{\pi})$  and the quark contribution

$$\Omega_{q\bar{q}}(T, \mu_q) = -d_q \int \frac{d^3 p}{(2\pi)^3} \left( E + T \ln \left( 1 + \exp \left( \frac{\mu_q - E}{T} \right) \right) + T \ln \left( 1 + \exp \left( \frac{-\mu_q - E}{T} \right) \right) \right), \quad (4.5)$$

where  $d_q = 12$  is the degeneracy factor of the quarks for  $N_f = 2$  flavors,  $N_c = 3$  colors and the two spin states. There is, however, a crucial difference from the calculation in appendix C.3. In the Lagrangian (4.1) there is no fermionic mass. The quark mass is generated by nonvanishing expectation values of the chiral fields due to spontaneous symmetry breaking. During the evaluation of the functional determinant in Dirac and isospin space one generates a term defined as the effective mass of the quarks

$$m_{\text{eff}}^2 = g^2(\sigma^2 + \vec{\pi}^2). \quad (4.6)$$

Then, the energy of the quarks and antiquarks is

$$E = \sqrt{\vec{p}^2 + m_{\text{eff}}^2} = \sqrt{\vec{p}^2 + g^2(\sigma^2 + \vec{\pi}^2)}. \quad (4.7)$$

This is obviously not a medium-independent quantity as the chiral expectation values depend on both medium parameters  $T$  and  $\mu_B$ . Thus, the divergent term in (4.5) cannot be subtracted as a simple zero-temperature contribution. It needs to be renormalized more carefully. By using standard renormalization techniques one part of the divergence can be absorbed in the parameters  $\lambda$  and  $\nu$  of the classical potential  $U(\sigma, \vec{\pi})$ , while a logarithmic term depending on  $m_{\text{eff}}$  and the renormalization scale remains. In [Sko10] it was shown that by neglecting this contribution fails to reproduce the second order phase transition for  $\mu_B = 0$  in the chiral limit. In [Mos04] the renormalization scale dependence was investigated phenomenologically. A thorough study of medium dependent corrections to mean-field calculations, perturbative and renormalization group approaches to Yukawa theory, also showed a crucial effect on the phase structure [Pal08, Fra09, Pal10a].

To achieve the goal of this work, namely the coupling of chiral nonequilibrium dynamics at the phase transition to a fluid dynamic expansion, we need a field-theoretical model exhibiting a phase transition. This is given by the mean-field approximation and we can neglect the effects of the vacuum correction.

The expectation values for the chiral fields are obtained from minimizing the thermodynamic potential (4.4) with respect to  $\sigma$  and  $\vec{\pi}$

$$\frac{\partial \Omega}{\partial \sigma} = \lambda^2(\sigma^2 + \vec{\pi}^2 - \nu^2)\sigma - h_q + g\rho_s = 0 \quad \text{and} \quad \frac{\partial^2 \Omega}{\partial \sigma^2} > 0, \quad (4.8a)$$

$$\frac{\partial \Omega}{\partial \vec{\pi}} = \lambda^2(\sigma^2 + \vec{\pi}^2 - \nu^2)\vec{\pi} + g\vec{\rho}_{ps} = 0 \quad \text{and} \quad \frac{\partial^2 \Omega}{\partial \vec{\pi}^2} > 0. \quad (4.8b)$$

Here, the one-loop scalar and the pseudo-scalar densities are

$$\rho_s = \langle \bar{q}q \rangle = g d_q \sigma \int \frac{d^3 p}{(2\pi)^3} \frac{1}{E} (n_q(T, \mu_q) + n_{\bar{q}}(T, \mu_q)), \quad (4.9a)$$

$$\vec{\rho}_{ps} = i \langle \bar{q} \gamma_5 \vec{\tau} q \rangle = g d_q \vec{\pi} \int \frac{d^3 p}{(2\pi)^3} \frac{1}{E} (n_q(T, \mu_q) + n_{\bar{q}}(T, \mu_q)), \quad (4.9b)$$

with the Fermi-Dirac distribution of quarks and antiquarks

$$n_q(T, \mu_q) = \frac{1}{1 + \exp((E - \mu_q)/T)}, \quad (4.10a)$$

$$n_{\bar{q}}(T, \mu_q) = \frac{1}{1 + \exp((E + \mu_q)/T)}. \quad (4.10b)$$

The net-baryon density is then

$$n_B = -\frac{1}{3} \frac{\partial \Omega}{\partial \mu_q} = \frac{d_q}{3\pi^2} \int_0^\infty dp p^2 (n_q(T, \mu_q) - n_{\bar{q}}(T, \mu_q)). \quad (4.11)$$

The minima of the thermodynamic potential  $\Omega$  obtained from (4.8a) and (4.8b) define the thermodynamically stable states of the matter. In this case the pressure of the system is

$$p(T, \mu_q) = -\Omega(T, \mu_q)|_{\phi=\phi_{\text{eq}}}, \quad (4.12)$$

from which all thermodynamic quantities can be calculated. We are especially interested in the energy density. It is given by the thermodynamic relation

$$e(T, \mu_q) = Ts(T, \mu_q) - p(T, \mu_q) + \mu_q n_B(T, \mu_q), \quad (4.13)$$

with the entropy density  $s = (\partial p / \partial T)_{\mu_q}$  and the baryon density  $n = -(\partial p / \partial \mu_q)_T$ . Then

$$e(T, \mu_q) = T \left( \frac{\partial p(T, \mu_q)}{\partial T} \right) \Big|_{\mu_q} - p(T, \mu_q) - \mu_q \left( \frac{\partial p(T, \mu_q)}{\partial \mu_q} \right) \Big|_T. \quad (4.14)$$

The masses of the sigma and the pions are given by the curvature of the thermodynamic potential at the equilibrium values of the chiral fields

$$m_\sigma^2 = \frac{\partial^2 \Omega}{\partial \sigma^2} \Big|_{\phi=\phi_{\text{eq}}}, \quad (4.15a)$$

$$m_\pi^2 = \frac{\partial^2 \Omega}{\partial \vec{\pi}^2} \Big|_{\phi=\phi_{\text{eq}}}. \quad (4.15b)$$

#### 4.1.2. Phase diagram of the linear sigma model with constituent quarks

The complete phase structure of the linear sigma model with constituent quarks can be obtained from the knowledge of the thermodynamic potential (4.4) [Sca01a]. Since the sigma field is the order parameter of chiral symmetry breaking, it is sufficient to solve

the gap equation (4.8a) to find the first order phase transition line in the  $T$ - $\mu_q$  plane. It is characterized by two minima separated by a barrier. These are the coexisting phases along the first order phase transition line. It terminates in a critical point where the barrier vanishes and there is only one global but very flat minimum, for which

$$\left. \frac{\partial^2 \Omega}{\partial \sigma^2} \right|_{\phi=\phi_{\text{eq}}} = 0. \quad (4.16)$$

The linear sigma model of constituent quarks exhibits the full spectrum of the suggested chiral phase structure of QCD. It has a crossover transition at vanishing  $\mu_B$  and a first order transition line at high  $\mu_B$  and lower temperatures, which terminates in a critical point at  $T_c$ . Naturally, the quantitative values for the phase transition are lower than the values for full QCD. Working with the linear sigma model with constituent quarks will, therefore, only give qualitative results for the true QCD phase transition.

As we are mainly interested in the qualitative analysis of the phase transition we can alternatively fix the baryochemical potential and tune the strength of the phase transition by changing the coupling constant  $g$ . At  $\mu_B = 0$  the thermodynamic potential is

$$\Omega(T, \phi) = U(\sigma, \vec{\pi}) + \Omega_{q\bar{q}} = U(\sigma, \vec{\pi}) - 2d_q T \int \frac{d^3 p}{(2\pi)^3} \ln \left( 1 + \exp \left( -\frac{E}{T} \right) \right), \quad (4.17)$$

which is an effective potential  $V_{\text{eff}}(T, \phi) = \Omega(T, \phi)$  for the chiral fields in presence of the quarks.

For the realistic coupling,  $g = 3.3$ , and  $\mu_B = 0$  the effective potential changes smoothly from the high-temperature phase to the low-temperature phase, see figure (4.1). For higher couplings  $g$  the effective potential starts to exhibit a first order phase transition. In figure (4.2) we show the effective potential for various temperatures and  $g = 5.5$ .

At high temperatures there is only one minimum at  $\sigma \simeq 0$ . Between the upper and the lower spinodal temperature there are two minima. The global minimum changes from the high-energy minimum at  $\sigma \simeq 0$  to the low-temperature minimum at  $\sigma \simeq f_\pi$  at a critical temperature of  $T_c = 123.27$  MeV. Here, the two minima are degenerate and form the two coexisting phases. Below  $T_c$  the high-temperature minimum becomes unstable but exists down to the spinodal temperature  $T_{\text{sp}} = 108$  MeV [Sca01b, Agu06].

If one carefully looks for the vanishing of the barrier by decreasing the coupling  $g$ , the effective potential shows the shape of a second order phase transition for  $g = 3.63$  with a critical temperature of  $T_c = 139.88$  MeV. Here, the curvature at the minimum becomes very flat, see figure 4.3, and the sigma mass decreases to  $m_\sigma = 26.6$  MeV. This value of  $m_\sigma$  is significantly smaller than the vacuum mass, but still finite. It would be necessary to tune the parameters  $g$  and  $T_c$  more precisely to achieve an even lower sigma mass. We work with the values presented here keeping in mind that  $m_\sigma$  at the critical point is very small, but finite.

For all three phase transition scenarios we show the temperature dependence of the equilibrium value of the sigma field  $\sigma_{\text{eq}}$  and the mass of the sigma field in equilibrium  $m_\sigma$  in figures 4.4 and 4.5.

Throughout this work we will explore these three scenarios depicted above: the crossover for  $g = 3.3$ , the first order phase transition for  $g = 5.5$  and the critical point for  $g = 3.63$ .

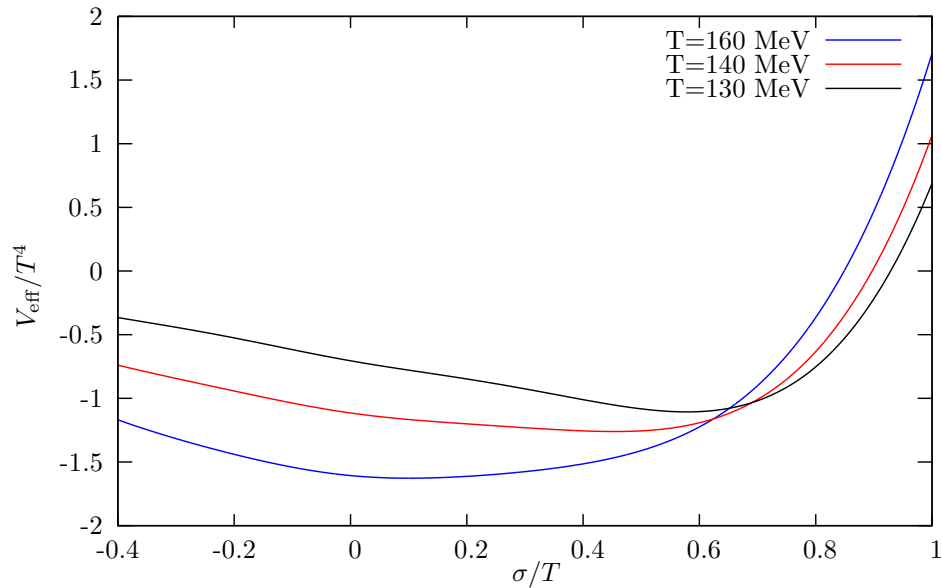


Figure 4.1.: The effective potential for a coupling  $g = 3.3$  and three different temperatures. The potential changes smoothly between the high and the low temperature phase. It describes a generic crossover transition.

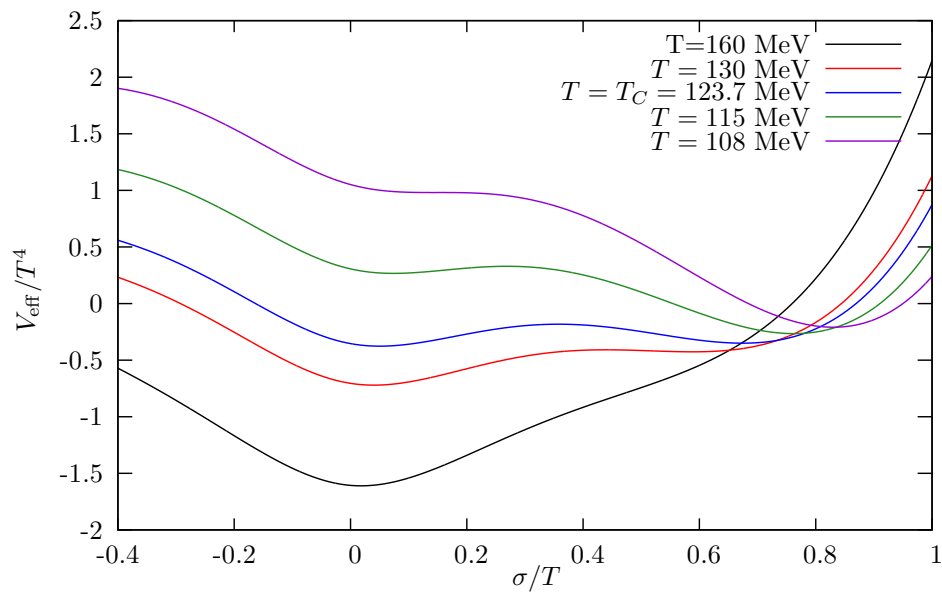


Figure 4.2.: The effective potential for a coupling  $g = 5.5$  and temperatures  $T > T_c$ ,  $T < T_c$  and the critical temperature. At the critical temperature the two minima are degenerate and represent the two coexisting phases for a first order phase transition.

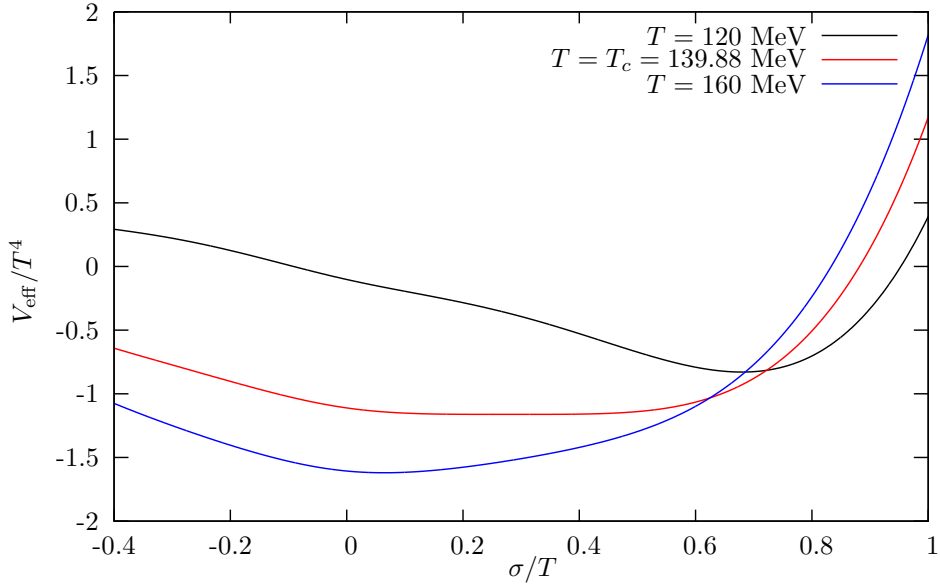


Figure 4.3.: The effective potential for a temperature above, a temperature below and the critical temperature at a coupling  $g = 3.63$ . At the critical temperature the curvature at the minimum becomes very flat. This indicates a second order phase transition.

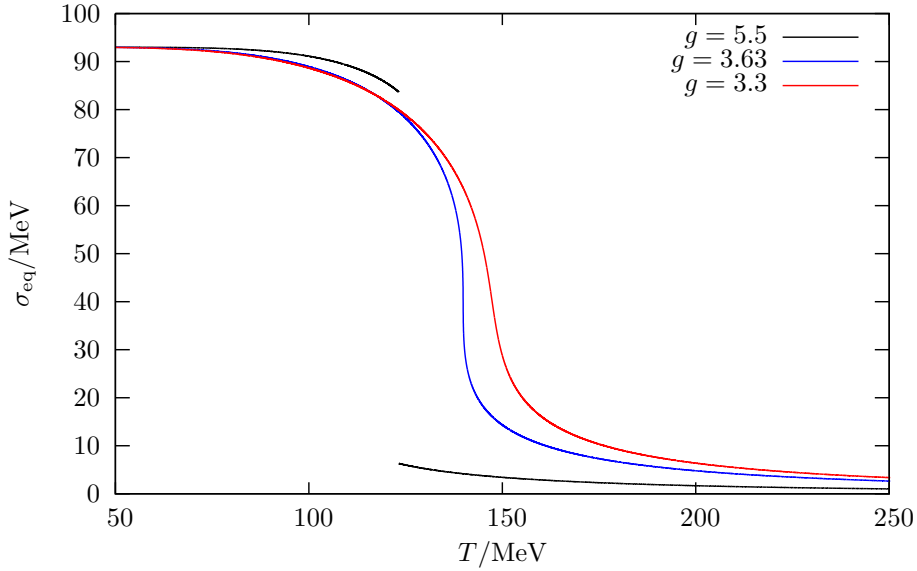


Figure 4.4.: The equilibrium value of the sigma field  $\sigma_{\text{eq}}$  for the three scenarios: with a first order phase transition  $g = 5.5$ , a critical point  $g = 3.63$  and a crossover  $g = 3.3$ . We see the discontinuity in  $\sigma_{\text{eq}}$  at the first order phase transition corresponding to the barrier between the two minima.

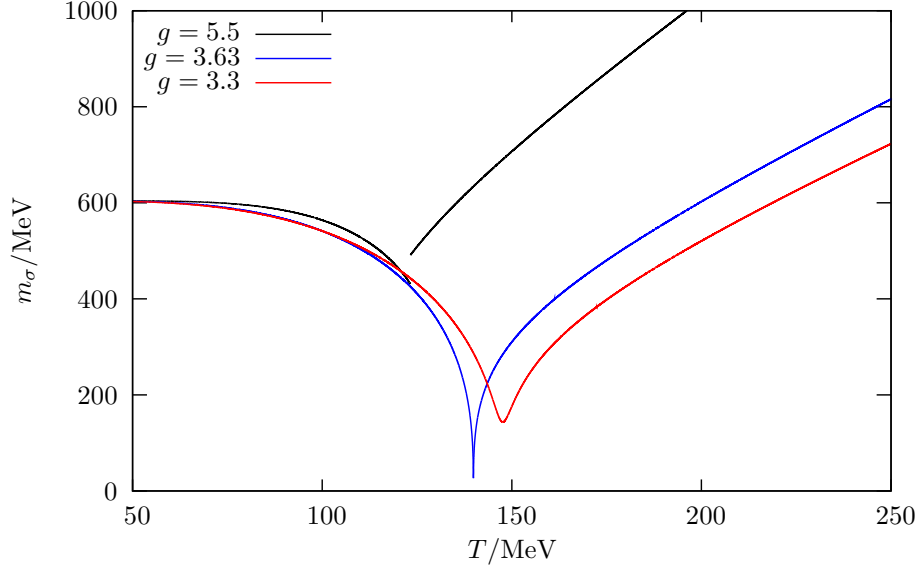


Figure 4.5.: The equilibrium value of the sigma mass  $m_\sigma$  for the three scenarios: with a first order phase transition  $g = 5.5$ , a critical point  $g = 3.63$  and a crossover  $g = 3.3$ . We also observe a discontinuity in  $m_\sigma$  at the first order phase transition.

#### 4.1.3. Thermal equilibrium

In thermal equilibrium the thermodynamic quantities are determined at their expectation value. There is, however, a certain probability to find fluctuations  $\delta x$  around these expectation values that lead to a decrease of the entropy

$$S = -\frac{V}{T} V_{\text{eff}} \simeq S_0 - \frac{1}{2} \kappa \delta x^2. \quad (4.18)$$

Then,

$$\kappa^{-1} = \frac{T}{V} \frac{\partial^2 V_{\text{eff}}}{\partial x^2} = \frac{T}{V} \frac{1}{m_x^2} = \frac{T}{V} \zeta_x^2 \quad (4.19)$$

is the variance of the fluctuations of the thermodynamic quantity  $x$  with mass  $m_x$  and correlation length  $\zeta_x$ . The probability distribution is Gaussian

$$P(\delta x) = \sqrt{\frac{\kappa}{2\pi}} \exp\left(-\frac{\kappa}{2} \delta x^2\right). \quad (4.20)$$

The variance of the sigma fluctuations from (4.19) with  $\delta x = \delta\sigma = \sigma - \sigma_{\text{eq}}$  is shown in figure 4.6 for a unit volume  $V = 1$  fm. We see the step increase of the fluctuations at the critical point.

## 4.2. Dynamics of the chiral fields and the quarks

We have just learned about the thermal equilibrium state of the chiral fields. Now, we want to include the explicit dynamics of the chiral fields. In this chapter we propagate the



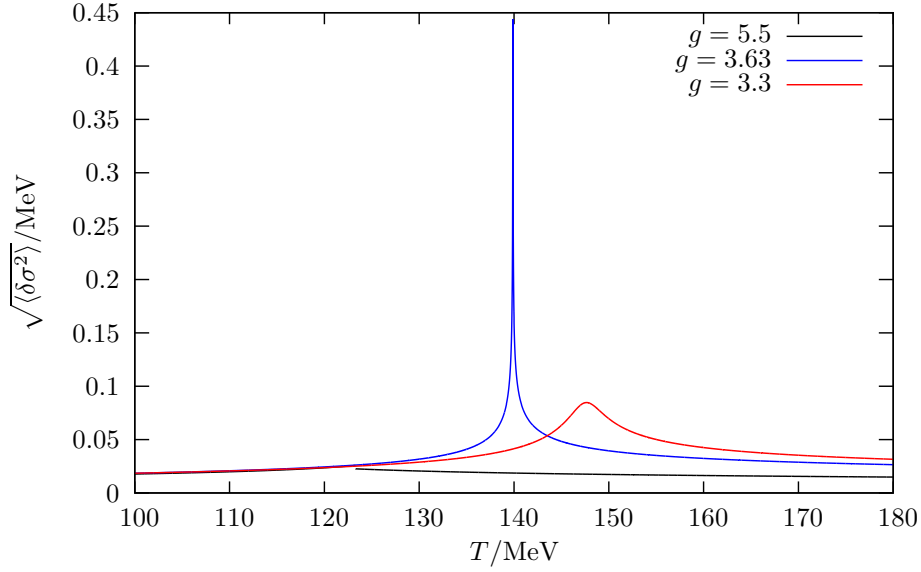


Figure 4.6.: The variance of the sigma fluctuations  $\sqrt{\langle \delta\sigma^2 \rangle}$  for the three scenarios: with a first order phase transition  $g = 5.5$ , a critical point  $g = 3.63$  and a crossover  $g = 3.3$ . The volume is  $V = 1$  fm.

chiral fields by the ordinary classical equations of motion, which result from applying the variational principle to an effective Lagrangian

$$\mathcal{L}_{\text{eff}} = \frac{1}{2} \partial_\mu \sigma \partial^\mu \sigma + \frac{1}{2} \partial_\mu \vec{\pi} \partial^\mu \vec{\pi} - U(\sigma, \vec{\pi}) - \Omega_{q\bar{q}}. \quad (4.21)$$

For the sigma field it reads

$$\partial_\mu \partial^\mu \sigma + \frac{\delta U(\phi)}{\delta \sigma} = -g\rho_S, \quad (4.22)$$

and for the pion fields

$$\partial_\mu \partial^\mu \vec{\pi} + \frac{\delta U(\phi)}{\delta \vec{\pi}} = -g\vec{\rho}_{\text{PS}}. \quad (4.23)$$

The time evolution of the quarks and antiquarks is given by the Dirac equation for quarks and antiquarks. Due to the effective mass acquired by the quarks and antiquarks from the interaction with the chiral fields, which are time and space dependent, the exact solution of the Dirac equation is extremely difficult to find. We need to make further approximations. In [Cse95, Mis97a, Aba97] a Vlasov-equation for the quark-antiquark Wigner-function was solved in the collisionless approximation. We adapt the concepts of [Mis99a, Pae03] and propagate the quarks and antiquarks fluid dynamically.

In section 2.4.1 we explained the basic ideas of a relativistic fluid dynamic approach to heavy-ion collisions. Comparisons of ideal fluid dynamic calculations to measurements at RHIC propose that the initial system created in a heavy-ion collision at high energies locally equilibrates fast. We do not include viscous effects in our fluid dynamic calculation and assume local equilibration of the fluid on times scales much smaller than the equilibration of the sigma field with the fluid heat bath. This allows us to ignore the microscopic

details of the quark dynamics. Since we explicitly want to study fluctuations we have to note that this puts further doubts on the applicability of ideal fluid dynamics as gradients become larger making viscous corrections more important. Its evolution is governed by local energy and momentum conservation. For the fluid dynamic expansion the chiral fields are treated on the level of an external, parametric field. According to their local value the local pressure of the quarks is

$$p(\phi, T) = -\Omega_{q\bar{q}}(T, \phi). \quad (4.24)$$

As in (4.14) the local energy density of the quark fluid is

$$\begin{aligned} e(\phi, T) &= T \frac{\partial p(\phi, T)}{\partial T} - p(\phi, T) \\ &= 2d_q \int \frac{d^3p}{(2\pi)^3} E n_F(p). \end{aligned} \quad (4.25)$$

Locally, the chiral fields interact with the quark fluid and exchange energy and momentum. In order to conserve energy and momentum of the coupled system we include a source term

$$S^v = -\partial_\mu T_\phi^{\mu\nu} = g\rho_\sigma \partial^\nu \sigma + g\vec{\rho}_\pi \partial^\nu \vec{\pi}, \quad (4.26)$$

where  $T_\phi^{\mu\nu}$  is the energy-momentum tensor of the purely mesonic part of the Lagrangian

$$\mathcal{L}_\phi = \frac{1}{2} \partial_\mu \sigma \partial^\mu \sigma + \frac{1}{2} \partial_\mu \vec{\pi} \partial^\mu \vec{\pi} - U(\phi). \quad (4.27)$$

Within the fluid dynamic description of the quarks we have to solve

$$\partial_\mu T_{\text{fluid}}^{\mu\nu} = S^v, \quad (4.28)$$

with the energy-momentum tensor of an ideal fluid as given in equation (2.44). The equation (4.28) with the source term (4.26) can alternatively be derived from the Vlasov-equation of quarks coupling to a background chiral field [Mis97b]. The coupled equations (4.22), (4.23) and (4.28) can together be obtained from a variational formulation [Agu06].

### 4.3. Numerical implementation

We have to solve the coupled equations of motion for the chiral fields (4.22) and (4.23) and the energy-momentum conserving equations of relativistic fluid dynamics (4.28) for the quark fluid numerically. We briefly explain the staggered leap-frog algorithm to solve the equations of motion for the chiral fields (4.22) and (4.23) and in more detail the full (3+1)d SHASTA fluid dynamic code.

#### 4.3.1. Staggered leap-frog algorithm

The equations of motion for the chiral fields (4.22) and (4.23) are solved by a staggered leap-frog algorithm. The second order equation is separated into two coupled equations,

one for  $\phi$  and one for the time derivative of the fields  $v = \partial_t \phi$ :

$$v = \partial_t \phi, \quad (4.29a)$$

$$\partial_t v - \vec{\nabla}^2 v + \frac{\partial U}{\partial \phi} = -g\rho_{s/ps}. \quad (4.29b)$$

$v$  is updated at half-time steps. This ensures the second order accuracy of the algorithm that is needed to work reliably for longer times. We apply boundary conditions of the Neumann type rather than periodic boundary conditions. The normal derivative is set to zero on the boundary of the grid. The implemented algorithm was tested and gave accurate results for analytically known results of the wave equation with various source terms, like for a soliton solution of the sine-Gordon equation.

### 4.3.2. SHASTA fluid dynamic code

For the solution of (4.28) we use the full (3+1)d SHarp And Smooth Transport Algorithm (SHASTA) fluid dynamic code [Ris95a, Ris95b, Pur93]. For this purpose the computational frame quantities are defined as

$$E = T^{00} = \gamma^2(e + p) - p, \quad (4.30a)$$

$$\vec{M} = T^{i0} = \gamma^2(e + p)\vec{v}. \quad (4.30b)$$

The fluid dynamic equations (2.43) and (2.45) in these computational frame quantities are

$$\partial_t E + \vec{\nabla} \cdot (E\vec{v}) = -\vec{\nabla} \cdot (p\vec{v}), \quad (4.31a)$$

$$\partial_t \vec{M} + \vec{\nabla}(\vec{M} \cdot \vec{v}) = -\vec{\nabla} p, \quad (4.31b)$$

$$\partial_t R + \vec{\nabla} \cdot (R\vec{v}) = 0. \quad (4.31c)$$

These equations are solved in the finite difference form on a Euclidean grid for the discretized quantities. The three-divergence operators are treated with the operator splitting method and each of the equations is solved sequentially in all three space directions alternating the sequence in each new time step. The remaining effectively one-dimensional equations are solved by a flux-corrected transport algorithm. The computation of the transported and diffused densities at the next time step is of second order accuracy due to the half-step in the terms on the right hand side of the equations (4.31). Numerical diffusion must be estimated and the resulting flux-corrected antidiffusion fluxes are subtracted to yield the propagated densities. This algorithm propagates quantities in the computational frame but requires values of the pressure and the velocity of the fluid cell. The pressure  $p$  is obtained from the equation of state, which expresses  $p$  as a function of the energy density and baryon number density in the local rest frame of the fluid cell. Therefore, one must calculate  $e$ ,  $\vec{v}$  and  $n$  from  $E$ ,  $\vec{M}$  and  $R$ .

The causal transport of matter is assured on a numerical level by fulfilling the Courant-Friedrichs-Levy criterion  $\Delta t / \Delta x \equiv \lambda < 1$ , where  $\Delta x$  is the cell size in one direction and  $\Delta t$  the time step. The averaging of the transported densities in a cell leads to prediffusion

that is larger for smaller  $\lambda$ , which thus cannot be chosen arbitrarily small. The SHASTA code requires values  $\lambda < 1/2$  for numerical stability. We choose  $\lambda = 0.4$ ,  $\Delta x = \Delta y = \Delta z = 0.2$  fm and thus  $\Delta t = 0.08$ . The grid size is  $(128\Delta x)^3$ .

### 4.3.3. Initial conditions

For a qualitative investigation the initial conditions are kept simple. We choose an initial temperature profile, which is uniform in  $z$ -direction over a length  $l_z = 6$  fm and ellipsoidal in the  $x/y$ -plane. The ellipsoidal shape should mimic the overlap region in a heavy-ion collision. Its major and minor radii are  $b = \sqrt{r_A^2 - \tilde{b}^2/4}$  and  $a = r_A - \tilde{b}/2$ , where  $\tilde{b} = 6$  fm is the supposed impact parameter and  $r_A = 6.5$  fm the radius of the nuclei. The temperature is smoothly distributed over this ellipsoidal region by a Wood-Saxon like distribution with the maximum at the initial temperature  $T_{\text{ini}} = 160$  MeV, which is well above either of the phase transitions,

$$T(\vec{x}, t = 0) = \frac{T_{\text{ini}}}{(1 + \exp((\tilde{r} - \tilde{R})/\tilde{a}))(1 + \exp((|z| - l_z)/\tilde{a}))} \quad (4.32)$$

with a surface thickness of  $\tilde{a} = 0.3$  fm,  $\tilde{r} = \sqrt{x^2 + y^2}$  and

$$\tilde{R} = \begin{cases} \frac{a\tilde{r}}{\sqrt{b^2x^2 + a^2y^2}} & \text{for } \tilde{r} \neq 0 \\ a & \text{for } \tilde{r} = 0 \end{cases} . \quad (4.33)$$

By minimizing the effective potential the equilibrium value of the sigma field  $\sigma_{\text{eq}}$  is found. The thermal equilibrium state has Gaussian fluctuations around the expectation value, the variance of which is

$$\langle \delta\sigma^2 \rangle = \frac{T}{V} \frac{1}{m_\sigma^2} . \quad (4.34)$$

Thus, the sigma field is initially Gaussian distributed around its equilibrium value,

$$\sigma(\vec{x}, t = 0) = \sigma_{\text{eq}} + \delta\sigma(\vec{x}) . \quad (4.35)$$

According to (4.25) the energy density of the quark fluid can be calculated with (4.32) and (4.35).

The velocity profile is  $v_z(\vec{x}, t = 0) = |z|/l_z \cdot v_{\text{max}}$ , where  $v_{\text{max}} = 0.2$ , while there are no transverse velocities initially  $v_x(\vec{x}, t = 0) = v_y(\vec{x}, t = 0) = 0$ . The time derivative of the sigma field  $\partial_t \sigma$  is initially set to zero.

The pion field is initially set to zero and neglected during the simulation, since we expect that mainly the sigma field as the order parameter of chiral symmetry is affected by the phase transition.

### 4.3.4. Equation of state

At the heart of the fluid dynamic expansion is the equation of state. It is elucidating to look at the equilibrium case of the present model first. We eliminate the temperature in the pressure (4.24) and the energy density (4.25) numerically for  $\phi = \phi_{\text{eq}}$ . In figure 4.7 the

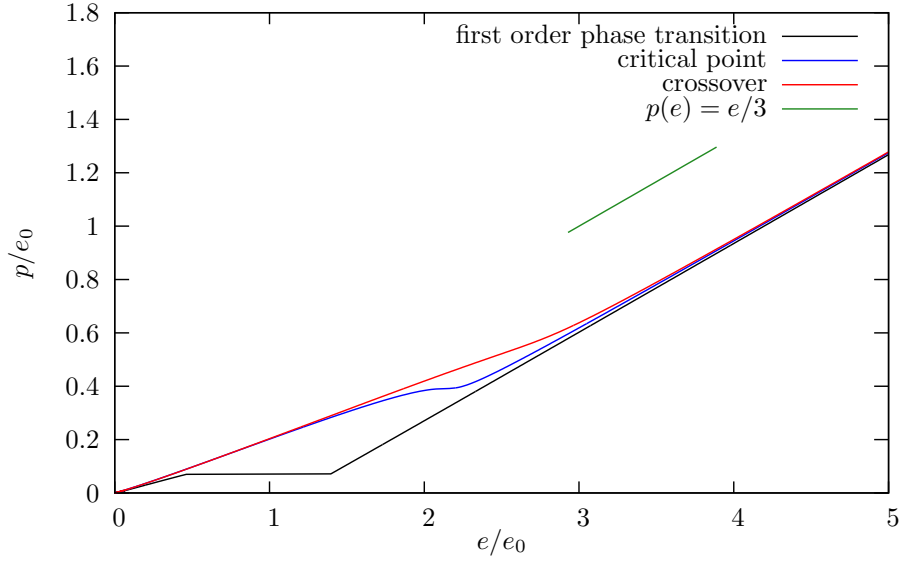


Figure 4.7.: The equation of state for the quark fluid with equilibrium values of the chiral fields  $\phi = \phi_{\text{eq}}$  for the different phase transition scenarios. For comparison of the slope we plot the equation of state of a relativistic ideal gas in a short interval.

obtained relation  $p = p(e)$  is plotted for the different couplings corresponding to a first order phase transition, a critical point and a crossover.

One sees that both in the high temperature and in the low temperature limit the three scenarios give the same equation of state. In the high temperature limit the system is in the chirally restored phase, where the quarks are almost massless. Therefore the slope of the pressure becomes that of the ideal gas equation of state  $p(e) = e/3$ . For the crossover the slope of the pressure varies continuously and smoothly. Already at the critical point the slope of the pressure becomes very small in the transition region at around  $e \simeq 2e_0$ . At the first order phase transition the energy density varies discontinuously with the pressure, which gives rise to the latent heat. It is the difference in the energy density at the two degenerate minima. As typical for a first order phase transition the speed of sound at the phase transition vanishes

$$c_s^2 = \left. \frac{\partial p}{\partial e} \right|_{\text{phase transition}} = 0. \quad (4.36)$$

This is called the softest point of the equation of state [Hun95].

In the case of the off-equilibrium propagation we do not obtain a simple relation  $p(e)$  because the sigma field is not fixed at its equilibrium value. Therefore, the pressure and the energy density depend explicitly on the local value of the field, which can be viewed as an external parameter in the thermodynamic sense. What needs to be done technically is the following. With the energy density from the fluid dynamic calculation at a given point  $x$ ,  $e_{\text{fluid}}(x)$  the equation for the thermodynamic energy density (4.25) needs to be inverted taking into account the local value of the sigma field  $\sigma(x)$ . The local temperature

$T(x)$  is given by the solution of

$$e_{\text{fluid}}(x) - e(\sigma, T) = 0. \quad (4.37)$$

The temperature  $T(x)$  and the local value of the sigma field  $\sigma(x)$  are then inserted into the thermodynamic pressure (4.24). For the transformations between the local rest frame of a fluid cell and the computational frame the equation of state is accessed very often in each time step. It is very time consuming to invert (4.25) numerically. We, therefore, parametrize the pressure as a polynomial in the energy density where the coefficients themselves are polynomials in the sigma field. The explicit values are obtained from fits to (4.24) and (4.25) for different temperatures and values of the sigma field and given in the appendix D.

#### 4.3.5. The inclusion of the source term

The source term (4.26) in explicit terms gives

$$\begin{aligned} S^0 &= -\partial_\mu T_\sigma^{\mu 0} = -\partial_t T_\sigma^{00} + \sum_i \partial_j T_\sigma^{j0} \\ &= -\partial_t E_\sigma + \vec{\nabla} \cdot \vec{M}_\sigma \\ &= -\partial_t E_\sigma - \vec{\nabla} \cdot (\vec{\nabla} \sigma) \partial_t \sigma, \end{aligned} \quad (4.38)$$

and

$$\begin{aligned} S^i &= -\partial_\mu T_\sigma^{\mu i} = -\partial_t T_\sigma^{0i} + \sum_j \partial_j T_\sigma^{ji} \\ &= -\partial_t \vec{M}_\sigma + \vec{\nabla} \cdot (\vec{\nabla} \sigma)^2 \end{aligned} \quad (4.39)$$

It appears on the right hand side of the fluid dynamic equations in computational frame quantities (4.31a) and (4.31b).

The numerical inclusion of the source term (4.26) is an intricate issue. We tested two possible methods. First, we treated the source term on the same footing as the right hand sides of equations (4.31a) and (4.31b). This is straight forward but violates the energy-momentum conservation severely. Second, we solve equation (4.28) in two steps. After performing the fluid dynamic step in the standard fashion for  $S^\nu = 0$  we subtract the source term  $S^\nu$  from the energy and momentum density in the computational frame. Then, we can again calculate the local rest frame quantities. This gives a very good conservation of energy and momentum of the entire system as we will show for the various calculations in this work. The latter method also proved to work well in multi-fluid dynamics [Bra97].

## 4.4. Results

In this section we first present a test scenario of an equilibrium expansion. Here, the sigma field is assumed to be thermally equilibrated with the quark fluid, which expands fluid dynamically. These results will serve as a reference for the off-equilibrium expansion presented thereafter and the nonequilibrium expansion, which is the subject of the following chapters. In the off-equilibrium case the chiral fields are propagated according to their classical equations of motion (4.22).

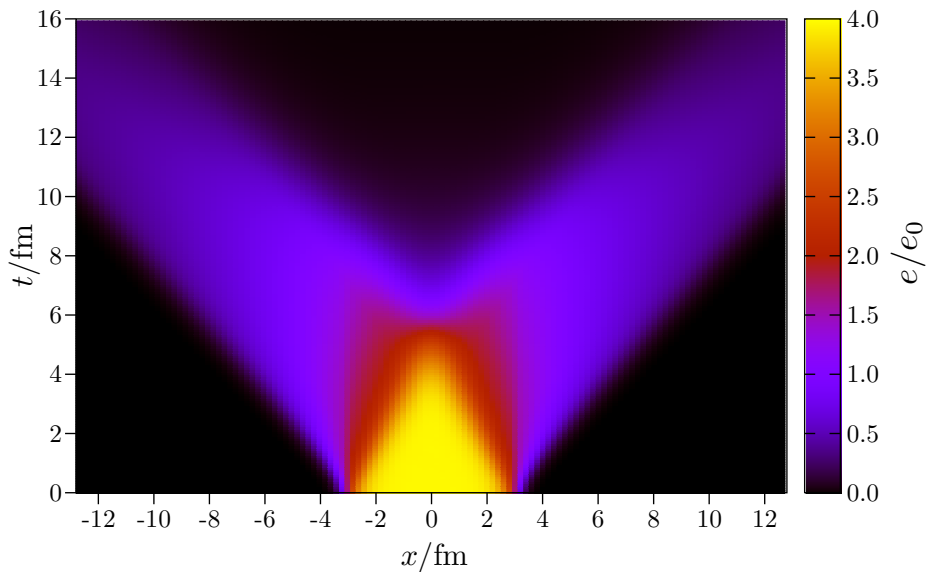


Figure 4.8.: The time evolution of the energy density in units of the ground state energy density  $e_0$  for a scenario with a critical point in an equilibrium expansion.

#### 4.4.1. Equilibrium expansion

By treating the sigma field as an external parameter that is always in thermal equilibrium with the quark fluid we can investigate the effects of a spatially inhomogeneous expansion. The quark fluid is propagated fluid dynamically with the initialization described above. The sigma field at each time step is

$$\sigma(x) = \sigma_{\text{eq}}(T(x)) + \delta\sigma(T(x)), \quad (4.40)$$

where the variance of the Gaussian fluctuations is given by (4.19). We define the volume of the system  $V$  over the number of fluid cells with nonzero energy density. Depending on the local temperature  $T(x)$  the variance of the sigma field varies spatially. Since the sigma field has no dynamics the source term (4.26) is zero.

The time evolution of the energy density in the laboratory frame in  $x$ -direction with  $y = z = 0$  is shown in figure 4.8 for a scenario with a critical point and in figure 4.9 for a scenario with a first order phase transition. They do not show a difference. In figures 4.10 and 4.11 the time evolution of the sigma field in  $x$ -direction with  $y = z = 0$  is plotted for a scenario with a critical point and with a first order phase transition, respectively. Here, we see very different evolutions around the phase transition. The sigma field in the critical point scenario evolves continuously from the chirally restored phase to the chirally broken phase. For a first order phase transition there is a region where both phases coexist and where there are larger spatial fluctuations.

The quantities shown in figures 4.12 and 4.13 are averaged over a sphere with radius  $r = 3$  fm in the center of the initially hot region. We see that already an inhomogeneous expansion of the quark fluid leads to a large deviation from the static equilibrium quantities. In figure 4.12 we compare the time evolution of the average values of the sigma

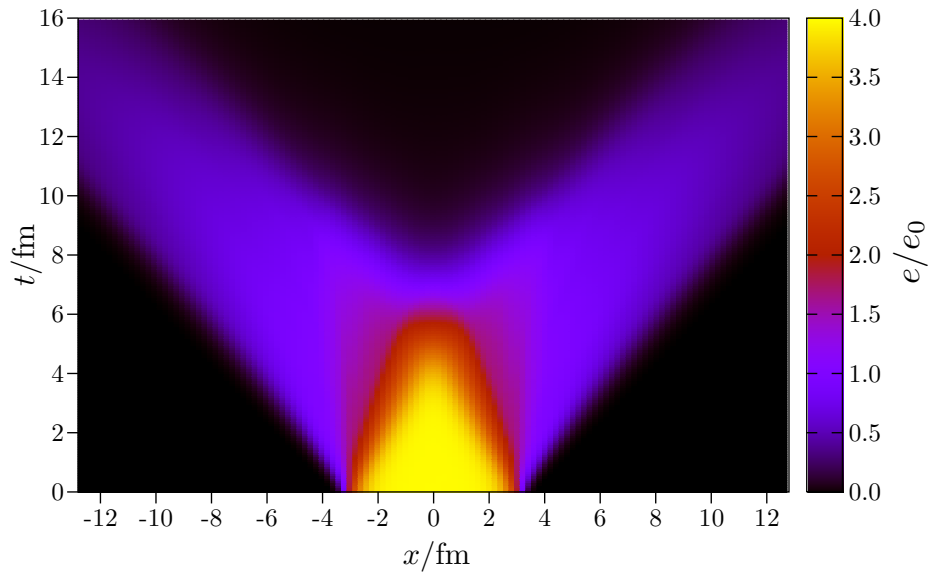


Figure 4.9.: The time evolution of the energy density in units of the ground state energy density  $e_0$  for a scenario with a first order phase transition and the sigma field in equilibrium.

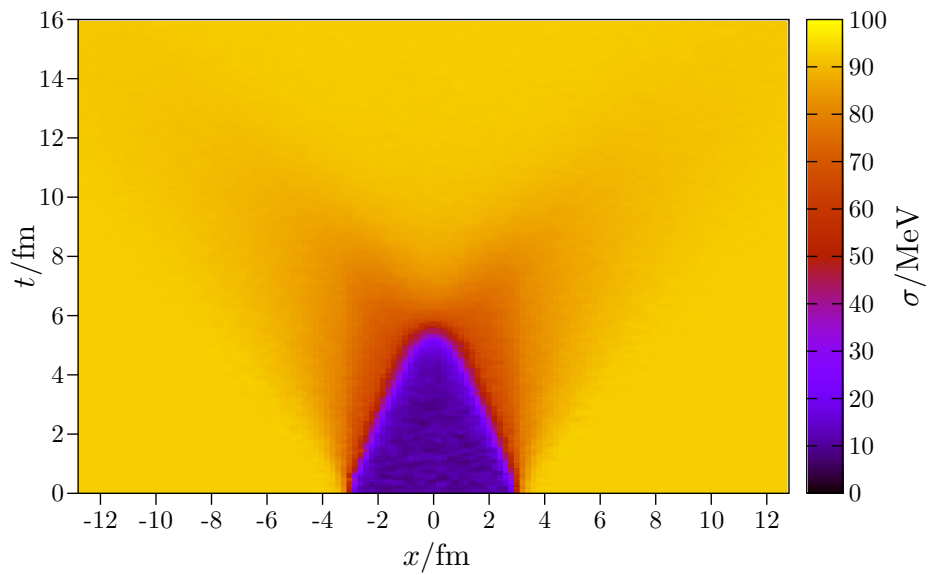


Figure 4.10.: The time evolution of the equilibrium sigma field for a scenario with a critical point.



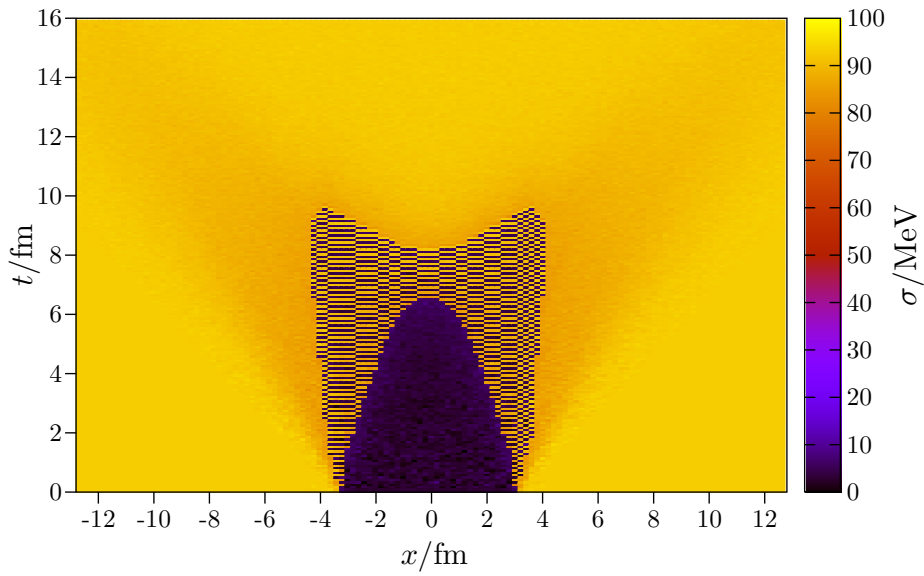


Figure 4.11.: The time evolution of the equilibrium sigma field for a scenario with a first order phase transition.

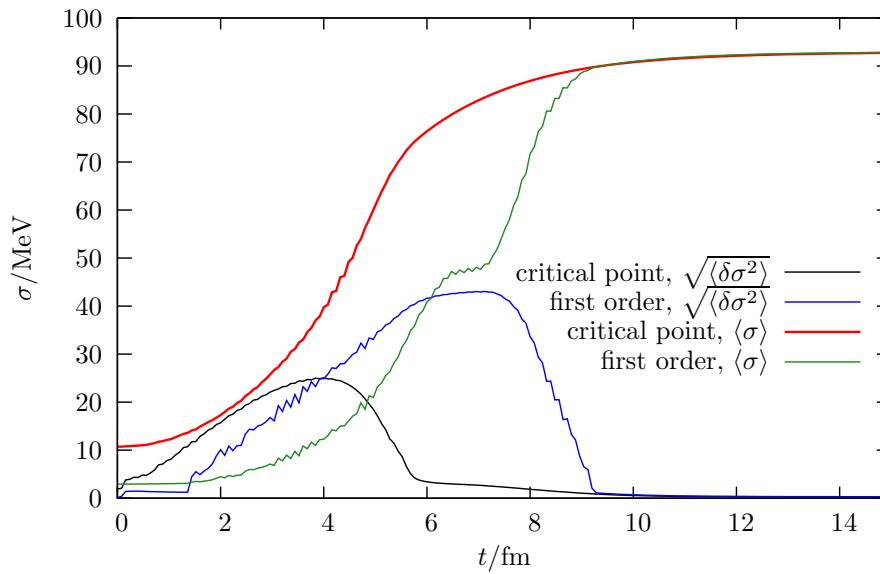


Figure 4.12.: The average values and the variances of the fluctuations  $\sqrt{\langle\delta\sigma^2\rangle}$  of the sigma field in an equilibrium expansion for a scenario with a critical point and with a first order phase transition

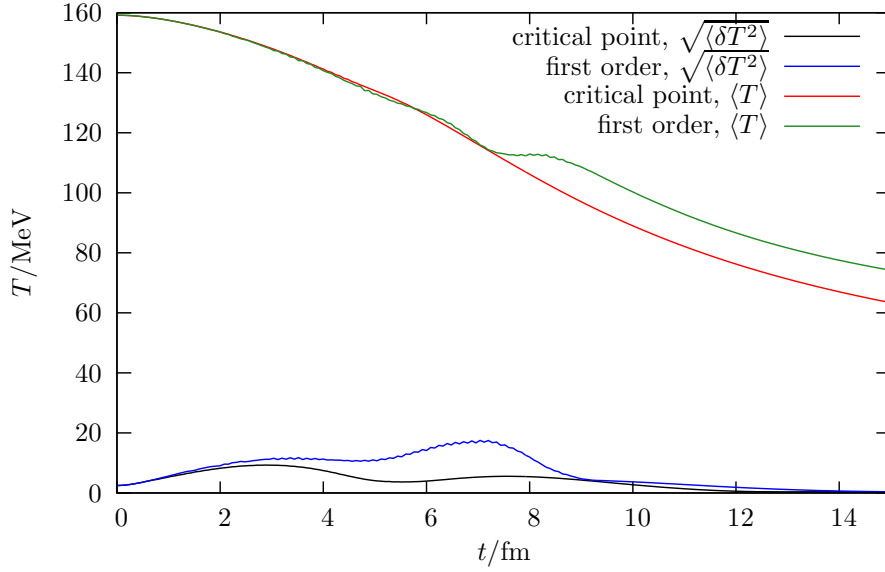


Figure 4.13.: The average temperature and temperature fluctuations in an equilibrium expansion for scenario with a critical point and with a first order phase transition.

field for a first order phase transition and a critical point. Due to the higher transition temperature the critical point scenario crosses the phase transition earlier than the first order phase transition scenario. Still, the final vacuum value  $\sigma_{\text{vac}} = f_\pi$  is reached at about the same time for both scenarios. At the phase transition the variance of the sigma fluctuations grows. Comparing to the global expectation values in figure 4.6, scaled with the respective volume, one sees that the fluctuations at the critical point are smaller while the fluctuations at the first order phase transition are larger. In global static equilibrium the variance of the fluctuations diverge for a critical point but are rather small for a first order phase transition. In figure 4.12 the fluctuations at the critical point stay finite and are even exceeded by the fluctuations at the first order phase transition. When we take a closer look at the evolution of the average of the sigma field in a first order phase transition, we see that at times between 6 and 7 fm it stays constant. At this time one part of the system is still in the high temperature and the other part is already in the low temperature phase. Both parts are approximately equally large as the average sigma field is almost exactly between the high temperature and the low temperature equilibrium value of the sigma field. This coexistence region was already observed in figure 4.11. A similar behavior can also be seen in the evolution of the average temperature in figure 4.13. Fluctuations in the temperature in a scenario with a first order phase transition have a maximum between 6 and 8 fm and then show a constant average value for slightly later times around 8 fm. Again, the fluctuations in the temperature are smaller for a critical point than for a first order phase transition.

To conclude a spatially inhomogeneous and time-dependent system seems to enhance fluctuations for a scenario with a first order phase transition because at different temperatures around the phase transition the true equilibrium values can be separated over

almost 80 MeV, which corresponds to the distances between the two minima, whereas at a critical point the sigma mass is small only in the vicinity of  $T_c$ . Averaging over space spoils the large fluctuations for global equilibrium.

#### 4.4.2. Off-equilibrium expansion

We now turn to the off-equilibrium expansion of the sigma field according to the classical equations of motion (4.22). First, we check the energy conservation of the entire system to show that the inclusion of the source term (4.26) described in section 4.2 indeed accounts for the energy exchange between the fluid and the sigma field. Violations of momentum conservation were found to be of the order of 1%. After having numerically convinced ourselves that the additional terms appearing in the source terms for the energy density (4.38) and the momentum density (4.39) are small compared to  $\partial_t E_\sigma$  and  $\partial_t \vec{M}_\sigma$ , we approximate

$$S^0 \simeq -\partial_t E_\sigma, \quad (4.41a)$$

$$S^i \simeq -\partial_t \vec{M}_\sigma. \quad (4.41b)$$

In figure 4.14 for a critical point and in figure 4.15 for a scenario with a first order phase transition the various contributions to the total energy of the entire system are shown. The total energy is the sum of the energy of the fluid, the classical potential and the kinetic and spatial fluctuation energy of the sigma field

$$\begin{aligned} E_{\text{tot}} &= E_{\text{fluid}} + E_\sigma \\ &= E_{\text{fluid}} + \frac{1}{2} \partial_t \sigma^2 + \frac{1}{2} \vec{\nabla} \sigma^2 + U(\sigma). \end{aligned} \quad (4.42)$$

In both scenarios the total energy is well conserved until the quark fluid reaches the edges of the grid between 8 and 9 fm and disappears. At  $T = 0$  the minimum of the classical potential is at  $\langle \sigma \rangle|_{T=0} = f_\pi$  with  $U(\sigma = f_\pi) = 0$ . Therefore, it initially contributes a finite energy. When the system cools this energy is transferred to the quarks. It is remarkable that in a system with a first order phase transition both the temporal and the spatial fluctuation energy of the sigma field are larger than in a system with a critical point.

Having shown that the total energy of the entire system is conserved in our approach we can take a look at the actual time evolution of the energy density and the sigma field. As in the equilibrium case we plot the energy density of the quark fluid and the sigma field in  $x$ -direction with  $y = z = 0$  for a critical point in figure 4.16 and 4.18 and for a first order phase transition in figure 4.17 and 4.19. Now, we can clearly see a different evolution of the energy density. In the critical point scenario the energy density develops broader structures around a time of 7 fm than in the first order phase transition scenario. In the latter at  $x = 3$  and  $x = -3$  fm and  $t = 7$  fm bubbles of higher energies densities are formed instead. Also for the sigma field the structures in the  $t/x$  diagram are broader for an expansion through the critical point and more localized at the first order phase transition. In both cases we see that the sigma field oscillates around the vacuum expectation value for large times. This finding can be backed by looking at the average sigma field and its variance in figure 4.20. While initially the average sigma field approaches the vacuum

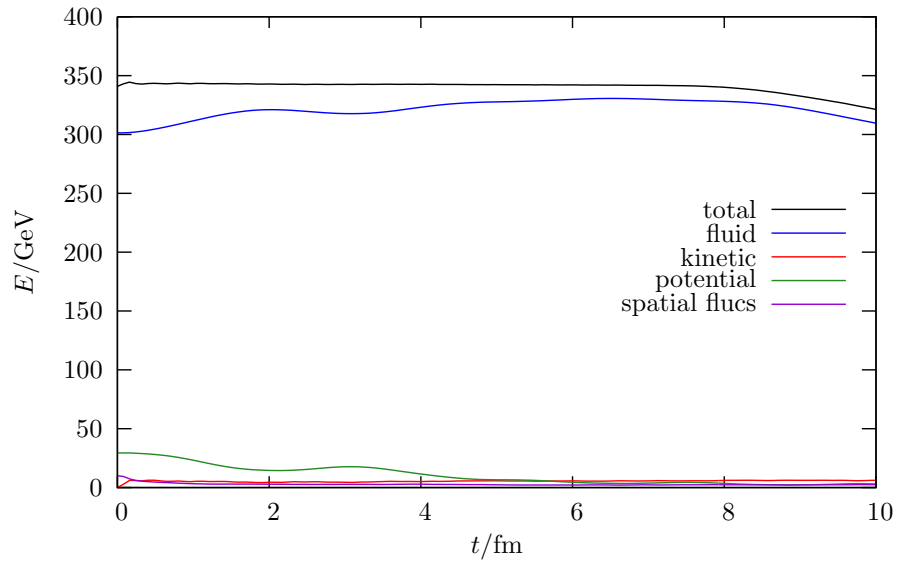


Figure 4.14.: The different contributions to the total energy of the entire system plotted versus the time for the critical point scenario. The total energy is well conserved until the quark fluid reaches the edges of the grid.

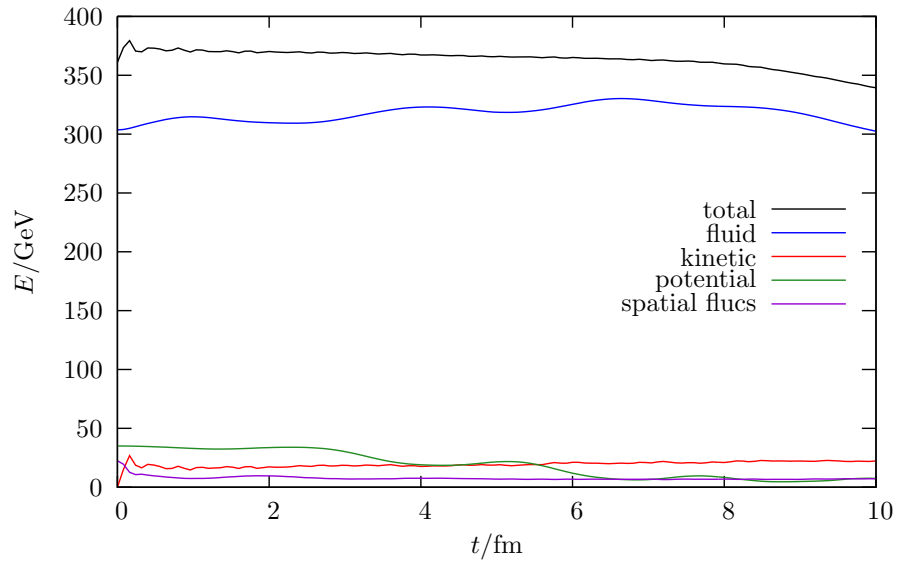


Figure 4.15.: The different contributions to the total energy of the entire system plotted versus the time for the first order scenario. The total energy is well conserved until the quark fluid reaches the edges of the grid. Even at late times there is a substantial amount of energy in the kinetic and spatial fluctuations of the sigma field.

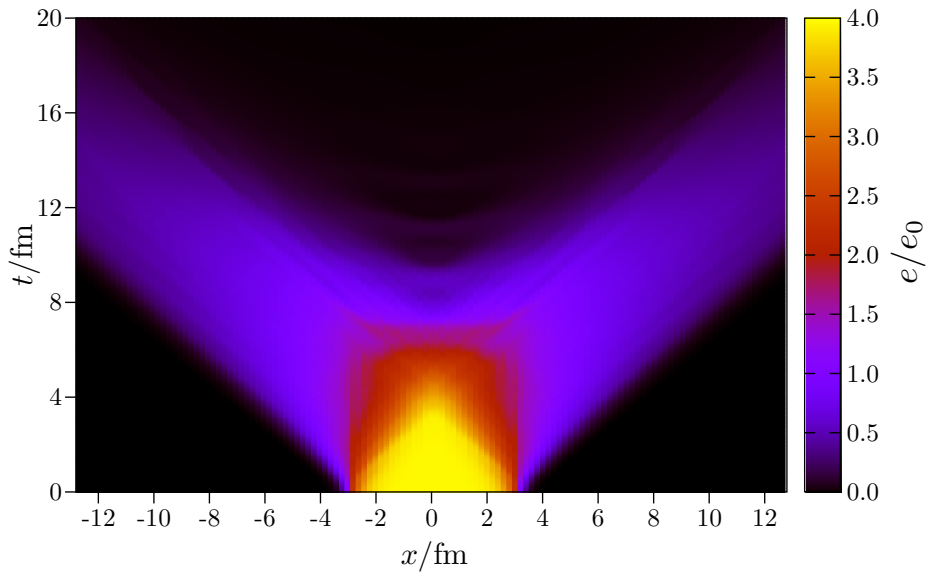


Figure 4.16.: The time evolution of the energy density in units of the ground state energy density  $e_0$  for a scenario with a critical point in the off-equilibrium expansion.

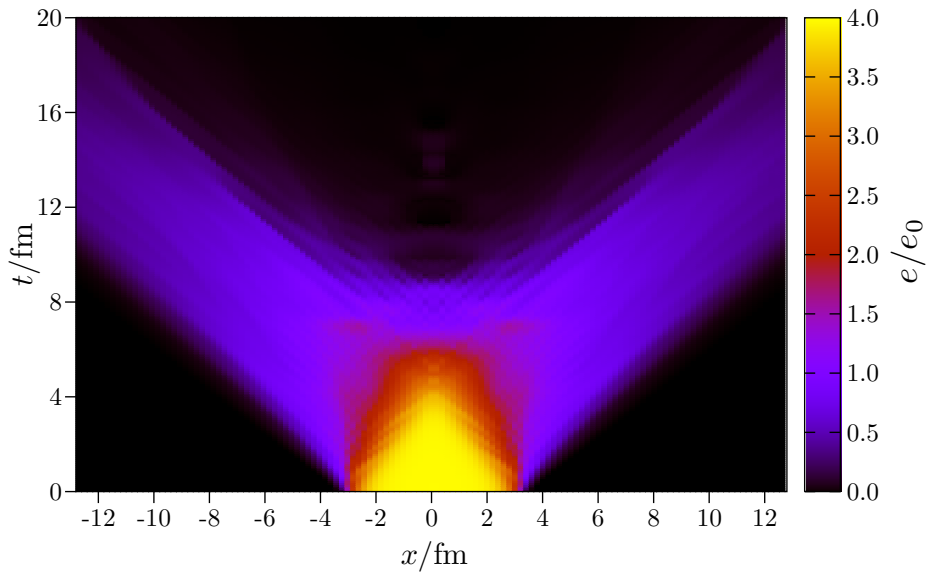


Figure 4.17.: The time evolution of the energy density in units of the ground state energy density  $e_0$  for a scenario with a first order phase transition in the off-equilibrium expansion.

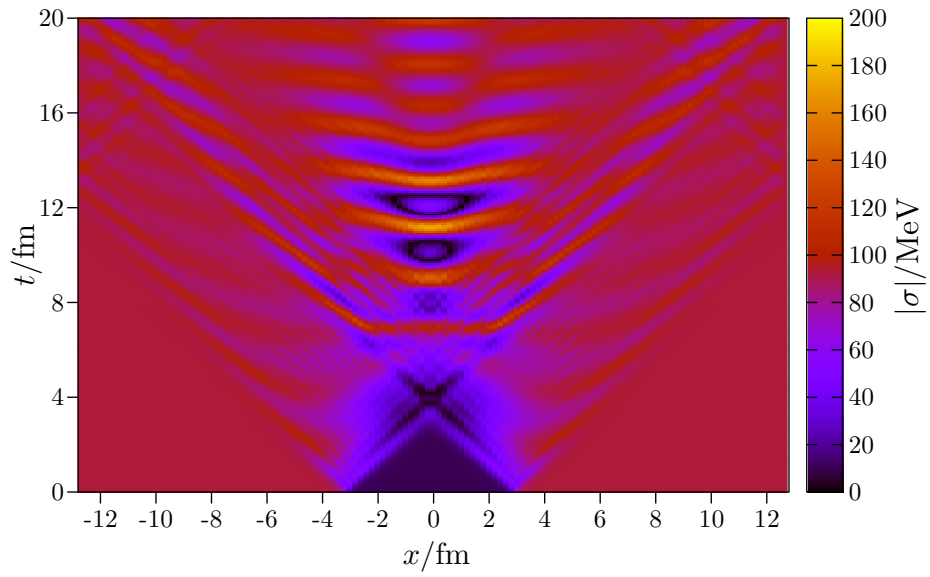


Figure 4.18.: The off-equilibrium evolution of the sigma field  $|\sigma|$  for a scenario with a critical point.

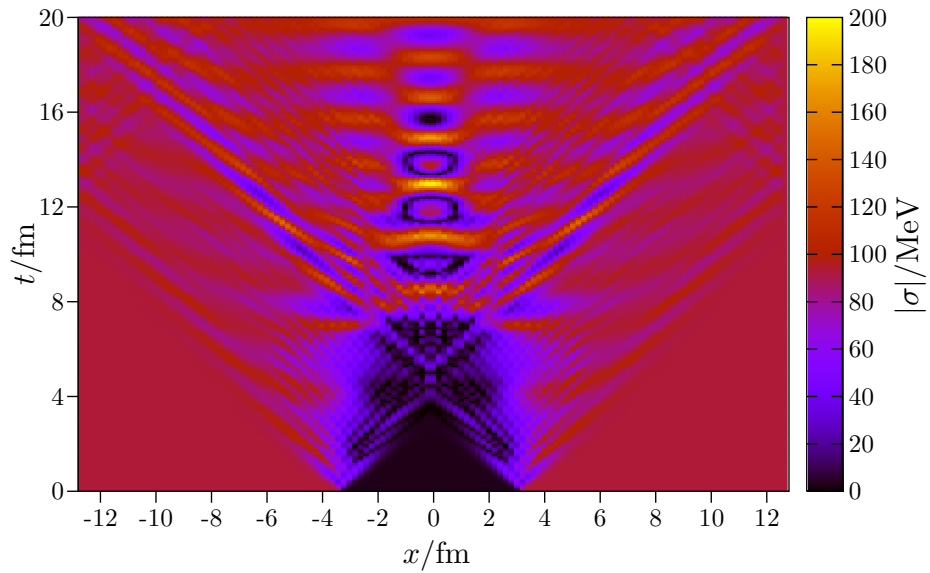


Figure 4.19.: The off-equilibrium evolution of the sigma field  $|\sigma|$  for a scenario with a first order phase transition.

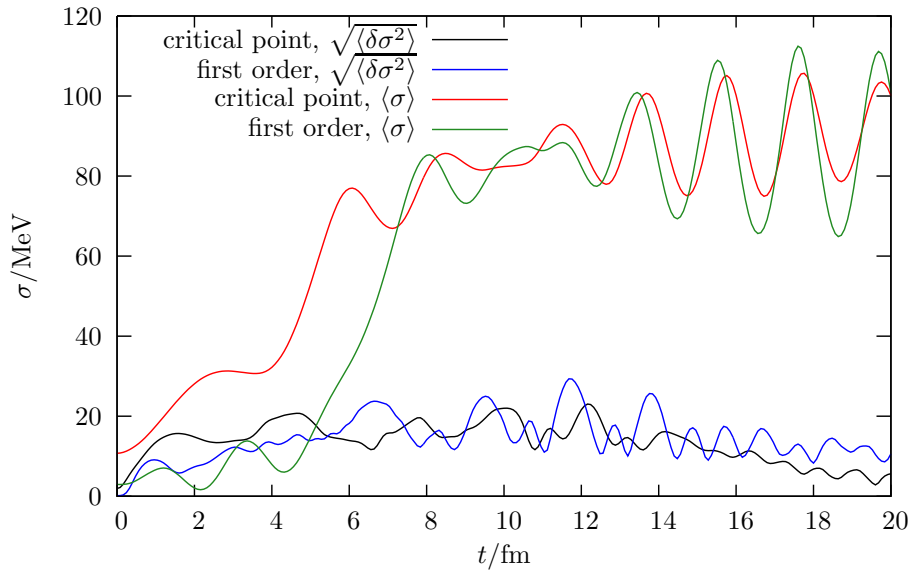


Figure 4.20.: The average values and the variances of the fluctuations  $\sqrt{\langle \delta\sigma^2 \rangle}$  of the sigma field in an off-equilibrium expansion for a scenario with a critical point and with a first order phase transition.

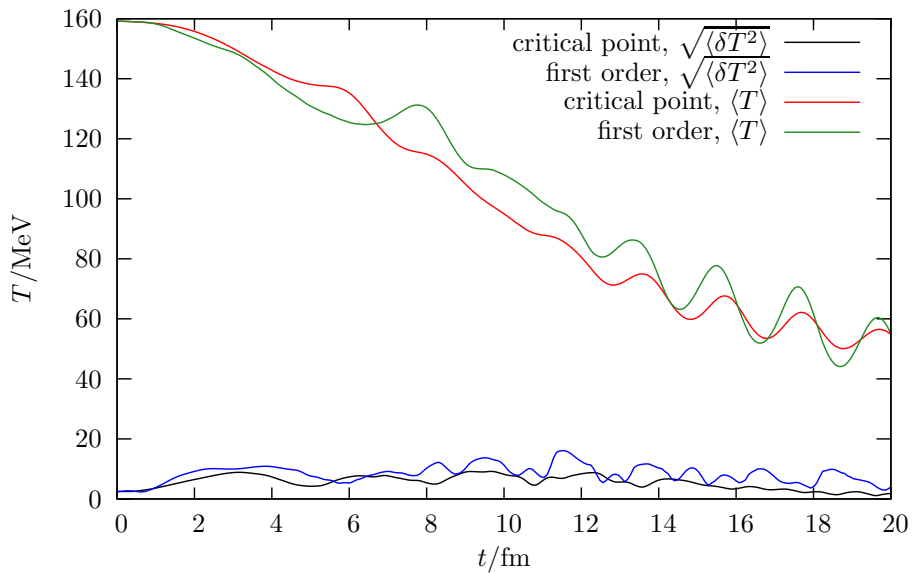


Figure 4.21.: The average temperature and temperature fluctuations in an off-equilibrium expansion for a scenario with a critical point and with a first order phase transition.

expectation value faster for a critical point the first order phase transition sets in later and drives the sigma field to the vacuum expectation value for around the same times  $t > 10$  fm. Then one clearly sees the large oscillations around  $f_\pi$ . The variances for both scenarios are small compared to the equilibrium expansion seen in figure 4.12. In figure 4.21 we can observe the reheating effect at a first order phase transition at  $t = 8$  fm and see that the oscillations of the average sigma field are imposed on the average temperature, which also oscillates.

In this chapter we investigated two expansion methods. First, we treated the sigma field in equilibrium with the quarks and included thermal fluctuations around the sigma expectation value. Second, we included the dynamics of the sigma field according to a classical equation of motion. We called this latter approach the off-equilibrium expansion in order to distinguish it from a nonequilibrium expansion. When the full nonequilibrium dynamics of the sigma field is taken into account it relaxes to its thermal equilibrium value. In the approach presented here we cannot see this relaxational dynamics. Instead the sigma field continues to oscillate around its equilibrium value. Obviously, we captured only part of the full nonequilibrium dynamics. It is the main goal of this thesis to improve the dynamics of the chiral fields by including relaxational dynamics. In the next chapter we develop the consistent analytic model for the coupled nonequilibrium dynamics of the sigma field and the quark fluid.



## 5. Selfconsistent system-heat bath coupling

The main focus of this work is on the extension of chiral fluid dynamic models to include nonequilibrium effects. We have seen in chapter 4 that the naïve formulation of the off-equilibrium dynamics of the chiral fields neglects relaxational and stochastic processes. In this chapter we derive a Langevin equation for the sigma field including dissipative and stochastic terms. In section 5.1 we apply the influence functional method to the linear sigma model with constituent quarks. The separation of the systems seems obvious in our approach to chiral fluid dynamics. We consider the quarks as the heat bath and treat the sigma field as the relevant sector. But we should not forget that it was the original decision to treat the chiral fields in the mean-field approximation and the quarks in local thermal equilibrium that led us to this separation. From the influence functional we can obtain the proper Langevin equation for the sigma field. However, it is not possible to control the local equilibrium properties of the quarks without further assumptions. We need to go beyond existing studies of Langevin equations by putting special emphasis on the properties and the evolution of the heat bath itself. We expect that the back reaction to the heat bath induced by the dynamics of the chiral fields can be important for the overall evolution of the system.

In order to derive the nonequilibrium propagation of the chiral fields and the equilibrium thermodynamic properties of the quarks selfconsistently within one approach we apply the formalism of the 2PI effective action in section 5.2. In section 5.3 we explicitly evaluate the expressions for the damping and the noise term. We discuss the additional heat bath of the hard chiral modes in section 5.4. In the exact formalism of the 2PI effective action a conserved energy-momentum tensor of the entire system can be constructed. We will derive this form and comment on the energy-momentum conservation of approximations to the full equations in section 5.5.

Large parts of this chapter are published in [Nah11b].

### 5.1. The influence functional for the linear sigma model with constituent quarks

The general idea of the influence functional method has been described in section 3.4. Here, we evaluate the influence functional (3.94) for the linear sigma model with constituent quarks starting from the perturbative expansion (3.96). A perturbative treatment for the coupling  $g$  might seem doubtful because  $g$  is of order  $\mathcal{O}(1)$ . The individual processes connected with the orders of the expansion must, however, be looked at more carefully. Higher orders in  $g$  involve more sigma modes and quark-antiquark pairs. The lower

the density of the system the less likely these processes become and, thus, they contribute less to the damping of the sigma field. Still, this is a crucial point in the application of the influence functional method.

### 5.1.1. Explicit calculation of the influence functional

For the linear sigma model with constituent quarks we assume the following splitting: the irrelevant degrees of freedom are the quarks and antiquarks and the relevant sector is that of the chiral fields. In (3.94) and (3.96) it is  $\Phi^{+,-} = \bar{q}^{+,-}, q^{+,-}$  and  $\phi^{+,-} = \sigma^{+,-}$  on the Keldysh contour. Again, we keep the pion fields fixed at their vacuum expectation value  $\langle \pi \rangle = 0$ . The free action of the quarks and antiquarks reads

$$S_0[q, \bar{q}] = i \int d^4x \bar{q}(x) \gamma^\mu \partial_\mu q(x), \quad (5.1)$$

and the interaction between the quarks and the sigma field is of Yukawa type

$$S_{\text{int}}[q, \bar{q}, \sigma] = -g \int d^4x \bar{q}(x) q(x) \sigma(x). \quad (5.2)$$

Then, the expansion of  $S_{\text{IF}}[\sigma^+, \sigma^-]$  becomes

$$\begin{aligned} \exp(iS_{\text{IF}}[\sigma^+, \sigma^-]) &= \int d\bar{q}_i^+ \int dq_i^+ \int d\bar{q}_i^- \int dq_i^- \rho_i^{\text{E}}(\bar{q}_i^+, q_i^+; \bar{q}_i^-, q_i^-) \times \\ &\times \int \mathcal{D}\bar{q}^+ \int \mathcal{D}q^+ \int \mathcal{D}\bar{q}^- \int \mathcal{D}q^- \exp(iS_0[\bar{q}^+, q^+] - iS_0[\bar{q}^-, q^-]) \times \\ &\times \left( 1 - ig \int d^4x (\bar{q}^+(x) q^+(x) \sigma^+(x) - \bar{q}^-(x) q^-(x) \sigma^-(x)) \right. \\ &\quad - \frac{1}{2} g^2 \int d^4x \int d^4y (\bar{q}^+(x) q^+(x) \bar{q}^+(y) q^+(y) \sigma^+(x) \sigma^+(y) \\ &\quad \quad - \bar{q}^+(x) q^+(x) \bar{q}^-(y) q^-(y) \sigma^+(x) \sigma^-(y) \\ &\quad \quad - \bar{q}^-(x) q^-(x) \bar{q}^+(y) q^+(y) \sigma^-(x) \sigma^+(y) \\ &\quad \quad \left. + \bar{q}^-(x) q^-(x) \bar{q}^-(y) q^-(y) \sigma^-(x) \sigma^-(y) \right). \end{aligned} \quad (5.3)$$

Due to the normalization of  $\rho_i^{\text{E}}(\bar{q}_i^+, q_i^+; \bar{q}_i^-, q_i^-)$  the zeroth order in (5.3) gives 1. The first order vanishes with the definition of the free quark propagator for  $a, b = +, -$ ,

$$\begin{aligned} iS_0^{ab}(x, y) &= \langle \mathcal{T}_C q^a(x) \bar{q}^b(y) \rangle_0 \\ &= \int d\bar{q}_i^+ \int dq_i^+ \int d\bar{q}_i^- \int dq_i^- \rho_i^{\text{E}}(\bar{q}_i^+, q_i^+; \bar{q}_i^-, q_i^-) \int \mathcal{D}\bar{q}^+ \int \mathcal{D}q^+ \int \mathcal{D}\bar{q}^- \int \mathcal{D}q^- \times \\ &\quad \times \exp(iS_0[\bar{q}^+, q^+] - iS_0[\bar{q}^-, q^-]) q^a(x) \bar{q}^b(y), \end{aligned} \quad (5.4)$$

and  $S^{++}(0) = S^{--}(0)$ . Only the second order gives a contribution,  $S_{\text{IF}}^{(2)}$  and is equal to  $i$ -times the influence functional itself, as can be seen by taking the logarithm of the expansion in (5.3)

$$iS_{\text{IF}}[\sigma^+, \sigma^-] = \ln(1 + S_{\text{IF}}^{(2)}[\sigma^+, \sigma^-]) \simeq S_{\text{IF}}^{(2)}[\sigma^+, \sigma^-]. \quad (5.5)$$

For the explicit evaluation, we need the four-point functions that appear in the influence functional (5.3). They are defined in the same way as the quark propagator (5.4) and can be obtained from the generating functional  $Z[\bar{\eta}, \eta]$  (3.62) by subsequent differentiation with respect to the external sources. In explicit terms

$$\begin{aligned} \langle \mathcal{T}_C \bar{q}^+(x) q^+(x) \bar{q}^+(y) q^+(y) \rangle &= \frac{1}{Z_0} \left( \frac{i\delta}{\delta\eta^+(x)} \right) \left( \frac{-i\delta}{\delta\bar{\eta}^+(x)} \right) \left( \frac{i\delta}{\delta\eta^+(y)} \right) \left( \frac{-i\delta}{\delta\bar{\eta}^+(y)} \right) Z[\bar{\eta}, \eta] \Big|_{\bar{\eta}=\eta=0} \\ &= S^{++}(0)^2 - S^{++}(x-y) S^{++}(y-x), \end{aligned} \quad (5.6a)$$

$$\begin{aligned} \langle \mathcal{T}_C \bar{q}^+(x) q^+(x) \bar{q}^-(y) q^-(y) \rangle &= \frac{1}{Z_0} \left( \frac{i\delta}{\delta\eta^+(x)} \right) \left( \frac{-i\delta}{\delta\bar{\eta}^+(x)} \right) \left( \frac{i\delta}{\delta\eta^-(y)} \right) \left( \frac{-i\delta}{\delta\bar{\eta}^-(y)} \right) Z[\bar{\eta}, \eta] \Big|_{\bar{\eta}=\eta=0} \\ &= S^{--}(0) S^{++}(0) - S^{+-}(x-y) S^{-+}(y-x), \end{aligned} \quad (5.6b)$$

$$\begin{aligned} \langle \mathcal{T}_C \bar{q}^-(x) q^-(x) \bar{q}^+(y) q^+(y) \rangle &= \frac{1}{Z_0} \left( \frac{i\delta}{\delta\eta^-(x)} \right) \left( \frac{-i\delta}{\delta\bar{\eta}^-(x)} \right) \left( \frac{i\delta}{\delta\eta^+(y)} \right) \left( \frac{-i\delta}{\delta\bar{\eta}^+(y)} \right) Z[\bar{\eta}, \eta] \Big|_{\bar{\eta}=\eta=0} \\ &= S^{++}(0) S^{--}(0) - S^{-+}(x-y) S^{+-}(y-x), \end{aligned} \quad (5.6c)$$

$$\begin{aligned} \langle \mathcal{T}_C \bar{q}^-(x) q^-(x) \bar{q}^-(y) q^-(y) \rangle &= \frac{1}{Z_0} \left( \frac{i\delta}{\delta\eta^-(x)} \right) \left( \frac{-i\delta}{\delta\bar{\eta}^-(x)} \right) \left( \frac{i\delta}{\delta\eta^-(y)} \right) \left( \frac{-i\delta}{\delta\bar{\eta}^-(y)} \right) Z[\bar{\eta}, \eta] \Big|_{\bar{\eta}=\eta=0} \\ &= S^{--}(0)^2 - S^{--}(x-y) S^{--}(y-x). \end{aligned} \quad (5.6d)$$

Then, neglecting all two-loop contributions, which cancel for  $S^{++}(0) = S^{--}(0)$ ,

$$\begin{aligned} iS_{\text{IF}}[\sigma^+, \sigma^-] &= -\frac{1}{2} g^2 \int d^4x \int d^4y \left( -S^{++}(x-y) S^{++}(y-x) \sigma^+(x) \sigma^+(y) \right. \\ &\quad \left. + S^{+-}(x-y) S^{-+}(y-x) \sigma^+(x) \sigma^-(y) \right. \\ &\quad \left. + S^{-+}(x-y) S^{+-}(y-x) \sigma^-(x) \sigma^+(y) \right. \\ &\quad \left. - S^{--}(x-y) S^{--}(y-x) \sigma^-(x) \sigma^-(y) \right). \end{aligned} \quad (5.7)$$

The structure of the influence functional becomes most obvious when rewriting it in terms of the center and relative field variable

$$\bar{\sigma} = \frac{1}{2} (\sigma^+ + \sigma^-), \quad (5.8a)$$

$$\Delta\sigma = \sigma^+ - \sigma^-. \quad (5.8b)$$

We obtain

$$\begin{aligned}
 iS_{\text{IF}}[\bar{\sigma}, \Delta\sigma] = & -\frac{1}{2}g^2 \int d^4x \int d^4y \times \\
 & \times \left[ \bar{\sigma}(x)\bar{\sigma}(y) \left( -S^{++}(x-y)S^{++}(y-x) + S^{+-}(x-y)S^{+-}(y-x) \right. \right. \\
 & \quad \left. \left. + S^{-+}(x-y)S^{-+}(y-x) - S^{--}(x-y)S^{--}(y-x) \right) \right. \\
 & + \frac{1}{2}\Delta\sigma(x)\bar{\sigma}(y) \left( -S^{++}(x-y)S^{++}(y-x) + S^{+-}(x-y)S^{+-}(y-x) \right. \\
 & \quad \left. - S^{-+}(x-y)S^{-+}(y-x) + S^{--}(x-y)S^{--}(y-x) \right) \\
 & + \frac{1}{2}\Delta\sigma(y)\bar{\sigma}(x) \left( -S^{++}(x-y)S^{++}(y-x) - S^{+-}(x-y)S^{+-}(y-x) \right. \\
 & \quad \left. + S^{-+}(x-y)S^{-+}(y-x) + S^{--}(x-y)S^{--}(y-x) \right) \\
 & \left. + \frac{1}{4}\Delta\sigma(x)\bar{\sigma}(y) \left( S^{++}(x-y)S^{++}(y-x) + S^{+-}(x-y)S^{+-}(y-x) \right. \right. \\
 & \quad \left. \left. + S^{-+}(x-y)S^{-+}(y-x) + S^{--}(x-y)S^{--}(y-x) \right) \right]. \tag{5.9}
 \end{aligned}$$

With the relations (3.50a) and (3.50b) the sums of products of propagators in the brackets in (5.9) can be evaluated. We write  $S^{+-} = S^<$  and  $S^{-+} = S^>$ . Finally, we are left with one term that is linear and one term that is quadratic in  $\Delta\sigma$ ,

$$\begin{aligned}
 iS_{\text{IF}}[\bar{\sigma}, \Delta\sigma] = & -g^2 \int d^4x \int_{y_0}^{x_0} d^4y \Delta\sigma(x)\bar{\sigma}(y) \left( S^<(x-y)S^>(y-x) - S^>(x-y)S^<(y-x) \right) \\
 & + \frac{1}{4}g^2 \int d^4x \int d^4y \Delta\sigma(x)\Delta\sigma(y) \left( S^<(x-y)S^>(y-x) + S^>(x-y)S^<(y-x) \right) \\
 = & i \int d^4x D(x)\Delta\sigma(x) - \frac{1}{2} \int d^4x \int d^4y \Delta\sigma(x)\mathcal{N}(x,y)\Delta\sigma(y), \tag{5.10}
 \end{aligned}$$

with the damping kernel

$$D(x) = ig^2 \int_{y_0}^{x_0} d^4y \bar{\sigma}(y) \left( S^<(x-y)S^>(y-x) - S^>(x-y)S^<(y-x) \right), \tag{5.11}$$

and the noise kernel

$$\mathcal{N}(x,y) = -\frac{1}{2}g^2 \left( S^<(x-y)S^>(y-x) + S^>(x-y)S^<(y-x) \right). \tag{5.12}$$

The influence functional

$$S_{\text{IF}}[\bar{\sigma}, \Delta\sigma] = \int d^4x D(x)\Delta\sigma(x) + \frac{i}{2} \int d^4x \int d^4y \Delta\sigma(x)\mathcal{N}(x,y)\Delta\sigma(y), \tag{5.13}$$

has an imaginary part. It is exactly this term that causes the underlying quantum system to decohere and allows for a classical description of the dynamics of the system. This means that every trajectory can be assigned a unique probability. For these trajectories the relative field variable vanishes  $\Delta\sigma(x) = 0$ , because trajectories that have a significantly large  $\Delta\sigma$  are exponentially suppressed. Together with the coarse graining of the environment, the decoherence leads to the quantum-to-classical transition of the system. Fluctuations in the classical equation of motion appear as a remnant of coarse graining and decoherence [Hu92, Hu93, Gel93, Cal95a, Cal95b].

### 5.1.2. The noise kernel and fluctuations

At first glance, the noise kernel seems to be redundant, because it is quadratic in  $\Delta\sigma(x)$  and, therefore, vanishes after variation with respect to  $\Delta\sigma(x)$ . However, the semiclassical concept of obtaining the equation of motion from varying the action is well-defined only for real actions. Here, the noise kernel introduces an imaginary part, which we need to rewrite in order to obtain a real action. This is done by introducing a new stochastic field  $\xi$ , which discloses the physical significance of the noise kernel. The imaginary part of  $S_{\text{IF}}$  can be rewritten by making use of the Gauss integral evaluation

$$\exp\left(-\frac{1}{2}\int d^4x \int d^4y \Delta\sigma(x) \mathcal{N}(x, y) \Delta\sigma(y)\right) = \int \mathcal{D}\xi P[\xi] \exp\left(i \int d^4x \xi(x) \Delta\sigma(x)\right). \quad (5.14)$$

Here, the stochastic weight  $P[\xi]$  is a Gauss distribution

$$P[\xi] = N' \exp\left(-\frac{1}{2}\int d^4x \int d^4y \xi(x) \mathcal{N}^{-1}(x, y) \xi(y)\right), \quad (5.15)$$

with a normalization constant  $N'$ . Then, the stochastic field  $\xi$  is fully determined by its first two moments, a vanishing expectation value and the variance:

$$\langle \xi(x) \rangle = 0, \quad (5.16a)$$

$$\langle \xi(x) \xi(y) \rangle = \mathcal{N}(x, y). \quad (5.16b)$$

This stochastic force  $\xi$  plays an essential role in the equilibration of the classical fields, as was discussed in general terms in section 3.3. By the dissipation-fluctuation theorem it enforces the relaxation to the correct equilibrium state.

### 5.1.3. The semiclassical equations of motion

The semiclassical equations of motion for the sigma field are obtained from the stochastic influence functional  $\tilde{S}_{\text{IF}}$ , defined in

$$\exp(iS_{\text{IF}}) = \int \mathcal{D}\xi P[\xi] \exp\left(i \int d^4x (D(x) + \xi(x)) \Delta\sigma(x)\right) = \int \mathcal{D}\xi P[\xi] \exp(i\tilde{S}_{\text{IF}}), \quad (5.17)$$

by varying

$$S_{\text{cl}}[\sigma^+] - S_{\text{cl}}[\sigma^-] + \tilde{S}_{\text{IF}}[\bar{\sigma}, \Delta\sigma] \quad (5.18)$$

with respect to  $\Delta\sigma$  and then setting  $\Delta\sigma = 0$ . From the classical action one obtains

$$\left. \frac{\delta(S_{\text{cl}}[\sigma^+] - S_{\text{cl}}[\sigma^-])}{\delta\Delta\sigma} \right|_{\Delta\sigma=0} = \frac{\delta S_{\text{cl}}[\bar{\sigma}]}{\delta\bar{\sigma}}. \quad (5.19)$$

The semiclassical Langevin equation for the sigma field is

$$-\frac{\delta S_{\text{cl}}[\bar{\sigma}]}{\delta\bar{\sigma}} - D = \zeta. \quad (5.20)$$

Note that the damping kernel  $D$  generally depends on  $\bar{\sigma}$ , too. We also note that in the perturbative approach to the influence functional we do not obtain the thermal mass correction of the sigma field. For the calculation of the mass correction one needs to include further information. For example, it is possible to find this term by directly calculating the equation of motion as it was done in [Ris98] for  $\phi^4$  theory.

## 5.2. The 2PI effective action for the linear sigma model with constituent quarks

The formalism of the 2PI effective action was introduced in section (3.6). It is well-suited for our purpose because it yields a selfconsistent and thermodynamically consistent description of the entire system. In the scheme that is developed in the following we want to make the semiclassical approximation for the sigma field. We restrict ourselves to the sigma mean-field and do not include the propagator of the sigma field. We, thus, work with a theory of fermions coupled to an external mean field. One often defines the mean field as an average over quantum and thermal fluctuations in which case there is neither damping nor noise. Within the 2PI effective action formalism the mean field is obtained from an integration over quantum fluctuations only and thus still contains the necessary information about dissipation and noise. Since the quarks have a vanishing mean field, they are represented by their propagators. Then the 2PI effective action is a functional of the sigma mean-field  $\sigma^a(x)$  and the full quark propagator  $S^{ab}(x, y)$

$$\Gamma[\sigma, S] = S_{\text{cl}}[\sigma] - i\text{Tr} \ln S^{-1} - i\text{Tr} S_0^{-1} S + \Gamma_2[\sigma, S], \quad (5.21)$$

where the trace operation includes  $\int_C d^4x \sum_{\text{flavor}} \sum_{\text{Dirac}}$  and  $S_{\text{cl}}[\sigma]$  is the classical action of the sigma mean-field. The free propagator for a fermion mass  $m_f$  reads

$$(i\not{\partial} - m_f)S_0^{ab}(x, y) = -i\delta_C^{ab}(x - y), \quad (5.22)$$

by which it is defined up to the boundary conditions. The free fermionic propagators on the contour are given in equations (3.61). The first three terms in (5.21) are the one-loop results. The additional term  $\Gamma_2[\sigma, S]$  is the sum of all 2PI diagrams.

In the absence of external sources the equation of motion for the sigma mean-field  $\sigma^a$ , obtained by variation of the effective action (5.21) with respect to  $\sigma^a$ , is

$$\frac{\delta\Gamma[\sigma, S]}{\delta\sigma^a} = 0, \quad (5.23)$$

and for the full quark propagator  $S^{ab}$ , obtained by variation with respect to  $S^{ab}$ ,

$$\frac{\delta\Gamma[\sigma, S]}{\delta S^{ab}} = 0. \quad (5.24)$$

The proper self energy of the quarks is

$$\Sigma^{ab}(x, y; S) = S_0^{ab}(x, y)^{-1} - S^{ab}(x, y)^{-1}. \quad (5.25)$$

Inserting the self energy (5.25) into the effective potential (5.21) and neglecting constant terms gives

$$\Gamma[\sigma, S] = S_{\text{cl}}[\sigma] - i\text{Tr} \ln S^{-1} - i\text{Tr} \Sigma S + \Gamma_2[\sigma, S]. \quad (5.26)$$

With  $\delta\Sigma/\delta S = 1/S^2$ , the variation (5.24) reads

$$-i\Sigma^{ab}(x, y) = -\frac{\delta\Gamma_2[\sigma, S]}{\delta S^{ab}(x, y)}. \quad (5.27)$$

This means that the equation of motion for the full quark propagator  $S^{ab}$  (5.24) is equivalent to equation (5.25), where the self energy is given by the expression (5.27). From equation (5.25) we obtain the Schwinger-Dyson equation

$$S_0^{-1}S - \Sigma S = 1, \quad (5.28)$$

which is in explicit terms

$$(i\partial - m_f)S^{ab}(x, y) - i \int_C d^4z \Sigma^{ac}(x, z)S^{cb}(z, y) = i\delta_C^{ab}(x - y). \quad (5.29)$$

Since implicit dependencies are not varied, the equation of motion for the sigma mean-field is

$$-\frac{\delta S_{\text{cl}}[\sigma]}{\delta\sigma^a} = \frac{\delta\Gamma_2[\sigma, S]}{\delta\sigma^a}. \quad (5.30)$$

To solve the equation of motion for the quark propagator (5.29) and for the sigma mean-field (5.30) we need the explicit form of the self energy and with expression (5.27) the explicit form of  $\Gamma_2[\sigma, S]$ .

### 5.2.1. The explicit form of $\Gamma_2[\sigma, S]$ and the self energy

Since all graphs with more than one mean-field insertion are necessarily two-particle reducible, they are not included in  $\Gamma_2[\sigma, S]$ . A single mean-field insertion represents them all, and we have to calculate only one diagram within the closed time path formalism, see figure 5.1. For the inclusion of such types of diagrams in the  $\Phi$ -functional approach see [Leu07]. Note, that this is exact within the mean-field approximation for the sigma field, because there are no quark self-interactions in the theory that could contribute to the 2PI effective action. It consists of one graph with a +- and one with a --vertex. The corresponding Feynman rules are given in appendix E.

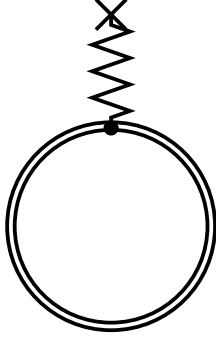


Figure 5.1.: The only diagram for  $\Gamma_2[\sigma, S]$ .

The diagram is

$$\Gamma_2[\sigma, S] = g \int_{\mathcal{C}} d^4x \operatorname{tr} (S^{++}(x, x)\sigma^+(x) + S^{--}(x, x)\sigma^-(x)), \quad (5.31)$$

with the trace operation  $\operatorname{tr} = \sum_{\text{flavor}} \sum_{\text{Dirac}}$ . Then, the self-energy from (5.27) reads

$$\Sigma^{ab}(x, y) = -ig\delta_{\mathcal{C}}^{ab}(x - y)\sigma^b(x). \quad (5.32)$$

### 5.2.2. The coupled equations of motion

With the explicit form of the self energy (5.32) the Schwinger-Dyson equation (5.29)

$$(i\cancel{\partial} - m_f)S^{ab}(x, y) - g\sigma^a(x)S^{ab}(x, y) = i\delta_{\mathcal{C}}^{ab}(x - y), \quad (5.33)$$

and the field equation for the sigma mean-field

$$-\frac{\delta S_{\text{cl}}[\sigma]}{\delta \sigma^a} = g \operatorname{tr} S^{aa}(x, x) \quad (5.34)$$

are a coupled set of equations. In principle, we have to solve (5.33) and put the solution for the full propagator  $S^{ab}$  into (5.34). Due to the space-time dependence of  $\sigma^a$  in (5.33) it is generally nontrivial to find the solution for  $S^{ab}$ , which is exact for the given form of  $\Gamma_2$  (5.31). We, therefore, have to approximate the full propagator. This is a crucial aspect because only the full approach of the 2PI effective action is a conserving, selfconsistent and thermodynamically consistent approximation to the exact quantum field theory [BayKad61, Bay62, Iva99]. For exact solutions of coupled propagator and mean-field dynamics for some model systems, see e.g. [Ber02, Juc04a, Juc04b].

We split the mean field into one component  $\sigma_0^a$  that has a slow variation compared to  $S^{ab}$  and a fluctuation part  $\delta\sigma^a$ , which we assume to be small. We will later disclose the actual meaning of this splitting

$$\sigma^a(x) = \sigma_0^a(x) + \delta\sigma^a(x). \quad (5.35)$$

We also expand the full propagator around the thermal propagator

$$S^{ab}(x, y) = S_{\text{th}}^{ab}(x, y) + \delta S^{ab}(x, y) + \delta^2 S^{ab}(x, y). \quad (5.36)$$

Then for the various orders of the expansion the Schwinger-Dyson equation reads

$$\mathcal{O}(0) : (i\cancel{\partial} - m_f)S_{\text{th}}^{ab}(x, y) - g\sigma_0^a(x)S_{\text{th}}^{ab}(x, y) = i\delta_{\mathcal{C}}^{ab}(x - y) \quad (5.37a)$$

$$\mathcal{O}(1) : (i\cancel{\partial} - m_f)\delta S^{ab}(x, y) - g\sigma_0^a(x)\delta S^{ab}(x, y) - g\delta\sigma^a(x)S_{\text{th}}^{ab}(x, y) = 0 \quad (5.37b)$$

$$\mathcal{O}(2) : (i\cancel{\partial} - m_f)\delta^2 S^{ab}(x, y) - g\sigma_0^a(x)\delta^2 S^{ab}(x, y) - g\delta\sigma^a(x)\delta S^{ab}(x, y) = 0. \quad (5.37c)$$

From the solution of (5.37a), we see that the  $\sigma_0^a$  part of the sigma field generates the mass of the quarks dynamically  $m = m_f + g\sigma_0$ . As already noted the idea is that the  $x$ -dependence of  $\sigma_0$  is weak compared to the  $x$ -dependence of the propagator  $S$ . We identify the spatial



and temporal variation of sigma with the corresponding variation of the local temperature in the fluid dynamic description of the quarks and antiquarks. In that spirit the solution of equation (5.37a) is given by (3.61). From (5.37b)

$$\delta S^{ab}(x, y) = -ig \int_C d^4z S_{\text{th}}^{ac}(x, z) \delta\sigma^c(z) S_{\text{th}}^{cb}(z, y), \quad (5.38)$$

and from (5.37c)

$$\delta^2 S^{ab}(x, y) = -g^2 \int_C d^4z d^4z' S_{\text{th}}^{ac}(x, z') \delta\sigma^c(z') S_{\text{th}}^{cd}(z', z) \delta\sigma^d(z) S_{\text{th}}^{db}(z, y). \quad (5.39)$$

The approximated propagator (5.36) rewritten in center and relative variables

$$\delta\bar{\sigma} = \frac{1}{2}(\delta\sigma^+ + \delta\sigma^-) \quad (5.40a)$$

$$\Delta\delta\sigma = \delta\sigma^+ - \delta\sigma^- \quad (5.40b)$$

yields

$$\begin{aligned} \text{tr} S^{ab}(x, y) &= \text{tr} S_{\text{th}}^{ab}(x, y) + ig \int_{y_0}^{x_0} d^4y \delta\bar{\sigma}(y) \left( S^<(x-y) S^>(y-x) - S^>(x-y) S^<(y-x) \right) \\ &\quad - \frac{i}{2}g \int d^4y \Delta\delta\bar{\sigma}(y) \left( S^<(x-y) S^>(y-x) + S^>(x-y) S^<(y-x) \right) \\ &\stackrel{\Delta\delta\sigma=0}{=} \text{tr} S_{\text{th}}^{ab}(x, y) + \frac{D(x)}{g}. \end{aligned} \quad (5.41)$$

In the last step we identified the same damping kernel as in (5.11). The term similar to the noise kernel in (5.12) vanishes by taking  $\Delta\delta\sigma = 0$ . In order to recover the noise kernel we need to calculate the effective action  $\Gamma[\sigma, S]$  explicitly from (5.21) with the approximations of the propagator (5.36) and (5.38-5.39). It is

$$\begin{aligned} \Gamma[\sigma, S] &= S_{\text{cl}}[\sigma] + g \text{tr} S_{\text{th}}^{++}(x, x) \Delta\sigma(x) \\ &\quad + \frac{i}{2}g^2 \int d^4x \int_{y_0}^{x_0} d^4y \Delta\delta\sigma(x) \delta\bar{\sigma}(y) \left( S^<(x-y) S^>(y-x) - S^>(x-y) S^<(y-x) \right) \\ &\quad - \frac{i}{4}g^2 \int d^4x \int d^4y \Delta\delta\sigma(x) \Delta\delta\sigma(y) \left( S^<(x-y) S^>(y-x) + S^>(x-y) S^<(y-x) \right) \end{aligned} \quad (5.42)$$

We can readily identify the same damping (5.11) and noise kernel (5.12) as we found in the influence functional approach.

The equation of motion for the sigma mean-field obtained by varying  $\Gamma[\sigma, S]$  with respect to  $\Delta\sigma$  is

$$-\frac{\delta S_{\text{cl}}[\sigma, S]}{\delta\sigma^a} = g \text{tr} S_{\text{th}}^{++}(x, x) + D(x) + \xi(x), \quad (5.43)$$

where we introduced the same stochastic field as was discussed in section 5.1.2. Note, that within the 2PI effective action we obtain the standard mean-field result as the first term on the right hand side of equation (5.43), which is formally of order  $g$ , while the damping and the noise kernel are of order  $g^2$ . Therefore, the standard mean-field result is the lowest order contribution.

### 5.2.3. The thermodynamic quantities of the quark fluid

Using the 2PI effective action we can include the local equilibrium properties of the quark fluid. In (5.42) the calculations were performed along the real-time contour from figure 3.2. For the calculation of equilibrium properties of a thermodynamic system we cannot, however, neglect the imaginary-time path  $\mathcal{C}_3$ . In the imaginary-time formalism the thermodynamic potential can be evaluated in a diagrammatic expansion [Kap94]. The perturbative expansion of the thermodynamic potential in real-time formalism is more difficult. The Bogoliubov assumption of an uncorrelated initial state [Bog62] leads to the factorization of the generating functional [Das97]. For the derivation of the Green's functions and the dynamics of the system the imaginary-time path  $\mathcal{C}_3$  of the contour can be neglected. To obtain the correct equilibrium properties of the coupled system it must be included since it contributes to the pressure

$$p = \frac{T}{V} \left( \ln Z_C[J_C = 0] + \ln Z_3[J_3 = 0] \right) = -\Gamma[\sigma, S] + \frac{T}{V} \ln Z_3[J_3 = 0]. \quad (5.44)$$

In equilibrium with  $\Gamma[\sigma, S]|_{\Delta\sigma=0} = 0$  the full pressure is given by the imaginary time path  $\mathcal{C}_3$  of the full contour. Due to the Bogoliubov initial conditions [Bog62] we are left only with the one-loop effective potential. More advanced techniques are required to set up a consistent real-time perturbation expansion for equilibrium properties [Lan86]. Since we restricted the model to the mean-field dynamics higher loop corrections to the pressure associated with propagators of the sigma field are discarded in the entire setting. This issue was briefly mentioned in the beginning of this section. Here, it assures that we capture the full equilibrium properties by the mean-field pressure calculated in section 4.1.1.

## 5.3. The equation of motion for the sigma field

We now turn to the explicit calculation of the terms in the equation of motion for the sigma field (5.43). On the right hand side, it includes the lowest order contribution, a damping term and the correlation of the noise.

### 5.3.1. Lowest order

For the lowest order contribution we calculate the first term on the right hand side of equation (5.43) with the thermal part of the free quark propagator (3.61a)

$$\begin{aligned} g \operatorname{tr} S^{++}(x, x) &= ig \int \frac{d^4 p}{(2\pi)^4} \operatorname{tr} 2i\pi n_F(|p^0|) (\gamma^\mu p_\mu + m_q(x)) \delta(p^2 - m_q^2) \\ &= -2d_q g^2 \sigma(x) \int \frac{d^3 p}{(2\pi)^3} \frac{n_F(E_p)}{E_p} \\ &= -g\rho_s(x) \end{aligned} \quad (5.45)$$

with the dynamically generated quark mass  $m_q(x) = g\sigma(x)$  and the degeneracy factor  $d_q = 12$  from the trace over flavor, color and spin. The energy of the quarks is  $E_p =$

$\sqrt{\vec{p}^2 + m_q^2}$ . We see that to this order the equation of motion does not include any terms leading to damping and noise. It is the same classical equation of motion with the scalar density (4.9a) that was used in chapter 4.

### 5.3.2. The damping kernel

The explicit form of the damping kernel  $D(x)$  is given in equation (5.11). For its evaluation we define the following quantity

$$\mathcal{M}(x-y) = \text{tr} (S^<(x-y)S^>(y-x) - S^>(x-y)S^<(y-x)) . \quad (5.46)$$

Its Fourier transform is

$$\mathcal{M}(\omega, \mathbf{k}) = \int \frac{d^4 p}{(2\pi)^4} \text{tr} (S^<(p+k)S^>(p) - S^>(p+k)S^<(p)) . \quad (5.47)$$

To explicitly evaluate  $\mathcal{M}(\omega, \mathbf{k})$  in (5.47) we need the trace over flavor, color and spin for products of propagators. This is obtained from the relations for the Dirac  $\gamma$ -matrices

$$\text{tr} \left( (\gamma^\mu (p_\mu + k_\mu) - m_q) (\gamma^\nu p_\nu - m_q) \right) = 4d_q \left( (p^\mu + k^\mu) p_\mu + m_q^2 \right) . \quad (5.48)$$

The integration over  $p^0$  is readily performed by the use of the delta functions from (3.61b) and (3.61c). With  $\Theta(-E_p) = 0$  and  $\Theta(E_p) = 1$ , it gives

$$\begin{aligned} \mathcal{M}(\omega, \mathbf{k}) = & -4\pi^2 d_q \int \frac{d^3 p}{(2\pi)^4} \frac{1}{E_p E_{k+p}} \times \\ & \times \left( (-E_p \omega - \mathbf{k} \cdot \mathbf{p} + 2m_q) (\delta(\omega - E_p + E_{k+p}) + \delta(\omega - E_p - E_{k+p})) \times \right. \\ & \times (n_F(E_p) \Theta(-\omega + E_p) + \Theta(\omega - E_p) - \Theta(\omega - E_p) - n_F(|\omega - E_p|)) \\ & + (E_p \omega - \mathbf{k} \cdot \mathbf{p} + 2m_q) (\delta(\omega + E_p + E_{k+p}) + \delta(\omega + E_p - E_{k+p})) \times \\ & \left. \times (n_F(E_p) \Theta(-\omega - E_p) - \Theta(-\omega - E_p) - \Theta(\omega + E_p) + n_F(|\omega + E_p|)) \right) . \end{aligned} \quad (5.49)$$

We can now sort the various scattering processes according to their energy balance, given

by the delta functions, in order to make the physical processes more obvious. We obtain

$$\begin{aligned}
 \mathcal{M}(\omega, \mathbf{k}) = & -\frac{d_q}{4\pi^2} \int d^3p \frac{1}{E_p E_{k+p}} \times \\
 & \times \left( (-E_p + E_{k+p}) E_p + 2m_q^2 - \mathbf{k} \cdot \mathbf{p} \right) \times \\
 & \times \left\{ \delta(\omega + E_p + E_{k+p}) (n_F(E_{k+p}) n_F(E_p) - (1 - n_F(E_p))(1 - n_F(E_{k+p}))) \right. \\
 & \quad \left. + \delta(\omega - E_p - E_{k+p}) ((1 - n_F(E_p))(1 - n_F(E_{k+p})) - n_F(E_{k+p}) n_F(E_p)) \right\} \\
 & + ((-E_p + E_{k+p}) E_p + 2m_q^2 - \mathbf{k} \cdot \mathbf{p}) \times \\
 & \times \left\{ \delta(\omega + E_p - E_{k+p}) ((1 - n_F(E_p)) n_F(E_{k+p}) - n_F(E_p) (1 - n_F(E_{k+p}))) \right. \\
 & \quad \left. + \delta(\omega - E_p + E_{k+p}) (n_F(E_p) (1 - n_F(E_{k+p})) - (1 - n_F(E_p)) n_F(E_{k+p})) \right\}
 \end{aligned} \tag{5.50}$$

Here, one sees the antisymmetric property  $\mathcal{M}(-\omega, \mathbf{k}) = -\mathcal{M}(\omega, \mathbf{k})$ . The structure of  $\mathcal{M}(\omega, \mathbf{k})$  is clear. It describes the difference between a gain and a loss term. The term  $n_F(E_{k+p}) n_F(E_p)$  is the probability for a quark-antiquark pair to form a sigma mode  $\bar{q}q \rightarrow \sigma$ , and the term  $(1 - n_F(E_p))(1 - n_F(E_{k+p}))$  is the statistical weight of the decay of a sigma mode to a quark-antiquark pair  $\sigma \rightarrow \bar{q}q$ . The mixed terms  $(1 - n_F(E_p)) n_F(E_{k+p})$  describe the scattering of a quark (antiquark) off a sigma mode to form an antiquark (quark). For each delta function, the ratio of the loss to the gain term is

$$\frac{\Gamma_{\text{loss}}}{\Gamma_{\text{gain}}} = \exp\left(\frac{\omega}{T}\right). \tag{5.51}$$

This is the detailed balance relation for the thermal quarks and antiquarks. For fixed quark masses the delta functions constrain the allowed scattering processes [Wel83].

The damping kernel is then

$$\begin{aligned}
 D(x) &= ig^2 \int_{y_0}^{x_0} d^4y \mathcal{M}(x - y) \delta\bar{\sigma}(y) \\
 &= ig^2 \int_{y_0}^{x_0} d^4y \int \frac{d^4k}{(2\pi)^4} \exp(-ik(x - y)) \mathcal{M}(\omega, \mathbf{k}) \delta\bar{\sigma}(y),
 \end{aligned} \tag{5.52}$$

where we take the spatial Fourier transform

$$\delta\bar{\sigma}(y_0, \mathbf{k}) = \int d^3y \exp(-i\mathbf{k} \cdot \mathbf{y}) \delta\bar{\sigma}(y_0, \mathbf{y}). \tag{5.53}$$

To simplify further calculations we make the substitution  $y_0 = x_0 - \tau$  and assume that the initial time  $x_0 - y_0 \rightarrow -\infty$ , such that  $\tau \rightarrow \infty$ . Then

$$D(x) = ig^2 \int \frac{d^3k}{(2\pi)^3} \exp(i\mathbf{k} \cdot \mathbf{x}) \int_0^\infty d\tau \int \frac{d\omega}{(2\pi)} \exp(-i\omega\tau) \mathcal{M}(\omega, \mathbf{k}) \delta\bar{\sigma}(x_0 - \tau, \mathbf{k}). \tag{5.54}$$

We see that the sigma mean-field now depends on the history  $t < x_0$ . It is known that an instantaneous approximation to this time dependence is too constraining because the dissipative terms vanish [Mor86, Gle93]. We assume that the effect of the past can be described by harmonic oscillations around a constant value

$$\bar{\sigma}(t - \tau, \mathbf{k}) \simeq a(t) \cos(E_k \tau) + b(t) \sin(E_k \tau). \quad (5.55)$$

This is the linear harmonic approximation which is also used in [Gre97, Ris98]. Here, we obtain the coefficients from the requirements at  $\tau = 0$

$$\bar{\sigma}(t - \tau, \mathbf{k})|_{\tau=0} = \bar{\sigma}_0(t, \mathbf{k}) \quad \Rightarrow \quad a(t) = \bar{\sigma}_0(t, \mathbf{k}) \quad (5.56)$$

$$\frac{\partial \bar{\sigma}(t - \tau, \mathbf{k})}{\partial \tau}|_{\tau=0} = -\frac{\partial \bar{\sigma}(t, \mathbf{k})}{\partial t} \quad \Rightarrow \quad b(t) = -\frac{1}{E_k} \partial_t \bar{\sigma}(t, \mathbf{k}). \quad (5.57)$$

Then, we find that

$$\begin{aligned} \bar{\sigma}(t - \tau, \mathbf{k}) &\simeq \sigma_0(t, \mathbf{k}) \cos(E_k \tau) - \frac{1}{E_k} \partial_t \bar{\sigma}(t, \mathbf{k}) \sin(E_k \tau) \\ &= \sigma_0(t, \mathbf{k}) + \delta \bar{\sigma}(t, \mathbf{k}). \end{aligned} \quad (5.58)$$

We now see the meaning of the splitting of  $\sigma(x)$  that was done in (5.35) and

$$\delta \bar{\sigma}(t, \mathbf{k}) = \sigma_0(t, \mathbf{k}) (\cos(E_k \tau) - 1) - \frac{1}{E_k} \partial_t \bar{\sigma}(t, \mathbf{k}) \sin(E_k \tau). \quad (5.59)$$

The first term gives a mass shift for the sigma field, which is only a correction to the leading order result (5.45). We assume that this correction is small as  $\cos(E_k \tau) - 1 \simeq 0$ . Then, we can replace the fluctuation  $\delta \bar{\sigma}(t, \mathbf{k})$  by the sine-modulated time derivative of the full field. With this we can evaluate the integral over the history and obtain quantities that are local in time. Such an approximation will later be used for the derivation of the noise correlator, too. Writing

$$\delta \bar{\sigma}(t - \tau, \mathbf{k}) = -\frac{1}{2iE_k} (\exp(iE_k \tau) - \exp(-iE_k \tau)) \partial_t \bar{\sigma}(t, \mathbf{k}) \quad (5.60)$$

and using the relation

$$\int_0^\infty d\tau \exp(i(\omega - E)\tau) = i\mathcal{P} \frac{1}{\omega - E} + \pi \delta(\omega - E) \quad (5.61)$$

we arrive at

$$\begin{aligned} D(x) &= -g^2 \int \frac{d^3 k}{(2\pi)^3} \exp(i\mathbf{k} \cdot \mathbf{x}) \int \frac{d\omega}{(2\pi)} \mathcal{M}(\omega, \mathbf{k}) \times \\ &\quad \times \frac{1}{2E_k} \left( i\mathcal{P} \frac{1}{E_k - \omega} + \pi \delta(E_k - \omega) - i\mathcal{P} \frac{1}{-\omega - E_k} - \pi \delta(-\omega - E_k) \right) \partial_t \bar{\sigma}(t, \mathbf{k}) \\ &= -g^2 \int \frac{d^3 k}{(2\pi)^3} \exp(i\mathbf{k} \cdot \mathbf{x}) \int \frac{d\omega}{(2\pi)} \mathcal{M}(\omega, \mathbf{k}) \frac{\pi}{E_k} \delta(\omega - E_k) \partial_t \bar{\sigma}(t, \mathbf{k}). \end{aligned} \quad (5.62)$$

## 5. Selfconsistent system-heat bath coupling

---

In the final step, we used that the principle integral terms cancel by applying the antisymmetry of  $\mathcal{M}(\omega, \mathbf{k})$ . We obtain for the damping kernel

$$D(x) = -g^2 \int \frac{d^3k}{(2\pi)^3} \exp(i\mathbf{k} \cdot \mathbf{x}) \frac{1}{2E_k} \mathcal{M}(E_k, \mathbf{k}) \partial_t \bar{\sigma}(t, \mathbf{k}). \quad (5.63)$$

$\mathcal{M}(\omega, \mathbf{k})$  contains the on-shell reaction rate of the processes given in equation (5.50). They lead to the dissipative part of the equation of motion.

In a perturbative expansion the damping term appears first at next-to-leading order  $g^2$  as one can immediately read off from (5.63). Also the thermal mass correction, which we have neglected is of this order  $g^2$ . However, it is in fact only a correction to the mass of the sigma meson, which gets contributions from leading order (5.45), i.e. from the standard mean-field contribution, and even more from the sigma field potential (4.2).

Being interested in the long-range oscillations of the sigma field we calculate the damping coefficient  $\eta$  for the zero mode,  $\mathbf{k} = 0$ , of the sigma mean-field and approximate  $\mathcal{M}(E_k, \mathbf{k}) \simeq \mathcal{M}(m_\sigma, 0)$ . Then for  $m_\sigma > 2m_q$  only the process  $\sigma \rightarrow \bar{q}q$  and the reverse reaction  $\bar{q}q \rightarrow \sigma$  are kinematically possible. We find

$$\begin{aligned} \mathcal{M}(m_\sigma, 0) &= -\frac{d_q}{2\pi^2} \int d^3p \frac{(m^2 - E_p^2)}{E_p^2} (1 - 2n_F(E_p)) \delta(m_\sigma - 2E_p) \\ &= 2\frac{d_q}{\pi} \left(1 - 2n_F\left(\frac{m_\sigma}{2}\right)\right) \frac{1}{m_\sigma} \left(\frac{m_\sigma^2}{4} - m_q^2\right)^{3/2} \end{aligned} \quad (5.64)$$

With the same approximation  $E_k \simeq m_\sigma$  the damping kernel becomes

$$\begin{aligned} D(x) &\simeq -g^2 \int \frac{d^3k}{(2\pi)^3} \exp(i\mathbf{k} \cdot \mathbf{x}) \frac{1}{2m_\sigma} \mathcal{M}(m_\sigma, 0) \partial_t \bar{\sigma}(t, \mathbf{k}) \\ &= -g^2 \frac{d_q}{\pi} \left(1 - 2n_F\left(\frac{m_\sigma}{2}\right)\right) \frac{1}{m_\sigma^2} \left(\frac{m_\sigma^2}{4} - m_q^2\right)^{3/2} \partial_t \bar{\sigma}(t, \mathbf{x}). \end{aligned} \quad (5.65)$$

With the equation of motion (5.43) the damping coefficient can be identified as

$$\eta = g^2 \frac{d_q}{\pi} \left(1 - 2n_F\left(\frac{m_\sigma}{2}\right)\right) \frac{1}{m_\sigma^2} \left(\frac{m_\sigma^2}{4} - m_q^2\right)^{3/2}. \quad (5.66)$$

We use the equilibrium value of the sigma field in  $m_q = g\sigma$  and the sigma mass  $m_\sigma$  determined in equilibrium via (4.15a). Alternatively one could try to use the actual value of the sigma field for the evaluation of the quark mass. For the determination of the sigma mass one presumably would have to study the (local) response of the sigma field to small variations on the basis of the equation of motion. At the critical point the equilibrium sigma mass becomes very small, but we expect to see fluctuations, which can locally change this effective mass. Concerning a first-order phase transition it is known that in nonequilibrium in the spinodal region the sigma mass becomes small, too, or even tachyonic. In principle, the explicit dependence of  $\eta = \eta(\sigma, T)$  could take these nonequilibrium effects into account. Still a lot of subtle questions need to be addressed, e.g., which ‘‘mass’’ should

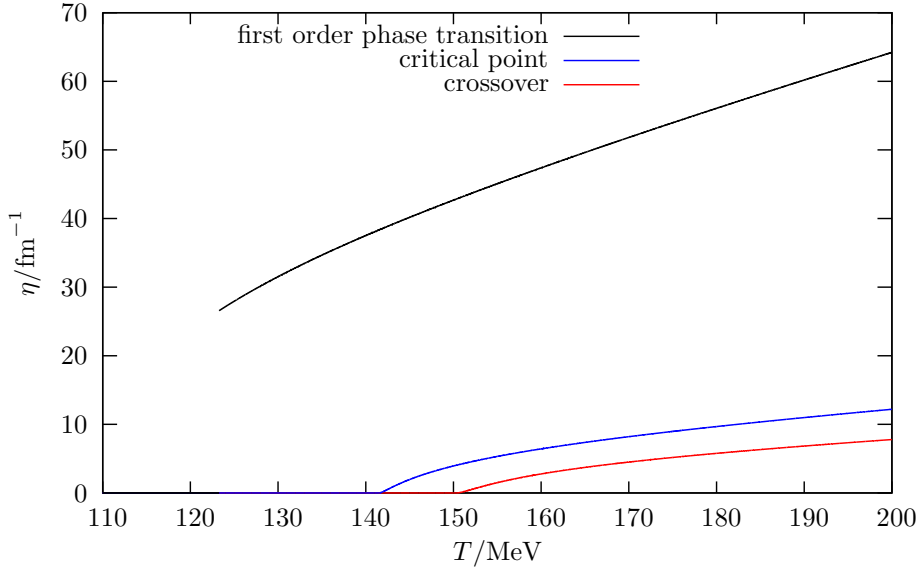


Figure 5.2.: Temperature dependence of the damping coefficient  $\eta$  for a the different couplings  $g = 5.5$ ,  $g = 3.63$  and  $g = 3.3$ , which correspond to scenarios with a first order phase transition, a critical point and a crossover.

enter formula (5.66), if the effective mass becomes tachyonic. In the present work, however, we disregard these issues and use the local equilibrium value for the determination of the sigma and quark masses which in turn enter the damping rate (5.66). Its temperature dependence is shown in figure 5.2 for the three different phase transition scenarios. Since  $\eta \propto g^2$  it is larger in a scenario with a first order phase transition than in a critical point scenario. This issue appears because we work at  $\mu_B = 0$  and tune the strength of the phase transition by different values of the coupling  $g$ . In the linear sigma model with constituent quarks a realistic constituent quark mass is obtained for  $g = 3.3$ . Moreover, the damping is very large compared to the value calculated in the chirally symmetric phase of the linear sigma model [Bir97], with  $\eta = 2.2/\text{fm}$ , and even larger than the damping terms calculated in the broken phase [Ris98]. Though the linear sigma model with constituent quarks does not include confinement the damping coefficient for the zero mode of the sigma field obtained from the interaction with the quarks vanishes below the phase transition. This gives a realistic description at low temperatures. The reason is that at high temperatures the (mostly dynamically generated) quark mass is small and therefore  $m_\sigma > 2m_q$  is satisfied. Hence the reactions  $\sigma \leftrightarrow \bar{q}q$  can take place. With lower temperatures  $m_q$  rises and at some point the reactions, which cause damping and noise in our model are kinematically forbidden. Physically, we expect that at low temperatures the decay and formation processes  $\sigma \leftrightarrow 2\pi$  become important since the pions as quasi-Goldstone bosons of chiral symmetry breaking become very light. In the present approach we have neglected the pions. This will be improved in the future. In that context it is interesting to note that our values for the damping are very large compared to the ones deduced from the linear sigma model *without* quarks [Bir97, Ris98].

### 5.3.3. Correlation of the noise fields

For the derivation of the correlation of the noise fields we perform the same steps for the noise kernel (5.12) as for  $\mathcal{M}(x-y)$ . For the Fourier transform of (5.12) we find analogously

$$\begin{aligned}
 \mathcal{N}(\omega, \mathbf{k}) &= \frac{d_q}{4\pi^2} \int d^3p \frac{1}{E_p E_{k+p}} \times \\
 &\times \left( (-E_p + E_{k+p}) E_p + 2m_q^2 - \mathbf{k} \cdot \mathbf{p} \right) \times \\
 &\times \left\{ \delta(\omega + E_p + E_{k+p}) (n_F(E_{k+p}) n_F(E_p) + (1 - n_F(E_p))(1 - n_F(E_{k+p}))) \right. \\
 &\quad \left. + \delta(\omega - E_p - E_{k+p}) ((1 - n_F(E_p))(1 - n_F(E_{k+p})) + n_F(E_{k+p}) n_F(E_p)) \right\} \cdot \\
 &+ \left( (-E_p + E_{k+p}) E_p + 2m_q^2 - \mathbf{k} \cdot \mathbf{p} \right) \times \\
 &\times \left\{ \delta(\omega + E_p - E_{k+p}) ((1 - n_F(E_p)) n_F(E_{k+p}) + n_F(E_p) (1 - n_F(E_{k+p}))) \right. \\
 &\quad \left. + \delta(\omega - E_p + E_{k+p}) (n_F(E_p) (1 - n_F(E_{k+p})) + (1 - n_F(E_p)) n_F(E_{k+p})) \right\}
 \end{aligned} \tag{5.67}$$

Since the noise term has the same microscopic origin as the damping term it is not surprising that the structure is very similar to (5.50). Especially, we find that  $\mathcal{N}(\omega, \mathbf{k})$  is proportional to the sum of the loss and the gain term of the same scattering processes. The variance of the noise fields is

$$\begin{aligned}
 \langle \tilde{\zeta}(t, \mathbf{x}) \tilde{\zeta}(t', \mathbf{x}') \rangle_{\tilde{\zeta}} &= \mathcal{N}(x, y) \\
 &= \int \frac{d^4k}{(2\pi)^4} \mathcal{N}(\omega, \mathbf{k}) \exp(-i\omega(t-t')) \exp(i\mathbf{k} \cdot (\mathbf{x} - \mathbf{x}')),
 \end{aligned} \tag{5.68}$$

where the average  $\langle \rangle_{\tilde{\zeta}}$  is taken with respect to the Gauss distribution (5.15). With the approximation  $\mathcal{N}(\omega, \mathbf{k}) \simeq \mathcal{N}(m_\sigma, 0)$  the integral over  $\mathbf{k}$  can be evaluated to yield a spatial delta-function, which is replaced by the inverse volume term. Then

$$\begin{aligned}
 \langle \tilde{\zeta}(t) \tilde{\zeta}(t') \rangle_{\tilde{\zeta}} &= \frac{1}{V} \int \frac{d\omega}{2\pi} \mathcal{N}(m_\sigma, 0) \exp(-i\omega(t-t')) \\
 &= \frac{1}{V} \mathcal{N}(m_\sigma, 0) \delta(t-t').
 \end{aligned} \tag{5.69}$$

With

$$2m_F^2(E_p) - 2n_F(E_p) + 1 = (1 - 2n_F(E_p)) \coth\left(\frac{E_p}{T}\right) \tag{5.70}$$

in (5.67) the relation between  $\mathcal{N}(m_\sigma, 0)$  and  $\mathcal{M}(m_\sigma, 0)$  reads

$$\mathcal{N}(m_\sigma, 0) = \mathcal{M}(m_\sigma, 0) \coth\left(\frac{m_\sigma}{2T}\right). \tag{5.71}$$



With the explicit form of  $\mathcal{M}(m_\sigma, 0)$  (5.64) and the damping coefficient (5.66), we finally find

$$\langle \xi(t)\xi(t') \rangle_\xi = \frac{1}{V} \delta(t-t') m_\sigma \eta \coth\left(\frac{m_\sigma}{2T}\right). \quad (5.72)$$

The approximation  $\mathbf{k} = 0$  and  $\omega = m_\sigma$  leads to the delta-function in the noise correlator. The noise fields are only correlated for equal times. This is the white-noise or Markovian approximation. It would be interesting to include the effect of higher modes and see how this leads to additional damping processes. This would require a non-Markovian description, where  $\mathcal{N}(\omega, \mathbf{k})$  and  $\mathcal{M}(\omega, \mathbf{k})$  have a full dependence on  $\mathbf{k}$ . The delta-function in (5.69) is replaced by a noise kernel that includes the memory effects of the history of the noise fields. In addition, the damping kernel in (5.65) is nonlocal. Non-Markovian noises pose a difficult problem for numerical studies [Xu00].

Finally, the equation of motion for the sigma field is

$$\partial_\mu \partial^\mu \sigma + \frac{\delta U}{\delta \sigma} + g\rho_s + \eta \partial_t \bar{\sigma}(x) = \xi(x) \quad (5.73)$$

with the scalar density  $\rho_s$  from (4.9a), the damping coefficient  $\eta$  given in (5.66) and the correlation of the noise field  $\xi$  given in (5.72).

## 5.4. Discussion of the hard-mesonic heat bath

In the above derivation we have restricted the analysis to the sigma mean-field. Besides having neglected the soft pion modes as explicit dynamic degrees of freedom we ignored the influence of the hard chiral modes, which constitute themselves a heat bath for the soft modes of the chiral fields. Due to the interaction with the hard modes, the soft modes undergo additional dissipative processes. Within the influence functional method this separation of the soft and hard modes at a scale  $k_c$  can be easily realized. The chiral fields are split according to

$$\sigma(\mathbf{x}, t) = \tilde{\sigma}(\mathbf{x}, t) + \Sigma(\mathbf{x}, t) \quad (5.74a)$$

$$\vec{\pi}(\mathbf{x}, t) = \vec{\tilde{\pi}}(\mathbf{x}, t) + \vec{\Pi}(\mathbf{x}, t), \quad (5.74b)$$

with the soft modes

$$\tilde{\sigma}(\mathbf{x}, t) = \int \frac{d^3k}{(2\pi)^3} \exp(i\mathbf{k} \cdot \mathbf{x}) \sigma(\mathbf{x}, t) \Theta(k_c - |\mathbf{k}|), \quad (5.75a)$$

$$\vec{\tilde{\pi}}(\mathbf{x}, t) = \int \frac{d^3k}{(2\pi)^3} \exp(i\mathbf{k} \cdot \mathbf{x}) \vec{\pi}(\mathbf{x}, t) \Theta(k_c - |\mathbf{k}|), \quad (5.75b)$$

and the hard modes

$$\Sigma(\mathbf{x}, t) = \int \frac{d^3k}{(2\pi)^3} \exp(i\mathbf{k} \cdot \mathbf{x}) \sigma(\mathbf{x}, t) \Theta(|\mathbf{k}| - k_c), \quad (5.76a)$$

$$\vec{\Pi}(\mathbf{x}, t) = \int \frac{d^3k}{(2\pi)^3} \exp(i\mathbf{k} \cdot \mathbf{x}) \vec{\pi}(\mathbf{x}, t) \Theta(|\mathbf{k}| - k_c). \quad (5.76b)$$

The influence functional can again be calculated from the perturbative expansion (3.96) with  $\Phi = \Sigma, \vec{\Pi}$  and  $\phi = \tilde{\sigma}, \vec{\pi}$ . The general structure is more complicated. There are multiplicative noises, which are field-dependent, accompanied by dissipative terms, which depend on the square of the fields [Gle93]. Calculations of the influence functional for a system of soft modes interacting with a heat bath of hard modes have extensively been studied in  $\phi^4$  theory [Mor86, Gle93, Boy96, Gre97], in gauge theories [Boe95, Son97] and in  $\mathcal{O}(N)$  chiral models [Ris98]. Below the phase transition we know that the sigma field can decay in two pions. This interaction is well known to result in a damping for the sigma field, too.

## 5.5. Energy-momentum conservation

From the Lagrangian (4.1) we calculate the divergence of the total averaged energy momentum tensor. On the operator level we have the Dirac equation for the quark operator and the conjugate for the adjoint operator

$$(i\overleftarrow{\not{D}} - g\sigma)q = 0 \quad \text{and} \quad \bar{q}(i\overrightarrow{\not{D}} + g\sigma) = 0. \quad (5.77)$$

Then, the energy-momentum tensor for the quarks reads

$$T_q^{\mu\nu}(x) = i\bar{q}(x)\gamma^\mu\partial^\nu q(x). \quad (5.78)$$

Taking the divergence yields

$$\begin{aligned} \partial_\mu T_q^{\mu\nu} &= i\bar{q}\overleftarrow{\not{D}}\partial^\nu q + i\bar{q}\partial^\nu\overrightarrow{\not{D}}q \\ &= g\bar{q}q\partial^\nu\sigma, \end{aligned} \quad (5.79)$$

where we used the Dirac equation (5.77). The energy-momentum tensor for the sigma field can easily be derived from the purely mesonic part of the Lagrangian (4.1)

$$\mathcal{L}_\sigma = \frac{1}{2}\partial_\mu\sigma\partial^\mu\sigma - U(\sigma, \vec{\pi} = 0). \quad (5.80)$$

The equation of motion for the sigma field is then found by the variational principle

$$\partial_\mu\partial^\mu\sigma + \frac{\delta U}{\delta\sigma} + g\bar{q}q = 0. \quad (5.81)$$

The divergence of the energy-momentum tensor for the sigma field is

$$\partial_\mu T_\sigma^{\mu\nu} = \left(\partial_\mu\partial^\mu\sigma + \frac{\delta U}{\delta\sigma}\right)\partial^\nu\sigma = -g\bar{q}q\partial^\nu\sigma. \quad (5.82)$$

From (5.79) and (5.82) it is clear that the sum  $\partial_\mu T_q^{\mu\nu} + \partial_\mu T_\sigma^{\mu\nu} = 0$  and, thus, the total energy of the system is conserved. Within the full formalism of the 2PI effective action we can now take the ensemble averages of the calculated quantities. Since the sigma field is treated in mean-field approximation we find with (3.49a),

$$\partial_\mu T_q^{\mu\nu}(x) = -S^{++}(x, x)\partial_x^\nu\sigma(x) \quad (5.83)$$

and

$$\partial_\mu T_\sigma^{\mu\nu} = S^{++}(x, x) \partial_x^\nu \sigma(x). \quad (5.84)$$

The total averaged energy-momentum tensor is, thus, conserved,

$$\partial_\mu T_{\text{total}}^{\mu\nu} = \partial_\mu (T_q^{\mu\nu}(x) + T_\sigma^{\mu\nu}(x)) = 0. \quad (5.85)$$

The situation is more difficult for any approximation to the full propagator due to the space-time dependence of the effective mass generated by the dynamic symmetry breaking. We write the energy-momentum tensor of the quarks in the symmetric form

$$\begin{aligned} T_q^{\mu\nu}(x) &= \frac{i}{4} \bar{q}(x) (\gamma^\mu \partial^\nu q(x) + \gamma^\nu \partial^\mu q(x)) - \frac{i}{4} (\partial^\mu \bar{q}(x) \gamma^\nu + \partial^\nu \bar{q}(x) \gamma^\mu) q(x) \\ &= \frac{i}{4} (\partial_x^\nu \bar{q}(y) q(x)|_{y=x} \gamma^\mu + \partial_x^\mu \bar{q}(y) q(x)|_{y=x} \gamma^\nu \\ &\quad - \partial_y^\mu \bar{q}(y) q(x)|_{x=y} \gamma^\nu - \partial_y^\nu \bar{q}(y) q(x)|_{x=y} \gamma^\mu). \end{aligned} \quad (5.86)$$

After a transformation to center and relative variable  $X = 1/2(x + y)$  and  $u = x - y$  we see that the differentiation with respect to the center variable cancels and the remaining expression for the energy-momentum tensor of the quarks reads

$$T_q^{\mu\nu}(X) = -\frac{i}{2} \partial_u^\nu S^{+-}(X, u)|_{u=0} \gamma^\mu - \frac{i}{2} \partial_u^\mu S^{+-}(X, u)|_{u=0} \gamma^\nu. \quad (5.87)$$

The energy-momentum tensor of the sigma field remains the same by using the equation of motion (5.34) defined on the center variable

$$\partial_\mu T_\sigma^{\mu\nu}(X) = \left( \partial_\mu \partial^\mu \sigma + \frac{\delta U}{\delta \sigma} \right) \partial^\nu \sigma = \frac{\delta \Gamma_2}{\delta \sigma} \partial^\nu \sigma = S^{++}(X) \partial_X^\nu \sigma(X). \quad (5.88)$$

With the approximation to the full propagator in equation (5.36) to first order (5.38) the energy-momentum balance of the entire system reads

$$\begin{aligned} \partial_\mu T_{q,\text{appr.}}^{\mu\nu}(X) + \partial_\mu T_{\sigma,\text{appr.}}^{\mu\nu}(X) &= \partial_\mu \left( -\frac{i}{2} \partial_u^\nu S_{\text{th}}^{+-}(X, u)|_{u=0} \gamma^\mu - \frac{i}{2} \partial_u^\mu S_{\text{th}}^{+-}(X, u)|_{u=0} \gamma^\nu \right. \\ &\quad \left. - \frac{i}{2} \partial_u^\nu \delta S^{+-}(X, u)|_{u=0} \gamma^\mu - \frac{i}{2} \partial_u^\mu \delta S^{+-}(X, u)|_{u=0} \gamma^\nu \right) \\ &\quad + S_{\text{th}}^{++}(X) \partial_X^\nu \sigma(X) + \delta S^{++}(X) \partial_X^\nu \sigma(X), \end{aligned} \quad (5.89)$$

where we identify the four contributions

$$\partial_\mu T_{q,\text{appr.}}^{\mu\nu}(X) + \partial_\mu T_{\sigma,\text{appr.}}^{\mu\nu}(X) = \partial_\mu T_{q,\text{th}}^{\mu\nu}(X) + \partial_\mu T_{\sigma,\text{th}}^{\mu\nu}(x) + \partial_\mu \delta T_q^{\mu\nu}(X) + \partial_\mu \delta T_\sigma^{\mu\nu}(x) \quad (5.90)$$

The first term evaluates to

$$\begin{aligned} T_{q,\text{th}}^{\mu\nu}(X) &= -\frac{i}{2} \partial_u^\nu S_{\text{th}}^{+-}(X, u)|_{u=0} \gamma^\mu - \frac{i}{2} \partial_u^\mu S_{\text{th}}^{+-}(X, u)|_{u=0} \gamma^\nu \\ &= 8\pi d_q \int \frac{d^4 p}{(2\pi)^4} p^\mu p^\nu n_{\text{F}}(|p^0|) \delta(p^2 - g^2 \sigma(X)^2) \\ &= 2d_q \int \frac{d^3 p}{(2\pi)^3} \frac{p^\mu p^\nu}{p^0} n_{\text{F}}(X, \vec{p}). \end{aligned} \quad (5.91)$$

It gives the energy-momentum tensor for an ideal fluid with the energy density and the pressure obtained from the equilibrium one-loop effective potential in mean-field approximation. This is exactly what we intend to use for the fluid dynamic expansion of the quark-antiquark fluid. What remains is the correction to the energy-momentum tensor of the quark fluid  $\delta T_q^{\mu\nu}(X)$ .

The thermal part of the divergence of the energy-momentum tensor of the sigma field  $\partial_\mu T_{\sigma,\text{th}}^{\mu\nu}$  gives exactly the same result (4.26) as was obtained in section 4.2. In the present nonequilibrium model we find a correction, which from (5.41) is given by

$$\partial_\mu \delta T_\sigma^{\mu\nu}(X) = D(X) \partial_X^\nu \sigma(X). \quad (5.92)$$

With the explicit result of the damping kernel  $D(X)$  for the zero mode (5.65), the total energy-momentum dissipation from the sigma field is

$$\partial_\mu T_{\sigma,\text{appr.}}^{\mu\nu} = (-g\rho_s - \eta \partial_t \sigma) \partial^\nu \sigma. \quad (5.93)$$

It includes the dissipative part of the dynamics of the sigma mean-field. It can, however, not account for the average energy transfer from the heat bath to the field given by the auxiliary noise field  $\zeta$ . We will see its consequences in the next chapter, in which we investigate the dynamics of the sigma field coupled to a static heat bath.

## 6. Equilibration and relaxation times

In the previous chapter we have derived the Langevin equation of motion for the sigma field coupled to quarks and given explicit expressions for the damping coefficient and the correlation of the noise term. In this chapter we want to investigate the relaxational dynamics of the sigma field and time scales associated with it. Equilibration of the sigma field with a heat bath can be understood on different levels. The first requirement is that the average of the sigma field relaxes to the global minimum of the effective potential for large times. The second requirement is the Gaussian thermal distribution around the average value. The relaxational properties of the sigma field are important for studies of the phase transition. In a nonequilibrium situation one expects the coexistence phase for a first order phase transition, and due to critical slowing down one also expects long relaxation times at the critical point.

In section 6.1 we explain the setup for the numerical investigation of the Langevin equation for the sigma mean field. We study the equilibration properties of the sigma field within our model for a static and isothermal heat bath in section 6.2. During the relaxation process the sigma field loses energy due to dissipation. This is studied in comparison with the energy conservation of the entire system in section 6.3. Finally, we include this energy exchange and take reheating of the heat bath into account in section 6.4.

This chapter is based on [Nah11c].

### 6.1. Numerical implementation of the Langevin equation

In chapter 4 we solved the classical equation of motion, which is a wave equation with a field-dependent source term, by a staggered leap-frog algorithm. The numerical implementation of an algorithm to solve the Langevin equation

$$\partial_\mu \partial^\mu \sigma(t, \mathbf{x}) + \frac{\delta U}{\delta \sigma} + g\rho_s + \eta \partial_t \sigma(t, \mathbf{x}) = \zeta(t, \mathbf{x}) \quad (6.1)$$

including a noise term on a lattice is more complicated. Here we apply the well tested algorithm used in [Cas07].

For the kinematic range  $m_\sigma > 2m_q$ , where the decay of the sigma in a quark-antiquark pair is allowed the damping coefficient  $\eta$  for the zero mode of the sigma field is given in (5.66). For the present calculations we use the respective equilibrium values of the sigma mass  $m_{\sigma_{\text{eq}}}(T) = (\partial^2 V_{\text{eff}}(T, \sigma) / \partial \sigma^2)|_{\sigma=\sigma_{\text{eq}}}$  and  $\sigma_{\text{eq}}(T)$  to evaluate this criterion. Then, the temperature dependence of  $\eta$  is shown in figure 5.2. We use (5.66) also for the nonzero modes in the Langevin equation (6.1). In this framework there would be no damping in the low-temperature phase because the quarks are not light enough to allow for the decay  $\sigma \rightarrow \bar{q}q$ . Physically this makes sense, because the quarks should be confined anyway. Additional damping is provided by the decay  $\sigma \rightarrow 2\pi$ . Strictly speaking this is not included

in our present framework. Nonetheless, to obtain a more realistic setup we include the zero-temperature damping coefficient from [Ris98] when the constituent quark mass is too large for the  $\sigma \rightarrow \bar{q}q$  decay. The damping coefficient for the present setup is

$$\eta = \begin{cases} g^2 \frac{d_q}{\pi} (1 - 2n_F(\frac{m_\sigma}{2})) \frac{1}{m_\sigma^2} \left( \frac{m_\sigma^2}{4} - m_q^2 \right)^{3/2}, & \text{for } m_\sigma(T) > 2m_q(T) = 2g\sigma_{\text{eq}}(T) \\ 3/\text{fm}, & \text{for } m_\sigma(T) < 2m_q(T) = 2g\sigma_{\text{eq}}(T) \end{cases}. \quad (6.2)$$

The noise correlation is given by (5.72).

In this chapter we investigate the time evolution of the following quantities. The volume average of the sigma field for one configuration of the noise field  $\xi_{ijk}$  is

$$\langle \sigma \rangle_n = \frac{1}{N^3} \sum_{ijk} \sigma_{ijk,n}, \quad (6.3)$$

where  $N$  is the number of cells in each direction. We average over several different configurations of the noise

$$\overline{\langle \sigma \rangle} = \frac{1}{N_r} \sum_{n=1}^{N_r} \langle \sigma \rangle_n, \quad (6.4)$$

typically between  $N_r = 5$  and  $N_r = 20$  depending on how different the trajectories really are for the various temperatures.

The variance of the sigma fluctuations for one noise configuration is

$$\langle \sigma^2 \rangle_n = \frac{1}{N^3} \sum_{ijk} (\sigma_{ijk,n} - \langle \sigma \rangle_n)^2, \quad (6.5)$$

and its average over noise configurations is

$$\overline{\langle \sigma^2 \rangle} = \frac{1}{N_r} \sum_{n=1}^{N_r} \langle \sigma^2 \rangle_n. \quad (6.6)$$

In the calculations presented here, we choose  $N = 32$ . The size of time steps is  $\Delta t = 0.02$  fm and the lattice spacing is  $\Delta x = 0.2$  fm.

## 6.2. Equilibration for a global, isothermal heat bath

In this section we study the equilibration of the sigma field with a global, i.e space-homogeneous, and isothermal heat bath. Concerning the energy exchange the back reaction of the sigma field on the heat bath is ignored. Therefore, the temperature of the heat bath is constant and determines the shape of the effective potential. This is very different for the first order phase transition and the critical point. We, therefore, expect a different evolution of the sigma field for these two scenarios.

While the initial conditions for the sigma field are varied in the next sections, the time derivative of the sigma field  $\partial_t \sigma$  is initially zero. There is no clear physical motivation for the choice of the initial  $\partial_t \sigma$ . When it is initialized in direction of the relaxation process the sigma field relaxes faster. A random distribution for the initial  $\partial_t \sigma$  averages out.

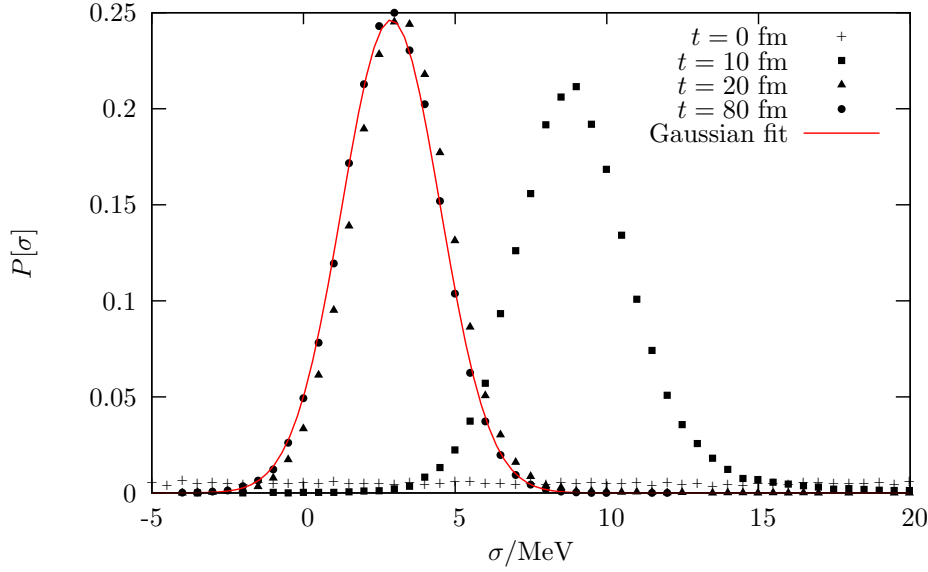


Figure 6.1.: The distribution of the sigma field for  $T = 160$  MeV at different times. The initial distribution is flat. It quickly turns into a Gaussian centered at a mean of 2.89 MeV with a width of 1.62 MeV. The Gaussian fit is to the distribution at  $t = 80$  fm

### 6.2.1. First order phase transition

The evolution in a first order scenario is especially interesting because the effective potential has two minima in the spinodal region  $108 \text{ MeV} \simeq T_{\text{sp}}^{(1)} < T_c < T_{\text{sp}}^{(2)} \simeq 128 \text{ MeV}$ . We expect that for some configurations the sigma field relaxes partly to the unstable minimum instead of the true thermal expectation value. This is even more likely in the vicinity of  $T_c$ , where both minima are almost degenerate.

In order to study the relaxation of the sigma field to its thermal equilibrium state at the temperature of the heat bath we need a clear nonequilibrium initial situation. In our investigation we distinguish between two cases for which the initial nonequilibrium situation is realized differently: the equilibration at temperatures above and at temperatures below the transition temperature.

#### Equilibration at high temperatures $T > T_c$

For the equilibration at temperatures above the phase transition temperature we initially distribute the sigma field linearly between  $\sigma_{\text{min}} \simeq 0$  and  $\sigma_{\text{max}} > 0$  such that the initial average of the sigma field is  $\langle \sigma \rangle_n \simeq 50 \text{ MeV}$ . The flat distribution is far from being thermal. For temperatures  $T$  above  $T_{\text{sp}}^{(2)}$  the time dependence of  $\overline{\langle \sigma \rangle} / \sigma_{\text{eq}}$  is shown in figure 6.2. As expected the sigma field relaxes more slowly for lower temperatures. The individual trajectories do not differ much for different realizations of the noise. This is clear because the potential has only one minimum and a steep curvature.

In figure 6.1 we see how the initially flat distribution develops for an example evolution at  $T = 160$  MeV. It becomes Gaussian after times  $t \simeq 20$  fm, which correspond to the re-

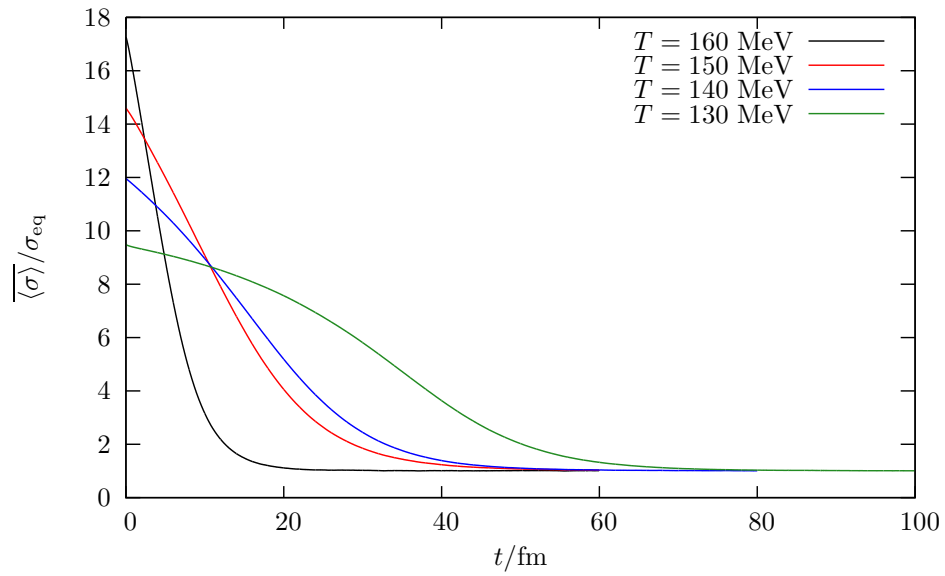


Figure 6.2.: The time evolution of the scaled noise average of the sigma field in a first order scenario for temperatures above the upper spinodal temperature  $T > T_{\text{sp}}^{(2)}$ .

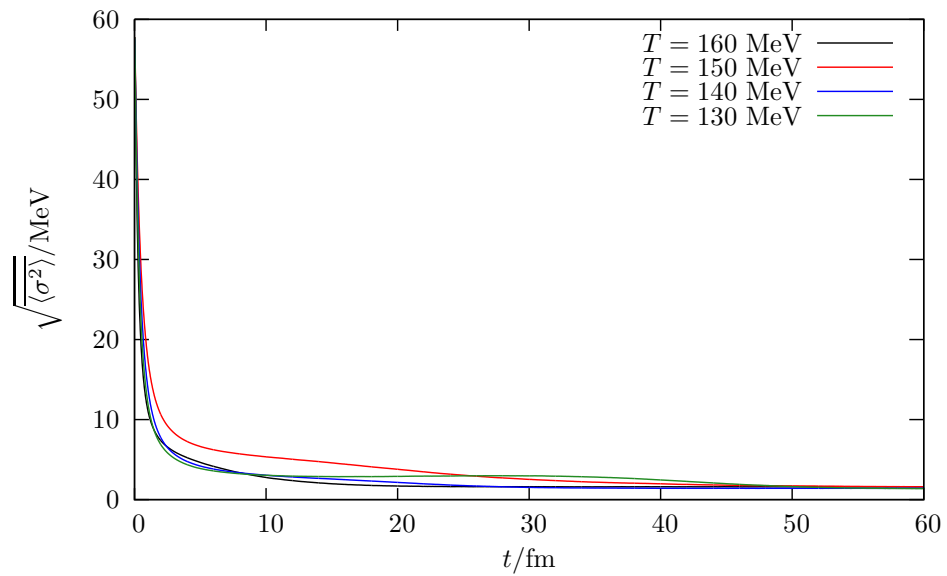


Figure 6.3.: The time evolution of the noise average of the sigma fluctuations in a first order scenario for temperatures above the upper spinodal temperature  $T > T_{\text{sp}}^{(2)}$ .



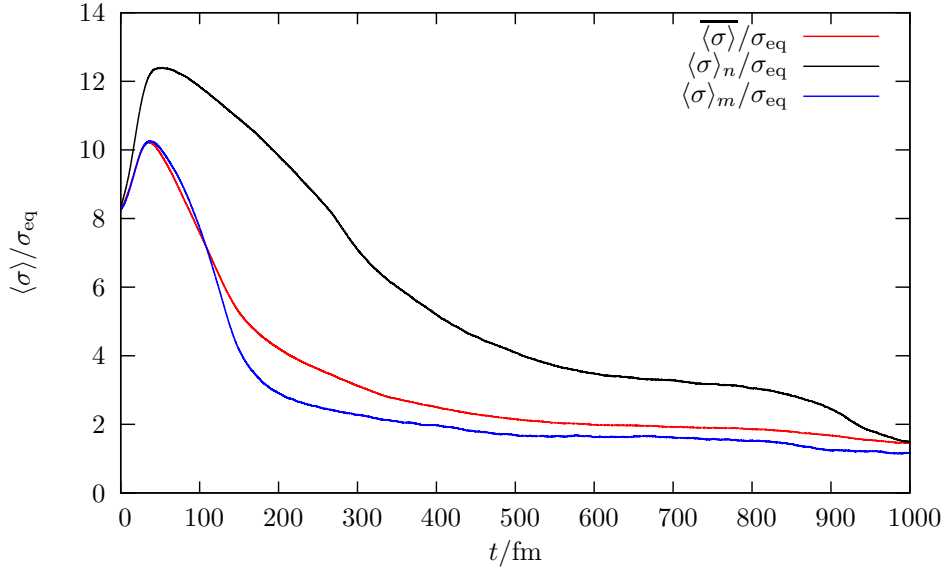


Figure 6.4.: The long relaxation process of the sigma field for  $T = 125$  MeV. The scaled noise average  $\overline{\langle \sigma \rangle} / \sigma_{\text{eq}}$  and two individual noise configurations are given. Due to the barrier between the two minima the relaxation to the global minimum is very slow. The individual noise configurations differ substantially.

laxation times in figure 6.2. It shows the equilibration of the sigma field to its proper equilibrium value at the respective temperature. This is ensured by the fluctuation-dissipation theorem (5.72), which relates the variance of the noise field to the damping coefficient.

The noise average of the sigma fluctuations is shown in figure 6.3. Here, we must note a small difference to the values one obtains from the effective potential via equation (4.19). We can attribute this discrepancy to the approximation we applied by using the equilibrium sigma mass to calculate the damping coefficient (5.66) and the noise correlation (5.72) instead of the local sigma mass calculated from the local shape of the potential. The variance of the noise is consequently slightly too small. Since the values of the final variances of the fluctuations of the sigma field are, however, of the same order, it still gives a reasonable description of the final equilibrium.

The dynamics of the system becomes different for  $T_{\text{sp}} > T > T_c$ . In figure 6.4 the scaled noise average  $\overline{\langle \sigma \rangle} / \sigma_{\text{eq}}$  and the volume average  $\langle \sigma \rangle_n / \sigma_{\text{eq}}$  for two individual noise realizations are shown for  $T = 125$  MeV. Because of the two minima the system takes a long time to relax to the global minimum at  $\sigma_{\text{eq}} \simeq 6$  MeV. Since the initial average is slightly shifted towards the low-temperature minimum the system first tends to this phase, but finally relaxes to the true minimum at very large times.

At the transition temperature  $T_c = 123.27$  MeV the distribution of the sigma field for one noise configuration is shown in figure 6.5. The system is in the expected phase coexistence and the sigma field does not relax at all. Instead we observe that the system is split into one part in the high-temperature and one part in the low-temperature minimum.

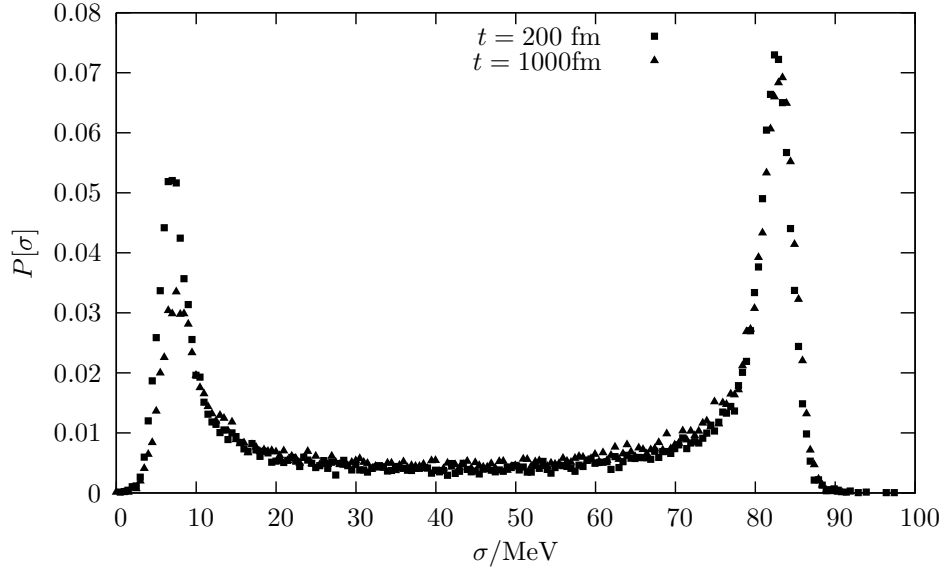


Figure 6.5.: The distribution of the sigma field at the transition temperature  $T_c = 123.27$  MeV of the first order phase transition scenario. The system shows phase coexistence.

### Equilibration for a quench to temperatures $T < T_c$

After initializing the sigma field in equilibrium with an initial temperature of  $T_{\text{ini}} = 160$  MeV the system is suddenly quenched to different temperatures  $T < T_c$  for which the Langevin equation for the sigma field is solved. It is known that for the linear sigma model with constituent quarks the nucleation rates are rather low and that the main relaxation mechanism is that of spinodal decomposition [Sca01b]. This is also observed in our calculations. In figure 6.6 we show the time evolution of the relaxation of the sigma field. For  $T = 115$  MeV, where we still have a substantial barrier between the two minima, the relaxation times are significantly larger than for lower temperatures. Here, the system remains in the local minimum  $\sigma \simeq 10$  MeV until at  $t \simeq 15$  fm it begins to decay to the global minimum, which is also a slow process. It resembles the case of an exponentially damped system, which decays without oscillations. At  $T = 100$  MeV we can clearly see the oscillating relaxation. It occurs much faster.

Figure 6.7 shows the variance of the fluctuations of the sigma field. During the relaxation process the size of the fluctuations develop a peak. For lower temperatures, significant fluctuations remain only for a short time, while they are enhanced during the whole long relaxation process at  $T = 115$  MeV. For  $T > T_{\text{sp}}^{(1)}$  the maximum size of the fluctuations is approximately half the distance of the two minima.

### 6.2.2. Critical point

The effective potential for a scenario with a critical point has only one minimum at all temperatures. It continuously shifts from  $\sigma \simeq 0$  to the vacuum expectation value  $\langle \sigma \rangle_{\text{vac}} = f_\pi$

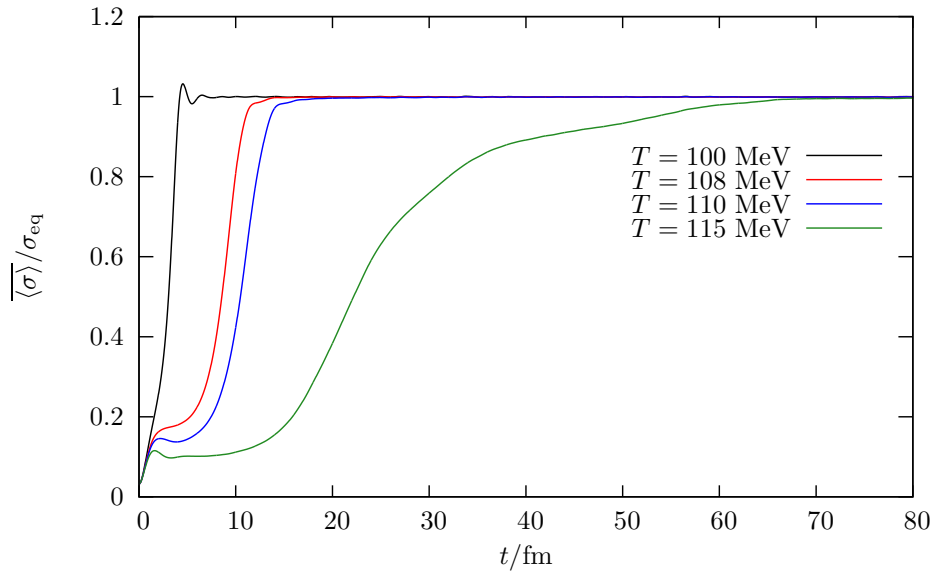


Figure 6.6.: The time evolution of the scaled noise average of the sigma field in different quenched scenarios for a first order phase transition scenario.

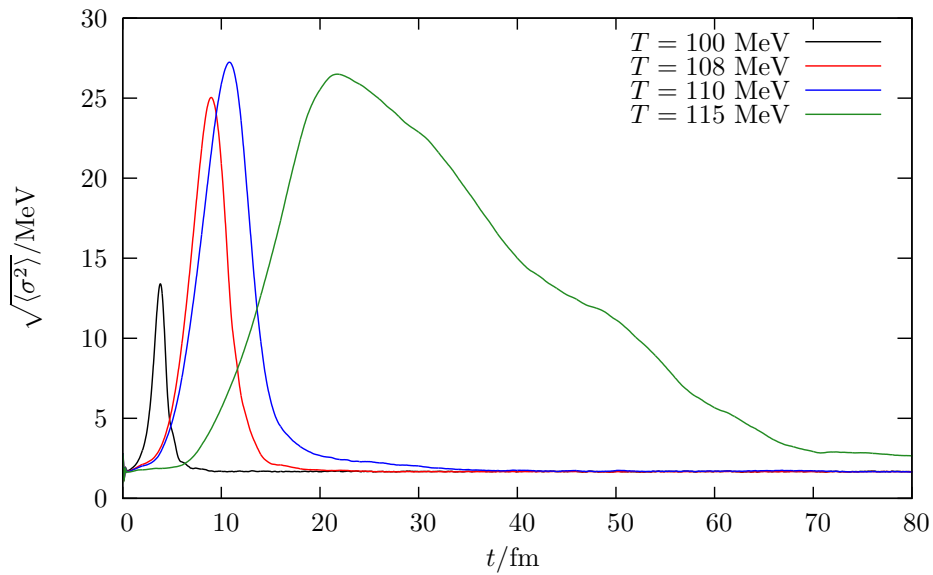


Figure 6.7.: The time evolution of the noise averaged fluctuations of the sigma field. They are enhanced during the relaxation process.

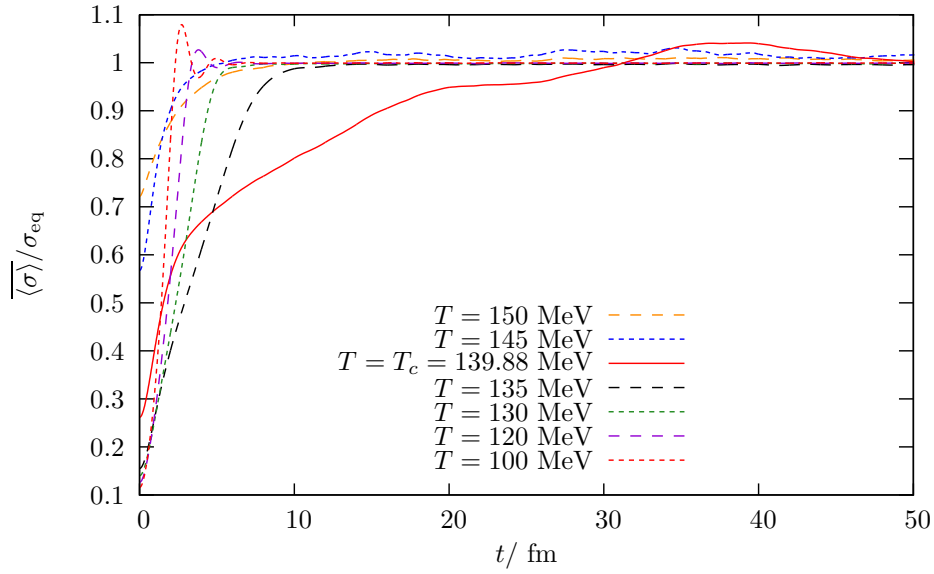


Figure 6.8.: The time evolution of the scaled noise average of the sigma field for a critical point scenario for various temperatures. The relaxation time becomes large at the critical point.

when lowering the temperature. At the critical point this minimum becomes very flat and we expect long relaxation times. For different temperatures, the evolution of the noise averaged sigma field can be best compared by choosing the same initial conditions, the thermal equilibrium state at  $T = 160 \text{ MeV}$ . The system is then quenched to temperatures  $T < 160 \text{ MeV}$ . The results are shown in figure 6.8. For low temperatures the potential is steeper and the relaxation process occurs faster. The field oscillates before relaxing. Approaching the critical temperature relaxation times become larger with a clear maximum at  $T_c$ . Here, fluctuations remain enhanced for long times, see figure 6.9. However, we have to note that the observed fluctuations are by far smaller than the expected fluctuations in thermal equilibrium, obtained from a Gaussian approximation to the effective potential. This effect is much larger for a critical point scenario than for the first order phase transition scenario.

### 6.3. The energy dissipation

During the relaxation of the sigma mean-field to its equilibrium value the dissipative term in the Langevin equation (6.1) causes energy dissipation. By the interaction with the quarks it is transferred to the heat bath. In section 5.5 we derived a conserved energy-momentum tensor of the entire system including a dynamics of the heat bath. In this paper, we do not include the fluid dynamic expansion of the heat bath. In this section we investigate the relevant energy exchange between the sigma field and the heat bath. The energy dissipation of the field to the heat bath can be obtained from the energy-momentum

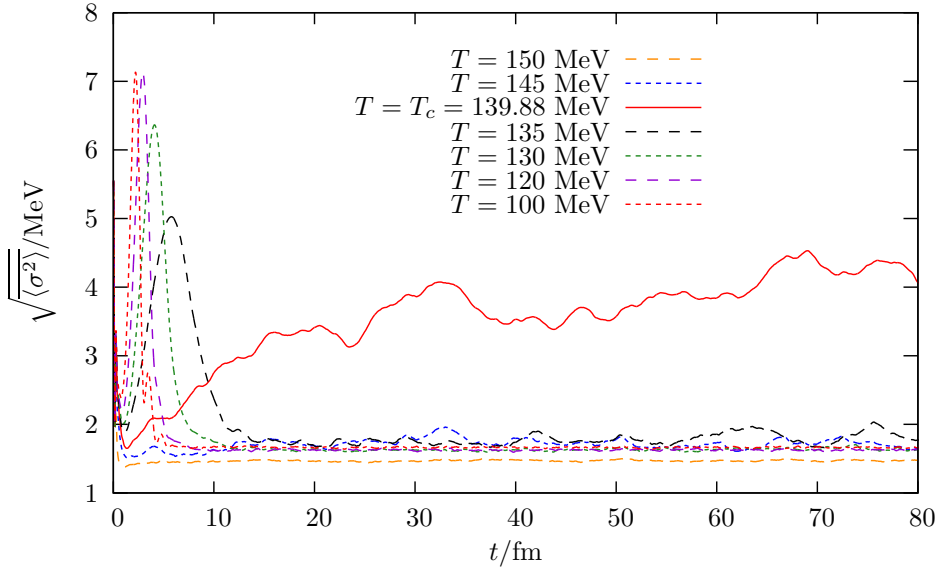


Figure 6.9.: The time evolution of the noise averaged variance of the sigma fluctuations. During the relaxation process fluctuations are enhanced. See text for the discussion of the fluctuations.

tensor of the sigma field

$$\partial_\mu T_\sigma^{\mu 0} = -(g\rho_s + \eta\partial_t\sigma)\partial_t\sigma, \quad (6.7)$$

where  $T_\sigma^{\mu\nu}$  is the energy-momentum tensor of the purely mesonic Lagrangian

$$\mathcal{L}_\sigma = \frac{1}{2}\partial_\mu\sigma\partial^\mu\sigma - U(\sigma). \quad (6.8)$$

We make the same approximation as in (4.41b). Then, the energy dissipation is described by

$$\Delta E_{\text{diss}} = (g\rho_s + \eta\partial_t\sigma)\partial_t\sigma\Delta t. \quad (6.9)$$

The total energy of the sigma field is given by

$$E_\sigma = \frac{1}{2}\partial_t\sigma^2 + \frac{1}{2}\vec{\nabla}\sigma^2 + U(\sigma). \quad (6.10)$$

It has a kinetic, potential and fluctuation energy term. During relaxation to the vacuum expectation value the potential energy is transferred to kinetic energy as  $\partial_t\sigma$  grows. Then, the damping becomes substantial and causes energy dissipation. This flow of energy from the field to the heat bath is given by (6.9). There is a reverse flow of energy from the heat bath to the field  $\Delta E_\zeta$  associated with the noise field  $\zeta$  in the Langevin equation (6.1), which is an averaged quantity balancing the energy dissipation  $\Delta E_{\text{diss}}$  in equilibrium and thus restoring the proper thermal equilibrium. Assuming that the made approximations in section 5.5 and (4.41b) cause only a small violation of energy conservation we can determine  $\Delta E_\zeta$  from comparing  $\Delta E_{\text{diss}}$  to the energy difference in the field before and after each numerical time step  $\Delta E_\sigma$ .

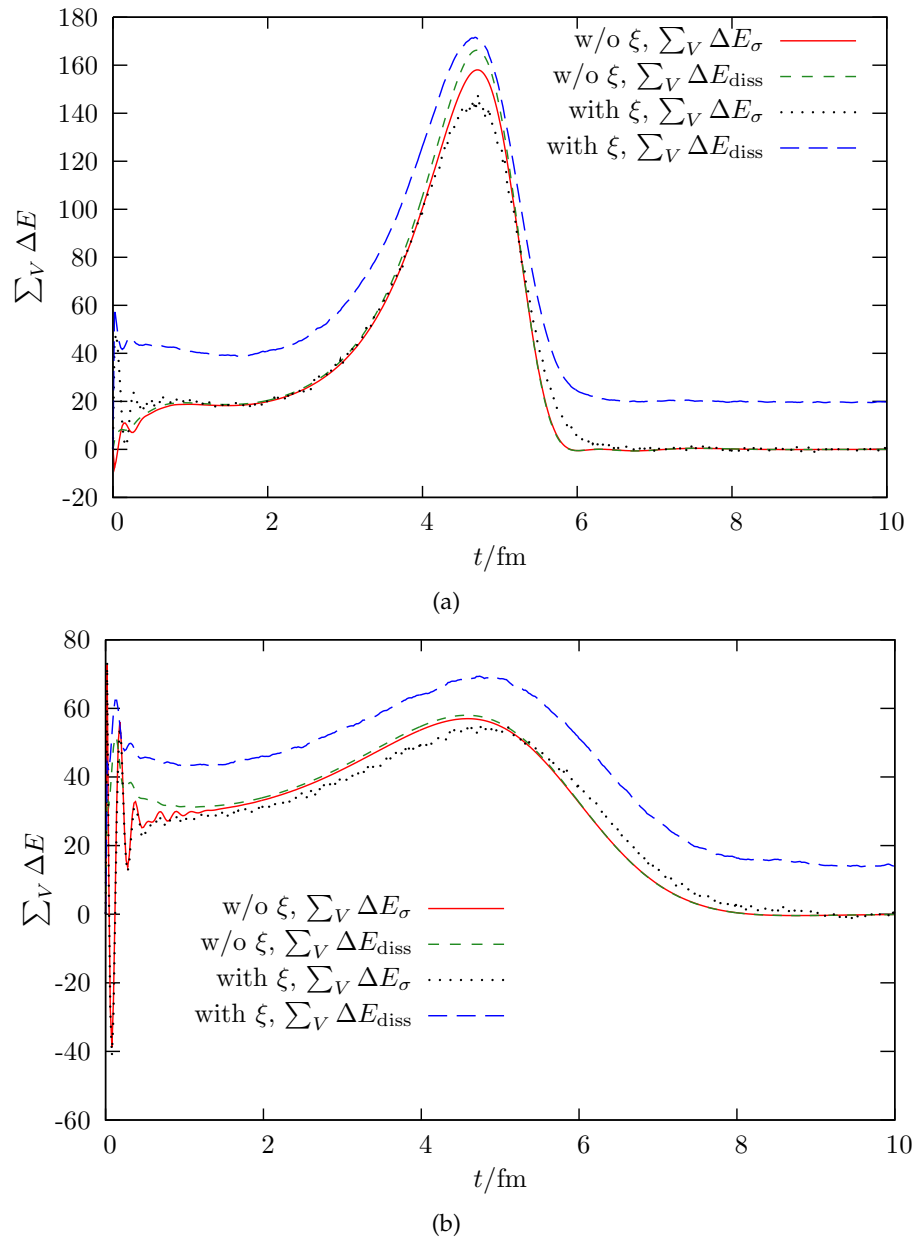


Figure 6.10.: Energy dissipation for a scenario with a first order phase transition (a) and for a critical point scenario (b). The system is quenched from  $T_{\text{ini}} = 160$  MeV to  $T = 100$  MeV in the first order phase transition scenario and from  $T_{\text{ini}} = 160$  MeV to  $T = 130$  MeV in the critical point scenario. The Langevin equation is once solved with the noise term  $\xi$  and once without it. For each case the comparison between the total energy dissipation  $\sum_V \Delta E_{\text{diss}}$  and the energy difference in the field  $\sum_V \Delta E_\sigma$  summed over the whole volume is shown.

Here, we first show that the difference between  $\Delta E_{\text{diss}}$  and  $\Delta E_{\sigma}$  is small if one ignores the noise term in the Langevin equation. This is shown in figure 6.10(a) for the quench from  $T_{\text{ini}} = 160$  MeV to  $T = 100$  MeV in a scenario with a first order phase transition and for a critical point scenario quenched from  $T_{\text{ini}} = 160$  MeV to  $T = 130$  MeV in figure 6.10(b). The resulting difference is a measure of the violation of energy conservation due to the approximations made in section 5.5 and (4.41b). It is numerically small. In figure 6.10 we also show the difference between  $\Delta E_{\text{diss}}$  and  $\Delta E_{\sigma}$  including the noise term. We identify this difference with  $\Delta E_{\xi}$ .

## 6.4. Equilibration for a heat bath with reheating

In this section we want to investigate the influence of the energy conservation on the equilibration of the entire system. While the sigma field relaxes after a sudden temperature quench energy dissipates from the system to the heat bath. This in return changes the temperature of the quark fluid and the effective potential. Thus, the evolution of the sigma field itself is altered. In the last section we discussed the energy transfer between the sigma field and the heat bath. It has the two components  $\Delta E_{\text{diss}}$  and  $\Delta E_{\xi}$ . In the following we locally calculate  $\Delta E_{\sigma}$  and add this to the local energy density of the heat bath given by (4.25). The new energy density is inverted to find the local temperature.

### 6.4.1. First order phase transition

We present four results for scenarios with a first order phase transition. We quench from  $T_{\text{ini}} = 160$  MeV to  $T_{\text{sys}} = 100, 80, 50$  and  $20$  MeV. During the relaxation of the volume averaged sigma field, see figure 6.11, the average temperature increases rapidly to  $T_{\text{fin}}$ , see figure 6.12. The exact values are shown in table 6.1. Three temperatures are above  $T_c$  and below or close to the upper spinodal temperature  $T_{\text{sp}}^{(2)}$ , where the effective potential has two minima. The sigma field initially relaxes towards the vacuum value. This relaxation reheats the heat bath and causes an increase in the temperature to above  $T_c$ . Large parts of the sigma field now remain in the unstable low-temperature minimum. We see that including reheating the entire system does not equilibrate for these temperatures. Obviously, the reheating locally changes the effective potential such that it counteracts the relaxational process. Only for the very low temperature  $T_{\text{sys}} = 20$  MeV, which is close to vacuum conditions, the final temperature is below  $T_c$ . Thus, the initial relaxation of the sigma field corresponds already to the equilibrium state at  $T_{\text{fin}}$ .

### 6.4.2. Critical point

In a scenario with a critical point the effective potential has only one minimum for all temperatures. Therefore, we expect the entire system to equilibrate. We consider the following four temperature quenches from  $T_{\text{ini}} = 160$  MeV to  $T_{\text{sys}} = 140, 130, 100,$  and  $80$  MeV respectively. The corresponding volume averaged values are shown in table 6.2. The volume averaged variances of both quantities are explicitly given. We clearly see that the entire system relaxes at a temperature  $T_{\text{fin}}$  and  $\sigma_{\text{fin}} \simeq \sigma_{\text{eq}}(T = T_{\text{fin}})$  in figures 6.13 and 6.14. We

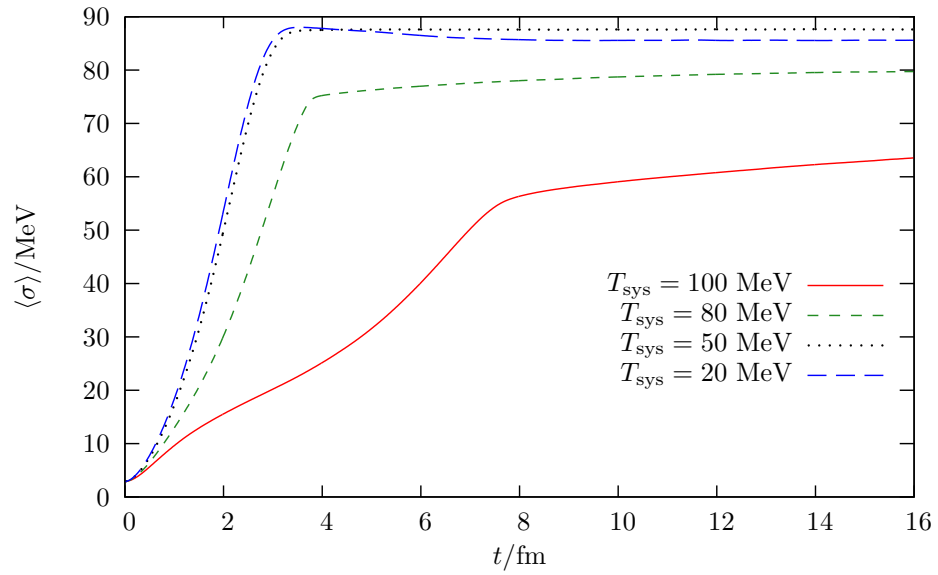


Figure 6.11.: Time evolution of the volume averaged sigma field in a scenario with a first order phase transition for different temperature quenches. The energy dissipation from the sigma field to the heat bath is taken into account.

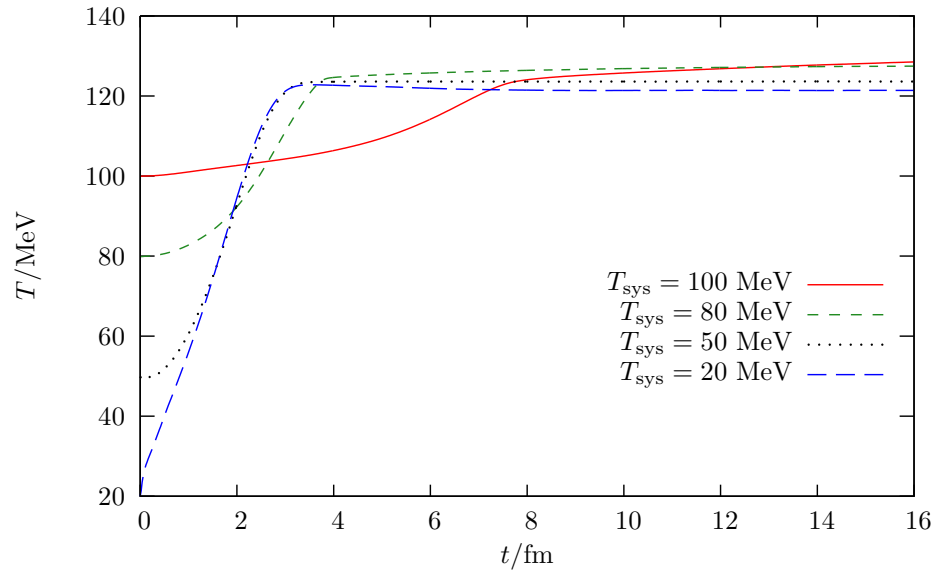


Figure 6.12.: Time evolution of the temperature in a scenario with a first order phase transition for different temperature quenches. The temperature is changed by the energy dissipation from the sigma field to the heat bath.



$T_{\text{sys}}/\text{MeV}$	$T_{\text{fin}}/\text{MeV}$	$\sigma_{\text{fin}}/\text{MeV}$	$\sigma_{\text{eq}}(T = T_{\text{fin}})/\text{MeV}$
100	131.89	69.06	5.00
80	127.69	80.11	5.56
50	123.59	87.57	6.25
20	121.41	85.60	84.82

Table 6.1.: Exact values for the relaxation of the volume averaged sigma field and the final temperatures for the different quenches for  $T_{\text{ini}} = 160$  MeV to  $T_{\text{sys}}$ . Here for a scenario with a first order phase transition.

observe that for a temperature quench to  $T_{\text{sys}} = 130$  MeV the final temperature comes closest to the critical temperature  $T_c = 139.88$  MeV. As seen in figure 6.13 and figure 6.14, relaxation times are longest for this quench.

$T_{\text{sys}}/\text{MeV}$	$T_{\text{fin}}/\text{MeV}$	$\sigma_{\text{fin}}/\text{MeV}$	$\sigma_{\text{eq}}(T = T_{\text{fin}})/\text{MeV}$
140	$141.42 \pm 0.31$	$23.33 \pm 1.92$	24.37
130	$138.96 \pm 0.47$	$53.43 \pm 1.52$	54.52
100	$124.53 \pm 0.57$	$78.46 \pm 1.40$	78.60
80	$115.44 \pm 0.62$	$83.82 \pm 1.43$	83.90

Table 6.2.: Exact values for the relaxation of the volume averaged sigma field and the final temperatures for the different quenches for  $T_{\text{ini}} = 160$  MeV to  $T_{\text{sys}}$ . Here for a critical point scenario.

We have studied the dynamics of the sigma field given by the Langevin equation (6.1) with the damping (6.2) and the noise correlator from chapter 5. It leads to the relaxation of the sigma field with a static isothermal heat bath. Including reheating of the heat bath we find full relaxational dynamics only for a scenario with a critical point. For a first order phase transition the system stays in the low-temperature minimum, which due to reheating becomes the unstable minimum at the final temperature. At the critical point we observed longest relaxation times which is in accordance with critical slowing down.

In the next chapter we will include the fluid dynamic expansion of the heat bath and thus study the full nonequilibrium chiral fluid dynamics.

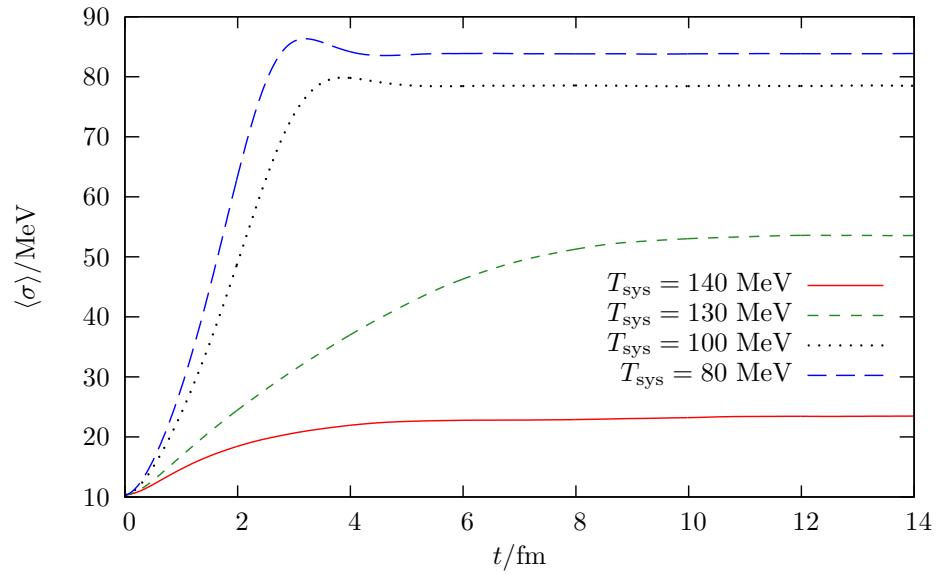


Figure 6.13.: Time evolution of the volume averaged sigma field in a critical point scenario for different temperature quenches. The energy dissipation from the sigma field to the heat bath is taken into account.

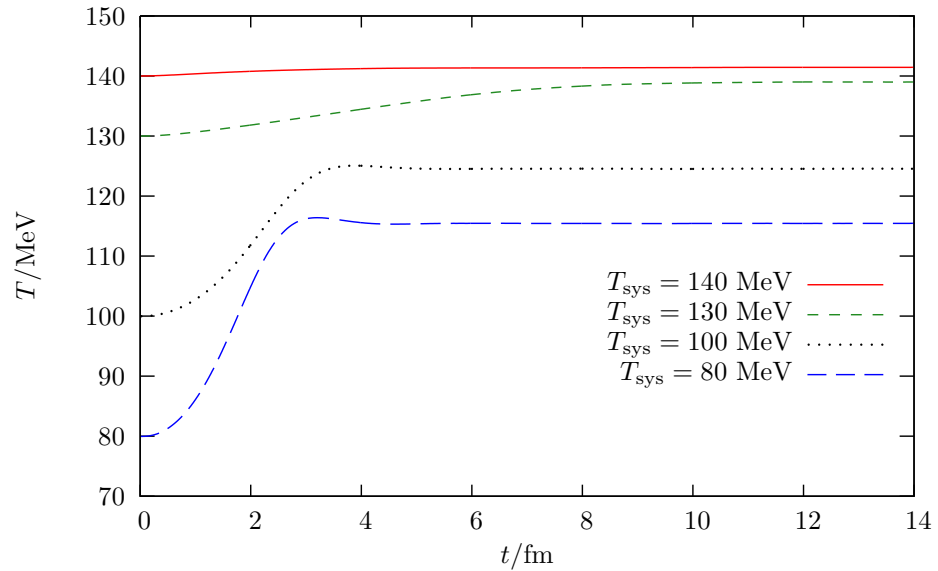


Figure 6.14.: Time evolution of the temperature in a critical point scenario for different temperature quenches. The temperature is changed by the energy dissipation from the sigma field to the heat bath.

## 7. Chiral fluid dynamics II

After having investigated the relaxational dynamics of the chiral sector in the previous chapter we are now ready to study the coupled dynamics of an expanding and cooling quark fluid and the relaxation of the sigma field. This coupling occurs on several points in the complete setup:

- The one-loop **effective potential**  $V_{\text{eff}}$  for the sigma field in presence of the quarks drives the chiral phase transition. By variation with respect to the sigma field it gives the one-loop scalar density  $\rho_s$ , which is the lowest order contribution to the equation of motion of the sigma field.
- The pressure and the energy density of the locally equilibrated quark fluid in the **equation of state**  $p(e)$  depend on the local value of the sigma field, which plays the role of an external parameter in the thermodynamic sense.
- The **damping coefficient**  $\eta$ , which describes the dissipative and stochastic processes in the equation of motion of the sigma field, is given by the interaction with the heat bath. It depends on the temperature of the heat bath and consistently on the sigma field itself via the masses of the quarks and of the sigma mesons.
- To account for the **energy-momentum exchange** between the two sectors we constructed an energy-momentum tensor, which is conserved for the full 2PI effective action. The approximations used for the derivation of the dynamics of the sigma field generate additional terms in the energy-momentum balance, which were derived in section 5.5.

We now implement this consistent coupling numerically and study the full dynamics of the entire system with respect to effects at the phase transition. We have seen in chapter 5 that the thermodynamic quantities, the pressure and the energy density, as calculated in chapter 4, are still consistent in the new setup including nonequilibrium effects. The issues discussed in chapter 4 can thus be adopted. We use the same parametrization of the equation of state, see section 4.3.4 and appendix D. The initial conditions are the same as in section 4.3.3 with one exception. Before we start the fluid dynamic expansion the equation of motion for the sigma field is solved a couple of times to generate an initial distribution of the time derivative of the sigma field. Section 4.3.5 on the inclusion of the source term remains largely valid. The additional aspects that have come in section 5.5 and 6.3 are discussed here in section 7.1. In section 7.2 we investigate the nonequilibrium effects of the coupled dynamics for three different damping coefficients. The sigma field is the order parameter of chiral symmetry breaking. It is expected to fluctuate characteristically at the phase transition. In section 7.3 we take a look at the intensity of the nonequilibrium fluctuations of the sigma field. At later times these numbers can be interpreted as the number

of sigma particles which are produced from the coherent decay of the field. The growth of the correlation length is an equilibrium phenomenon at a critical point and the basis for the large thermodynamic fluctuations. We see that the correlation function exhibits more structure in nonequilibrium and the definition of a correlation length becomes more difficult in an inhomogeneous and dynamic system in section 7.4. Finally, in section 7.5 we take a look at the momentum anisotropy in the fluid.

Parts of this chapter are published in [Nah10b, Nah11a, Nah11d].

### 7.1. Energy-momentum conservation

The energy-momentum conservation was discussed in section 5.5, where we found a conserved energy-momentum tensor for the full 2PI effective action. In the approximated theory additional terms contribute to the energy-momentum balance in equation (5.89). The thermal contributions for the quark fluid and the sigma field were already investigated in chapter 4 and yielded energy-momentum conservation to a very good degree. The correction to the divergence of the energy-momentum tensor of the sigma field is given by the dissipative part of the equation of motion. It describes the energy that dissipates out of the field. We assume that it is most important for the energy exchange between the field and the fluid. In section 6.3 we studied the behavior of this source term. As was expected, it well describes the dissipation of energy. It does not, however, account for the average energy transfer from the heat bath to the sigma field given by the stochastic field in the Langevin equation. As in section 6.4, where we studied the relaxation of the sigma field in a static heat bath with reheating, we will use the numerically determined energy and momentum difference in the sigma field for each time step.

In the beginning of the simulation the field configuration gains energy due to the increase of fluctuations. Locally this might exceed the energy in the fluid. In these cells the energy density is set to zero at the end of each numerical time step. In the beginning we, thus, observe a net increase of the total energy by  $\lesssim 10\%$  in the scenario with a first order phase transition the energy conservation is well fulfilled during the expansion. In a scenario with a critical point the energy is very well conserved during the entire evolution. The quark fluid reaches the edges of the grid at around  $t \simeq 8$  fm and disappears. In a test case with a larger grid energy was conserved well for a longer time. In addition, the evolution of the system in the inner region was not altered. The figures showing the energy balance for the different damping and phase transition scenarios are deferred to appendix F.

In addition to the energy conservation we also have to show momentum conservation when we include the expansion of the system. The total momentum of the system is close to zero. Due to the finite initial time derivative of the sigma field each initial field configuration has a small overall momentum, which is slightly enhanced in the beginning of the simulation. The total momentum in each of the three directions is of the order of 0.1% of the total momentum in positive direction.

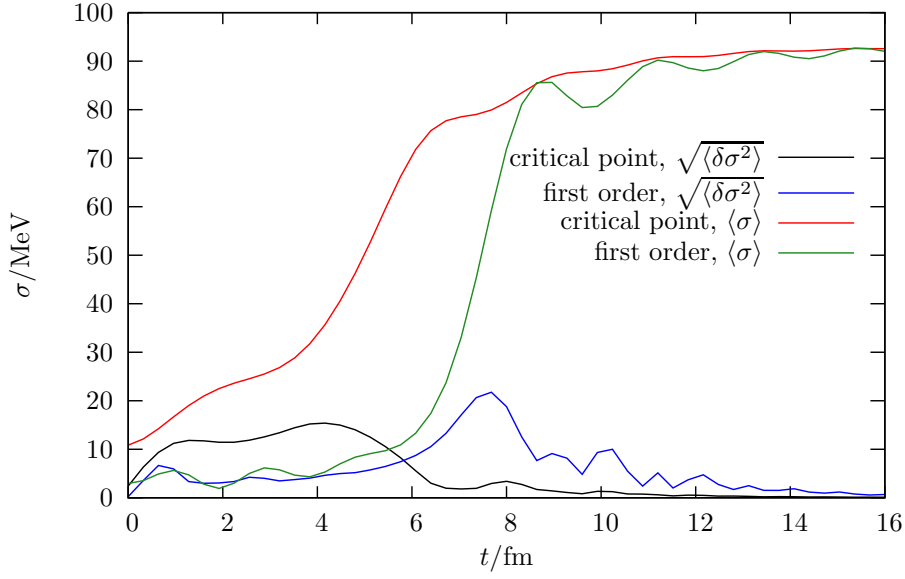


Figure 7.1.: The average values and the variances of the fluctuations  $\sqrt{\langle\delta\sigma^2\rangle}$  of the sigma field for  $\eta = 2.2/\text{fm}$  and both phase transition scenarios.

## 7.2. Supercooling and reheating

In this first section we investigate the coupled dynamics of the system for two constant damping coefficients,  $\eta = 2.2/\text{fm}$  and  $\eta = 10/\text{fm}$ , and a temperature-dependent damping coefficient  $\eta = \eta(T)$ . A parametric, constant damping coefficient  $\eta$  generally investigates dissipation and relaxation. The temperature dependence of  $\eta = \eta(T)$  includes more aspects of the phase transition scenario. The time evolution of the energy density and the sigma field for all scenarios are shown in appendix G and H.

### 7.2.1. Constant damping coefficient $\eta = 2.2/\text{fm}$

The constant damping coefficient of  $\eta = 2.2/\text{fm}$  is motivated by the study of the DCC formation within a Langevin approach [Bir97]. The time evolution of the average value of the sigma field  $\langle\sigma\rangle$  and its fluctuations  $\sqrt{\langle\delta\sigma^2\rangle} = \sqrt{\langle(\sigma - \langle\sigma\rangle)^2\rangle}$  are shown in figure 7.1. Figure 7.2 shows the time evolution of the average temperature  $\langle T\rangle$  and its fluctuations  $\sqrt{\langle\delta T^2\rangle} = \sqrt{\langle(T - \langle T\rangle)^2\rangle}$ . The average is taken over an initially hot and dense sphere with radius  $r = 3 \text{ fm}$ . The phase transition temperature in a critical point scenario  $T_c = 139.88 \text{ MeV}$  is crossed at around  $t = 5 \text{ fm}$ , after which the slightly enhanced fluctuations fall off. The average sigma field smoothly relaxes towards its vacuum value. As the phase transition temperature of the first order phase transition,  $T_c = 123.27 \text{ MeV}$ , is lower than at a critical point the system relaxes later but the relaxational process itself is faster in a first order phase transition scenario. The vacuum value is reached around the same time, but the average sigma field shows strong oscillations and the fluctuations are enhanced in the first order phase transition scenario.

When the first order phase transition temperature is reached after  $t \simeq 5 \text{ fm}$  large parts of

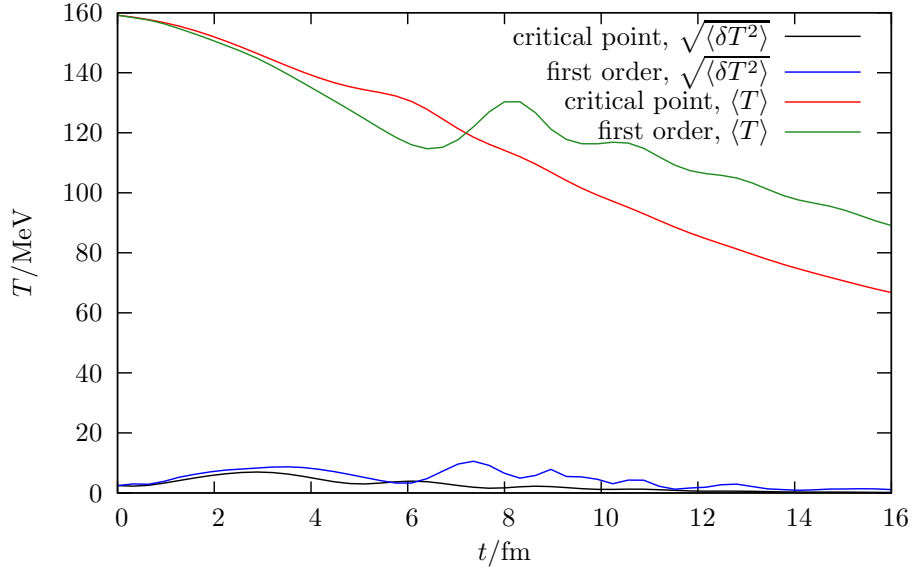


Figure 7.2.: The average values and the variances of the fluctuations  $\sqrt{\langle \delta T^2 \rangle}$  of the temperature for  $\eta = 2.2/\text{fm}$  and both phase transition scenarios.

the system are still in the chirally broken phase as the average value of the sigma field is still  $\langle \sigma \rangle \lesssim 10$  MeV. These large deviations of the sigma field from its equilibrium value is the nonequilibrium effect of supercooling.

Due to the steep curvature in the effective potential experienced by the system once the barrier is overcome, the potential energy is transformed effectively in kinetic energy, which leads to the dissipation of energy via  $\eta(\partial_t \sigma)^2$  in the source term. In figure 7.2 we can clearly observe the reheating effect at the first order phase transition. Between  $t = 7$  fm and  $t = 9$  fm the system is reheated from  $T \simeq 118$  MeV below  $T_c$  to  $T \simeq 125$  MeV above  $T_c$ , followed by a subsequent cooling. Thus, the reheating causes the system to cross the phase transition two more times, once in the reverse direction from the low temperature phase to the high temperature phase around  $t = 8$  fm and again at around  $t = 9$  fm. This contributes to a slower relaxation of the average sigma field.

The effective potential with a critical point is very flat at the transition temperature and reheating is not observed. Instead the cooling is slightly decelerated as seen in figure 7.2 between  $t = 5$  fm and  $t = 6$  fm.

### 7.2.2. Constant damping coefficient $\eta = 10/\text{fm}$

The damping coefficient in the linear sigma model with constituent quarks is larger at higher temperatures, as shown in figure 5.2. An average value for the whole time and both phase transition scenarios is of the order of  $\eta = 10/\text{fm}$ . The larger the constant damping coefficient the longer are the relaxation times, especially for a first order phase transition, because here the system is locally damped to the unstable minimum first.

If we chose the damping coefficient to be even larger, the relaxation time would by far

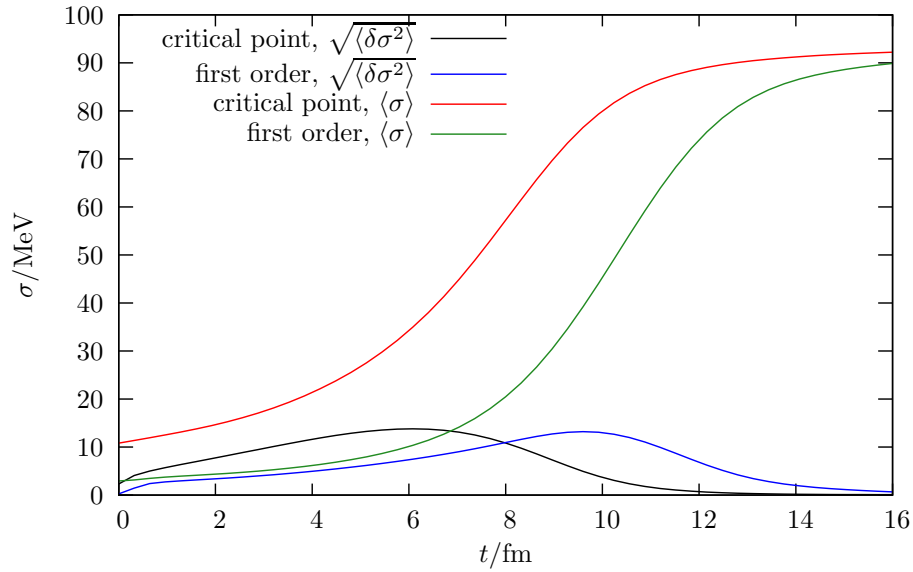


Figure 7.3.: The average values and the variances of the fluctuations  $\sqrt{\langle\delta\sigma^2\rangle}$  of the sigma field for  $\eta = 10/\text{fm}$  and both phase transition scenarios.

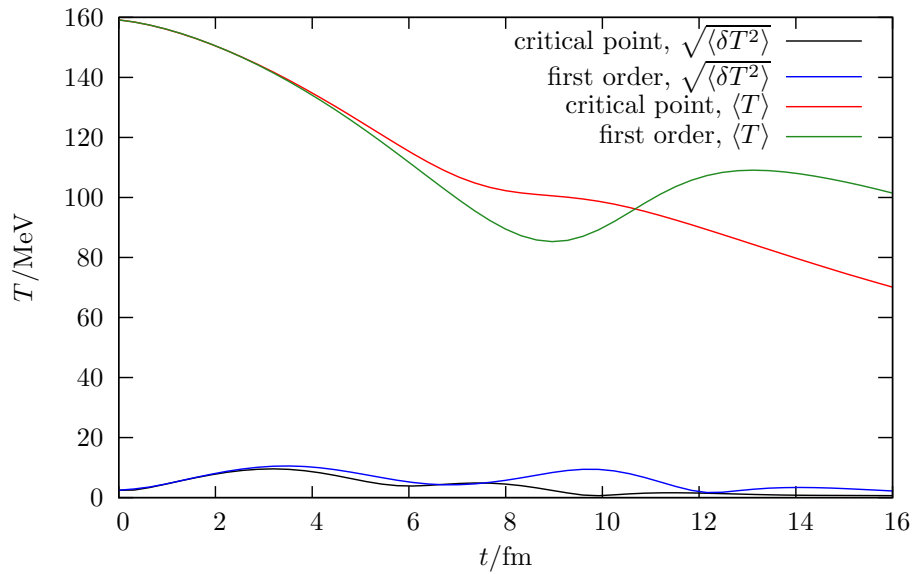


Figure 7.4.: The average values and the variances of the fluctuations  $\sqrt{\langle\delta T^2\rangle}$  of the temperature for  $\eta = 10/\text{fm}$  and both phase transition scenarios.

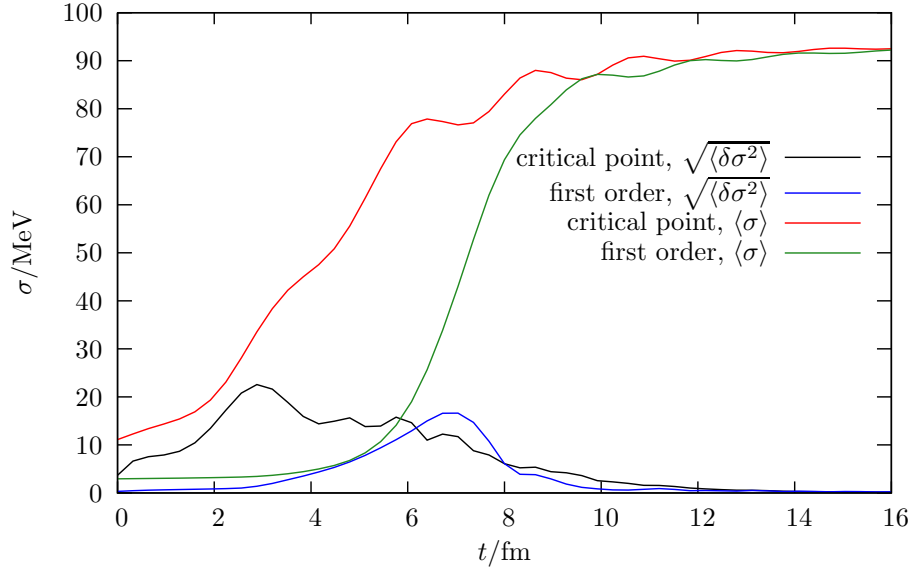


Figure 7.5.: The average values and the variances of the fluctuations  $\sqrt{\langle \delta\sigma^2 \rangle}$  of the sigma field for  $\eta = \eta(T)$  and both phase transition scenarios.

exceed the expansion time of the fluid. This contradicts the goal to investigate realistically coupled dynamics.

The time evolution of the average sigma field and its fluctuations are shown in figure 7.3 and of the average temperature and fluctuations of the temperature in figure 7.4. The relaxation times of the sigma field are larger than in the previous section for  $\eta = 2.2/\text{fm}$ . In both phase transition scenarios the average temperature is already below  $T = 100$  MeV, when the average sigma field approaches its equilibrium value at around  $t = 12$  fm for a critical point scenario and  $t = 16$  fm in a first order phase transition scenario.

The overall evolution is very smooth and the oscillations in a first order phase transition scenario are damped. In figure 7.4 we observe that the reheating process is more pronounced and takes longer time.

### 7.2.3. Temperature dependent damping coefficient $\eta = \eta(T)$

We now take the temperature dependence of the damping coefficient into account. As calculated in equation (5.66) the damping coefficient depends on the local value of the sigma field via the sigma mass and the quark mass. We calculated these masses by using the local equilibrium value of sigma. This results in a temperature dependence as shown in figure 5.2.

At lower temperatures it vanishes because the decay of the zero mode of the sigma field in a quark-antiquark pair is kinematically forbidden as  $m_\sigma(T) < 2m_q(T) = 2g\sigma_{\text{eq}}(T)$ . Albeit confinement is not included in the model, the vanishing of the damping process  $\sigma \rightarrow \bar{q}q$  at low temperatures is in agreement with confinement. Physically the sigmas get further damped by interactions with the hard chiral modes [Gre97, Ris98], as discussed in



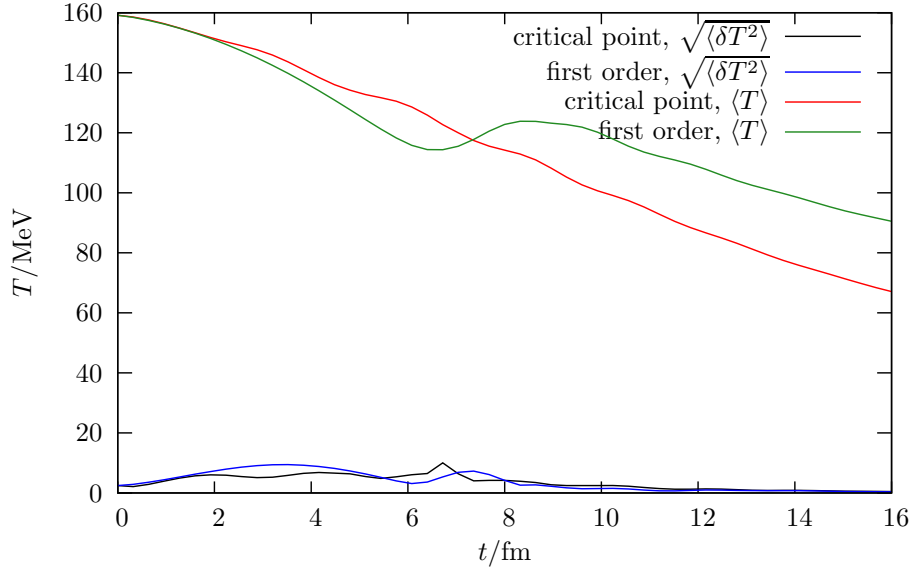


Figure 7.6.: The average values and the variances of the fluctuations  $\sqrt{\langle \delta T^2 \rangle}$  of the temperature for  $\eta = \eta(T)$  and both phase transition scenarios.

section 5.4. These effects are not included in our mean-field approach. To account for them we add by hand a value of  $\eta = 2.2/\text{fm}$  [Bir97]. We interpret this value of  $\eta$  as processes coming from the reactions  $\sigma \leftrightarrow 2\pi$ . Consequently this damping effect should vanish when the sigma mass undershoots two times the pion mass. This occurs only in a critical point scenario, where the sigma mass is very small.

To summarize,

$$\eta = \begin{cases} g^2 \frac{d_q}{\pi} \left(1 - 2n_F\left(\frac{m_\sigma}{2}\right)\right) \frac{1}{m_\sigma^2} \left(\frac{m_\sigma^2}{4} - m_q^2\right)^{3/2}, & \text{for } m_\sigma(T) > 2m_q(T) \\ 2.2/\text{fm}, & \text{for } 2m_q > m_\sigma(T) > 2m_\pi \\ 0, & \text{for } m_\sigma(T) < 2m_\pi, 2m_q \end{cases} \quad (7.1)$$

In a scenario with a critical point the vanishing of the damping coefficient leads to strong oscillations of the average sigma field during the relaxational process, as seen in figure 7.5. In a scenario with a first order phase transition the sigma field is strongly damped at high temperatures. At the phase transition temperature  $T_c$  the sigma mass drops below the threshold of quark-antiquark production but is larger than twice the pion mass. The damping coefficient shows a discontinuity from  $\eta(T > T_c) \simeq 26.6/\text{fm}$  to  $\eta(T < T_c) = 2.2/\text{fm}$ . In this scenario the average of the sigma field stays constant up to almost  $t \simeq 5$  fm and the relaxational process starts only when the average temperature is close to the phase transition temperature as can be seen by comparing figure 7.5 with 7.6. The cooling of the system is inhomogeneous. While the center is still very hot, outer parts have cooled down already. The fluctuations of temperature within the inner region with radius  $r = 3$  fm have a variance of almost 10 MeV. We conclude that even in this small inner region the outer parts have already cooled below the phase transition temperatures at  $t = 5$  fm and that it

is these parts that relax first due to the lower damping coefficient  $\eta$ .

For the average temperature we again see the effect of reheating in a scenario with a first order phase transition, which resembles the case for constant  $\eta = 2.2/\text{fm}$  as this is the predominant value for the damping for average temperatures below  $T_c$ . However, when the system is reheated to a temperature close to  $T_c$  parts of the system again experience a larger damping so that the subsequent cooling is slightly delayed. The average temperature in a critical point scenario is influenced by the oscillations of the average sigma field.

### 7.3. The intensity of sigma fluctuations

In various studies on the formation of DCC a large amplification of pion fields was observed at the phase transition [Raj93, Bir97, Mis99a, Xu00]. The pionic excitations were found to be triggered by violent oscillations of the sigma modes. Moreover, the zero mode of the sigma field is the order parameter of chiral symmetry breaking. The soft modes are thus expected to show large fluctuations at a critical point in thermodynamic systems. We are, therefore, especially interested in the intensity of sigma fluctuations at the phase transition.

The intensity of the sigma fluctuations is given by [Aba97, Ame97]

$$\frac{dN_\sigma}{d^3k} = \frac{a_k^* a_k}{(2\pi)^3 2\omega_k} = \frac{1}{(2\pi)^3 2\omega_k} (\omega_k^2 |\delta\sigma_k|^2 + |\partial_t \sigma_k|^2), \quad (7.2)$$

where  $a_k^*$  and  $a_k$  are the fourier coefficients in the expansion of the field and its conjugate momentum field

$$\delta\sigma(x) = \int \frac{d^3k}{(2\pi)^3 2\omega_k} (a_k \exp(-ikx) + a_k^* \exp(ikx)) \quad (7.3a)$$

$$\partial_t \sigma(x) = \int \frac{d^3k}{(2\pi)^3 2\omega_k} \frac{i}{2} (-a_k \exp(-ikx) + a_k^* \exp(ikx)) \quad (7.3b)$$

and read

$$a_k = \int d^3x (i\partial_t \sigma(x) + \omega_k \delta\sigma(x)) \exp(ikx) \quad (7.4a)$$

$$a_k^* = \int d^3x (\omega_k \partial_t \delta\sigma(x) + i\partial_t \sigma(x)) \exp(-ikx). \quad (7.4b)$$

$\delta\sigma_k$  and  $\partial_t \sigma_k$  are the Fourier transforms of the fluctuations of the sigma field and the time derivative. Here, it is a crucial issue of how we define the fluctuations of the sigma field. In the last section we showed results of the variance of the sigma fluctuations around the average sigma field in a hot region of radius  $r = 3 \text{ fm}$ . Now, we are interested in quantities that can be defined over the entire volume of the system but have a meaning locally. In a typical potential for a critical point fluctuations around the thermal equilibrium are large. We define the sigma fluctuations as the fluctuations around the local thermal equilibrium value of the sigma field. This is the average sigma field in the initial state and after relaxation and takes nonequilibrium effects at the first order phase transition into account. At

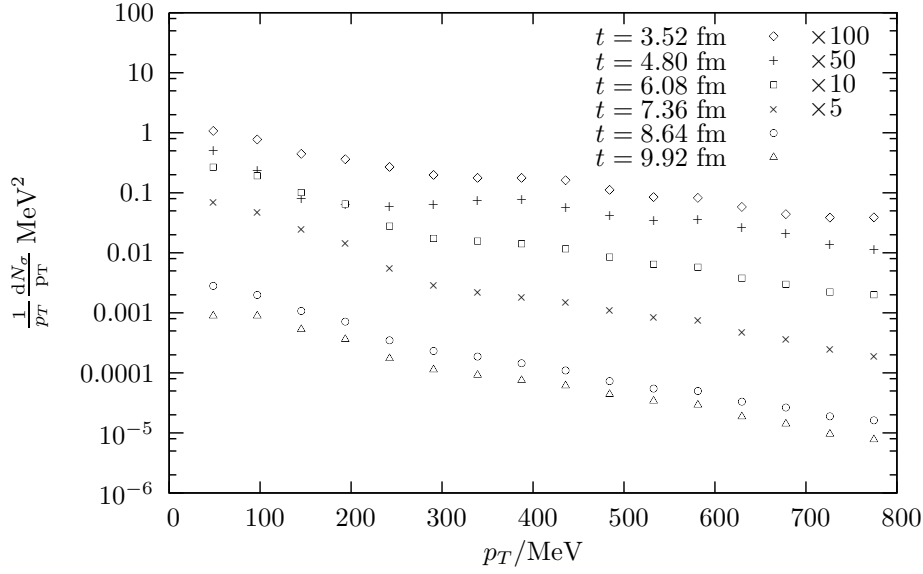


Figure 7.7.: Transverse momentum spectra for different times during the expansion and a critical point scenario.

later times when the nonlinearities in the equation of motion can be neglected the quantity  $N_\sigma$  in equation 7.2 gives the number of sigma particles produced from the excitations of the sigma field. The energy  $\omega_k$  of the  $k$ th mode of the sigma field is given by

$$\omega_k = \sqrt{|k|^2 + m_\sigma^2}. \quad (7.5)$$

We define the sigma mass via the curvature of the effective potential at its equilibrium value corresponding to the average temperature  $T_{\text{av}}$  in a hot region of radius  $r = 3$  fm. It turns out that the intensity of sigma fluctuations does not depend strongly on the choice of the radius.

At the end of each time step the Fourier transform of the sigma field is calculated by a Fast Fourier Transform algorithm [NumRec]. These algorithms are implemented effectively only on lattices with  $N = 2^n$ ,  $n \in \mathbb{N}$ , cells in each direction. This limits the realistic choice of how to define the entire volume of the system. We simply perform Fourier transformations of the entire grid.

Spectra of transverse momentum at different times are shown in figure 7.7 for a critical point scenario and in figure 7.8 for a scenario with a first order phase transition.

For the three damping coefficients and the two phase transition scenarios we show the intensity of sigma fluctuations for the zero mode and low momentum modes in momentum ranges of  $\Delta|k| = 50$  MeV. Finally, we compare these values to the development of the deviations of the sigma field from its thermal equilibrium value. The initial conditions, see section 4.3.3, are chosen such that the sigma field is in equilibrium with the quark fluid at the initial temperature given in equation 4.32. In all three damping scenarios the intensity of sigma fluctuations is increased during the expansion and cooling. For a critical point scenario the results are shown in figure 7.9 for  $\eta = 2.2/\text{fm}$ , in figure

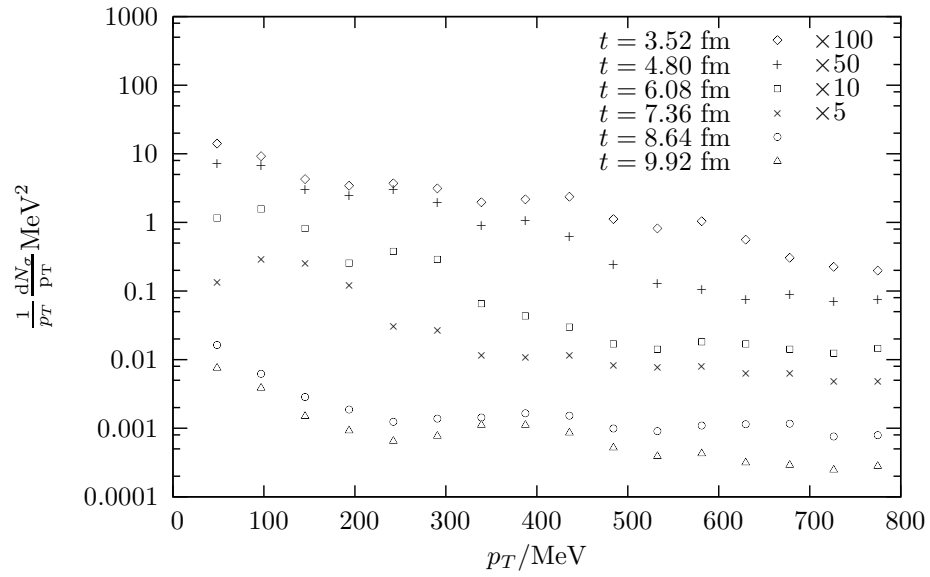


Figure 7.8.: Transverse momentum spectra for different times during the expansion and a scenario with a first order phase transition.

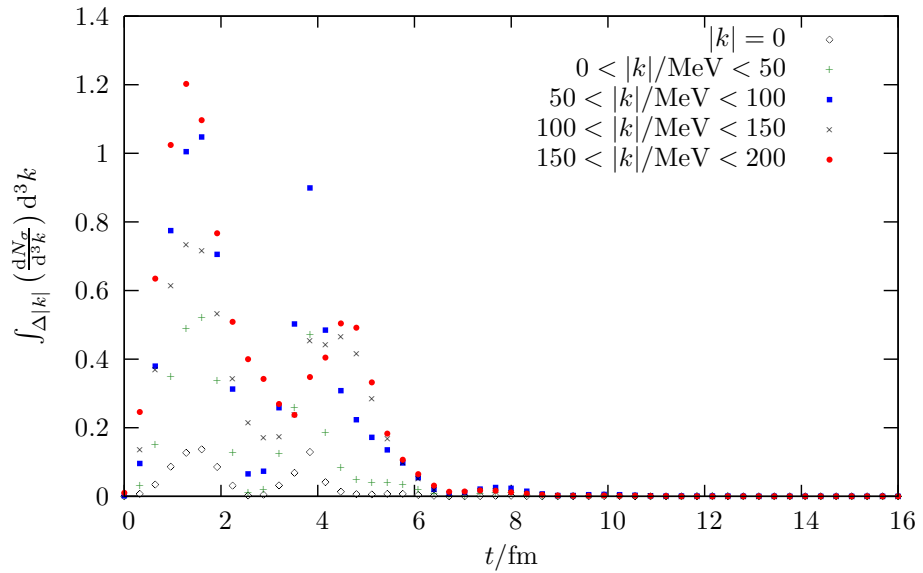


Figure 7.9.: The time evolution of the intensity of sigma fluctuations for  $\eta = 2.2/\text{fm}$  and a critical point scenario.

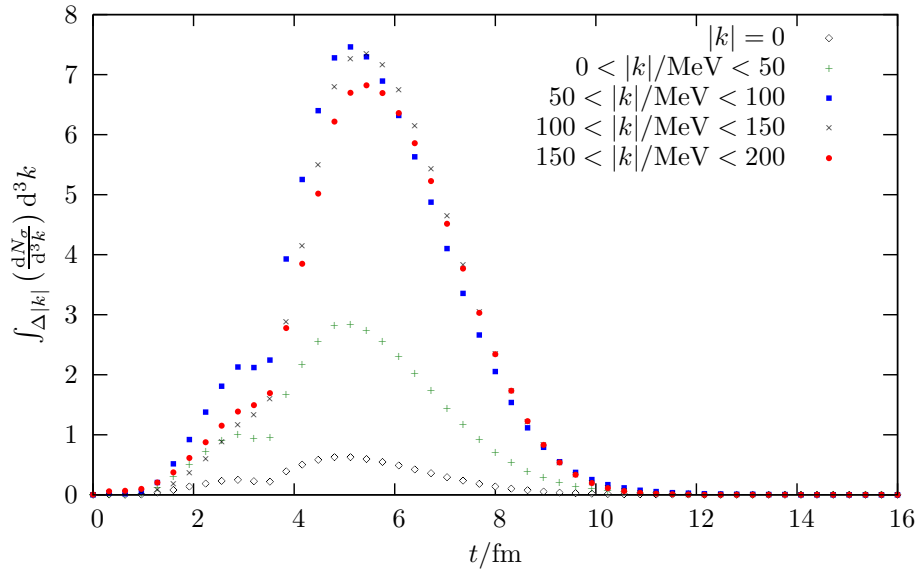


Figure 7.10.: The time evolution of the intensity of sigma fluctuations for  $\eta = 10/\text{fm}$  and a critical point scenario.

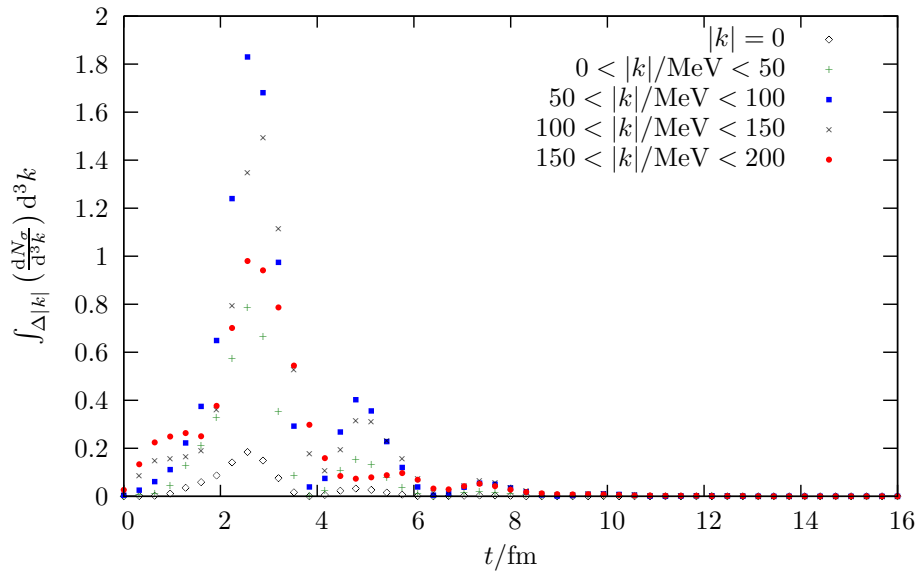


Figure 7.11.: The time evolution of the intensity of sigma fluctuations for  $\eta = \eta(T)/\text{fm}$  and a critical point scenario.

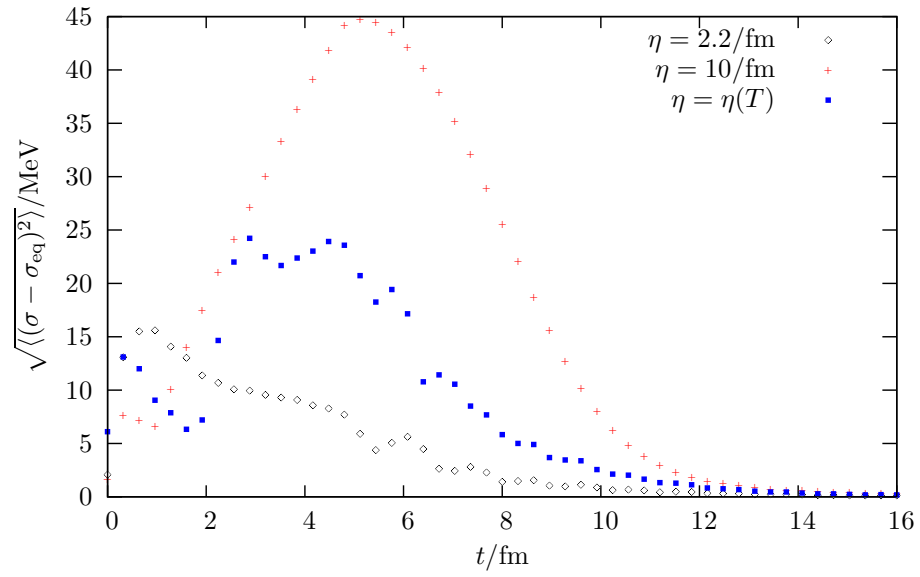


Figure 7.12.: The time evolution of the deviation of the sigma field from its equilibrium value for all three damping coefficients and a scenario with a critical point.

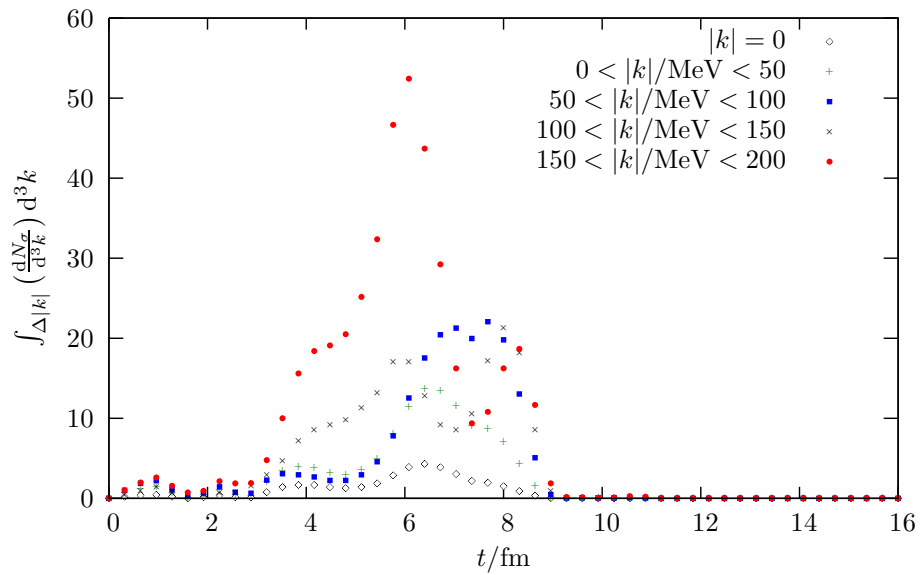


Figure 7.13.: The time evolution of the intensity of sigma fluctuations for  $\eta = 2.2/\text{fm}$  and a scenario with a first order phase transition.

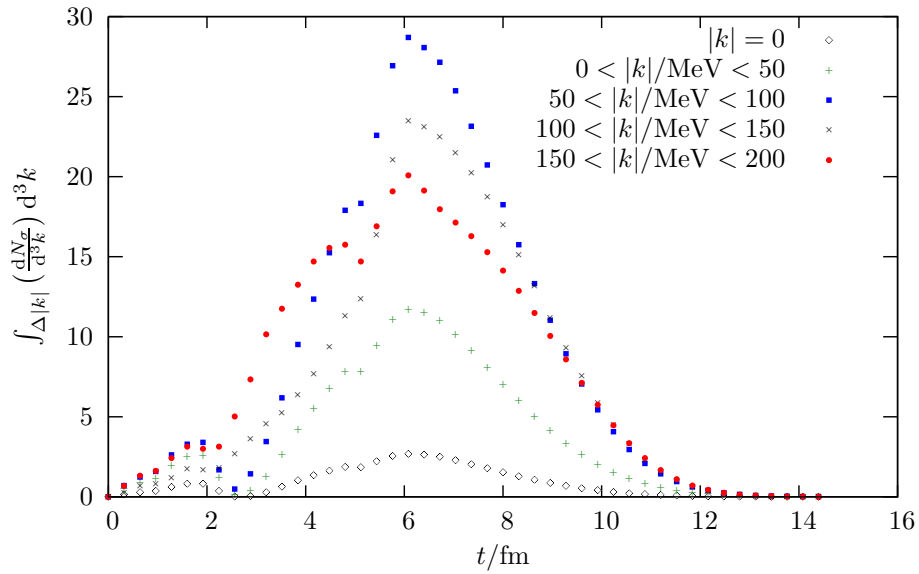


Figure 7.14.: The time evolution of the intensity of sigma fluctuations for  $\eta = 10/\text{fm}$  and a scenario with a first order phase transition.

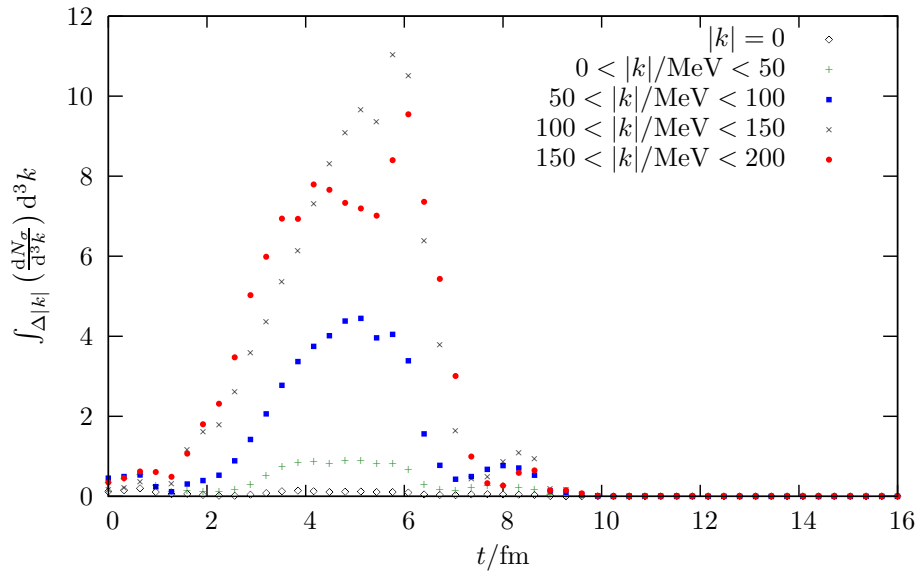


Figure 7.15.: The time evolution of the intensity of sigma fluctuations for  $\eta = \eta(T)$  and a scenario with a first order phase transition.

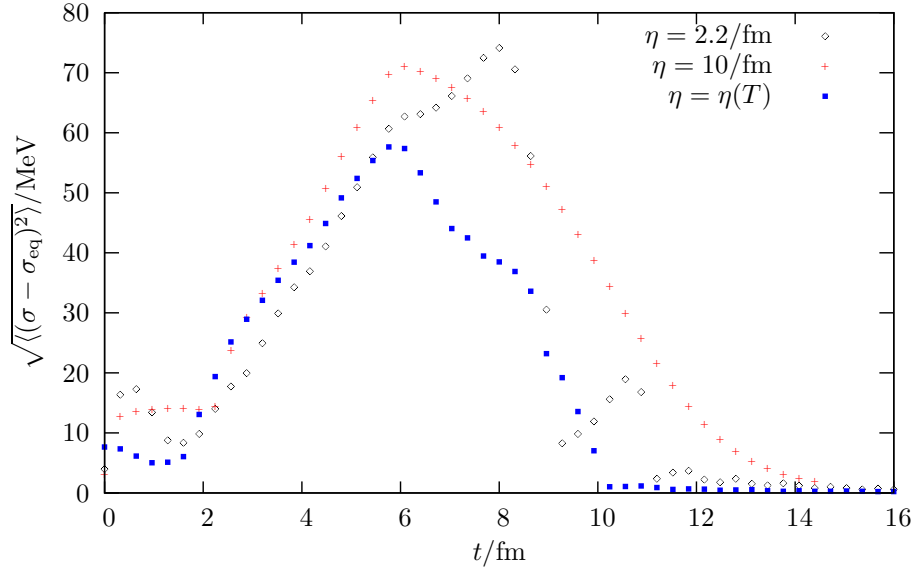


Figure 7.16.: The time evolution of the deviation of the sigma field from its equilibrium value for all three damping coefficients and a scenario with a first order phase transition.

7.10 for  $\eta = 10/\text{fm}$  and in figure 7.11 for the temperature-dependent damping coefficient  $\eta = \eta(T)$ . We see that the intensity of the soft modes is increased the most for the constant damping  $\eta = 10/\text{fm}$ . This can be understood by looking at the time evolution of the sigma fluctuations around the thermal equilibrium value plotted in figure 7.12 averaged over a region of radius  $r = 4$  fm. These are maximally increased for times between  $t = 5$  fm and  $t = 6$  fm for  $\eta = 10/\text{fm}$ . Here, the fluctuations reach the width of the effective potential. Fluctuations for the temperature-dependent damping are enhanced over the small constant damping which also results in an enhanced intensity of sigma fluctuations.

For the scenario with a first order phase transition the time evolution of the intensity of sigma fluctuations is shown in figure 7.13 for  $\eta = 2.2/\text{fm}$ , in figure 7.14 for  $\eta = 10/\text{fm}$  and in figure 7.15 for the temperature-dependent damping coefficient  $\eta = \eta(T)$ . Figure 7.16 shows the sigma fluctuations around the thermal equilibrium value. Since these fluctuations are larger than for the scenario with a critical point, the intensity of sigma fluctuations is also larger for all damping scenarios. We observe that for the smaller damping the higher modes are extremely populated at  $t \simeq 6$  fm slightly before the lower modes are intensified between  $t = 7$  fm and  $t = 8$  fm. We attribute this behavior to the relaxation of parts of the system outside of the region with radius  $r = 4$  fm, for which the sigma fluctuations around the equilibrium value are shown.

#### 7.4. Correlation length at the critical point

The growth of the correlation length at a critical point is the driving force for the predicted large fluctuations in observables like mean transverse momentum and particle multiplicities. The divergence of the correlation length only occurs in static infinite and homoge-



neous systems. In finite systems the correlation length is necessarily limited by the size of the system. Here, however, finite size scaling [Car96] developed within renormalization group methods can be applied to heavy-ion collisions [Pal10b]. More crucial are the issues of inhomogeneity, where temperature is defined only locally, and the dynamics of the system, which leads to critical slowing down, as discussed in section 2.4.2. Within a phenomenological model inspired by the  $\mathcal{O}(4)$ -Ising model and the dynamic universality class it was shown that finite time effects are more limiting on the growth of the correlation length than finite size [Ber00]. These calculations were, however, performed in a homogeneous system.

Here, we want to extract the correlation length of the fluctuations of the sigma field from the numeric simulation. We consider only the case of the temperature-dependent damping coefficient  $\eta = \eta(T)$ . Three measures of the correlation length are shown in figure 7.17 versus time. In mean-field approximations the correlation length is the inverse sigma mass and can thus be obtained from the curvature of the effective potential at the minimum ( $\xi_3$  in figure 7.17) or at the local value of the sigma field ( $\xi_1$  in figure 7.17). Both of these values are averaged over the inner sphere of radius  $r = 3$  fm.

The growth of the correlation length  $\xi_3$  is severely limited by the inhomogeneity of the system. The average correlation length  $\xi_1$  inherits the oscillations of the sigma mean field during the relaxational process.

The correlation length is also defined as the characteristic length, over which the radial correlation function in equation (2.35) exponentially decreases. It is generally difficult to obtain the thermodynamic correlation function from numeric simulations on finite and discretized spacetime. From fits to the correlation function (2.35) we obtain the correlation length  $\xi_2$  in figure 7.17. It also shows an increase at the phase transition. This, however, is where the error becomes rather large.

## 7.5. Momentum anisotropy

Fluctuations in well-defined thermodynamic systems lead to the most obvious observables of a phase transition. In heavy-ion collisions there are a couple of other signals, which are supposed to change characteristically at the phase transition. One of the most famous is the elliptic flow measured in noncentral collisions. Here, the overlap region of the two colliding nuclei has a spatial eccentricity in the transverse plane. If the system locally thermalizes early and shows collective fluid dynamic behavior, this spatial anisotropy leads to an anisotropy in the pressure gradients. This mechanism causes a momentum anisotropy and thus the build-up of elliptic flow in the transverse plane. It can be measured in the azimuthal angular dependence of particle multiplicity distributions and is characterized by the second Fourier coefficient

$$\frac{dN}{d\varphi} = \frac{dN}{2\pi p_T dp_T} \left( 1 + 2 \sum_{n=1}^{\infty} v_n \cos(n\varphi) \right). \quad (7.6)$$

Here,  $\varphi$  is the azimuthal angle with respect to the collision plane, which is defined by the direction of the beam axis and the impact parameter  $\vec{b}$ .  $v_1$  is called the directed flow

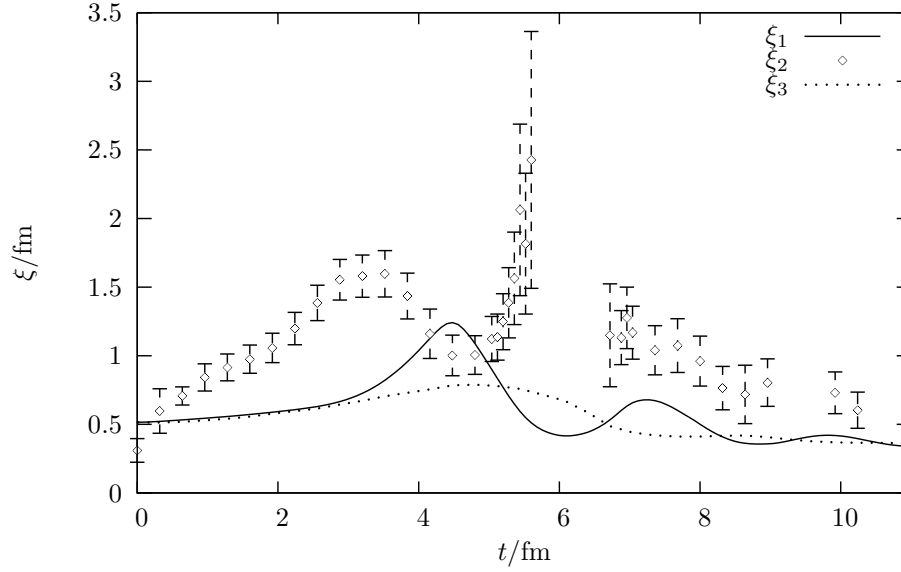


Figure 7.17.: The time evolution of the correlation length  $\xi$  obtained from different extraction methods:  $\xi_1$  from the sigma mass defined at the local value of the field,  $\xi_2$  from fits to the correlation function and  $\xi_3$  from the sigma mass defined at the global minimum of the potential.

and  $v_2$  is the elliptic flow. The collective flow depends on the equation of state and is, thus, expected to be affected by the phase transition. At a first order phase transition the equation of state has a softest point, see section 4.3.4, where  $p/e$  is very small. This weakens the build-up of the elliptic flow and one expects to observe less  $v_2$  in a scenario with a first order phase transition. Since by the same argument the fluid spends more time in the transition region it has a longer time for building up the elliptic flow. It has been found in many calculations that these effects cancel [Kol99, Kol00].

In order to determine the elliptic flow one has to perform a freeze-out, see section 2.4.1, to obtain the particle multiplicity distributions. We can, however, investigate the momentum anisotropy of the fluid even during the fluid dynamic expansion. It is

$$\epsilon_p = \frac{\langle T_{xx} - T_{yy} \rangle}{\langle T_{xx} + T_{yy} \rangle} \quad (7.7)$$

with

$$T_{ii}(x) = v_i(x)m_i(x) + p(x). \quad (7.8)$$

In [Kol99, Kol00] it was found that at the time of the freeze-out it is nearly identical to the  $p_T$ -weighted elliptic flow

$$v_{2,p_T^2} = \frac{\langle p_T^2 \cos(2\varphi) \rangle}{\langle p_T^2 \rangle}, \quad (7.9)$$

where the average is taken over the distribution of particle momenta.  $\epsilon_p$  gives a measure for the time evolution of the build-up of elliptic flow.

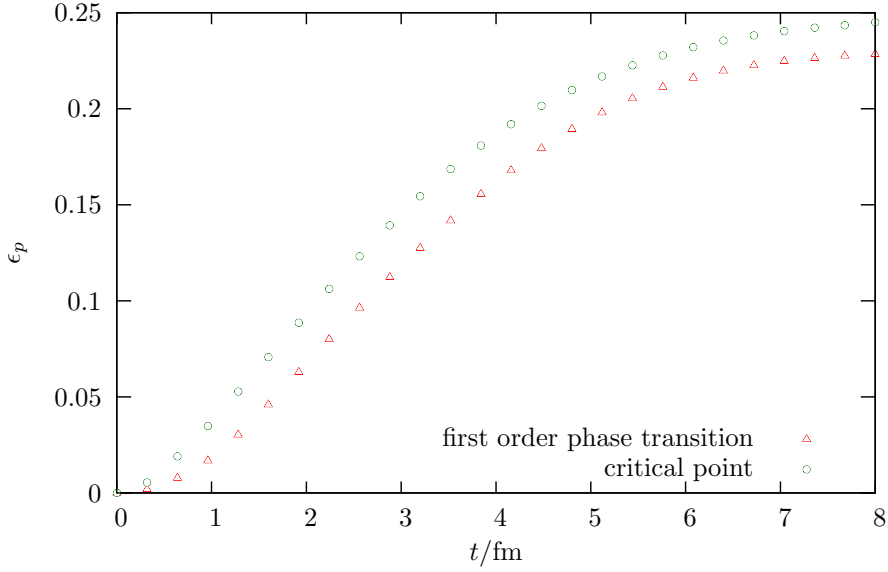


Figure 7.18.: The time evolution of the momentum anisotropy  $\epsilon_p$  for temperature-dependent damping.

In figure 7.18 we show  $\epsilon_p$  as a function of time for the temperature-dependent damping coefficient  $\eta = \eta(T)$  and both phase transition scenarios. By and large, the different calculations do not differ much. The momentum anisotropy is build up by the pressure gradients during the expansion and levels off when the initial spatial anisotropy is gone. For the smaller damping  $\epsilon_p$  is slightly below that for the larger damping. Generally, the values of  $\epsilon_p$  for a first order phase transition are only slightly lower than those for a scenario with a critical point. We do not observe any characteristic time evolution. It very much resembles the results obtained for an ideal gas equation of state in [Kol00]. We want to remark that the softest point in the equation of state is an equilibrium effect of the entire system and we cannot expect to see its effect in a nonequilibrium situation. This does still not contradict the plateau found in  $\epsilon_p/\epsilon_x$  in [Sor99], where the microscopic dynamics are solved according to a transport equation of one-particle distribution functions, claiming this to be a nonequilibrium effect. Here, the investigated nonequilibrium effects here are of Langevin type and therefore different. What we can expect to see is the effect of bubble formation at a first order phase transition. Since these bubbles do not show a spatial anisotropy on average it should lower the final value of  $v_2$ . We can observe this effect, when we take the local temperature dependence of the damping coefficient into account.



## 8. Summary and outlook

Nonequilibrium effects become important in the investigation of the QCD phase diagram by heavy-ion collisions. In this thesis we presented a combined approach to the chiral phase transition by embedding a field theoretical effective model of QCD into the realistic description of heavy-ion collisions by fluid dynamics.

While first principle calculations of the thermodynamics of QCD on the lattice predict the phase transition to be a crossover at zero baryochemical potential, at the present status they cannot give reliable results for finite baryonic densities. Concentrating on certain aspects of QCD, effective models cover broad ranges of the phase diagram. Studies of effective models strongly suggest that the phase transition is of first order at large baryonic densities. Thus, the existence of a critical point at the end of the first order phase transition line is conjectured. Effective models give, however, only a phenomenological picture of the strong interaction. Heavy-ion collisions can close the gap between phenomenology and the quantum field theory of the strong interaction, QCD, as they provide the only experimental tool to study the properties of strongly interacting matter. In order to study thermodynamic aspects of the underlying theory experimentally, one needs large systems, for which over long times the external parameters like temperature and pressure can be controlled. A heavy-ion collision is not like this. The size of the fireball created is of about the same order as the relevant length scales of the interaction, the dynamics is very fast and the external control of parameters is limited and possibly restricted to the beam energy and the type of the colliding nuclei. Still, fluid dynamic descriptions requiring local thermalization are in reasonable agreement with collective observables like elliptic flow measurements at RHIC and statistical model fits can reproduce the ratios of different particle yields. It should, therefore, be possible to observe signals of a phase transition, which is a thermodynamic concept, in heavy-ion collisions if one properly takes nonequilibrium effects into account.

In equilibrium, systems of very different microscopic nature show universal macroscopic properties at a second order phase transitions. Here, fluctuations and their correlation lengths diverge. This leads to critical phenomena like opalescence at the critical point of water. The growth of the correlation length is accompanied with very long relaxation times. In dynamic environments the system is necessarily driven out of equilibrium at a second order phase transition and the correlation length stays finite. All signals based on the divergence of the correlation are, therefore, crucially weakened. One of the questions we studied was how much of these fluctuation signals survive in the dynamics of a heavy-ion collision. At a first order phase transition nonequilibrium effects lead to supercooling and the subsequent relaxation of the systems via nucleation and spinodal decomposition. Both can lead to the formation of regions where the system is in the unstable phase. The

average size of these regions grows for the case of spinodal decomposition. This is predicted to be seen in the formation of disoriented chiral condensates. Thus, another question was how likely these nonequilibrium signals at a first order phase transition develop in a heavy-ion collision.

In this work we studied both of these questions within chiral fluid dynamics based on the linear sigma model with constituent quarks. The dynamics of the quarks and antiquarks is reduced to a fluid dynamic evolution of densities, while the order parameter of chiral symmetry breaking the sigma field is propagated explicitly. This gives rise to the name chiral fluid dynamics. As a first reference calculation we showed that fixing the sigma field to its equilibrium value and including thermal equilibrium fluctuations the growth of the fluctuations in an expansion scenario with a critical point is limited by the inhomogeneous temperature distribution.

In a first naïve approach to the dynamics of the sigma field the equation of motion was derived as a deterministic, classical Euler-Lagrange equation. It has a nontrivial source term, which depends on the local temperature and thus on the fluid dynamic expansion of the quarks. The equation of state is obtained from the one-loop thermodynamic potential in mean-field approximation and explicitly depends on the local value of the sigma field. In the relativistic fluid dynamic equations we found a source term describing the energy-momentum exchange between the field and the fluid. This source term showed to ensure energy-momentum conservation to a very good extent in the numerical simulation. The expansion and cooling of the quark fluid changes the effective potential for the sigma field and thus drives the system through the phase transition. The sigma field evolves towards its vacuum expectation. However, large oscillations develop during the evolution, since relaxational processes are not included in the dynamics. We call this the off-equilibrium expansion. The time evolution of the sigma field and the energy density was found to be qualitatively different: while fluctuations are more extended in space in a scenario with a critical point, bubble formation was observed in a scenario with a first order phase transition.

It was the main intention of this work to extend off-equilibrium chiral fluid dynamics by the consistent inclusion of nonequilibrium effects.

We succeeded in deriving the relaxational dynamics of the sigma mean-field from the two-particle irreducible (2PI) effective action. The 2PI effective action includes dissipative processes and gives rise to a damping term and a stochastic field. We explicitly evaluated the damping coefficient and the correlation of the stochastic field in Markovian approximation for the zero mode of the sigma mean-field. Although there is no confining in the underlying theory, the damping coefficient caused by the interaction of the sigma field with the quarks vanishes below the phase transition temperature due to kinematic reasons. While the quarks gain the constituent quark mass, the sigma mass gets smaller at the first order phase transition and very small at a critical point. Even at a realistic coupling of  $g = 3.3$  the vacuum sigma mass is smaller than twice the constituent quark mass. The damping coefficient can similarly be derived in the influence functional method, where an explicit splitting of the system in a relevant sector, here the sigma mean-field,

---

and an environment, here the quarks, must a priori be assumed. In these terms the quark fluid acts as a locally equilibrated heat bath. In the formalism of the influence functional it is, however, not possible to control the equilibrium properties of the quark fluid without further assumptions.

In the work presented, we put special emphasis on the consistent equilibrium properties of the heat bath. This is the main advantage of the 2PI effective action. It is a conserving and selfconsistent approximation to the full quantum theory. Besides the equation of motion for the sigma mean-field we obtain a Dyson-Schwinger equation for the real-time quark propagators. From the exact (for a given 2PI effective action) solution for the quark propagator we constructed a conserved energy-momentum tensor. For an explicit solution to the Dyson-Schwinger equation we had to make further approximations.

We were able to identify different terms in the divergence of the energy-momentum tensor of the entire system: a thermal part which coincides with the energy-momentum tensor for the classical fields and a correction term for both the quark and the sigma contributions to the energy-momentum balance. The correction to energy-momentum tensor of the sigma field includes the dissipative dynamics of the mean-field.

Next, we investigated the relaxational dynamics of the sigma mean-field for a global, i.e. space-homogeneous and isothermal heat bath for both phase transition scenarios according to the derived Langevin equation. For an initial distribution out of equilibrium we found that the system quickly develops a Gaussian distribution around the equilibrium value. For an initial equilibrium distribution at a high temperature the system relaxes after a temperature quench to the new equilibrium state. In both phase transition scenarios the relaxation times are larger for temperatures near the transition temperature. In a scenario with a first order phase transition this is due to the coexistence of the two phases and in a critical point scenario the very flat curvature of the effective potential leads to critical slowing down. During these relaxational processes we compared the energy of the sigma field to the source term derived in the 2PI effective action formalism. We saw that the net-energy flow consists of the energy dissipation from the sigma field to the heat bath and of the averaged energy transfer from the heat bath to the system via the stochastic noise field. For the investigation of the equilibration of the system coupled to a heat bath including reheating we determined the net-energy transfer. During the relaxation the local temperature of the heat bath increased. For the critical point scenario the entire coupled system finally reached equilibrium. Again, relaxation times were found to be longest for quenches that led the system to equilibrate near the critical temperature. For a scenario with a first order phase transition, however, local reheating prevented the system from an entire relaxation. Except of quenches to very low temperatures, the phase transition temperature was crossed once more in the reverse direction, but the system had already relaxed to the low-temperature phase now being a local minimum.

Finally, we studied the phase transition in the complete nonequilibrium description of the coupled chiral fluid dynamics. Here, we tested three different damping scenarios, two constant damping coefficients and the temperature dependent damping coefficient, which was derived for the linear sigma model with constituent quarks. In the energy-momentum balance we neglected the correction to the energy-momentum tensor of the quarks and

found that this is obviously a small quantity. In the time evolution of the average sigma mean-field and the temperature we observed the nonequilibrium effects of supercooling and reheating in a first order phase transition scenario. The intensity of this effect depends on the damping scenario. For the larger damping coefficients relaxation times are found to be unrealistically large. The most realistic picture is given by the temperature-dependent damping coefficient. Still, it only takes part of the nonequilibrium effects into account as it is derived with the equilibrium sigma mass. The intensity of sigma fluctuations, which gives the number of produced sigma particles at later stages of the evolution, was found to increase at the phase transition in all scenarios investigated. In a first order phase transition this is caused by supercooling and the subsequent relaxation via spinodal decomposition. The intensity of sigma fluctuations turned out to be larger in a scenario with a first order phase transition. While scanning the phase diagram of QCD by heavy-ion collisions it is thus more likely to observe nonequilibrium fluctuations of the first order phase transition than equilibrium fluctuations of the critical point. The inhomogeneity of the system given by the temperature being defined only locally makes it moreover difficult to define equilibrium quantities like the correlation length. However, these are aspects which also occur in the realistic scenario of a heavy-ion collision and make the experimental detection of equilibrium fluctuations of the critical point even more unlikely. The question about the existence and the location of a conjectured critical point could also be decided by an experimental proof of the first order phase transition. Combined with the lattice results on the crossover at zero baryochemical potential this is obvious for the existence of a critical point. The location could be determined by the beam energy, at which the signal of the first order phase transition disappears.

The main achievements of this thesis are the following:

- The development of a complete, selfconsistent quantum field theoretical approach to the treatment of dynamic phase transitions in nonequilibrium. Besides its application to the chiral phase transition in heavy-ion collisions it could be of interest for other fields of physics where phase transitions occur in a dynamic and expanding medium.
- The successful investigation of nonequilibrium phenomena at the phase transition embedded into a realistic evolution of a heavy-ion collision including relaxational dynamics. The effects of critical slowing down, supercooling and reheating were thoroughly studied and proved an increase of nonequilibrium fluctuations at the first order phase transition.

Our new approach allows for a couple of further developments leading towards a more quantitative description of the chiral phase transition in heavy-ion collisions. These cover both analytic and numeric aspects of the model. It would be interesting to implement the full nonequilibrium dependence of the damping coefficient  $\eta = \eta(\sigma, T)$ . The full dependence on the local value of the sigma mean-field would however capture more effects of spinodal decomposition at the first order phase transition.

So far we have only propagated the sigma field explicitly and fixed the pion degrees of freedom to their vacuum expectation value  $\langle \vec{\pi} \rangle = 0$ . Including the pions in the calculation



---

is the next step for a complete description. It also implies that the decay of the sigma particle into two pions need to be considered for a final spectrum of pions. It is also interesting to perform a freeze-out of the fluid and include this as a background of pions and see if the pions, which are characteristically produced at the phase transition, leave a significant imprint on the total pion distribution. This is also an important step towards studies of event-by-event fluctuations.

Below the phase transition the zero-mode damping coefficient originating from the quark interaction of the sigma field with the quarks vanishes. It would be interesting to include the effect of higher modes and see how this leads to additional damping processes. However, this would go beyond the Markovian approximation and thus complicates future numerical studies. Additional damping processes potentially also come from the interaction of the soft modes of the sigma field with the hard sigma and pion modes. These processes definitely occur below the phase transition and assure relaxational dynamics of the sigma field. Especially the decay and formation processes  $\sigma \leftrightarrow 2\pi$  become important at low temperatures where the pions are light.

For a more quantitative description it would be necessary to improve the model by the extension to finite baryochemical potential and the inclusion of the Polyakov loop. Moreover, the fluid dynamic treatment of the quarks might not always be valid, e.g. in the dilute phase. Starting from the Dyson-Schwinger equation one can derive a Vlasov-equation for the quark-antiquark Wigner function. It is a more challenging task to derive dissipation and noise from a Vlasov treatment of the quarks and antiquarks and is subject of ongoing research.

## 8. Summary and outlook

---

# Appendix A.

## SU(2) and SU(3)

Here, we summarize some important relations corresponding to the special unitary groups SU(2) and SU(3).

The special unitary group SU(2) consists of all unitary matrices with determinant 1 and is of special importance to the electroweak part in the standard model. It also appears in the two-flavor description of chiral symmetry. Every matrix  $U \in \text{SU}(2)$  can be written as

$$U = \exp(i\alpha^k \sigma^k), \quad (\text{A.1})$$

where  $\alpha^k$  are three real parameters and  $\sigma^k$  the Pauli spin matrices, which are the generators of SU(2).

$$\sigma^1 = \begin{pmatrix} 0 & 1 \\ 1 & 0 \end{pmatrix}, \quad \sigma^2 = \begin{pmatrix} 0 & -i \\ i & 0 \end{pmatrix}, \quad \sigma^3 = \begin{pmatrix} 1 & 0 \\ 0 & -1 \end{pmatrix}. \quad (\text{A.2})$$

They satisfy

$$[\sigma^j, \sigma^k] = 2i\sigma^l \varepsilon^{jkl}, \quad (\text{A.3})$$

with the Levi-Civita tensor  $\varepsilon^{ijk}$ .

The special unitary group SU(3) is the group of all 3x3 unitary matrices with determinant 1. It has 8 independent generators, which are represented by 3x3 hermitian ( $t_a = t_a^\dagger$ ) and traceless ( $\text{Tr } t_a = 0$ ) matrices. A matrix  $U \in \text{SU}(3)$  can be expressed as

$$U = \exp(i\beta^a t^a), \quad (\text{A.4})$$

where  $\beta^a$  are real parameters. In the fundamental representation the generators of SU(3) are given by the Gell-Mann matrices

$$t_a = \frac{\lambda_a}{2}, \quad (\text{A.5})$$

with

$$\begin{aligned} \lambda_1 &= \begin{pmatrix} 0 & 1 & 0 \\ 1 & 0 & 0 \\ 0 & 0 & 0 \end{pmatrix}, & \lambda_2 &= \begin{pmatrix} 0 & -i & 0 \\ i & 0 & 0 \\ 0 & 0 & 0 \end{pmatrix}, & \lambda_3 &= \begin{pmatrix} 1 & 0 & 0 \\ 0 & -1 & 0 \\ 0 & 0 & 0 \end{pmatrix}, \\ \lambda_4 &= \begin{pmatrix} 0 & 0 & 1 \\ 0 & 0 & 0 \\ 1 & 0 & 0 \end{pmatrix}, & \lambda_5 &= \begin{pmatrix} 0 & 0 & -i \\ 0 & 0 & 0 \\ i & 0 & 0 \end{pmatrix}, & \lambda_6 &= \begin{pmatrix} 0 & 0 & 0 \\ 0 & 0 & 1 \\ 0 & 1 & 0 \end{pmatrix}, \\ \lambda_7 &= \begin{pmatrix} 0 & 0 & 0 \\ 0 & 0 & -i \\ 0 & i & 0 \end{pmatrix}, & \lambda_8 &= \frac{1}{\sqrt{3}} \begin{pmatrix} 1 & 0 & 0 \\ 0 & 1 & 0 \\ 0 & 0 & -2 \end{pmatrix}. \end{aligned} \quad (\text{A.6})$$

The Gell-Mann matrices satisfy the commutation relation (cf. equation (2.5))

$$[\lambda_a, \lambda_b] = 2if_{abc}\lambda^c, \quad (\text{A.7})$$

with the structure constants  $f_{123} = 1$ ,  $f_{147} = f_{246} = f_{257} = f_{345} = f_{516} = f_{637} = 1/2$ ,  $f_{458} = f_{678} = \sqrt{3}/2$ .  $f_{abc}$  are odd under the transposition of any two indices and vanish for any two identical indices.

## Appendix B.

### The Grassmann algebra

The most complete and mathematically rigorous explanation of the Grassmann algebra in physics can be found in [Ber66].

#### B.1. The basic formulation

In the path integral formulation of the partition sum for fermions one integrates over classical fields, which by virtue of the spin-statistics theorem anticommute. They are described by the Grassmann algebra  $\mathcal{G}$ , which is an algebra with dimension  $N$  over a field  $\mathcal{K}$ . Any two elements from this algebra  $\eta, \theta \in \mathcal{G}$  anticommute

$$\eta\theta = -\theta\eta, \quad (\text{B.1})$$

from which immediately follows that the square of any Grassmann number vanishes

$$\eta^2 = 0. \quad (\text{B.2})$$

Consequently, the Taylor expansion of a general function  $f : \mathcal{G} \mapsto \mathcal{G}$  terminates after the linear term

$$f(\eta) = a + b\eta, \quad (\text{B.3})$$

with any  $a, b \in \mathcal{K}$ .

For the description of Dirac fields one needs to introduce a complex Grassmann algebra, which is simply a  $2N$  dimensional real Grassmann algebra over the field of complex numbers. Then, any Grassmann number  $\eta$  is defined by a real  $\eta_1$  and an imaginary part  $\eta_2$

$$\eta = \frac{\eta_1 + i\eta_2}{\sqrt{2}}. \quad (\text{B.4})$$

The complex conjugation is defined like the Hermitian conjugation of operators

$$(\eta\theta)^* = \theta^*\eta^* = -\eta^*\theta^*. \quad (\text{B.5})$$

#### B.2. Differentiation

Due to the anticommuting property the sign in derivatives must be defined. The usual convention is

$$\frac{\partial}{\partial\eta}\eta\theta = \theta \quad \text{and} \quad \frac{\partial}{\partial\eta}\theta\eta = -\theta. \quad (\text{B.6})$$

With the property (B.3) one sees immediately that the second derivative with respect to the same variable of any function always vanishes

$$\frac{\partial^2}{\partial^2 \eta} f(\eta) = 0. \quad (\text{B.7})$$

### B.3. Integration

For the evaluation of path integrals over Grassmann variables one needs to define the integration over Grassmann-valued functions and integration measures of the Grassmann algebra. This can not be done in the same manner as for complex numbers. Because of (B.7) one can not simply define the integration as the inverse operation to differentiation. This means that there is no indefinite integral. Every integral must be translationally invariant

$$\int d\eta f(\eta + \theta) \stackrel{!}{=} \int d\eta f(\eta). \quad (\text{B.8})$$

This leads to

$$\begin{aligned} \int d\eta f(\eta + \theta) &= \int d\eta (a + b(\eta + \theta)) \\ &= \int d\eta (a + b\theta) + \int db\eta \\ &\stackrel{!}{=} \int d\eta f(\eta) = \int d\eta a + \int d\eta b\eta, \end{aligned} \quad (\text{B.9})$$

which for any  $a, b \in \mathbb{C}$  and  $\theta \in \mathcal{G}$  can be solved nontrivially only for

$$\int d\eta = 0 \quad \text{and} \quad \int d\eta \eta = \text{const.} = 1. \quad (\text{B.10})$$

A one-dimensional Gauss integral with  $b \in \mathbb{C}$  reads

$$\int d\eta^* d\eta \exp(-\eta^* b \eta) = \int d\eta^* d\eta (1 - \eta^* b \eta) = b, \quad (\text{B.11})$$

by Taylor expanding the exponential function. In the same manner a  $N$ -dimensional Gauss integral evaluates to

$$\int d\eta_1^* d\eta_1 \dots \int d\eta_N^* d\eta_N \exp\left(-\sum_{i,j} \eta_i^* B_{ij} \eta_j\right) = \det B, \quad (\text{B.12})$$

for any hermitian matrix  $B \in \mathbb{C}^{N \times N}$ .

## Appendix C.

### The one-loop partition function in imaginary time formalism

The imaginary-time formalism, which was presented in section 3.1, is best suited to study systems in equilibrium. Here, we explain the explicit calculation of the partition functions for free bosons and fermions.

#### C.1. The free propagators in imaginary time

The free bosonic and fermionic imaginary-time propagators are obtained from solving the Klein-Gordon and Dirac equations in Euclidean space. The calculations are the same as for zero temperature, except for the definition on the discrete Matsubara frequencies instead of continuous frequencies. For bosons the propagator is

$$D(\vec{k}, \omega_n) = \frac{1}{\omega_n^2 + \vec{k}^2 + m^2}, \quad (\text{C.1})$$

with the Matsubara frequencies (3.17a). And the fermionic propagator reads

$$S(\vec{k}, \omega_n) = \frac{1}{\not{k} - m}, \quad (\text{C.2})$$

with  $k_0 = i\omega_n$  and the Matsubara frequencies (3.17b).

#### C.2. Partition function for free bosons

The starting point for the evaluation of the partition function is equation (3.4). The Euclidean action for a noninteracting real Klein-Gordon field  $\phi$  is obtained by a Wick rotation  $t \mapsto -i\tau$

$$\begin{aligned} S_E &= \int_0^\beta d\tau \int d^3x \mathcal{L}_E = \frac{1}{2} \int_0^\beta d\tau \int d^3x \left[ \left( \frac{\partial \phi}{\partial \tau} \right)^2 + (\vec{\nabla} \phi)^2 + m^2 \phi^2 \right] \\ &= \frac{1}{2} \int_0^\beta d\tau \int d^3x \phi \left( -\frac{\partial^2}{\partial \tau^2} + \vec{\nabla}^2 + m^2 \right) \phi, \end{aligned} \quad (\text{C.3})$$

after partial integration and applying the periodicity  $\phi(\vec{x}, \beta) = \phi(\vec{x}, 0)$ . The Fourier transform of the field  $\phi(\vec{x}, \tau)$

$$\phi(\vec{x}, \tau) = \sqrt{\frac{\beta}{V}} \sum_{n=-\infty}^{\infty} \sum_{\vec{p}} \exp[i(\vec{p} \cdot \vec{x} + \omega_n \tau)] \phi_n(\vec{p}), \quad (\text{C.4})$$

is defined on the discrete Matsubara frequencies (3.17a). With  $\phi_{-n}(-\vec{p}) = \phi_n^*(\vec{p})$  for real fields the action can be evaluated to

$$S_E = \frac{1}{2} \beta^2 \sum_n \sum_{\vec{p}} (\omega_n^2 + \vec{p}^2 + m^2) \phi_n(\vec{p}) \phi_n^*(\vec{p}). \quad (\text{C.5})$$

The integrand in (3.4) does not depend on the phase of  $\phi$  but only on its amplitude  $A_n$

$$Z = \mathcal{N} \int_{\text{periodic}} \mathcal{D}\phi \prod_n \prod_{\vec{p}} \int_{-\infty}^{\infty} dA_n(\vec{p}) \exp \left[ -\frac{1}{2} \beta^2 (\omega_n^2 + \omega^2) A_n^2(\vec{p}) \right], \quad (\text{C.6})$$

with  $\omega = \sqrt{\vec{p}^2 + m^2}$ . Gauss integration gives by ignoring a volume and temperature independent factor, which does not affect the thermodynamics,

$$Z = \prod_n \prod_{\vec{p}} (\beta^2 (\omega_n^2 + \omega^2))^{-1/2}. \quad (\text{C.7})$$

Then, taking the logarithm gives

$$\ln Z = -\frac{1}{2} \sum_n \sum_{\vec{p}} \ln [\beta^2 (\omega_n^2 + \omega^2)]. \quad (\text{C.8})$$

With the Matsubara frequencies (3.17a) the frequency sums can be evaluated by using the identities

$$\int_1^{\beta^2 \omega^2} d\theta^2 \frac{1}{\theta^2 + (2\pi n)^2} = \ln[\beta^2 \omega^2 + (2\pi n)^2] - \ln[1 + (2\pi n)^2] \quad (\text{C.9})$$

and

$$\sum_{n=-\infty}^{\infty} \frac{1}{n^2 + (\theta/2\pi)^2} = \frac{2\pi^2}{\theta} \left( 1 + \frac{2}{\exp \theta - 1} \right). \quad (\text{C.10})$$

Neglecting temperature independent terms yields

$$\ln Z = - \sum_{\vec{p}} \left( \frac{1}{2} \beta \omega + \ln(1 - \exp(-\beta \omega)) \right) = V \int \frac{d^3 p}{(2\pi)^3} \left( \frac{1}{2} \beta \omega + \ln(1 - \exp(-\beta \omega)) \right). \quad (\text{C.11})$$

The first term in (C.11) is not finite. It corresponds to the zero-temperature energy

$$E_0 = -\frac{\partial}{\partial \beta} \ln Z_0 = V \int \frac{d^3 p}{(2\pi)^2} \omega, \quad (\text{C.12})$$

and pressure

$$p_0 = T \frac{\partial}{\partial V} \ln Z_0 = -\frac{E_0}{V}. \quad (\text{C.13})$$



For a proper definition of the vacuum it should be subtracted. Starting from (C.3) one can express the partition function as

$$Z = \mathcal{N} \int_{\text{periodic}} \mathcal{D}\phi \exp \left[ -\frac{1}{2} \phi D \phi \right] = \mathcal{N}' (\det D)^{-1/2} \quad (\text{C.14})$$

with the functional determinant of  $D = \beta^2(\omega_n^2 + \omega^2)$  in momentum space and  $D = -\partial^2/\partial^2\tau + \vec{\nabla}^2 + m^2$  in coordinate space. This formulation allows for a simple extension to a charged field  $\Phi = (\phi_1, \phi_2)$ .  $\Phi$  is complex and describes particles and antiparticles. A chemical potential  $\mu$  is associated with the conserved charge corresponding to the U(1) symmetry of a complex Klein-Gordon field. For this theory

$$D = \beta^2 \begin{pmatrix} \omega_n^2 + \omega^2 - \mu^2 & -2\mu\omega_n \\ 2\mu\omega_n & \omega_n^2 + \omega^2 - \mu^2 \end{pmatrix} \quad (\text{C.15})$$

and

$$\begin{aligned} \ln Z &= -\frac{1}{2} \ln(\det D) \\ &= -\frac{1}{2} \ln \left( \prod_n \prod_{\vec{p}} \beta^4 ((\omega_n^2 + \omega^2 - \mu)^2 + 4\mu^2 \omega_n^2) \right) \\ &= -\frac{1}{2} \ln \left( \prod_n \prod_{\vec{p}} \beta^2 (\omega_n^2 + (\omega - \mu)^2) \right) - \frac{1}{2} \ln \left( \prod_n \prod_{\vec{p}} \beta^2 (\omega_n^2 + (\omega + \mu)^2) \right). \end{aligned} \quad (\text{C.16})$$

Thus, with a simple substitution  $\omega \mapsto \omega \pm \mu$  for the terms in (C.16) the results from (C.11) can be transferred to

$$\ln Z = -V \int \frac{d^3p}{(2\pi)^2} (\beta\omega + \ln [1 - \exp(-\beta(\omega - \mu))] + \ln [1 - \exp(-\beta(\omega + \mu))]). \quad (\text{C.17})$$

### C.3. Partition function for free fermions

The partition function of noninteracting fermions can be evaluated very analogously to the case of free bosons, but we have to take into account that fermionic operators obey the anticommutation relations

$$\left[ \hat{\psi}_\alpha(x), \hat{\psi}_\beta^\dagger(y) \right]_+ = \hbar \delta_{\alpha\beta} \delta(x - y) \quad (\text{C.18})$$

$$\left[ \hat{\psi}_\alpha(x), \hat{\psi}_\beta(y) \right]_+ = \left[ \hat{\psi}_\alpha^\dagger(x), \hat{\psi}_\beta^\dagger(y) \right]_+ = 0. \quad (\text{C.19})$$

In the path integral formulation of the partition function one integrates over classical fields, which in the limit  $\hbar \rightarrow 0$  anticommute. Fermions must, therefore, be described by Grassmann numbers, see appendix B.

The Euclidean action for free fermions is

$$S_E = \int_0^\beta d\tau \int d^3x \mathcal{L}_E = \bar{\psi} (\gamma^0 \frac{\partial}{\partial \tau} - i\vec{\gamma} \cdot \vec{\nabla} + m - \mu\gamma^0) \psi. \quad (\text{C.20})$$

After Fourier transformation of the fields the partition function reads

$$\begin{aligned}
 Z &= \mathcal{N} \int_{\text{antiper.}} \mathcal{D}\bar{\psi} \int_{\text{antiper.}} \mathcal{D}\psi \exp \left[ -\beta \sum_n \sum_{\vec{p}} \bar{\psi}_n(\vec{p}) (i\gamma^0(\omega_n + i\mu) + \vec{\gamma}\vec{p} + m) \psi_n(\vec{p}) \right] \\
 &= \det [\beta(i\gamma^0(\omega_n + i\mu) + \vec{\gamma}\vec{p} + m)] ,
 \end{aligned} \tag{C.21}$$

with antiperiodic boundary conditions in the fermionic path integral.

It is useful to evaluate the determinant over Dirac indices first and then use  $\ln \det A = \text{Tr} \ln A$  to trace over momenta and frequencies

$$\begin{aligned}
 \ln Z &= 2 \sum_n \sum_{\vec{p}} \ln [\beta^2((\omega_n + i\mu)^2 + \omega^2)] \\
 &= \sum_n \sum_{\vec{p}} (\ln [\beta^2(\omega_n^2 + (\omega - \mu)^2)] + \ln [\beta^2(\omega_n^2 + (\omega + \mu)^2)]) ,
 \end{aligned} \tag{C.22}$$

where it was used that the sum over Matsubara frequencies is symmetric. The subsequent evaluation of the Matsubara sums is carried out by using (C.9) and similarly to (C.10)

$$\sum_{n=-\infty}^{\infty} \frac{1}{(2n+1)^2\pi^2 + \theta^2} = \frac{1}{\theta} \left( \frac{1}{2} + \frac{1}{\exp \theta + 1} \right) . \tag{C.23}$$

By neglecting terms independent of  $\beta$  and  $V$  the final integration yields

$$\ln Z = 2V \int \frac{d^3p}{(2\pi)^3} (\beta\omega + \ln [1 + \exp(-\beta(\omega - \mu))] + \ln [1 + \exp(-\beta(\omega + \mu))]) . \tag{C.24}$$

The factor 2 describes the two spin degrees of freedom accounting for the spin-1/2 nature of fermions. Again, we have to subtract the zero-temperature energy.

Imaginary-time formalism in its path integral formulation is analogous to field theoretical methods at zero temperature. It is, therefore, not astonishing that the diagrammatic perturbation expansion and the Feynman rules can be derived from the path integral in exactly the same manner [Kap94]. The only difference is in the boundary conditions, which give rise to the temperature dependence.

## Appendix D.

### Parametrization of the equation of state

In the relativistic fluid dynamic code one often needs the equation of state, which is the relation between the energy density and the pressure in the local rest frame of the fluid  $p = p(e)$ . In order to obtain the local pressure  $p(x) = p(\phi(x), T(x))$  one has to invert the local energy density  $e(x) = e(\phi(x), T(x))$  (4.25) for a given local energy density of the fluid  $e_{\text{fluid}}(x)$  and a given local value of the chiral fields  $\phi(x)$ . This gives the local temperature  $T(x)$  from the solution of

$$e_{\text{fluid}}(x) - e(\phi(x), T(x)) = 0. \quad (\text{D.1})$$

The local temperature  $T(x)$  is then inserted in (4.24). Finding the solution of (D.1) is very time consuming. It is, therefore, numerically not feasible to do the inversion every time the equation of state  $p = p(e)$  is needed. The dependence on the chiral fields is through the energy of the quarks,  $E = \sqrt{p^2 + g^2|\phi|^2}$ . It can be parametrized with

$$p(e) = a_0(|\phi|)e + a_1(|\phi|)e^2 + a_2(|\phi|)e^3 \quad (\text{D.2})$$

and with the coefficients for  $g|\phi| < 500$  MeV:

$$\begin{aligned} a_0(|\phi|) = & 0.333333 + 1.63924 \cdot 10^{-05}g|\phi| - 3.40087 \cdot 10^{-06}(g|\phi|)^2 \\ & + 1.32825 \cdot 10^{-08}(g|\phi|)^3 - 2.46749 \cdot 10^{-11}(g|\phi|)^4 + 2.31484 \cdot 10^{-14}(g|\phi|)^5 \\ & - 8.73269 \cdot 10^{-18}(g|\phi|)^6 \end{aligned} \quad (\text{D.3})$$

$$\begin{aligned} a_1(|\phi|) = & -1.18556 \cdot 10^{-08}(g|\phi|) + 1.91555 \cdot 10^{-09}(g|\phi|)^2 - 1.00771 \cdot 10^{-11}(g|\phi|)^3 \\ & + 2.35985 \cdot 10^{-14}(g|\phi|)^4 - 2.73812 \cdot 10^{-17}(g|\phi|)^5 + 1.28238 \cdot 10^{-20}(g|\phi|)^6 \end{aligned} \quad (\text{D.4})$$

$$\begin{aligned} a_2(|\phi|) = & 2.56706 \cdot 10^{-12}(g|\phi|) - 3.78345 \cdot 10^{-13}(g|\phi|)^2 + 2.13608 \cdot 10^{-15}(g|\phi|)^3 \\ & - 5.33201 \cdot 10^{-18}(g|\phi|)^4 + 6.55426 \cdot 10^{-21}(g|\phi|)^5 - 3.23409 \cdot 10^{-24}(g|\phi|)^6 \end{aligned} \quad (\text{D.5})$$

and for larger values of  $g|\phi|$ :

$$\begin{aligned} a_0(|\phi|) = & 0.343264 - 0.000485805(g|\phi|) + 5.22853 \cdot 10^{-07}(g|\phi|)^2 \\ & - 3.34684 \cdot 10^{-10}(g|\phi|)^3 + 1.24058 \cdot 10^{-13}(g|\phi|)^4 - 2.4531 \cdot 10^{-17}(g|\phi|)^5 \\ & + 2.00151 \cdot 10^{-21}(g|\phi|)^6 \end{aligned} \quad (\text{D.6})$$

$$\begin{aligned} a_1(|\phi|) = & 3.17691 \cdot 10^{-05} + 2.83658 \cdot 10^{-08}(g|\phi|) - 8.03578 \cdot 10^{-11}(g|\phi|)^2 \\ & + 7.11458 \cdot 10^{-14}(g|\phi|)^3 - 3.10115 \cdot 10^{-17}(g|\phi|)^4 + 6.79465 \cdot 10^{-21}(g|\phi|)^5 \\ & - 5.96383 \cdot 10^{-25}(g|\phi|)^6 \end{aligned} \quad (\text{D.7})$$

*Appendix D. Parametrization of the equation of state*

---

$$\begin{aligned} a_2(|\phi|) = & -6.71523 \cdot 10^{-09} + 1.82283 \cdot 10^{-12}(g|\phi|) + 4.17458 \cdot 10^{-15}(g|\phi|)^2 \\ & - 5.20079 \cdot 10^{-18}(g|\phi|)^3 + 2.5609 \cdot 10^{-21}(g|\phi|)^4 - 6.03135 \cdot 10^{-25}(g|\phi|)^5 \quad (\text{D.8}) \\ & + 5.57109 \cdot 10^{-29}(g|\phi|)^6 \end{aligned}$$

These two parts connect continuously.

Alternatively, the equation of state can be read in from a table, which is the appropriate way when including more quantities like the baryochemical potential or the Polyakov-loop variable.

## Appendix E.

### Feynman rules on the closed time path

The diagrammatic Feynman rules for the calculation of  $\Gamma_2$  on the closed time path are taken from [Iva99]. For a Yukawa interaction  $\mathcal{L}_{\text{int}}(x) = -g\bar{q}(x)\sigma(x)q(x)$  the vertex factor is  $v(x) = -ig$ . The sigma mean-field  $\sigma$  is given by zigzag lines closed by a cross to indicate that it is not an external line.

1. Draw all topological distinct, connected diagrams with  $N$  internal vertices  $x_1, \dots, x_N$  contributing to  $\Gamma_2$ . There are no external lines.
2. Keep only two-particle irreducible diagrams, i.e. those that cannot be separated by cutting two lines.
3. Assign a sign  $i_k \in \{+, -\}$  for the contour branch to each internal vertex  $x_k^{i_k}$ . Each line, which connects two vertices  $x_k^{i_k}$  and  $x_l^{i_l}$  gives a factor  $iS^{i_k i_l}(x_k, x_l)$ .
4. Assign a sigma mean-field  $\sigma(x_k)$  to all zigzag lines at  $x_k$ .
5. Assign a vertex factor  $v(x)$  to each vertex  $x_k$ .
6. Integrate over all internal vertices  $x_1, \dots, x_N$  on the real-time axis, multiply each internal  $\pm$ -vertex by  $(-1)$  and sum over all internal contour branches  $i_1, \dots, i_N$  with  $i_k \in \{+, -\}$ .
7. Sum all diagrams, including an extra factor of  $1/N$  for each diagram.
8. Multiply all fermion loops with a factor  $(-1)$ .



## Appendix F.

# Energy conservation in nonequilibrium chiral fluid dynamics

### F.1. Constant damping coefficient $\eta = 2.2/\text{fm}$

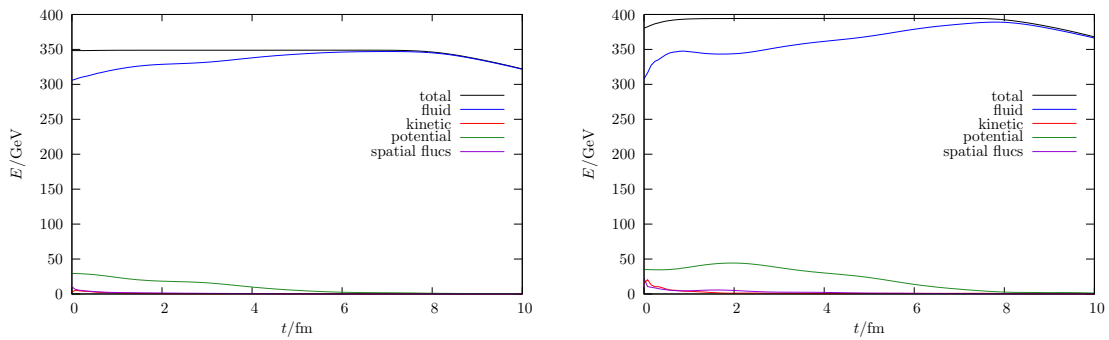


Figure F.1.: The total energy of the system for  $\eta = 2.2/\text{fm}$  and a critical point scenario (left) and a scenario with a first order phase transition (right).

### F.2. Constant damping coefficient $\eta = 10/\text{fm}$

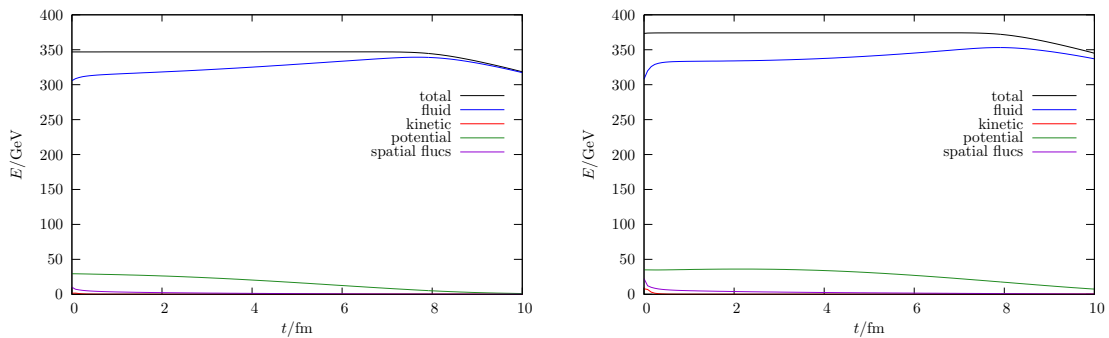


Figure F.2.: The total energy of the system for  $\eta = 10/\text{fm}$  and a critical point scenario (left) and a scenario with a first order phase transition (right).

### F.3. Temperature dependent damping coefficient $\eta = \eta(T)$

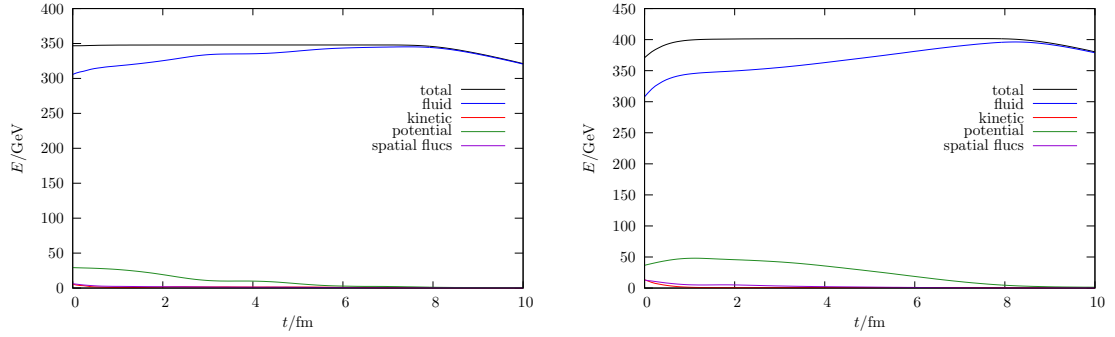


Figure F.3.: The total energy of the system for  $\eta = \eta(T)$  and a critical point scenario (left) and a scenario with a first order phase transition (right).



## Appendix G.

# Energy density in nonequilibrium chiral fluid dynamics

### G.1. Constant damping coefficient $\eta = 2.2/\text{fm}$

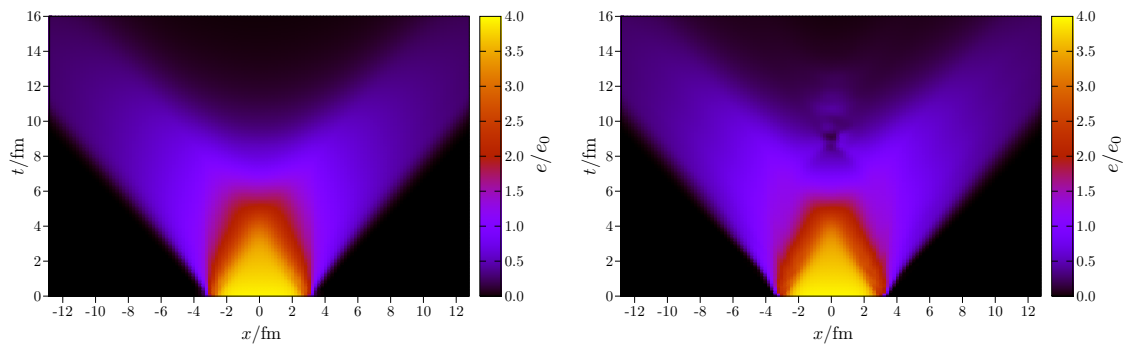


Figure G.1.: Time evolution of the energy density for  $\eta = 2.2/\text{fm}$  and a critical point scenario (left) and a scenario with a first order phase transition (right).

### G.2. Constant damping coefficient $\eta = 10/\text{fm}$

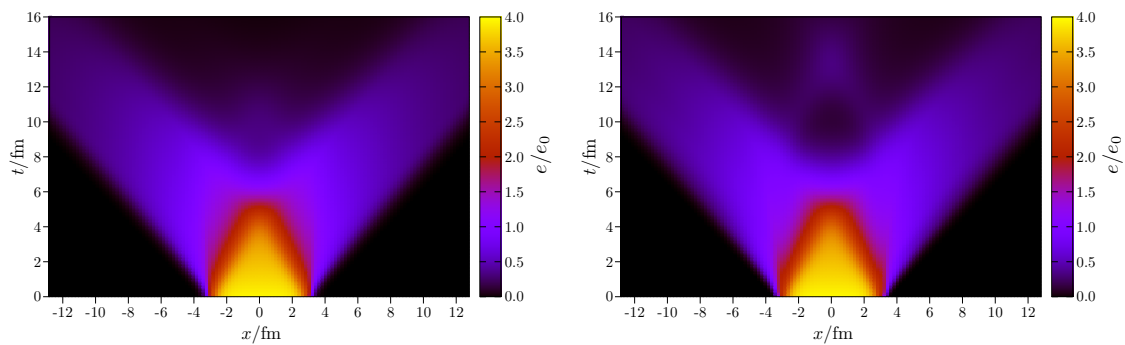


Figure G.2.: Time evolution of the energy density for  $\eta = 10/\text{fm}$  and a critical point scenario (left) and a scenario with a first order phase transition (right).

### G.3. Temperature dependent damping coefficient $\eta = \eta(T)$

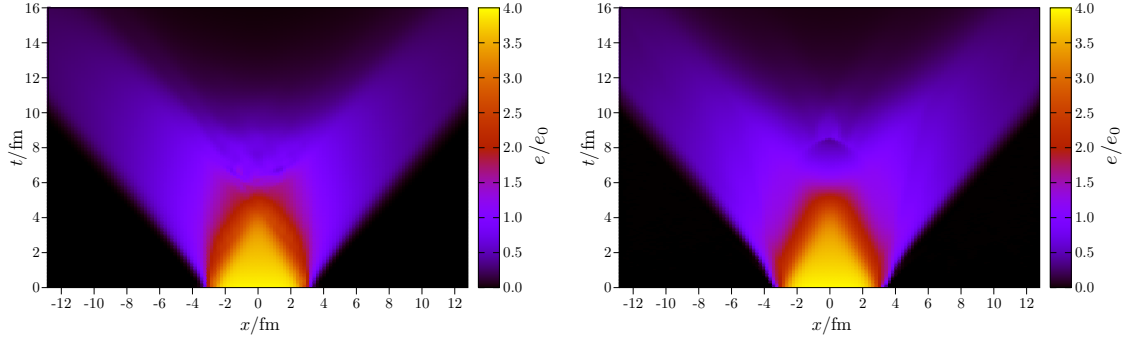


Figure G.3.: Time evolution of the energy density for  $\eta = \eta(T)$  and a critical point scenario (left) and a scenario with a first order phase transition (right).

## Appendix H.

# Sigma field in nonequilibrium chiral fluid dynamics

### H.1. Constant damping coefficient $\eta = 2.2/\text{fm}$

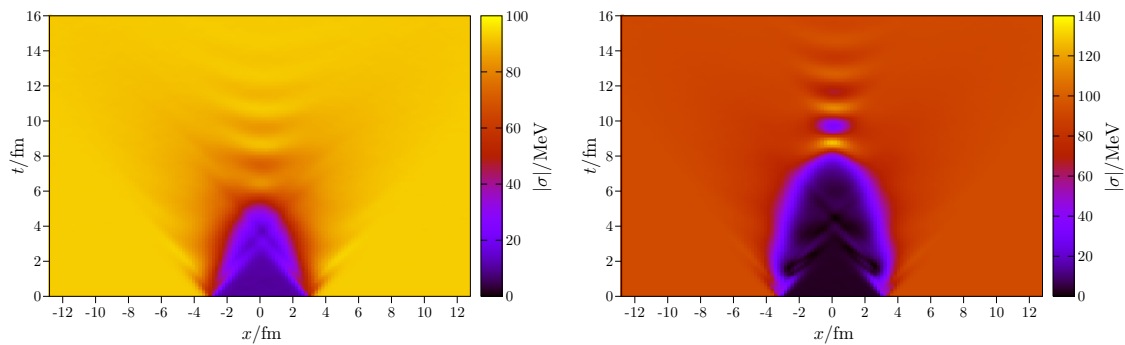


Figure H.1.: Time evolution of the sigma field for  $\eta = 2.2/\text{fm}$  and a critical point scenario (left) and a scenario with a first order phase transition (right).

### H.2. Constant damping coefficient $\eta = 10/\text{fm}$

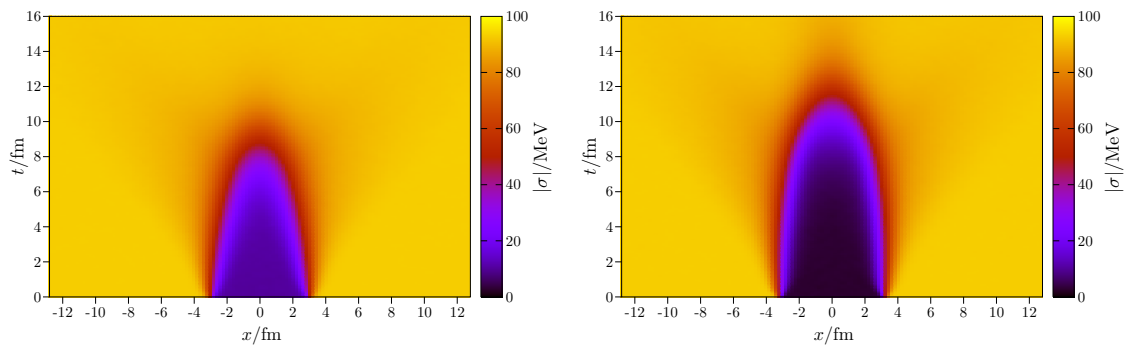


Figure H.2.: Time evolution of the sigma field for  $\eta = 10/\text{fm}$  and a critical point scenario (left) and a scenario with a first order phase transition (right).

### H.3. Temperature dependent damping coefficient $\eta = \eta(T)$

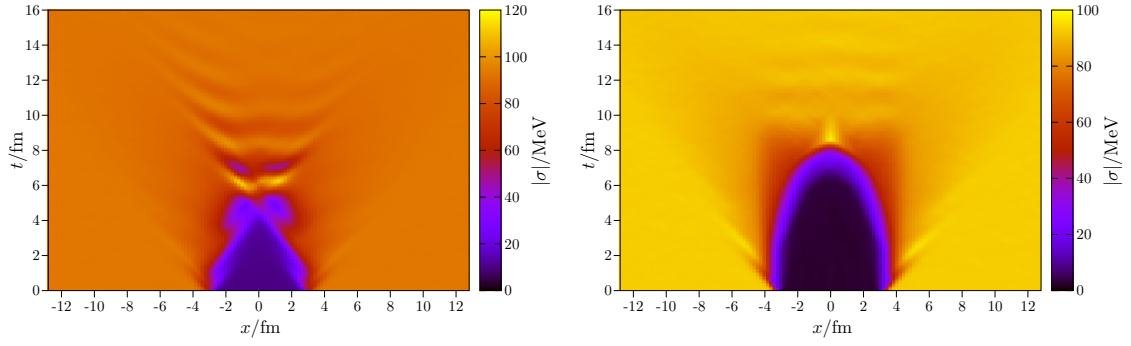


Figure H.3.: Time evolution of the sigma field for  $\eta = \eta(T)$  and a critical point scenario (left) and a scenario with a first order phase transition (right).

# Bibliography

- [Aba97] A. Abada, M. C. Birse, "Coherent amplification of classical pion fields during the cooling of droplets of quark plasma", *Phys. Rev.* **D55** (1997) 6887-6899.
- [Agu06] C. E. Aguiar, E. S. Fraga, T. Kodama, "Hydrodynamical instabilities beyond the chiral critical point", *J. Phys. G* **G32** (2006) 179-188.
- [Alf07] M. G. Alford, A. Schmitt, K. Rajagopal, T. Schafer, "Color superconductivity in dense quark matter", *Rev. Mod. Phys.* **80** (2008) 1455-1515.
- [ALICE08] P. Crochet [ ALICE Collaboration ], "The ALICE experiment at the LHC", *Phys. Part. Nucl.* **39** (2008) 1074-1081.
- [All02] C. R. Allton, S. Ejiri, S. J. Hands, O. Kaczmarek, F. Karsch, E. Laermann, C. Schmidt, L. Scorzato, "The QCD thermal phase transition in the presence of a small chemical potential", *Phys. Rev.* **D66** (2002) 074507.
- [Ame97] G. Amelino-Camelia, J. D. Bjorken, S. E. Larsson, *Phys. Rev.* **D56** (1997) 6942-6956.
- [And06] R. Andrade, F. Grassi, Y. Hama, T. Kodama and O. J. Socolowski, "On the necessity to include event-by-event fluctuations in experimental evaluation of elliptical flow", *Phys. Rev. Lett.* **97** (2006) 202302.
- [Aok06] Y. Aoki, G. Endrodi, Z. Fodor, S. D. Katz, K. K. Szabo, "The Order of the quantum chromodynamics transition predicted by the standard model of particle physics", *Nature* **443** (2006) 675-678.
- [Asa06] M. Asakawa and C. Nonaka, "Critical end point and its consequences", *Nucl. Phys. A* **774** (2006) 753.
- [Asa09] M. Asakawa, S. Ejiri, M. Kitazawa, "Third moments of conserved charges as probes of QCD phase structure", *Phys. Rev. Lett.* **103** (2009) 262301.
- [Bai08] R. Baier, P. Romatschke, D. T. Son, A. O. Starinets, M. A. Stephanov, "Relativistic viscous hydrodynamics, conformal invariance, and holography", *JHEP* **0804** (2008) 100.
- [Bar05] A. Barducci, R. Casalbuoni, G. Pettini, L. Ravagli, "A NJL-based study of the QCD critical line", *Phys. Rev.* **D72** (2005) 056002.
- [Bas98] S. A. Bass, M. Belkacem, M. Bleicher, M. Brandstetter, L. Bravina, C. Ernst, L. Gerland, M. Hofmann *et al.*, "Microscopic models for ultrarelativistic heavy ion collisions", *Prog. Part. Nucl. Phys.* **41** (1998) 255-369.

- [Bas99] S. A. Bass, M. Bleicher, W. Cassing, A. Dumitru, H. J. Drescher, K. Eskola, M. Gyulassy, D. Kharzeev *et al.*, "Last call for RHIC predictions", Nucl. Phys. **A661** (1999) 205-260.
- [Bay62] G. Baym, "Selfconsistent approximation in many body systems", Phys. Rev. **127** (1962) 1391-1401.
- [BayKad61] G. Baym, L. P. Kadanoff, "Conservation Laws and Correlation Functions", Phys. Rev. **124** (1961) 287-299.
- [Baz09] A. Bazavov, T. Bhattacharya, M. Cheng, N. H. Christ, C. DeTar, S. Ejiri, S. Gottlieb, R. Gupta *et al.*, "Equation of state and QCD transition at finite temperature", Phys. Rev. **D80** (2009) 014504.
- [Bec02] F. Becattini, G. Passaleva, "Statistical hadronization model and transverse momentum spectra of hadrons in high-energy collisions", Eur. Phys. J. **C23** (2002) 551-583.
- [Ber66] F. A. Berezin: The Method of Second Quantization, Academic Press, New York 1966.
- [Ber00] B. Berdnikov and K. Rajagopal, "Slowing out of equilibrium near the QCD critical point", Phys. Rev. D **61** (2000) 105017.
- [Ber02] J. Berges, "Controlled nonperturbative dynamics of quantum fields out-of-equilibrium", Nucl. Phys. **A699** (2002) 847-886.
- [Ber03] J. Berges, D. U. Jungnickel, C. Wetterich, "Quark and nuclear matter in the linear chiral meson model", Int. J. Mod. Phys. **A18** (2003) 3189-3220.
- [Bin73] K. Binder, "Time-Dependent Ginzburg-Landau Theory of Non-equilibrium Relaxation", Phys. Rev. **B8** (1973) 3423-3438.
- [Bin87] K. Binder, "Theory of First-order Phase Transitions", Rep. Progr. Phys. **50** (1987) 783-859 .
- [Bir97] T. S. Biro and C. Greiner, "Dissipation and fluctuation at the chiral phase transition", Phys. Rev. Lett. **79** (1997) 3138.
- [Bjo92] J. D. Bjorken, "A Full acceptance detector for SSC physics at low and intermediate mass scales: An Expression of interest to the SSC", Int. J. Mod. Phys. A **7** (1992) 4189.
- [Bla94] J. P. Blaizot and E. Iancu, "Soft collective excitations in hot gauge theories", Nucl. Phys. B **417** (1994) 608.
- [Ble99] M. Bleicher, E. Zabrodin, C. Spieles, S. A. Bass, C. Ernst, S. Soff, L. Bravina, M. Belkacem, "Relativistic hadron hadron collisions in the ultrarelativistic quantum molecular dynamics model", J. Phys. G **G25** (1999) 1859-1896.

- [Ble00] M. J. Bleicher, S. A. Bass, L. V. Bravina, W. Greiner, S. Soff, H. Stoecker, N. Xu, E. E. Zabrodin, "Global observables and secondary interactions in central Au + Au reactions at  $s^{1/2} = 200\text{-GeV}/A$ ", *Phys. Rev.* **C62** (2000) 024904.
- [Boe95] D. Bodeker, L. D. McLerran, A. V. Smilga, "Really computing nonperturbative real time correlation functions", *Phys. Rev.* **D52** (1995) 4675-4690.
- [Bog62] N. N. Bogoliubov, in "Studies in Statistical Mechanics", edited by I. de Boer and G. E. Uhlenbeck (North-Holland, Amsterdam, 1962), Vol. I.
- [Boy96] D. Boyanovsky, I. D. Lawrie, D. S. Lee, "Relaxation and kinetics in scalar field theories", *Phys. Rev.* **D54** (1996) 4013-4028.
- [Boy98] D. Boyanovsky, H. J. de Vega, R. Holman, S. Kumar, R. D. Pisarski, "Nonequilibrium evolution of a 'Tsunami': Dynamical symmetry breaking", *Phys. Rev.* **D57** (1998) 3653-3669.
- [Boy99] D. Boyanovsky, H. J. de Vega, R. Holman, J. Salgado, "Nonequilibrium Bose-Einstein condensates, dynamical scaling and symmetric evolution in the large  $N$   $\Phi^4$  theory", *Phys. Rev.* **D59** (1999) 125009.
- [BRAHMS05] I. Arsene *et al.* [BRAHMS Collaboration], "Quark Gluon Plasma an Color Glass Condensate at RHIC? The perspective from the BRAHMS experiment", *Nucl. Phys. A* **757**, 1 (2005).
- [Bra92] E. Braaten and R. D. Pisarski, "Simple effective Lagrangian for hard thermal loops", *Phys. Rev. D* **45** (1992) 1827.
- [Bra97] J. Brachmann, A. Dumitru, J. A. Maruhn, H. Stoecker, W. Greiner and D. H. Rischke, "Non-equilibrium fluid-dynamics in the early stage of ultrarelativistic heavy-ion collisions", *Nucl. Phys. A* **619** (1997) 391.
- [Bra04] E. L. Bratkovskaya, M. Bleicher, M. Reiter, S. Soff, H. Stoecker, M. van Leeuwen, S. A. Bass, W. Cassing, "Strangeness dynamics and transverse pressure in relativistic nucleus-nucleus collisions", *Phys. Rev.* **C69** (2004) 054907.
- [BrM95] P. Braun-Munzinger, J. Stachel, J. P. Wessels, N. Xu, "Thermal equilibration and expansion in nucleus-nucleus collisions at the AGS", *Phys. Lett.* **B344** (1995) 43-48.
- [BrM96] P. Braun-Munzinger, J. Stachel, J. P. Wessels, N. Xu, "Thermal and hadrochemical equilibration in nucleus-nucleus collisions at the SPS", *Phys. Lett.* **B365** (1996) 1-6.
- [Bro92] L. S. Brown, *Quantum Field Theory*, Cambridge University Press (1992)
- [Bro99] G. Brown, P. A. Rikvold, M. Sutton, M. Grant "Evolution of speckle during spinodal decomposition", *Phys. Rev. E* **60** (1999) 5151 .
- [Bub03] M. Buballa, "NJL model analysis of quark matter at large density," *Phys. Rept.* **407** (2005) 205-376.

- [Cai09] H. Caines [ STAR Collaboration ], “The RHIC Beam Energy Scan: STAR’S Perspective”, [arXiv:0906.0305 [nucl-ex]].
- [Cal95a] E. Calzetta, B. L. Hu, “Quantum fluctuations, decoherence of the mean field, and structure formation in the early universe”, *Phys. Rev.* **D52** (1995) 6770-6788.
- [Cal95b] E. Calzetta, B. L. Hu, “Correlations, decoherence, dissipation, and noise in quantum field theory”, [hep-th/9501040].
- [Cal08] E. Calzetta and B.-L. Hu, *Nonequilibrium Quantum Field Theory* (University Press, Cambridge, 2008).
- [Car96] J. L. Cardy, *Scaling and Renormalization in Statistical Physics* (University Press, Cambridge, 1996).
- [Cas99] W. Cassing, E. L. Bratkovskaya, “Hadronic and electromagnetic probes of hot and dense nuclear matter”, *Phys. Rept.* **308** (1999) 65-233.
- [Cas07] N. C. Cassol-Seewald, R. L. S. Farias, E. S. Fraga, G. Krein, R. O. Ramos, “Langevin Simulation of Scalar Fields: Additive and Multiplicative Noises and Lattice Renormalization”, [arXiv:0711.1866 [hep-ph]].
- [Cas08] W. Cassing, E. L. Bratkovskaya, “Parton transport and hadronization from the dynamical quasiparticle point of view”, *Phys. Rev.* **C78** (2008) 034919.
- [CBM] B. Friman, C. Höhne, J. Knoll, S. Leupold, J. Randrup, R. Rapp, P. Senger (eds.), “The CBM physics book: Compressed baryonic matter in laboratory experiments,” *Lect. Notes Phys.* **814** (2011) 1-980.
- [Che09] M. Cheng, P. Hengde, C. Jung, F. Karsch, O. Kaczmarek, E. Laermann, R. D. Mawhinney, C. Miao *et al.*, “Baryon Number, Strangeness and Electric Charge Fluctuations in QCD at High Temperature”, *Phys. Rev.* **D79** (2009) 074505.
- [Cho74a] A. Chodos, R. L. Jaffe, K. Johnson, C. B. Thorn, V. F. Weisskopf, “A New Extended Model of Hadrons”, *Phys. Rev.* **D9** (1974) 3471-3495.
- [Cho74b] A. Chodos, R. L. Jaffe, K. Johnson, C. B. Thorn, “Baryon Structure in the Bag Theory”, *Phys. Rev.* **D10** (1974) 2599.
- [Cho04] P. Chomaz, M. Colonna, J. Randrup, “Nuclear spinodal fragmentation”, *Phys. Rept.* **389** (2004) 263-440.
- [Cle99] J. Cleymans, K. Redlich, “Chemical and thermal freezeout parameters from 1-A/GeV to 200-A/GeV”, *Phys. Rev.* **C60** (1999) 054908.
- [CoJaTo74] J. M. Cornwall, R. Jackiw and E. Tomboulis, “Effective Action For Composite Operators”, *Phys. Rev. D* **10** (1974) 2428.
- [Coo94] F. Cooper, S. Habib, Y. Kluger, E. Mottola, J. P. Paz, P. R. Anderson, “Nonequilibrium quantum fields in the large N expansion”, *Phys. Rev.* **D50** (1994) 2848-2869.



- [Coo95] F. Cooper, Y. Kluger, E. Mottola, J. P. Paz, "Nonequilibrium quantum dynamics of disoriented chiral condensates", *Phys. Rev.* **D51** (1995) 2377-2397.
- [Coo97] F. Cooper, S. Habib, Y. Kluger, E. Mottola, "Nonequilibrium dynamics of symmetry breaking in  $\lambda \Phi^4$  field theory", *Phys. Rev.* **D55** (1997) 6471-6503.
- [CooFry74] F. Cooper, G. Frye, "Comment on the Single Particle Distribution in the Hydrodynamic and Statistical Thermodynamic Models of Multiparticle Production", *Phys. Rev.* **D10** (1974) 186.
- [Cse95] L. P. Csernai, I. N. Mishustin, "Fast hadronization of supercooled quark - gluon plasma", *Phys. Rev. Lett.* **74** (1995) 5005-5008.
- [Das97] A. Das, *Finite Temperature Field Theory*, (World Scientific Publishing Company, 1997).
- [deF02] P. de Forcrand, O. Philipsen, "The QCD phase diagram for small densities from imaginary chemical potential", *Nucl. Phys.* **B642** (2002) 290-306.
- [deF03] P. de Forcrand, O. Philipsen, "The QCD phase diagram for three degenerate flavors and small baryon density," *Nucl. Phys.* **B673** (2003) 170-186. [hep-lat/0307020].
- [deF06] P. de Forcrand, O. Philipsen, "The Chiral critical line of  $N(f) = 2+1$  QCD at zero and non-zero baryon density," *JHEP* **0701** (2007) 077.
- [Dex10] V. A. Dexheimer and S. Schramm, "A Novel Approach to Model Hybrid Stars", *Phys. Rev. C* **81** (2010) 045201.
- [DolJac73] L. A. Dolan and R. Jackiw, "Symmetry Behavior At Finite Temperature", *Phys. Rev. D* **9** (1974) 3320.
- [Dum05] A. Dumitru, R. D. Pisarski, D. Zschiesche, "Dense quarks, and the fermion sign problem, in a  $SU(N)$  matrix model", *Phys. Rev.* **D72** (2005) 065008.
- [E864-97] T. A. Armstrong *et al.* [ E864 Collaboration ], "Anti-proton production in 11.5 A-GeV/c Au + Pb nucleus-nucleus collisions", *Phys. Rev. Lett.* **79** (1997) 3351-3354.
- [E864-99] T. A. Armstrong *et al.* [ E864 Collaboration ], "Search for neutral strange quark matter in high-energy heavy ion collisions", *Phys. Rev.* **C59** (1999) 1829-1833.
- [E878-95] D. Beavis [ E878 Collaboration ], "Centrality dependence of anti-proton production in Au + Au collisions", *Phys. Rev. Lett.* **75** (1995) 3633-3636.
- [E878-97] M. J. Bennett *et al.* [ E878 Collaboration ], "Anti-proton distributions in Au + nucleus collisions", *Phys. Rev.* **C56** (1997) 1521-1535.
- [Ehr33] P. Ehrenfest, "Phasenumwandlungen im ueblichen und erweiterten Sinn, clasifiziert nach den entsprechenden Singularitaeten des thermodynamischen Potentiales", *Verhandlingen der Koninklijke Akademie van Wetenschappen (Amsterdam)* **36**: 153-157; *Communications from the Physical Laboratory of the University of Leiden*, Supplement No. 75b (1933).

- [Ein05] A. Einstein, *Annalen der Physik* **322** (1905) 549.
- [Eji06] S. Ejiri, "Lee-Yang zero analysis for the study of QCD phase structure", *Phys. Rev. D* **73** (2006) 054502.
- [Fer88] A. M. Ferrenberg, R. H. Swendsen, "New Monte Carlo Technique for Studying Phase Transitions", *Phys. Rev. Lett.* **61** (1988) 2635-2638.
- [FetWal71] L. Fetter and J. D. Walecka, *Quantum Theory of Many- Particle Systems* (McGraw-Hill, New York, 1971).
- [Fey63] R. P. Feynman and F. L. . Vernon, "The Theory of a general quantum system interacting with a linear dissipative system", *Annals Phys.* **24** (1963) 118 [*Annals Phys.* **281** (2000) 547].
- [Fod02] Z. Fodor and S. D. Katz, "Lattice determination of the critical point of QCD at finite T and mu", *JHEP* **0203** (2002) 014.
- [Fod04] Z. Fodor and S. D. Katz, "Critical point of QCD at finite T and mu, lattice results for physical quark masses", *JHEP* **0404** (2004) 050.
- [Fra09] E. S. Fraga, L. F. Palhares, M. B. Pinto, "Nonperturbative Yukawa theory at finite density and temperature", *Phys. Rev.* **D79** (2009) 065026.
- [Fre92] J. Frenkel and J. C. Taylor, "Hard thermal QCD, forward scattering and effective actions", *Nucl. Phys. B* **374** (1992) 156.
- [Gav99] S. Gavin, "Extraordinary baryon fluctuations and the QCD tricritical point", [*nucl-th/9908070*].
- [Gav05] R. V. Gavai, S. Gupta, "The Critical end point of QCD", *Phys. Rev.* **D71** (2005) 114014.
- [Gel60] M. Gell-Mann, MLevy, "The axial vector current in beta decay", *Nuovo Cim.* **16** (1960) 705.
- [Gel64] M. Gell-Mann, "A Schematic Model Of Baryons And Mesons", *Phys. Lett.* **8** (1964) 214.
- [Gel93] M. Gell-Mann, J. B. Hartle, "Classical equations for quantum systems", *Phys. Rev.* **D47** (1993) 3345-3382.
- [Gel10] F. Gelis, E. Iancu, J. Jalilian-Marian, R. Venugopalan, "The Color Glass Condensate" , [*arXiv:1002.0333 [hep-ph]*].
- [Gen93] N. A. Gentile, M. B. Aufderheide, G. J. Mathews, F. D. Swesty, G. M. Fuller, "The QCD phase transition and supernova core collapse", *Astrophys. J.* **414** (1993) 701-711.
- [Gla70] R. J. Glauber, G. Matthiae, "High-energy scattering of protons by nuclei", *Nucl. Phys.* **B21** (1970) 135-157.

- 
- [Gle93] M. Gleiser and R. O. Ramos, "Microphysical approach to nonequilibrium dynamics of quantum fields", *Phys. Rev. D* **50** (1994) 2441.
- [GinLan50] V. L. Ginzburg and L. D. Landau, "On the Theory of superconductivity", *Zh. Eksp. Teor. Fiz.* **20** (1950) 1064.
- [Gor04] M. I. Gorenstein, M. Gazdzicki, O. S. Zozulya, "Fluctuations of strangeness and deconfinement phase transition in nucleus nucleus collisions", *Phys. Lett.* **B585** (2004) 237-242.
- [Gre97] C. Greiner and B. Muller, "Classical Fields Near Thermal Equilibrium", *Phys. Rev. D* **55** (1997) 1026.
- [Gre98] C. Greiner and S. Leupold, "Stochastic interpretation of Kadanoff-Baym equations and their relation to Langevin processes", *Annals Phys.* **270** (1998) 328.
- [GroWil74] D. J. Gross and F. Wilczek, "Asymptotically free Gauge Theories. 2", *Phys. Rev. D* **9** (1974) 980.
- [Hat03] Y. Hatta and M. A. Stephanov, "Proton number fluctuation as a signal of the QCD critical end-point", *Phys. Rev. Lett.* **91** (2003) 102003 [Erratum-ibid. **91** (2003) 129901]
- [Hee02a] H. van Hees, J. Knoll, "Renormalization in selfconsistent approximations schemes at finite temperature. 1. Theory", *Phys. Rev.* **D65** (2002) 025010.
- [Hee02b] H. Van Hees, J. Knoll, "Renormalization of selfconsistent approximation schemes. 2. Applications to the sunset diagram", *Phys. Rev.* **D65** (2002) 105005.
- [Hee02c] H. van Hees, J. Knoll, "Renormalization in selfconsistent approximation schemes at finite temperature. 3. Global symmetries", *Phys. Rev.* **D66** (2002) 025028.
- [Hei06] U. W. Heinz, H. Song, A. K. Chaudhuri, "Dissipative hydrodynamics for viscous relativistic fluids", *Phys. Rev.* **C73** (2006) 034904.
- [Hir04] T. Hirano and Y. Nara, "Hydrodynamic afterburner for the color glass condensate and the parton energy loss", *Nucl. Phys. A* **743** (2004) 305.
- [Hir07] T. Hirano, "Relativistic hydrodynamics at RHIC and LHC", *Prog. Theor. Phys. Suppl.* **168** (2007) 347.
- [HohHal77] P. C. Hohenberg, B. I. Halperin, "Theory of Dynamic Critical Phenomena", *Rev. Mod. Phys.* **49** (1977) 435-479.
- [HotQCD10] W. Söldner [for the HotQCD collaboration], "Chiral Aspects of Improved Staggered Fermions with 2+1-Flavors from the HotQCD Collaboration", *PoS LATTICE2010* (2010) 215.
- [Hu92] B. L. Hu, J. P. Paz, Y. -h. Zhang, "Quantum Brownian motion in a general environment: 1. Exact master equation with nonlocal dissipation and colored noise", *Phys. Rev.* **D45** (1992) 2843-2861.

- [Hu93] B. L. Hu, J. P. Paz, Y. Zhang, ‘Quantum Brownian motion in a general environment. 2: Nonlinear coupling and perturbative approach’, *Phys. Rev.* **D47** (1993) 1576-1594.
- [Hun95] C. M. Hung, E. V. Shuryak, “Hydrodynamics near the QCD phase transition: Looking for the longest lived fireball”, *Phys. Rev. Lett.* **75** (1995) 4003-4006.
- [IlltMa75] J. Iliopoulos, C. Itzykson, A. Martin, “Functional Methods and Perturbation Theory”, *Rev. Mod. Phys.* **47** (1975) 165.
- [Iva99] Yu. B. Ivanov, J. Knoll and D. N. Voskresensky, “Self-consistent approximations to non-equilibrium many-body theory”, *Nucl. Phys. A* **657** (1999) 413.
- [Jac74] R. Jackiw, “Functional evaluation of the effective potential”, *Phys. Rev. D* **9** (1974) 1686.
- [Juc04a] S. Juchem, W. Cassing, C. Greiner, “Quantum dynamics and thermalization for out-of-equilibrium  $\phi^4$  theory”, *Phys. Rev.* **D69** (2004) 025006.
- [Juc04b] S. Juchem, W. Cassing, C. Greiner, “Nonequilibrium quantum field dynamics and off-shell transport for  $\phi^4$  theory in (2+1)-dimensions”, *Nucl. Phys.* **A743** (2004) 92-126.
- [Jun96] D. U. Jungnickel, C. Wetterich, “Effective action for the chiral quark-meson model”, *Phys. Rev.* **D53** (1996) 5142-5175.
- [Kap94] J. I. Kapusta, *Finite-Temperature Field Theory*, (University Press, Cambridge, 1994).
- [Kel64] L. V. Keldysh, “Diagram technique for nonequilibrium processes”, *Zh. Eksp. Teor. Fiz.* **47** (1964) 1515 [*Sov. Phys. JETP* **20** (1965) 1018].
- [Koc86] P. Koch, B. Muller, J. Rafelski, “Strangeness in Relativistic Heavy Ion Collisions”, *Phys. Rept.* **142** (1986) 167-262.
- [Kha08] D. E. Kharzeev, L. D. McLerran, H. J. Warringa, “The Effects of topological charge change in heavy ion collisions: ‘Event by event P and CP violation’ ”, *Nucl. Phys.* **A803** (2008) 227-253.
- [Kol99] P. F. Kolb, J. Sollfrank, U. W. Heinz, “Anisotropic flow from AGS to LHC energies”, *Phys. Lett.* **B459** (1999) 667-673.
- [Kol00] P. F. Kolb, J. Sollfrank, U. W. Heinz, “Anisotropic transverse flow and the quark hadron phase transition”, *Phys. Rev.* **C62** (2000) 054909.
- [Kol01a] P. F. Kolb, U. W. Heinz, P. Huovinen, K. J. Eskola, K. Tuominen, “Centrality dependence of multiplicity, transverse energy, and elliptic flow from hydrodynamics”, *Nucl. Phys.* **A696** (2001) 197-215.
- [Kol01b] P. F. Kolb, P. Huovinen, U. W. Heinz, H. Heiselberg, “Elliptic flow at SPS and RHIC: From kinetic transport to hydrodynamics”, *Phys. Lett.* **B500** (2001) 232-240.

- 
- [Kub57] R. Kubo, "Statistical Mechanical Theory Of Irreversible Processes. 1. General Theory And Simple Applications In Magnetic And Conduction Problems", J. Phys. Soc. Jap. **12** (1957) 570.
- [Kuh06] A. Kuhlman, U. W. Heinz and Y. V. Kovchegov, "Gluon saturation effects in relativistic U + U collisions," Phys. Lett. B **638** (2006) 171
- [LaLiPi80] L. Landau, E. Lifshitz and L. Pitaevskii, Statistical Physics, vol. I (Pergamon Press, London, 1980).
- [Lan86] N. P. Landsman and C. G. van Weert, "Real and Imaginary Time Field Theory at Finite Temperature and Density", Phys. Rept. **145** (1987) 141.
- [Lap06] T. Lappi, L. McLerran, "Some features of the glasma," Nucl. Phys. **A772** (2006) 200-212.
- [Lat80] C. M. G. Lattes, Y. Fujimoto and S. Hasegawa, "Hadronic Interactions Of High-Energy Cosmic Ray Observed By Emulsion Chambers", Phys. Rept. **65** (1980) 151.
- [LeeYan60] T. D. Lee, C. N. Yang, "Many-Body Problem in Quantum Statistical Mechanics. 4. Formulation in Terms of Average Occupation Number in Momentum Space", Phys. Rev. **117** (1960) 22-36.
- [Leu07] S. Leupold, "Selfconsistent approximations, symmetries and choice of representation", Phys. Lett. B **646** (2007) 155
- [LutWar60] J. M. Luttinger, J. C. Ward, "Ground state energy of a many fermion system. 2.", Phys. Rev. **118** (1960) 1417-1427.
- [Luz08] M. Luzum, P. Romatschke, "Conformal Relativistic Viscous Hydrodynamics: Applications to RHIC results at  $\sqrt{s(NN)} = 200$ -GeV", Phys. Rev. **C78** (2008) 034915.
- [MarSch59] P. C. Martin and J. S. Schwinger, "Theory of many particle systems. I", Phys. Rev. **115** (1959) 1342.
- [Mat55] T. Matsubara, "A New Approach To Quantum Statistical Mechanics", Prog. Theor. Phys. **14** (1955) 351.
- [McL94a] L. D. McLerran, R. Venugopalan, "Green's functions in the color field of a large nucleus", Phys. Rev. **D50** (1994) 2225-2233.
- [McL94b] L. D. McLerran, R. Venugopalan, "Gluon distribution functions for very large nuclei at small transverse momentum", Phys. Rev. **D49** (1994) 3352-3355.
- [McL94c] L. D. McLerran, R. Venugopalan, "Computing quark and gluon distribution functions for very large nuclei", Phys. Rev. **D49** (1994) 2233-2241.
- [McL07] L. McLerran, R. D. Pisarski, "Phases of cold, dense quarks at large  $N(c)$ ", Nucl. Phys. **A796** (2007) 83-100.

- [Mis97a] I. N. Mishustin, O. Scavenius, "Dynamical generation of the constituent mass in expanding plasma", *Phys. Lett.* **B396** (1997) 33-38.
- [Mis97b] I. N. Mishustin, J. A. Pedersen, O. Scavenius, "Fluid dynamical description of the chiral transition", *Heavy Ion Phys.* **5** (1997) 377-386.
- [Mis99a] I. N. Mishustin and O. Scavenius, "Chiral fluid dynamics and collapse of vacuum bubbles", *Phys. Rev. Lett.* **83** (1999) 3134.
- [Mis99b] I. N. Mishustin, "Nonequilibrium phase transition in rapidly expanding QCD matter", *Phys. Rev. Lett.* **82** (1999) 4779-4782.
- [Mol10] E. Molnar, H. Niemi, D. H. Rischke, "Numerical tests of causal relativistic dissipative fluid dynamics", *Eur. Phys. J.* **C65** (2010) 615-635.
- [Mor86] M. Morikawa, "Classical Fluctuations In Dissipative Quantum Systems", *Phys. Rev.* **D33** (1986) 3607.
- [Mos04] A. Mocsy, I. N. Mishustin, P. J. Ellis, "Role of fluctuations in the linear sigma model with quarks", *Phys. Rev.* **C70** (2004) 015204.
- [NA49-02] S. V. Afanasiev *et al.* [ The NA49 Collaboration ], "Energy dependence of pion and kaon production in central Pb + Pb collisions", *Phys. Rev.* **C66** (2002) 054902.
- [NA49-08a] M. Rybczynski *et al.* [ NA49 Collaboration ], "Energy dependence of fluctuations in central Pb+Pb collisions from NA49 at the CERN SPS", *J. Phys. G* **G35** (2008) 104091.
- [Nah09] M. Nahrgang, M. Bleicher, "The phase transition in chiral fluid dynamics", *Acta Phys. Polon. B Proc. Suppl.* **2** (2009) 405.
- [Nah10a] M. Nahrgang, "Fluid dynamics with a critical point", *Russ. Phys. J.* **53** (2010) 103
- [Nah10b] M. Nahrgang, M. Bleicher, "Non-equilibrium fluctuations at the QCD phase transition", *J. Phys. Conf. Ser.* **270** (2010) 012059.
- [Nah11a] M. Nahrgang, C. Herold, S. Schramm, M. Bleicher, "Hybrid approaches to heavy ion collisions and future perspectives", [arXiv:1103.0753 [hep-ph]].
- [Nah11b] M. Nahrgang, S. Leupold, C. Herold, M. Bleicher, "Nonequilibrium chiral fluid dynamics including dissipation and noise", [arXiv:1105.0622 [nucl-th]].
- [Nah11c] M. Nahrgang, S. Leupold, M. Bleicher, "Equilibration and relaxation times at the chiral phase transition including reheating", [arXiv:1105.1396 [nucl-th]].
- [Nah11d] M. Nahrgang, M. Bleicher, S. Leupold, I. Mishustin, "The impact of dissipation and noise on fluctuations in chiral fluid dynamics", [arXiv:1105.1962 [nucl-th]].
- [NaJoLa61a] Y. Nambu, G. Jona-Lasinio, "Dynamical Model of Elementary Particles Based on an Analogy with Superconductivity. 1.", *Phys. Rev.* **122** (1961) 345-358.

- 
- [NaJoLa61b] Y. Nambu, G. Jona-Lasinio, "Dynamical Model Of Elementary Particles Based On An Analogy With Superconductivity. Ii", Phys. Rev. **124** (1961) 246-254.
- [Nak09] E. Nakano, B. -J. Schaefer, B. Stokic, B. Friman, K. Redlich, "Fluctuations and isentropes near the chiral critical endpoint", Phys. Lett. **B682** (2010) 401-407.
- [Non04] C. Nonaka, M. Asakawa, "Hydrodynamical evolution near the QCD critical endpoint", Phys. Rev. **C71** (2005) 044904.
- [NumRec] W. H. Press, B.P.Flannery, S.A.Teukolsky, W.T.Vetterling, Numerical Recipes in Fortran, (Cambridge University Press, 1992).
- [Pae03] K. Paech, H. Stoecker and A. Dumitru, "Hydrodynamics near a chiral critical point", Phys. Rev. C **68** (2003) 044907.
- [Pal08] L. F. Palhares, E. S. Fraga, "Perturbative Yukawa theory at finite density: The Role of masses and renormalization group flow at two loops", Phys. Rev. **D78** (2008) 025013. [arXiv:0803.0262 [hep-ph]].
- [Pal10a] L. F. Palhares, E. S. Fraga, "Droplets in the cold and dense linear sigma model with quarks", Phys. Rev. **D82** (2010) 125018.
- [Pal10b] L. F. Palhares, E. S. Fraga, T. Kodama, "Finite-size effects and signatures of the QCD critical endpoint", J. Phys. G **G37** (2010) 094031.
- [Pap99] P. Papazoglou, D. Zschesche, S. Schramm, J. Schaffner-Bielich, H. Stoecker, W. Greiner, "Nuclei in a chiral SU(3) model", Phys. Rev. **C59** (1999) 411-427.
- [Pet08] H. Petersen, J. Steinheimer, G. Burau, M. Bleicher and H. Stoecker, "A Fully Integrated Transport Approach to Heavy Ion Reactions with an Intermediate Hydrodynamic Stage", Phys. Rev. C **78** (2008) 044901.
- [PHENIX05] K. Adcox *et al.* [PHENIX Collaboration], "Formation of dense partonic matter in relativistic nucleus nucleus collisions at RHIC: Experimental evaluation by the PHENIX collaboration", Nucl. Phys. A **757**, 184 (2005).
- [Phi10] O. Philipsen, "Lattice QCD at non-zero temperature and baryon density", [arXiv:1009.4089 [hep-lat]].
- [PHOBOS05] B. B. Back *et al.*, "The PHOBOS perspective on discoveries at RHIC", Nucl. Phys. A **757**, 28 (2005).
- [Pur93] Y. Pürsün, diploma thesis, Goethe-Universität Frankfurt am Main (1993).
- [Raf82a] J. Rafelski, B. Muller, "Strangeness Production in the Quark - Gluon Plasma", Phys. Rev. Lett. **48** (1982) 1066.
- [Raf82b] J. Rafelski, "Formation and Observables of the Quark-Gluon Plasma", Phys. Rept. **88** (1982) 331.

- [Raj93] K. Rajagopal and F. Wilczek, "Emergence of coherent long wavelength oscillations after a quench: Application to QCD", Nucl. Phys. B **404** (1993) 577.
- [Ran96] J. Randrup, "Amplification of pionic instabilities in high-energy collisions?", Phys. Rev. Lett. **77** (1996) 1226.
- [Ran97] J. Randrup, "Mean-field treatment of the linear sigma model in dynamical calculations of DCC observables", Nucl. Phys. A **616** (1997) 531.
- [Ran04] J. Randrup, "Spinodal decomposition during the hadronization stage at RHIC?", Phys. Rev. Lett. **92** (2004) 122301.
- [Ran06] J. Randrup, J. Cleymans, "Maximum freeze-out baryon density in nuclear collisions", Phys. Rev. **C74** (2006) 047901.
- [Rat06] C. Ratti, M. A. Thaler, W. Weise, "Phases of QCD: Lattice thermodynamics and a field theoretical model," Phys. Rev. **D73** (2006) 014019.
- [Rat07] C. Ratti, S. Roessner, M. A. Thaler, W. Weise, "Thermodynamics of the PNJL model," Eur. Phys. J. **C49** (2007) 213-217.
- [Ris95a] D. H. Rischke, S. Bernard, J. A. Maruhn, "Relativistic hydrodynamics for heavy ion collisions. 1. General aspects and expansion into vacuum", Nucl. Phys. **A595** (1995) 346-382.
- [Ris95b] D. H. Rischke, Y. Pursun, J. A. Maruhn, "Relativistic hydrodynamics for heavy ion collisions. 2. Compression of nuclear matter and the phase transition to the quark - gluon plasma", Nucl. Phys. **A595** (1995) 383-408.
- [Ris98] D. H. Rischke, "Forming disoriented chiral condensates through fluctuations", Phys. Rev. C **58** (1998) 2331.
- [Roe06] S. Roessner, C. Ratti, W. Weise, "Polyakov loop, diquarks and the two-flavour phase diagram," Phys. Rev. **D75** (2007) 034007.
- [Roe07] S. Roessner, T. Hell, C. Ratti, W. Weise, "The chiral and deconfinement crossover transitions: PNJL model beyond mean field," Nucl. Phys. **A814** (2008) 118-143.
- [Rom07] P. Romatschke, U. Romatschke, "Viscosity Information from Relativistic Nuclear Collisions: How Perfect is the Fluid Observed at RHIC?", Phys. Rev. Lett. **99** (2007) 172301.
- [Roo74] R. G. Root, "Effective Potential for the O(N) Model to Order 1/N", Phys. Rev. **D10** (1974) 3322.
- [Sas08] C. Sasaki, B. Friman, K. Redlich, "Chiral phase transition in the presence of spinodal decomposition", Phys. Rev. **D77** (2008) 034024.
- [Sca99] O. Scavenius and A. Dumitru, "A first-order chiral phase transition may naturally lead to the 'quench' initial condition and strong soft-pion fields", Phys. Rev. Lett. **83** (1999) 4697.



- [Sca01a] O. Scavenius, A. Mocsy, I. N. Mishustin and D. H. Rischke, “Chiral phase transition within effective models with constituent quarks”, *Phys. Rev. C* **64** (2001) 045202.
- [Sca01b] O. Scavenius, A. Dumitru, E. S. Fraga, J. T. Lenaghan and A. D. Jackson, “First order chiral phase transition in high-energy collisions: Can nucleation prevent spinodal decomposition?”, *Phys. Rev. D* **63** (2001) 116003.
- [Sch61] J. S. Schwinger, “Brownian motion of a quantum oscillator”, *J. Math. Phys.* **2** (1961) 407.
- [Sch07] B. -J. Schaefer, J. M. Pawłowski, J. Wambach, “The Phase Structure of the Polyakov–Quark-Meson Model,” *Phys. Rev.* **D76** (2007) 074023.
- [Sch08] B. -J. Schaefer, J. Wambach, “Renormalization group approach towards the QCD phase diagram”, *Phys. Part. Nucl.* **39** (2008) 1025-1032.
- [Sch09] T. Schuster, M. Nahrgang, M. Mitrovski, R. Stock, M. Bleicher, “Analysis of the baryon-, proton-, and charged particle kurtosis in heavy ion collisions within a relativistic transport approach”, [arXiv:0903.2911 [hep-ph]].
- [Sko10] V. Skokov, B. Friman, E. Nakano, K. Redlich, B. -J. Schaefer, “Vacuum fluctuations and the thermodynamics of chiral models”, *Phys. Rev.* **D82** (2010) 034029.
- [Son97] D. T. Son, “Effective nonperturbative real time dynamics of soft modes in hot gauge theories”, [hep-ph/9707351].
- [Son07] D. T. Son, A. O. Starinets, “Viscosity, Black Holes, and Quantum Field Theory”, *Ann. Rev. Nucl. Part. Sci.* **57** (2007) 95-118.
- [Son09a] H. Song, U. W. Heinz, “Extracting the QGP viscosity from RHIC data - A Status report from viscous hydrodynamics”, *J. Phys. G* **G36** (2009) 064033.
- [Son09b] H. Song, U. W. Heinz, “Viscous hydrodynamics with bulk viscosity: Uncertainties from relaxation time and initial conditions”, *Nucl. Phys.* **A830** (2009) 467C-470C.
- [Son04] D. T. Son and M. A. Stephanov, “Dynamic universality class of the QCD critical point”, *Phys. Rev. D* **70** (2004) 056001
- [Sor99] H. Sorge, “Highly sensitive centrality dependence of elliptic flow: A novel signature of the phase transition in QCD”, *Phys. Rev. Lett.* **82** (1999) 2048-2051.
- [Spl05] K. Splittorff, “Lattice simulations of QCD with  $\mu(B) \neq 0$  versus phase quenched QCD”, arXiv:hep-lat/0505001.
- [STAR05] J. Adams *et al.* [STAR Collaboration], “Experimental and theoretical challenges in the search for the quark gluon plasma: The STAR collaboration’s critical assessment of the evidence from RHIC collisions”, *Nucl. Phys. A* **757**, 102 (2005).
- [STAR10] M. M. Aggarwal *et al.* [ STAR Collaboration ], “Higher Moments of Net-proton Multiplicity Distributions at RHIC,” *Phys. Rev. Lett.* **105** (2010) 022302.

- [Ste99] M. A. Stephanov, K. Rajagopal and E. V. Shuryak, "Event-by-event fluctuations in heavy ion collisions and the QCD critical point", *Phys. Rev. D* **60** (1999) 114028.
- [Ste06] M. A. Stephanov, "QCD phase diagram: An overview", *PoS LAT2006* (2006) 024.
- [Ste09] M. A. Stephanov, "Non-Gaussian fluctuations near the QCD critical point", *Phys. Rev. Lett.* **102** (2009) 032301.
- [Ste10] J. Steinheimer, V. Dexheimer, H. Petersen, M. Bleicher, S. Schramm and H. Stoecker, "Hydrodynamics with a chiral hadronic equation of state including quark degrees of freedom", *Phys. Rev. C* **81** (2010) 044913.
- [Sto09] B. Stokic, B. Friman, K. Redlich, "Kurtosis and compressibility near the chiral phase transition", *Phys. Lett.* **B673** (2009) 192-196.
- [Tea01] D. Teaney, J. Lauret and E. V. Shuryak, "A hydrodynamic description of heavy ion collisions at the SPS and RHIC", arXiv:nucl-th/0110037.
- [Tet03] N. Tetradis, "The Quark meson model and the phase diagram of two flavor QCD", *Nucl. Phys.* **A726** (2003) 93-119.
- [Wan10] F. Wang, M. Bleicher, "Nuclear absorption effects on Lambda-bar/p-bar ratio in heavy ion collisions", [arXiv:1011.4289 [nucl-th]].
- [Wel83] H. A. Weldon, "Simple Rules For Discontinuities In Finite Temperature Field Theory", *Phys. Rev. D* **28** (1983) 2007.
- [Wil74a] K. G. Wilson and J. B. Kogut, "The Renormalization group and the epsilon expansion," *Phys. Rept.* **12** (1974) 75.
- [Wil74b] K. G. Wilson, "Confinement of Quarks", *Phys. Rev. D* **10** (1974) 2445.
- [Wil92] F. Wilczek, "Application of the renormalization group to a second order QCD phase transition", *Int. J. Mod. Phys.* **A7** (1992) 3911-3925.
- [WUPBUD10] S. Borsanyi, Z. Fodor, C. Hoelbling, S. D. Katz, S. Krieg, C. Ratti and K. K. Szabo [Wuppertal-Budapest Collaboration], "Is there still any  $T_c$  mystery in lattice QCD? Results with physical masses in the continuum limit III", *JHEP* **1009** (2010) 073.
- [Xu00] Z. Xu and C. Greiner, "Stochastic treatment of disoriented chiral condensates within a Langevin description", *Phys. Rev. D* **62** (2000) 036012.
- [Xu05] Z. Xu and C. Greiner, "Thermalization of gluons in ultrarelativistic heavy ion collisions by including three-body interactions in a parton cascade", *Phys. Rev. C* **71** (2005) 064901.
- [Xu07] Z. Xu and C. Greiner, "Transport rates and momentum isotropization of gluon matter in ultrarelativistic heavy-ion collisions", *Phys. Rev. C* **76** (2007) 024911.

- [YanMil54] C. N. Yang and R. L. Mills, "Conservation of isotopic spin and isotopic gauge invariance", *Phys. Rev.* **96** (1954) 191.
- [Zsc02] D. Zschesche, S. Schramm, J. Schaffner-Bielich, H. Stoecker, W. Greiner, "Particle ratios at RHIC: Effective hadron masses and chemical freezeout", *Phys. Lett.* **B547** (2002) 7-14.
- [Zsc07] D. Zschesche, G. Zeeb, S. Schramm, "Phase structure in a hadronic chiral model", *J. Phys. G* **G34** (2007) 1665-1672.



# Deutsche Kurzfassung

## Einleitung: Das Phasendiagramm der Quantenchromodynamik

Mehr als 99% der Masse der sichtbaren Materie in unserem Universum entsteht am Phasenübergang von einem Plasma aus Quarks und Gluonen zu einer Welt, die hauptsächlich aus Hadronen, Protonen und Neutronen, aufgebaut ist. In der Natur ereignete sich dieser Phasenübergang zirka  $10^{-5}$  Sekunden nach dem Urknall bei einer Temperatur von etwa  $10^{12}$  Kelvin. Neben dem frühen Universum kann der Phasenübergang auch im Inneren extrem dichter Sterne vorkommen.

Der Phasenübergang hat zwei interessante Aspekte: die spontane Brechung der chiralen Symmetrie und den Übergang von partonischen zu hadronischen Freiheitsgraden. Oberhalb der Übergangstemperatur haben die Up- und Down-Quarks sehr kleine aber endliche Massen von 1,5 MeV und 3 MeV. Die Herkunft dieser Massen wird am Large Hadron Collider (LHC) in Gestalt des Higgs-Bosons gesucht. Unterhalb der Übergangstemperatur haben Protonen und Neutronen eine Masse von ungefähr 940 MeV, was einer Masse der Konstituentenquarks von ungefähr 300 MeV entspricht. Diese Masse entsteht am chiralen Phasenübergang.

Die grundlegende Theorie der starken Wechselwirkung zwischen Quarks und Gluonen und zwischen Nukleonen im Atomkern ist die Quantenchromodynamik (QCD). Die Ladung in der QCD heißt Farbe und hat drei Ausrichtungen: rot, blau und grün. In keinem der in der Hochenergiephysik durchgeführten Experimente wurde jemals ein einzelnes isoliertes Quark gefunden. Unterhalb der Phasenübergangstemperatur sind Quarks und Gluonen immer in farbneutralen Hadronen gebunden. Dieses Phänomen heißt Farbeinschluss und hat seinen Ursprung in der nicht-Abelschen Struktur der zugrunde liegenden Eichgruppe. Da die Gluonen ebenfalls Farbladung tragen wechselwirken sie miteinander. Durch die Quantisierung der Feldtheorie führt dies zu einer laufenden Kopplungskonstanten, die am Phasenübergang von der Ordnung eins ist. Dies ist technisch ein großes Problem, da jede störungstheoretische Herangehensweise am Phasenübergang zwischen Quarks und Gluonen und Hadronen zusammenbricht.

Genau wie der Phasenübergang von Wasser kann der Phasenübergang der QCD erster oder zweiter Ordnung oder ein rascher Phasenwechsel sein. Am Phasenübergang erster Ordnung gibt es einen Bereich, in dem beide Phasen stabile Gleichgewichtszustände darstellen. Dies wird Phasenkoexistenz genannt. Am Phasenübergang zweiter Ordnung verschwindet die Phasenkoexistenz. Stattdessen zeigen hier viele mikroskopisch verschiedene Systeme makroskopisch gleiches Verhalten, man spricht von Universalitätseigenschaften. Die Fluktuationen und die Korrelationslänge am Phasenübergang zweiter

Ordnung divergiert. Im Phasendiagramm von Wasser endet die Phasenübergangslinie erster Ordnung in einem kritischen Punkt, der ein Phasenübergang zweiter Ordnung ist. Hier wächst die Korrelationslänge der Fluktuationen bis in den Wellenlängenbereich des sichtbaren Lichts an. Die eigentlich durchsichtige Flüssigkeit wird durch die Streuung des Lichts undurchsichtig.

Die Untersuchung des QCD Phasendiagramms ist ungleich schwieriger. Es gibt drei verschiedene Herangehensweisen:

- Erstens, man ist tapfer und berechnet die Zustandssumme der QCD ausgehend vom Lagrangian der Theorie mittels nichtstörungstheoretischer Methoden. Die vielversprechendste ist die numerische Behandlung der QCD auf einem diskretisierten Raumzeitgitter, die Gitter-QCD. Allerdings ist die Effektivität auf verschwindend kleine baryochemische Potenziale beschränkt. Hier ist der Phasenübergang ein rascher Phasenwechsel. Das linke Bild in Abbildung 1.1 zeigt, was wir von der Gitter-QCD über das Phasendiagramm wissen.
- Zweitens, man ist stark und bringt Schwerionen bei ultrarelativistischen Energien zur Kollision. Dies ist die einzige Methode stark wechselwirkende Materie unter extremen Bedingungen im Labor herzustellen. Dieses Unternehmen startete mit relativ niedrigen Energien zur Untersuchung der Kernstruktur und des Übergangs zwischen flüssiger und gasförmiger Kernmaterie. Die Möglichkeit den Phasenübergang der QCD zu untersuchen ermöglichte sich durch den Bau leistungsfähigerer Beschleuniger und Detektoren am CERN (Organisation européenne pour la Recherche nucléaire) und am BNL (Brookhaven National Laboratory). Bislang konnten jedoch noch keine Observablen gefunden werden, mittels derer die Daten eindeutig zu erklären wären. Neue Messungen am RHIC (Relativistic Heavy Ion Collider), BNL, bei verschiedenen Energien sollen Aufschluss über Existenz und Position eines kritischen Punkts geben. Die zukünftige Beschleunigungsanlage FAIR (Facility for Antiproton and Ion Research) am GSI Helmholtzzentrum für Schwerionenforschung bietet dem CBM (Compressed Baryonic Matter) Experiment hervorragende Möglichkeiten das Phasendiagramm bei besonders hohen Dichten zu untersuchen. Der bisherige experimentelle Kenntnisstand über das Phasendiagramm stark wechselwirkender Materie ist in Abbildung 1.1 rechts gezeigt.
- Drittens, man ist kreativ und konstruiert phänomenologisch ein effektives, feldtheoretisches Modell der QCD. Die Kreativität ist jedoch nicht unbeschränkt, denn das Modell soll eine möglichst gute quantitative Beschreibung messbarer Größen, wie Wirkungsquerschnitte, liefern und wesentliche Aspekte des Phasendiagramms beschreiben, wie den chiralen Phasenübergang und/oder den Farbeinschluss. Diese Modelle zeigen eine Phasenübergangslinie erster Ordnung bei hohen baryochemischen Potenzialen, die in einem kritischen Punkt endet. Eine bildhafte Vorstellung des Phasendiagramms der QCD ist in Abbildung 1.2 zu sehen.

Die vorliegende Arbeit leistet einen Beitrag zu dem ehrgeizigen Ziel den Phasenübergang der QCD unter realistischen Bedingungen einer Schwerionenkollision theoretisch zu ver-

---

stehen. Die Vorhersagen von Observablen am Phasenübergang sind hauptsächlich aus thermodynamischen Systemen im Gleichgewicht abgeleitet. Es ist allerdings fraglich, ob das System, das in einer Schwerionenkollision erzeugt wird am Phasenübergang, wo Relaxationszeiten lang werden, im thermodynamischen Gleichgewicht ist. Selbst wenn das System oberhalb der Übergangstemperatur im Gleichgewicht ist, kommt es in einem dynamischen System am Phasenübergang aus dem Gleichgewicht. An einem Phasenübergang zweiter Ordnung nennt man dies kritische Verlangsamung. Sie führt dazu, dass das Anwachsen der Korrelationslänge beschränkt ist, und somit jedes Fluktuationssignal erheblich abgeschwächt wird. Im Nichtgleichgewicht gibt es jedoch interessante Phänomene am Phasenübergang erster Ordnung, die auf der möglichen Unterkühlung des Systems basieren.

Wir untersuchen beide Fragen:

- Wieviel von den Gleichgewichtssignalen eines kritischen Punkts übersteht die Nichtgleichgewichtssituation eines dynamischen Systems?
- Wie stark können Nichtgleichgewichtseffekte am Phasenübergang erster Ordnung in einer Schwerionenkollision entwickelt werden?

Zu diesem Zweck entwickeln wir einen gekoppelten Nichtgleichgewichtsansatz, der auf dem linearen Sigmamodell mit Konstituentenquarks beruht. Dieses Modell wird vielfach zur Beschreibung der dynamischen Brechung der chiralen Symmetrie verwendet.

## Chirale Fluiddynamik I

Inspiziert durch den Erfolg fluiddynamischer Beschreibungen von Schwerionenkollisionen reduzieren wir die Dynamik der Quarkfelder zu einer Propagation von Dichten gemäß Energie- und Impulserhaltung. Das Sigmafeld wird hingegen als Ordnungsparameter des chiralen Phasenübergangs explizit propagiert. In einem ersten Ansatz verwenden wir hierfür die deterministische klassische Euler-Lagrange Bewegungsgleichung. Sie besitzt einen nichttrivialen Quellterm, der über die Temperatur von der Expansion der Quarkflüssigkeit abhängt. Die Zustandsgleichung erhalten wir durch das thermodynamische Potenzial in Mittlerer-Feld-Näherung, das explizit vom lokalen Wert des Sigmafelds abhängt. In den Gleichungen der relativistischen Fluiddynamik finden wir einen Quellterm, der den Energie-Impuls-Austausch zwischen Feld und Flüssigkeit beschreibt. In der numerischen Simulation sehen wir, dass die Expansion und Kühlung der Quarkflüssigkeit das System durch den Phasenübergang führt. Das Sigmafeld erhält hier einen endlichen Erwartungswert, aber starke Oszillationen verhindern das Erreichen dieses Gleichgewichtszustands. Dieses Verhalten ist darauf zurück zu führen, dass Relaxationsprozesse in einer einfachen deterministischen Bewegungsgleichung im Sinne der klassischen Mechanik nicht enthalten sind. Diese Ergebnisse finden sich in Kapitel 4. Das Hauptaugenmerk dieser Arbeit liegt auf der Erweiterung der chiralen Fluiddynamik um eine konsistente Beschreibung von Nichtgleichgewichtseffekten am Phasenübergang.

## Selbstkonsistente Kopplung von Feld und Flüssigkeit

Um eine selbstkonsistente Kopplung der relaxierenden und expandierenden Dynamiken des Feldes und der Flüssigkeit herzuleiten wenden wir in Kapitel 5 zwei Methoden der Nichtgleichgewichtsquantenfeldtheorie an, das Influenzfunktional und die zwei-Teilchen irreduzible (2PI) effektive Wirkung. Erstere hat breite Anwendung in Nichtgleichgewichtsstudien der  $\Phi^4$ -Theorie, von Eichtheorien und  $\mathcal{O}(4)$ -Modellen gefunden.

Wir berechnen das Influenzfunktional für das lineare Sigmamodell mit Konstituentenquarks perturbativ. Es enthält damit die gesamte Wechselwirkung zwischen dem Sigmafeld und dem lokalen Wärmebad der Quarks. Hieraus erhalten wir einen Dämpfungsterm und ein stochastisches Feld in der Bewegungsgleichung des Sigmafelds. Innerhalb dieser Methode ist es jedoch nicht ohne Weiteres möglich die lokalen Gleichgewichtseigenschaften der Quarkflüssigkeit konsistent herzuleiten. Deshalb berechnen wir im Weiteren die 2PI effektive Wirkung. Der große Vorteil ist, dass in den zu berücksichtigenden Diagrammen bereits die vollen Propagatoren stehen, und somit große Klassen an Diagrammen summiert sind. In diesem Formalismus ist es möglich Transportgleichungen herzuleiten, für die die makroskopischen Erhaltungssätze erfüllt sind, konsistente Gleichgewichtseigenschaften zu erhalten und die thermodynamischen Relationen zwischen diesen zu bewahren. Man erhält gekoppelte Gleichungen für das mittlere Sigmafeld und die vollen Propagatoren der Quarks. Um diese allerdings zu lösen muss man weitere Näherungen einführen. Es gelingt uns die vollständige Langevin-Bewegungsgleichung für das mittlere Sigmafeld herzuleiten, deren Dämpfungs- und Rauschterm mit denen aus der Influenzfunktionalmethode übereinstimmen. Da wir vor allem an den langreichweitigen Fluktuationen interessiert sind, berechnen wir den Dämpfungskoeffizienten für die Nullmode des mittleren Sigmafelds explizit. Hier finden wir, dass, obwohl der Farbeinschluss in dem Modell nicht vorkommt, unterhalb des Phasenübergangs, wo die Quarks durch die Symmetriebrechung eine Masse erhalten, der Zerfall des Sigmamesons in ein Quark-Antiquarkpaar kinematisch nicht mehr möglich ist. Generell sollte hier die Wechselwirkung der langwelligen Moden mit den kurzwelligen Moden der chiralen Felder zu weiteren Dämpfungsprozessen führen. Im Speziellen ist das für das Sigmameson der Zerfall in zwei Pionen.

Darüberhinaus erhalten wir den lokalen Druck der Quarkflüssigkeit und können für diese aus der Schwinger-Dyson Gleichung für den vollen Propagator die Gleichungen der relativistischen Fluiddynamik ableiten. Entscheidend ist nun, dass für die exakte Lösung der gekoppelten Gleichungen bei vorgegebener 2PI effektiven Wirkung ein erhaltener Energie-Impulstensor hergeleitet werden kann. Die gemachten Näherungen erzeugen jedoch weitere Terme, die zum einen eine Korrektur zum Quarkanteil liefern, zum anderen von der Dissipation des mittleren Sigmafelds stammen. Letztere führt zu einer Korrektur über den herkömmlichen (siehe Kapitel 4) Anteil des Quellterms in den fluiddynamischen Gleichungen hinaus und beschreibt somit den Energietransfer aus dem Feld in die Flüssigkeit, zu der es aufgrund der Dämpfung während des Relaxationsprozesses kommt. In der numerischen Umsetzung müssen wir schauen, ob die Korrekturen des Quarkanteils



---

klein sind und ihre Vernachlässigung dadurch gerechtfertigt ist.

## Äquilibration und Relaxationszeiten

In Kapitel 6 untersuchen wir zunächst das Relaxationsverhalten des mittleren Sigmafelds bei einem globalen, d.h. räumlich homogenen, und isothermen Wärmebad. In der Langevin-Gleichung verwenden wir in dem kinematisch erlaubten Bereich den berechneten Dämpfungskoeffizienten aus Abbildung 5.2, wo die Masse der Quarks und des Sigma mesons über die Gleichgewichtswerte des mittleren Sigmafelds bestimmt werden. Verschwindet dieser Dämpfungskoeffizient, verwenden wir einen konstanten Dämpfungskoeffizienten, der als Ergebnis von Berechnungen in der gebrochenen Phase des  $O(4)$ -Modells motiviert ist.

Wir initialisieren das Sigmafeld oberhalb der Phasenübergangstemperatur im Gleichgewicht mit dem Wärmebad bei vorgegebener Temperatur und lassen diese dann instantan auf verschiedene Werte absinken. Der Relaxationsprozess verläuft sehr unterschiedlich für die verschiedenen Phasenübergangsszenarien. In der Nähe der Übergangstemperatur am Phasenübergang erster Ordnung, wo das Potenzial zwei Minima aufweist, beobachten wir die Phasenkoexistenz. Ein Teil des Systems befindet sich im globalen Minimum, während der andere Teil im lokalen Minimum ist. Die Relaxationszeiten sind sehr lang. Direkt an der Phasenübergangstemperatur befinden sich ungefähr gleich große Teile des Systems in den entarteten Minima.

Das Potenzial in einem Szenario mit einem kritischen Punkt hat nur ein Minimum. Bei der kritischen Temperatur wird es extrem flach. Hier zeigt sich, dass die Relaxationszeit sehr viel länger ist und selbst nach sehr großen Zeiten das System noch nicht relaxiert ist.

Im Folgenden untersuchen wir die Energiebilanz des Felds während des Relaxationsprozesses. Einerseits verliert das Feld Energie durch die Dissipation. Dies wird durch den Dämpfungsbeitrag im hergeleiteten Quellterm der fluiddynamischen Gleichungen beschrieben. Darüber hinaus erhält das System Energie durch das stochastische Feld. Dieser Beitrag lässt sich ermitteln, indem man sich nach jedem Zeitschritt die Feldenergie anschaut und mit der dissipierten Energie vergleicht. Die Differenz ist dann die Energiezufuhr vom Wärmebad ins Feld. Aufgrund des Dissipations-Fluktuationstheorems heben sich diese beiden Beiträge im Gleichgewicht auf. Während des Relaxationsprozesses hat die Energiedissipation ein Maximum. Dieser Nettoenergiefluss vom Feld muss ins Wärmebad gehen. Nun erweitern wir das Modell um diesen Effekt der Rückreaktion auf das Wärmebad und untersuchen erneut das Relaxationsverhalten des gekoppelten Systems. Wieder initialisieren wir das Feld im Gleichgewicht bei einer Temperatur oberhalb der Phasenübergangstemperatur und senken diese dann abrupt ab. Mit dieser neuen Temperatur berechnen wir nun über die Zustandsgleichung die Energiedichte des Wärmebads. Durch den dissipativen Energiefluss vom Feld in das Wärmebad heizt diese sich auf, woraufhin sich das effektive Potenzial des Felds ändert und so wiederum den Relaxations-

verlauf beeinflusst. In einem Szenario mit einem Phasenübergang erster Ordnung wird das Wärmebad so stark aufgeheizt, dass der Phasenübergang erneut in die Hochtemperaturphase überquert wird. Da das System zu diesem Zeitpunkt bereits in das Minimum der Niedrigtemperaturphase relaxiert ist und der weitere Energiefluss lokal einer Relaxations ins globale Minimum entgegen wirkt, bleibt das System für alle untersuchten, großen Zeiträume im lokalen Minimum. Für ein anfängliches Absinken auf sehr niedrige Temperaturen relaxiert das Gesamtsystem auf eine Temperatur, bei der das Feld im Gleichgewicht ist. Für ein Szenario mit einem kritischen Punkt relaxiert das Feld immer bei der Endtemperatur des Wärmebads. Kommt diese in die Nähe der kritischen Temperatur, so beobachten wir erneut den Effekt der kritischen Verlangsamung, nämlich sehr große Relaxationszeiten.

## Chirale Fluidodynamik II

Zur vollständigen Beschreibung der chiralen Fluidodynamik berücksichtigen wir in Kapitel 7 zusätzlich die fluiddynamische Expansion der Quarkflüssigkeit. Hierfür wählen wir einfache Anfangsbedingungen, die aber die Überlappregion einer Kern-Kern-Kollision im Wesentlichen nachbilden. Dazu initialisieren wir das Feld im Gleichgewicht. Für jedes Phasenübergangsszenario untersuchen wir die Expansion mit verschiedenen Dämpfungskoeffizienten: zwei konstanten Werten und einem temperaturabhängigen. Letzterer besteht im kinematisch erlaubten Bereich aus dem Dämpfungskoeffizienten in Abbildung 5.2. Ist die Sigmamasse zu klein für den Zerfall in ein Quark-Antiquarkpaar, so kann das Sigmameson noch in zwei Pionen zerfallen und daher eine Dämpfung erfahren. Wenn die Sigmamasse auch hierfür zu klein ist, wie es am kritischen Punkt der Fall ist, so verschwindet der Dämpfungskoeffizient.

Wir überzeugen uns in allen beschriebenen Szenarien, dass auch in dem dynamischen Modell die Gesamtenergie während der Expansion sehr gut erhalten ist. Beim Betrachten einzelner Komponenten sieht man sehr schön, dass die Energie aus dem Feld in die Quarkflüssigkeit dissipiert.

Die Zeitentwicklung des Sigmafelds, der Temperatur und der Energiedichte sind qualitativ sehr unterschiedlich für die verschiedenen Dämpfungs- und Phasenübergangsszenarien. Am Phasenübergang erster Ordnung finden wir die Effekte der Unterkühlung des Systems und das Aufheizen der Quarkflüssigkeit, so dass auch in dem gekoppelten System die Phasenübergangstemperatur wieder überschritten wird. Durch die weitere Expansion der Quarkflüssigkeit relaxiert das mittlere Sigmafeld schließlich zum Vakuumserwartungswert.

Wir untersuchen für alle Szenarien die Intensität der Fluktuationen des Sigmafelds. Zu späteren Zeiten, wenn Nichtlinearitäten klein sind, ergibt sie die Anzahl der aus dem kohärenten Zerfall des Felds produzierten Sigmamesonen. Wir finden, dass die Nichtgleichgewichtseffekte in einem Szenario mit einem Phasenübergang erster Ordnung die

---

Intensität dieser Fluktuationen stark erhöhen gegenüber einem Szenario mit einem kritischen Punkt. Wir zeigen die Spektren des transversalen Impulses der Sigmamesonen.

Die Korrelationslänge in einem Szenario mit einem kritischen Punkt kann dynamisch berechnet werden. Wir finden ein leichtes Anwachsen am Phasenübergang.

Schließlich berechnen wir während der Expansion die Impulsanisotropie. Für einen temperaturabhängigen Dämpfungskoeffizienten ist diese in einem Szenario mit einem Phasenübergang erster Ordnung kleiner als für ein Szenario mit einem kritischen Punkt.

## Zusammenfassung und Ausblick

Die wesentlichen Errungenschaften dieser Arbeit sind die folgenden:

- Die Entwicklung eines vollständigen und selbstkonsistenten quantenfeldtheoretischen Ansatzes zur dynamischen Untersuchung von Phasenübergängen im Nichtgleichgewicht.
- Die erfolgreiche Untersuchung von Nichtgleichgewichtseffekten am Phasenübergang innerhalb einer realistischen fluiddynamischen Entwicklung einer Schwerionenkollision. Wir konnten die Phänomene der Unterkühlung, des Aufheizens und der kritischen Verlangsamung untersuchen und zeigen, dass die Intensität der Nichtgleichgewichtsfluktuationen am Phasenübergang erster Ordnung stark anwächst.

Über die Verbesserung des verwendeten Modells hinaus, wie die Betrachtung bei endlichen baryonischen Dichten und die Einbeziehung der Polyakov-Schleife, werden wir in zukünftiger Arbeit die Pionen berücksichtigen. Diese sind einerseits wichtig als explizit propagierte Freiheitsgrade, andererseits spielen sie eine wichtige Rolle bei zusätzlichen Dämpfungsprozessen des mittleren Sigmafelds. Darüber hinaus ist es interessant vollständige Pionenspektren zu errechnen, also auch das Wärmebad durch Ausfrieren in Pionen zu überführen. So sollten in Zukunft auch Fluktuationen zwischen verschiedenen Kollisionen zu untersuchen sein.



# Danke!

Es bleibt mir die angenehme Aufgabe allen denjenigen meinen herzlichsten Dank auszusprechen, die zum Gelingen dieser Arbeit maßgeblich beigetragen haben.

Zu allererst gilt dieser Dank Prof. Dr. Marcus Bleicher für die interessante Themenstellung und die engagierte Betreuung dieser Arbeit. Besonders danke ich ihm für seine motivierende Unterstützung während der letzten drei Jahre und die vielen Möglichkeiten auf Konferenzen und Forschungsaufenthalte zu fahren und diese Arbeit vorzustellen.

Ich danke Prof. Dr. Horst Stöcker nicht nur für seine freundliche Bereitschaft die Zweitkorrektur dieser Arbeit zu übernehmen, sondern auch für seine vielen aufmunternden und unterstützenden Worte.

Für die intensive Betreuung und die vielen Stunden Rechnen und Erklären danke ich Prof. Dr. Stefan Leupold. Während meines Aufenthalts am Institut für Physik und Astronomie der Universität Uppsala sind wesentliche Teile dieser Arbeit entstanden. Ich danke dem Institut für die konzentrierte Arbeitsatmosphäre und die Gastfreundschaft, mit der ich dort aufgenommen wurde.

Für ihr fortwährendes Interesse an dieser Arbeit und viele nützliche Diskussionen und Anregungen danke ich Prof. Dr. Carsten Greiner und Prof. Dr. Igor Mishustin. Prof. Dr. Dirk Rischke danke ich für die Zurverfügungstellung des SHASTA-Codes.

Für zahlreiche Anregungen und Diskussionen danke ich Prof. Dr. Reinhard Stock, Prof. Dr. Eduardo Fraga, Prof. Dr. Misha Stephanov, Prof. Dr. Volker Koch und Prof. Dr. Pedro Bicudo.

Es war nicht nur physikalisch ein enormer Zugewinn, es hat auch immer Spaß gemacht, an Veranstaltungen der Graduiertenschule HGS-HiRe teilzunehmen. Für diese Möglichkeiten und dafür, dass sie immer versuchen alles möglich zu machen, danke ich Prof. Dr. Henner Büsching und allen MitarbeiterInnen der Graduiertenschule ganz herzlich.

Für die finanzielle und ideelle Unterstützung dieser Arbeit danke ich der Stiftung der Polytechnischen Gesellschaft Frankfurt am Main und der Studienstiftung des deutschen Volkes. Ein besonderer Dank geht an Dr. Wolfgang Eimer und Tobias Ullrich.

Ein ganz besonderer Dank geht an Gabriela Meyer für ihr offenes Ohr, ihre große Unterstützung und die vielen Hilfen!

Zu besonderem Dank bin ich all denjenigen verpflichtet, die meinen Aufenthalt in Upp-

sala nicht nur physikalisch mit Leben gefüllt haben. Besonders danke ich Gunjana und Arpana Sharma für die tolle Zeit, die ich bei ihnen verbracht habe. Ich danke Pär für die ein oder andere schwedische Party. Danke, Stefan und Sabrina für die vielen Einladungen zum Fußball gucken und/oder zum Essen!

Ich danke allen jenen, die diese Arbeit ganz oder in Teilen Korrektur gelesen haben: Björn, Christoph und Thomas L. Bei Björn und Christian bedanke ich mich außerdem für die Hilfe mit dem Gestalten der Bilder in dieser Arbeit. Ist irgendetwas dennoch falsch oder ein Bild nicht schön geworden, liegt es natürlich alleine an mir. Für Hilfe bei jeglicher Art von Computerproblem bedanke ich mich bei Alex, Thomas W. und Guido.

Für viele interessante Gespräche, Ratschläge, Hilfen und viele schöne Momente auf Konferenzen und bei Treffen danke ich Marcus Bluhm, Clement Gombeaud, Claudia Ratti, Magdalena Malek und Vincent Mathieu.

Dafür, dass wir immer eine nette Arbeitsatmosphäre hatten, die ein oder andere Appelweinpause eingelegt haben und mit Hilfe zur Stelle waren, wenn sie benötigt wurde, danke ich meinen lieben Bürokollegen: Hannah, Christoph, Björn, Martin K. und Martin S. Den weiteren Mitgliedern unserer Arbeitsgruppe danke ich ebenso: Jan, Gunnar, Thomas L., Elvira und Michi.

Als Eintracht-Fans haben wir es nicht leicht, und zur Zeit besonders schwer. Ich danke daher Christoph, Alex, Guido, Tobias und Joe fürs gemeinsame Leiden an der Uni und darüber hinaus. Ein besonderer Dank geht an Joe für viele gemeinsame Appelwein am Gleisdreieck.

Ich danke meinen lieben Freunden, die nicht nur dafür gesorgt haben, dass der Uni-Alltag nie langweilig wurde, sondern auch ansonsten dazu beigetragen haben, dass meine Zeit in der schönsten Stadt der Welt unvergesslich bleiben wird. Danke Christoph, Alex, Björn, Hannah und Thomas! Ich danke auch von ganzem Herzen meiner lieben Freundin Yixian, mit der ich zwar kein Büro mehr teile, dafür aber vieles, vieles andere!

Dafür, dass er zu mir hält, meine Physik fast so sehr mag wie mich und mich daher besonders in den letzten Monaten mit allen Kräften unterstützt hat, danke ich meinem lieben Freund Christian.

Ich danke meiner lieben Familie dafür, dass sie immer zu mir halten und ich mich immer auf sie verlassen kann, dass sie mich, meine Pläne, Entscheidungen und Wünsche unterstützen, auch wenn das heißt, dass ich mal wieder unterwegs bin, obwohl sie mich doch am liebsten immer bei sich hätten. Für diese Liebe danke ich euch am allermeisten.

# Akademischer Lebenslauf

Dipl.-Phys. Marlene Nahrgang  
Frankfurt Institute for Advanced Studies  
Ruth-Moufang-Str. 1  
60438 Frankfurt am Main  
Deutschland

[www.th.physik.uni-frankfurt.de/~nahrgang](http://www.th.physik.uni-frankfurt.de/~nahrgang)

geboren am 02. August 1982 in Marburg an der Lahn

## AUSBILDUNG

---

1989 – 1993	Bärenbachschule, Grundschule, Stadtallendorf
1993 – 1999	Georg-Büchner-Schule, Gesamtschule, Stadtallendorf
1999 – 2002	Martin-Luther-Schule, Marburg an der Lahn
06/2002	Abitur
10/2002 – 03/2008	<b>Philipps-Universität Marburg an der Lahn,</b> Studium der Physik
10/2004	Vordiplom
2005 – 2006	<b>Staatlich-Technische Universität und Staatliche Universität Novosibirsk</b> Forschungsaufenthalt zum Thema: Solitonen und inverse Streutheorie
03/2008	Diplom Betreuer: Prof. Dr. Florian Gebhard Titel der Arbeit: "Multichain Approach to the Single-Impurity Anderson Model in the Dynamical Mean-Field Theory"
seit Mai 2008	<b>Johann Wolfgang Goethe-Universität Frankfurt am Main</b> und <b>Frankfurt Institute for Advanced Studies</b> , Doktorandin Betreuer: Prof. Dr. Marcus Bleicher

06/2010 – 10/2010    **Uppsala Universitet, Ångströmlaboratoriet**  
Institutionen for fysik och astronomi  
Forschungsaufenthalt bei Prof. Dr. Stefan Leupold

---

**ERFAHRUNGEN UND STIPENDIEN**

---

11/2002 – 03/2008    Stipendiatin der Studienstiftung des deutschen Volkes

08/2005 – 08/2006    Stipendium “Metropolen in Osteuropa” der Studienstiftung des deutschen Volkes und der Alfried Krupp von Bohlen und Halbach-Stiftung

09/2005 – 06/2006    Auslandsstipendium des DAAD

2006 – 2007            **Naturwissenschaftliches Kolleg** der Studienstiftung des deutschen Volkes  
“Urknall im Labor: Erforschung von Urknallmaterie mit Schwerionenstößen”  
Leitung: Prof. Dr. Peter Braun-Munzinger

seit 10/2008            Promotionsstipendium der Stiftung der Polytechnischen Gesellschaft Frankfurt am Main

seit 11/2008            Stipendiatin in der Promotionsförderung der Studienstiftung des deutschen Volkes

seit 02/2009            Studentin in der Helmholtz Graduate School for Hadron and Ion Research, HGS-HIRe



# Meine akademischen Lehrer

Prof. Dr. Marcus Bleicher

Prof. Dr. Stefan Leupold (Universität Uppsala)

Prof. Dr. Florian Gebhard (Philipps-Universität Marburg)

Prof. Dr. Peter Thomas (Philipps-Universität Marburg)

Prof. Dr. Stephan Koch (Philipps-Universität Marburg)

Prof. Dr. Angela Thränhardt (jetzt: Technische Universität Chemnitz)

Prof. Dr. Sergei Baranovski (Philipps-Universität Marburg)

Dr. Jörg Bünemann (Philipps-Universität Marburg)

Prof. Dr. Wolfgang Rühle (Philipps-Universität Marburg)

Prof. Dr. Ulrich Höfer (Philipps-Universität Marburg)

Prof. Dr. Heinz Jänsch (Philipps-Universität Marburg)

Prof. Dr. Wolfgang Stolz (Philipps-Universität Marburg)

Prof. Dr. Kerstin Volz (Philipps-Universität Marburg)

Prof. Dr. Gerhard Weiser (Philipps-Universität Marburg)

Dr. Bernd Kohlmeyer (Philipps-Universität Marburg)

Prof. Dr. Wolfgang Gromes (Philipps-Universität Marburg, Fachbereich Mathematik)

Prof. Dr. Hans-Peter Schlickewei (Philipps-Universität Marburg, Fachbereich Mathematik)

Prof. Dr. Harald Upmeier (Philipps-Universität Marburg, Fachbereich Mathematik)

Prof. Dr. Claude Portenier (Philipps-Universität Marburg, Fachbereich Mathematik)

Prof. Dr. Vladislav Dubrovsky (Staatlich-Technische Universität Novosibirsk)

